THE UNIVERSITY
of EDINBURGH

The Design and Development of Novel mTOR and SRC Family Kinase Inhibitors via a Phenotypic Drug Discovery Approach

By

Craig Fraser

Doctor of Philosophy

The University of Edinburgh

2015

Abstract

Traditionally, drug discovery programs have focused on prioritising compounds by their affinity to a specific target in isolation, which was hypothesised to be the cause of a particular disease. Through chemical inhibition, the disease could, thus, be prevented or at the very least, controlled. These hypotheses require significant validation before drug screening can begin which relates to lengthy and expensive programs. Furthermore, drug screening against a single target in isolation is not a realistic model of cellular behaviour and is not appropriately tailored to more complex diseases such as cancer.

Phenotypic drug discovery, on the other hand, bypasses any involvement of known targets, instead focusing on the desired outcome – the phenotype. In this way, drugs are biased by their potency on the phenotype and not against any particular targets. The molecular mechanism of action need not be known at all, however, it can be useful to later reveal the target(s) involved by various deconvolution methods.

This thesis describes a cooperative ligand based phenotypic drug discovery approach, undertaken in order to develop more suitable small molecule drugs for cancer treatment. For this purpose, the promiscuous pyrazolopyrimidine inhibitor PP1 was chosen as a starting model compound. Modification of PP1 on the N1 position allowed a series of water solubilising groups to be incorporated into the pyrazolopyrimidine scaffold which created an initial 12-membered library. Testing against MCF7 breast cancer cells and looking at phenotypic end points such as cell proliferation, cell mobility and cell cycle, generated early target-agnostic structure/anti-proliferative activity relationships. These early results, along with compounds published in recent literature, were used to generate further libraries.

Profiling lead compounds against a selection of 18 kinases known to be targeted by PP1, showed the compounds were inhibiting either SRC family or mTOR kinases which enabled the creation of two, structure specific, groups of inhibitors. Further lead optimisation led to the rapid discovery of preclinical candidates with excellent drug-like properties and potencies in both cellular assays and against their respective targets. Compounds also showed improved selectivity profiles compared to PP1 and commonly known inhibitors of SRC and mTOR kinases. Reported, herein, is the discovery of the first sub-nanomolar SRC inhibitor which does not inhibit the kinase ABL and shows excellent properties suitable for further preclinical development.

Declaration

This thesis has been entirely written by me, Craig Fraser. All experiments and analysis have been performed by me unless otherwise stated. All figures, schemes and tables have been composed by me unless stated. Permission was sought for any figures not composed by me and is indicated in the figure description. This work is not submitted for any other degree or professional qualification. A patent was filed on the 21st of May, 2015 protecting the rights to the compounds described in this thesis.

Intellectual Property Office Patent Application Number: 1508747.1

Signed:.....

Date:.....

Acknowledgements

First of all, my upmost gratitude goes to Dr Asier Unciti-Broceta. Your down-to-earth attitude and excellent supervision has made my PhD experience a very positive one, and has been paramount to the success of this project, and thesis. Your seemingly endless supply of ideas and 'wee blue books' will be worth millions someday. 'I have an idea' is a phrase I have come to both love, and loath.

A special mention goes out to Dr Jason Weiss, the other co-founder of the Unciti-Broceta lab (who managed to beat me on both publishing, and submitting his thesis). We have worked great together from the start and if there ever was an example of excellent team work, we would be it. The rest of the Unciti-Broceta group also deserve special thanks - Dr Belén Rubio-Ruiz, Dr Teresa Valero, Dr Ana Pérez-López, Sam Myers, Thomas Bray and Richard Crispin. The good times we have shared both in the lab and out have made this PhD worthwhile.

I must thank both Dr Neil Carragher and Dr John Dawson for both teaching me your knowledge and answering my constant questions regarding biology. John, your hands-on experience is second to none and your no-messing-about approach to science is something I admire. A particular mention must go to Alison Munro for always pointing me in the right direction and keeping tissue culture in tip top condition. I also thank the rest of the Carragher group for their guidance, and good times had during the post-lab meeting pub trips.

The strong collaboration between the Unciti-Broceta and Patton groups deserves a mention and I thank Dr Liz Patton and Reece Dowling for their perseverance and patience during the zebrafish work. I hope the collaboration will continue to grow.

Special thanks go to Jan at reception. Your welcoming smile and help during my 3 years have made this experience so much easier.

I must thank my parents, Andrea and John, for their support during, not just my PhD, but all through my undergraduate, and also my brother, Stephen, for the collective nodding of your heads in agreement when I try to explain what I actually do. My gratitude goes far beyond words. To all my friends in Edinburgh, and beyond, I thank you for all the good nights had and the accompanying, uncomfortable, hangovers.

Síðast, en ekki síst, vil ég þakka kærustunni minni, Ylfu. Öllu mínu doktorsnámi deildi ég með þér og þú hefur umborið allt mitt nöldur meðan á því stóð. Ég hef vaxið mikið á síðustu þremur árum og þú hefur verið stór hluti af því. Þú kynntir mig fyrir heimalandi þínu, Íslandi, sem ég varð strax mjög hrifin af. Stundirnar sem við höfum átt saman, bæði í Edinborg og erlendis mun ég minnast um ókomna tíð og ég hlakka til upplifa enn fleiri ævintýri með þér.

Contents

Abbreviations

^{1}H NMR	Proton Nuclear Magnetic Resonance
4E-BP1	eIF4E Binding Protein 1
5-FU	5-Fluorouracil
^{13}C NMR	Carbon-13 Nuclear Magnetic Resonance
δ	Chemical Shift
μM	Micro Molar
ABL	Abelson murine leukaemia viral oncogene homolog 1
ADMET	Absorption Distribution, Metabolism, Excretion and Toxicology
AKT	a.k.a Protein Kinase B
AMPK	Adenosine Monophosphate-activated Protein Kinase
ATG13	Autophagy-related Gene 13
ATP	Adenosine Triphosphate
BCR	Breakpoint Cluster Region
BLK	B Lymphocyte Kinase
BRK/PTK6	Breast tumour Kinase/Protein Tyrosine Kinase 6
BSA	Bovine Serum Albumin
CAS	CRK-Associated Substrate
$CDCl_3$	Deuterated Chloroform
CML	Chronic Myeloid Leukaemia
CRPC	Castration Resistant Prostate Cancer
CSK	C-terminal SRC Kinase
CYP	Cytochrome P450 enzyme
d	Doublet
DCM	Dichloromethane
dd	Doublet of doublets
ddd	Doublet of doublet of doublet
DDT	Dichlorodiphenyltrichloroethane
Deptor	DEP-domain-containing mTOR-interacting protein
DMEM	Dulbecco's Modified Eagle Medium
DMF	*N*,*N*-Dimethylformamide
DMPK	Drug Metabolism and Pharmacokinetics
DMSO	Dimethylsulphoxide
DNA	Deoxyribonucleic Acid
dpf	Days Post Fertilisation
EC_{50}	Half maximal Effective Concentration
ECM	Extracellular Matrix
eEF2K	Eukaryotic Elongation Factor-2-Kinase
EGFR	Epidermal Growth Factor Receptor
eIF4B	Eukaryotic Initiation Factor 4B
eIF4E	Eukaryotic Initiation Factor 4E
eq.	Equivalents

ER	Estrogen Receptor or Endoplasmic Reticulum
ERBB2	a.k.a HER2
ES	Electrospray Ionisation
EtOAc	Ethyl Acetate
FAK	Focal Adhesion Kinase
FAS	Fatty Acid Synthase
FBS	Fetal Bovine Serum
FDA	Food and Drug Administration
FGR	Gardner-Rasheer Feline sarcoma viral oncogene homolog
FIP200	Focal adhesion kinase family-Interacting Protein of 200 kDa
FKBP12	FK506-binding Protein of 12 kDa
FRB	FKB12-Rapamycin Binding domain
FRK/PTK5	Fyn-Related Kinase/Protein Tyrosine Kinase 5
FYN	Proto-oncogene FYN
g	Grams
G_2	Gap 2
GPCR	G-Protein Coupled Receptor
HCK	Proto-oncogene HCK
HEPES	4-(2-hydroxyethyl)-1-piperazineethanesulfonic acid
hERG	Human Ether-a-go-go-Related Gene
HER2	Human Epidermal Growth factor Receptor 2
HIF1α	Hypoxia-Inducible Factor 1 Alpha
HLM	Human Liver Microsomes
HRMS	High Resolution Mass Spectrometry
HRP	Horseradish Peroxidase
HTS	High Throughput Screening
Hz	Hertz
IC_{50}	Half maximal Inhibitory Concentration
IGF	Insulin Growth Factor
IV	Intravenous
c-KIT	a.k.a. Mast/stem cell growth factor receptor
J	Coupling Constant
LCK	Lymphocyte-specific protein tyrosine Kinase
LC-MS/MS	Liquid Chromatography Mass Spectrometry
LYN	Lck/Yes Novel tyrosine kinase
LRMS	Low Resolution Mass Spectrometry
m	Multiplet
M	Mitosis
mg	Milligram
M+H	Mass + Proton
ml	Millilitre
mmol	Millimoles
m/z	Mass to charge ratio
MCF7	Michigan Cancer Foundation-7 (Origin of cell line)
MDA-MB-231	Breast adenocarcinoma cell line
MeOD	Deuterated Methanol

MeOH	Methanol
MIPDD	Mechanism Informed Phenotypic Drug Discovery
MHz	Mega Hertz
mLST8	Mammalian Lethal with Sec13 protein 8
MOA	Mechanism Of Action
mRNA	Messenger Ribonucleic Acid
MS	Mass Spectrometry
mSIN1	Mammalian Stress activated protein kinase Interacting protein
mTOR	Mammalian Target of Rapamycin
mTORC	mTOR Complex
mw	Microwave
MW	Molecular Weight
NADPH	Nicotinamide Adenine Dinucleotide Phosphate-oxidase
NIS	*N*-iodosuccinimide
nm	Nanometer
NME	New Molecular Entity
NMR	Nuclear Magnetic Resonance
NSCLC	Non-Small Cell Lung Cancer
PAGE	Polyacrylamide Gel Electrophoresis
PBS	Phosphate Buffered Saline
PC3	Prostate Cancer 3
PDCD4	Programmed Cell Death protein 4
PDGFR	Platelet-Derived Growth Factor Receptor
PFA	Poly Formaldehyde
pHH3	Phospho-Histone H3
PI3K	Phosphatidylinositol 3-Kinase
PK	Pharmacokinetic
PKCα	Protein Kinase C-alpha
POD ECL	Peroxidase Enhanced Chemiluminescence
PPAR-γ	Peroxisome Proliferator-Activated Receptor-gamma
PPB	Plasma Protein Binding
PRAS40	Proline Rich AKT Substrate 40 kDa
PTEN	Phosphatase and Tensin homolog
Protor-1	Protein Observed with Rictor-1
PVDF	Polyvinyllidene Fluoride
q	Quartet
Rac1	Ras-related C3 botulinum toxin substrate 1
Raptor	Regulatory Associated Protein of mTOR
RED	Rapid Equilibrium Dialysis
RET	Rearranged during Transfection
R_f	Retention Factor
RhoA	Ras Homolog family member A
Rictor	Rapamycin Insensitive Companion of mTOR
RLU	Relative Light Units
RNA	Ribonucleic Acid
RPMI	Roswell Park Memorial Institute

RPPA	Reverse Phase Protein Micro Array
r.t.	Room Temperature
s	Singlet
S6	Ribosomal protein S6
S6K1	p70 ribosomal S6 Kinase 1
SAR	Structure Activity Relationship
SDS	Sodium Dodecyl Sulphate
SFK	SRC Family Kinase
SH	SRC Homology
SMO	Smoothened Receptor
SREBP1	Sterol Regulatory Element Binding Protein 1
SRC	Sarcoma
STAT3	Signal Transducer and Activator of Transcription 3
SYF	SRC, YES and FYN deficient mouse embryonic fibroblasts
TBS/T	Tris Buffered Saline/Tween
TFA	Trifluoroacetic Acid
THF	Tetrahydrofuran
TLC	Thin Layer Chromatography
TSC1/2	Tuberous Sclerosis 1/2
td	Triplet of Doublets
Tyr	Tyrosine
ULK1	Unc-51-Like Kinase 1
VEGF	Vascular Endothelial Growth Factor
YES	Proto-Oncogene YES
YRK	Yes Related Kinase

1. Introduction

1.1 Targeted Drug Discovery

Traditional drug discovery programs begin with a target based hypothesis.[1-5] That is, a single biological target (e.g. Enzyme, GPCR, ion channel, DNA/mRNA etc.) is hypothesised to cause an undesired effect and so inhibiting or blocking said target should render the pathophysiological effect mute and regain normal function, in an organism. Such hypotheses require extensive biological validation before the onset of drug screening. This represents the first problem associated with traditional target based drug discovery; target validation is often challenging due to a lack of disease relevant preclinical model systems and typically involves months of work, with knockout mice commonly required. This can prove to be very expensive and often the target hypothesis does not correlate well *in vivo*. Additionally, diseases caused by multiple factors/genes, such as cancer, are not appropriately tailored to this approach.[6-8] That is not to say that the targeted drug discovery approach is ineffective. Indeed, it has proven itself several times over in the later stages of the 20th and early 21st century of drug discovery. However, the increased costs associated with target directed drug discovery and high attrition rates have contributed to an overall decline in pharmaceutical productivity.[9]

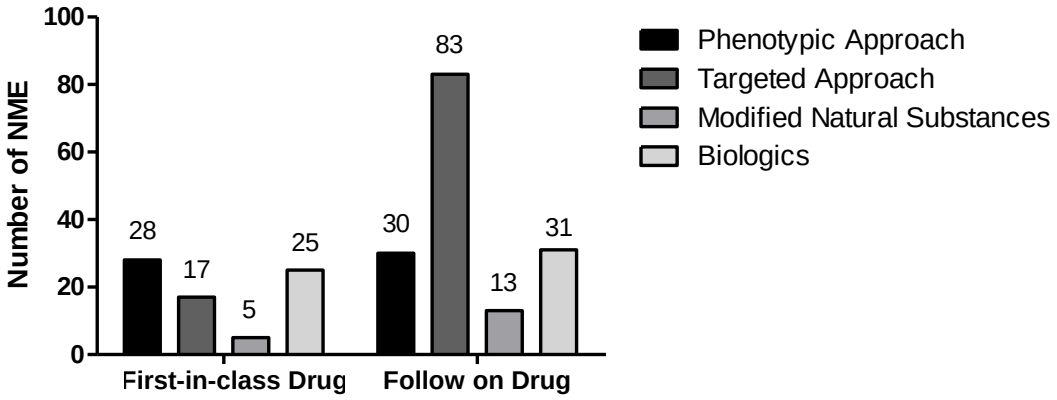

Figure 1.1: *New molecular entities approved between 1999 and 2008 arranged by their discovery stategy.*

As described in a recent review by David C. Swinney and Jason Anthony, targeted drug discovery programs accounted for 43% of new molecular entities (NME) approved between

1999 and 2008 with phenotypic based drug discovery programs producing 25%, figure 1.1.[10]

This is by no means a fair comparison of both routes as neither attrition rates nor costs were taken into consideration. It is also worthy to note that target-directed drug discovery was less successful in the production of first in class drugs but far superior in 'follow on' drugs. These analyses may be expected as 'follow on' drugs have the target pre-validated and new drugs are simply developed to offer incremental improvements in potency, or pharmacokinetic properties, over the original drug.

Shown in figure 1.2 is a schematic representation of the traditional drug discovery route. Priority is placed on validating a molecular target corresponding to a particular disease. Once the target has been validated and one is confident that inhibition of the target will reduce the effects of the disease, priority is then shifted to developing a drug against the target. There are many methods for discovering a starting compound, listed below:

1. High throughput screening (HTS)
2. Structure based techniques (eg. X-ray, NMR)
3. Improving previous drugs (follow on drug)
4. Modification of natural ligands
5. Modification of natural inhibitors

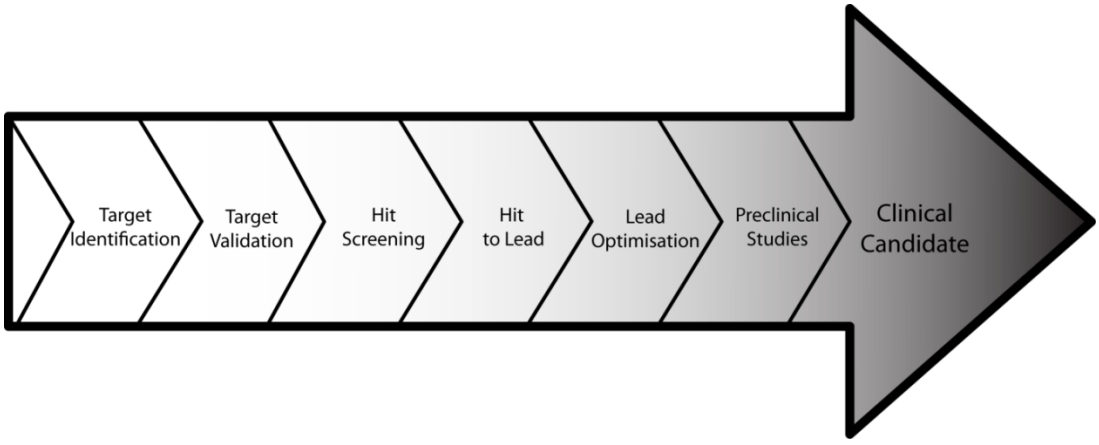

Figure 1.2: *Traditional target-directed drug project operating model from target identification to clinical candidate.*

However, when it comes to the treatment of cancer, disappointing results in recent clinical trials have shown that even compounds showing promising results *in vitro* often translate poorly when taken into the clinic. An important point to consider when advancing a drug

candidate is the emergence of drug resistance in patients. In many cancers, the major issue when administering chemotherapy is overcoming heterogeneity within patients. Consequently, more effective targeted drug therapies are still very much sought after.[11, 12]

When drugs do get approved for use in humans, targeted drug discovery does have one strong advantage. That is the ability to pair up the patient with the correct drug. If the drug has a well-defined target, patients can be selected by predictive biomarkers of target expression or activity and tailored to the correct therapy. This enables more personalised therapy rather than a 'stab in the dark' approach where generic drugs are prescribed to groups of patients with 'similar' cancers.

One must be careful, however, as there have been a few reported cases of drugs assigned to the wrong targets – although the drug may inhibit the target, its true mechanism of action exerts through another, perhaps unknown, pathway. Such an example is Sorafenib, thought to be a Raf inhibitor but later shown to exert it's clinical effects through VEGFR inhibition.[13] This can lead to the selection of the wrong population of patients in trials and, consequently, apparent failed efficacy of the drug.[13-16] Even drugs with well validated targets may present significant problems when taken into the clinic as complex signalling pathways and feedback mechanisms within cells coupled with intricate resistance mechanisms may prove overwhelming for the drug, contrary to the success observed in more basic preclinical cellular studies.

In order to break away from the resistance prone targeted drug discovery approach, one may take a variety of steps. For example, phenotypic drug discovery is an alternative route which frontloads the phenotype of the disease model rather than the genotype, therefore, biasing the development on the desired therapeutic outcome regardless of the molecular targets involved.[17] Adopting pro-drug therapies for administering drugs to specific disease areas permits the safer use of cytotoxic agents and helps to reduce the side effects associated with them.[18] The pre-clinical use of advanced imaging techniques coupled with clinically relevant *in vitro* models may also steer drug development towards more successful outcomes by informing chemical selection and design strategies based upon robust biological evidence.[19] Although perhaps not appropriately tailored for more complex diseases such as neurodegeneration and the majority of cancers, which do not fall into molecular subtypes characterised by defined genetic mutations, targeted drug discovery remains a valuable route for the discovery of compounds suited to single gene defect diseases.

1. Introduction

1.2 Phenotypic Drug Discovery

As an alternative to the current targeted drug discovery route, modern phenotypic drug discovery offers promise in overcoming the difficult transition from lab to clinic. Drugs developed on the basis of selectivity to one target only, often do not possess known mechanisms of action. That is to say that although the target may be validated via knockout mice etc., and the drug does indeed inhibit the target effectively, the exact mechanism by which it exerts its phenotypic response (i.e. cell death, reduced cell mobility/division) is unknown. Many cases of failed clinical programs may be caused by gaps in the knowledge of molecular pathways. On the other hand, phenotypic drug discovery offers the advantage of not being constrained by target selectivity and instead, focuses on the desired outcome. Drugs produced from such a technique are, therefore, more likely to possess validated and clinically relevant mechanisms of action.[20]

Classic phenotypic endpoints in cancer drug discovery include: reduced cell proliferation, reduced cell migration/invasion, induction of apoptosis, cell cycle arrest and changes in cell morphology. These classical 'hallmarks of cancer' are relatively simple to measure in *in vitro* assays. Consequently, whether a drug can reduce cancer cell viability in culture has become the bedrock of cancer drug discovery. Indeed, this phenotypical based technique has outdated any knowledge of the mechanisms of action of drugs or the targets involved.[21] However, there are many phenotypes which are not so easily measured (e.g. inhibition of angiogenesis, cell motility, and evasion of the immune system) as they require more complex modelling and assay formats than simply cultured cancer cells in a monolayer.

Figure 1.3 shows how phenotypic screening bypasses biased knowledge of a compound's target. Starting at the 'hit screening' stage, one can progress a compound right through to the clinic without any prior knowledge of the target involved. In essence, the route is shorter, however, knowing the target can often help the optimisation of a drug and will prove more useful in a preclinical setting. In practice, it is often wise to deconvolute the target after an early lead compound has been identified (lead optimisation stage). There are various ways to deconvolute a target including: reverse protein micro arrays (RPPA), screening against members of a target family (e.g. the kinome for a suspected kinase inhibitor), affinity

chromatography, phage display, mRNA display, yeast/mammalian three hybrid system, reverse transfected cell microarrays etc.[22]

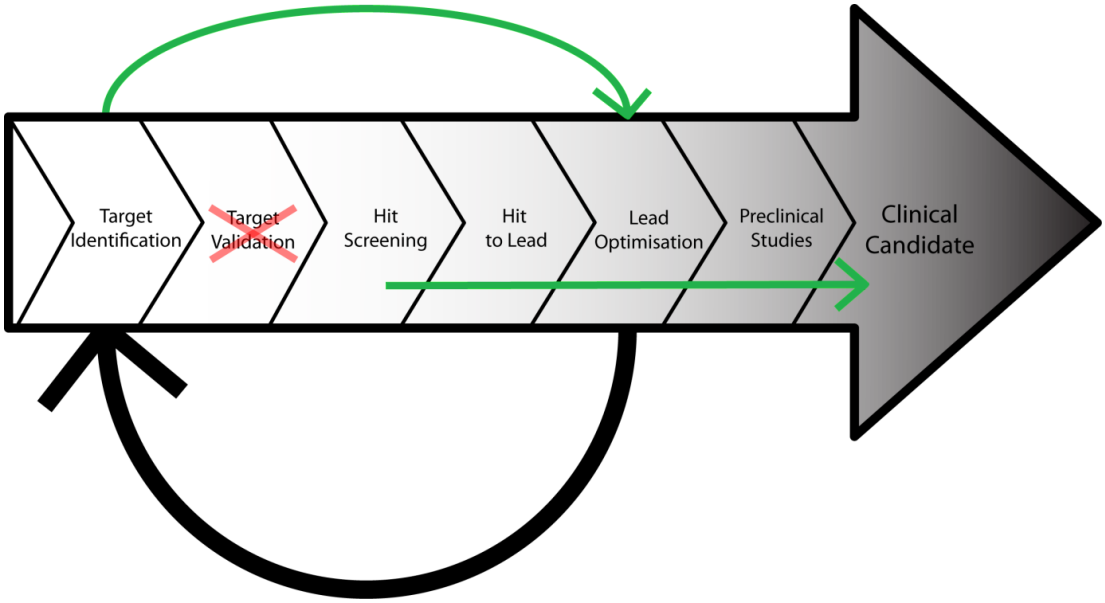

Figure 1.3: *Adapted schematic diagram from figure 1.1 showing the typical phenotypic approach.*

As an extension to the two sided, black or white argument (targeted or phenotypic), John G. Moffat *et Al.* described a more fluid classification on the origins of NMEs.[23] They analysed drugs approved for cancer treatment between 1999 and 2013 and categorised them according to a 'matrix system', table 1.1.

It is clear from the data that the majority of drugs were discovered solely via a targeted approach where both the initial hit and further development was based upon on-target potency alone. Interestingly, most of these drugs (21 out of 29) were kinase inhibitors. The well-established ATP assays available for determining kinase inhibition and their ease of expression in bacterial systems along with the ability to create X-ray crystal structures attribute to this high number.

		Lead Discovery		
Lead Optimisation		**Target Inhibition Only Screen**	**Mechanism Informed Phenotypic Screen**	**Unbiased Phenotypic Screen**
	Inhibition of Known Target	29	4	3
	Mechanism Informed Phenotypic Assay	2	2	3*
	Unbiased Phenotypic Assay	0	1	4

Table 1.1: *Origins of cancer drugs approved between 1999 and 2013 by Moffat et al.[23] *Compounds discussed in this thesis belong to this category.*

This study, most importantly, included an 'in-between' category which Moffat *et al.* have termed *'mechanism-informed phenotypic drug discovery (MIPDD)'*.[23] This category comprises drugs that have either been initially discovered or optimised by a phenotypic screen but the main target(s) of the compounds are known. Knowing the target involved allows further development of novel compounds with both well-defined molecular mechanisms of action and proven phenotypic properties, at least *in vitro*.

The compounds discussed in this thesis belong to the MIPDD category because the core structure is derived from a known promiscuous kinase inhibitor (PP1) and, therefore, any phenotypic hit should be expected to target one or more proteins of the human kinome. However, apart from their biased starting design, the initial hits were discovered solely through a phenotypic screen with no regard to the target involved. Thus, they belong to a further novel category halfway in between MIPDD and unbiased phenotypic screen: discovered by an unbiased phenotypic screen but subsequently optimised by mechanism informed phenotypic assays and target selectivity profiling, based on the original chemical design.

1. Introduction

1.3 Pyrazolopyrimidines as Kinase Inhibitors

Pyrazolopyrimidines are the fused heterocyclic system comprising a 5-membered pyrazole moiety joined to a 6-membered pyrimidine, figure 1.4. Different orientations of the rings leads to different isomers, however, this chapter only focuses on pyrazolo[3,4-d]pyrimindines as the drugs described later contain only this isomer.

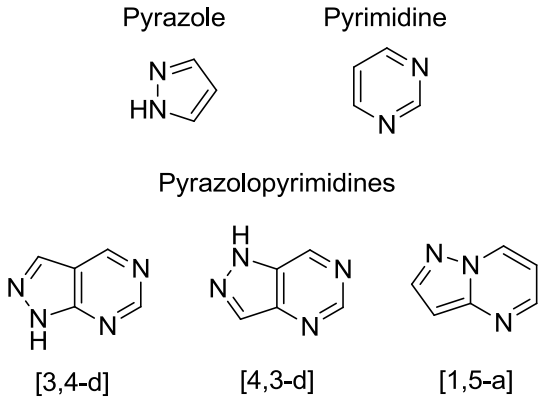

Figure 1.4: *Structures of the different isomers of pyrazolopyrimidines*.

The first reported compound containing the pyrazolo[3,4-d]pyrimidine system was in 1938 by Justoni and Fusco.[24] They synthesised the compound 6-methyl-1,3-diphenyl-pyrazolo[3,4-d]pyrimidin-4-ol from 5-acetamido-1,3-diphenyl-pyrazole-4-carboxamide as shown in figure 1.5.

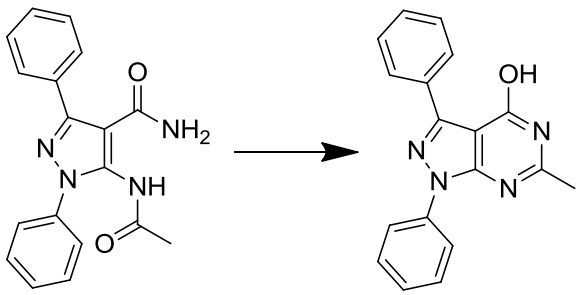

Figure 1.5: *Structure of the first reported compound containing the pyrazolo[3,4-d]pyrimidine scaffold.*

Commonly reported pyrazolopyrimidines are substituted pyrazolo[3,4-d]pyrimidin-4-amine compounds. The similarity of this group to the purines, most importantly to adenine, allows the development of compounds which show similar properties to the natural nucleobases etc. and indeed some of the earliest pyrazolopyrimidines were shown to be adenosine receptor antagonists.[25-27] As early as the 1980s, pyrazolopyrimidines were being substituted for adenine in ribonucleosides in order to mimic adenosine and create synthetic drugs.[28] Cottam *et Al*. synthesised 3,4-disubstituted pyrazolo[3,4-d]pyrimidine ribonucleosides in order to treat parasitic infections. The unique metabolic pathways of the parasites allowed the incorporation of the synthetic ribonucleosides into RNA, whereas, this process did not occur in mammals.

1.3.1 Pyrazolopyrimidines as Kinase Inhibitors

Kinases are an important class of enzyme contained within cells. Kinases, by definition, are enzymes which use adenosine triphosphate (ATP) to transfer phosphate groups to other molecules, thereby, phosphorylating them. These phosphorylation sites of proteins, and other cellular substrates such as lipids and carbohydrates, act as on/off switches governing enzyme activity or protein-protein interactions and the presence or absence of a phosphate group on a key site (amino acids such as tyrosine, serine, threonine or histidine may be phosphorylated in proteins) determines the function and activity within cells. Kinases are, therefore, highly involved in the signalling networks that exist within cells. Kinases not only control basic pathways within and across cells but they also contribute to the dynamic signalling that exists between cells and the extracellular matrix (ECM) by regulating the functions of adhesion complexes and transmitting signals from extracellular ligands. This influences the dynamics of the cell and controls cellular movement and overall tissue physiology. Due to their important role in cell functions, unnaturally high or low levels of kinase expression can lead to a variety of diseases including cancer and inflammation of various tissues.[29]

The high importance of kinases within cells has prompted a search for tools in order to study their function or even control their activity. One of the earliest reported cases of synthetic pyrazolopyrimidine kinase inhibitors was by Cottam *et. Al.* in 1993.[30] They synthesised pyrazolo[3,4-d]pyrimidine analogues of 5-iodotubercidin, shown in figure 1.6, as inhibitors of adenosine kinase.

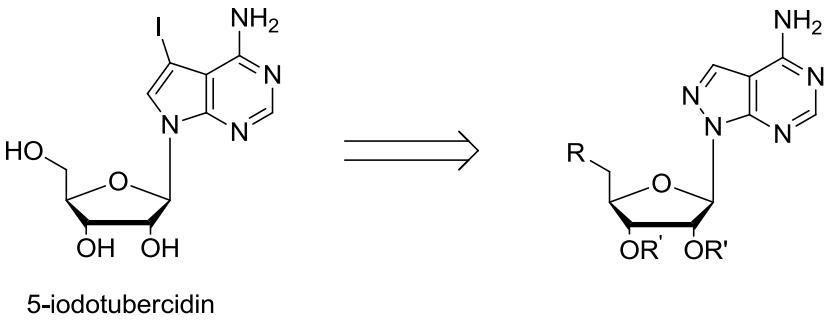

Figure 1.6: *Pyrazolo[3,4-d]pyrimidine analogues of 5-iodotubercidin synthesised by Cottam et Al. for use as adenosine inhibitors.*

The first clinically approved kinase inhibitor for cancer was Imatinib in May 2001. In terms of medicinal chemistry this is relatively recent and so kinase inhibition for cancer therapy remains a fresh and exciting area of drug discovery. Currently, the only pyrazolopyrimidine kinase inhibitor approved by the FDA is Ibrutinib which was approved in November 2013 for the treatment of mantle cell lymphoma.

1.3.2 Pyrazolo[3,4-d]pyrimidines as SRC Family Kinase Inhibitors

SRC is short for 'sarcoma'. Cellular-SRC (c-SRC) and the constitutively active avian viral form (v-SRC) are two of the oldest oncogenes reported.[31] SRC is, therefore, one of the most studied and familiar human proto-oncogenes.[32] The SRC family of proteins are non-receptor tyrosine kinases and contain the following members: BLK, FGR, FRK, FYN, HCK, LCK, LYN, YES and c-SRC. These proteins are all structurally similar and so inhibition of one usually results in some off-target binding to the other members. Due to increasing examples of acquired drug resistance in patients, however, multi-targeted kinase inhibitors are often sought after. SRC has been shown to be involved in many cellular pathways and is responsible for a variety of cell phenotypes including adhesion, migration and invasion, proliferation, angiogenesis and metastasis.[32]

The earliest reported SRC family inhibitors were the pyrazolo[3,4-d]pyrimidines, PP1 and PP2, figure 1.7.[33] Synthesised in 1996 by J. H. Hanke *et Al.*, PP1 and PP2 were designed to be inhibitors of LCK and FYN. IC_{50} values of 5 and 6 nM against LCK and FYN, respectively, were reported for PP1 and values of 4 and 5 nM for PP2.[33] Although, these compounds are still both widely used as biological tools for studying SRC family kinases (SFKs), neither of them have made it into clinical studies. Recent studies have also shown

PP1 and PP2 to be non-selective towards the SRC family which further limits their usefulness.

One of the earliest reported specific SRC inhibitors is 1-naphthyl-PP1 (1-NA-PP1), very similar to PP1. Designed in 1998, by Anthony C. Bishop *et. Al.*, 1-NA-PP1 selectively inhibits a mutant form of v-SRC (Ile338Gly v-Src) over wild-type SRC, however, 1-NA-PP1 is still non-selective to other kinases.[34]

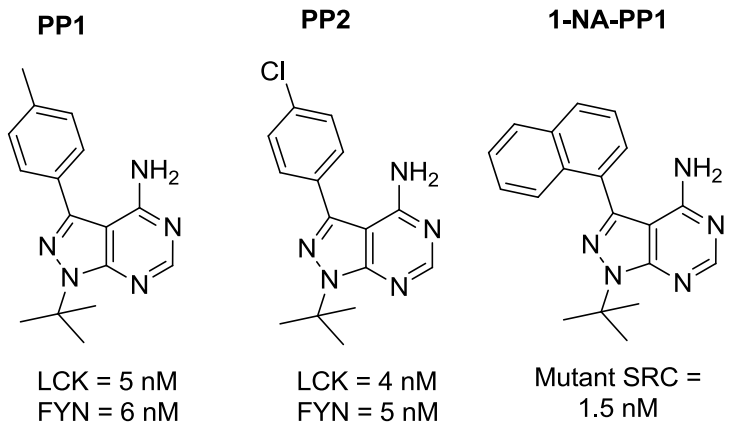

Figure 1.7: *Structure of SFK inhibitors PP1, PP2 and 1-NA-PP1.*

1. Introduction

1.4 The Mechanistic Target of Rapamycin

The mechanistic target of rapamycin (mTOR), also known as the mammalian target of rapamycin, is a key serine/threonine protein kinase with roles in many cellular mechanisms and pathways such as protein synthesis, cell cycle, survival, proliferation and even migration/invasion.[35] Consequently, mTOR is highly involved in cancer, metabolic diseases such as obesity and type-2 diabetes, neurodegenerative diseases and even aging.[36] mTOR belongs to the phosphatidylinositol 3-kinase (PI3K)-related family and shares many pathways with the PI3Ks. Their interaction in pathways is critical to mTOR's function.

mTOR exists as part of a complex of proteins in which there are two forms – mTOR complex 1 (mTORC1) and mTOR complex 2 (mTORC2). mTORC1 and 2 behave differently in cells and also function as separate multi-protein complexes.[36]

1.4.1 mTORC1

mTORC1 consists of 5 proteins: mTOR, Raptor (regulatory associated protein of mTOR), mLST8 (mammalian lethal with Sec13 protein 8, aka GβL), PRAS40 (proline rich AKT substrate 40 kDa) and Deptor (DEP-domain-containing mTOR-interacting protein).[37] Of these proteins, mTOR is the main component containing the catalytically active site; little is known about the function of the other 4 proteins, although many experiments suggest they may function as regulators of mTOR kinase activity.[37]

The functions of mTORC1 are much better defined than those of mTORC2 and many of these discoveries can be credited to the fact that one of the first discovered inhibitors of mTOR, Rapamycin (a macrolide isolated from the bacterium *Streptomyces hygroscopicus*), inhibits mTORC1 but not mTORC2, in general. Rapamycin binds to the FK506-binding protein of 12 kDa (FKBP12) which then binds to the FKB12-rapamycin binding domain (FRB) of mTOR.[38] This inhibits mTORC1, however, FKBP12 and rapamycin cannot inhibit mTORC2.[39, 40]

mTORC1 has been termed "a master regulator of cell growth and metabolism" as it is involved in many pathways and interacts with many different proteins concerning cell

growth and cell cycle.[37] The synthesis of proteins and lipids within the cell are all controlled by mTOR which is highly sensitive to nutrients such as glucose and amino acids and also to hormones such as insulin and growth factors. By far the most important aspect of mTORC1 is the control of protein synthesis. Downstream of mTORC1 is the eukaryotic initiation factor 4E (eIF4E) binding protein 1 (4E-BP1) and the p70 ribosomal S6 kinase 1 (S6K1) which are phosphorylated by mTORC1 to initiate protein synthesis. Phosphorylated 4E-BP1 cannot bind to its partner, eIF4E, which enables eIF4E promotion of cap-dependent translation.[41] Phosphorylation of S6K1 leads to cap-dependent translocation, translation elongation, mRNA biogenesis and ribosome biogenesis via the proteins eIF4B, PDCD4, eEF2K, SKAR and S6, respectively, figure 1.8.[42]

mTORC1 has also been shown to control autophagy, whereby, mTOR inhibition increases autophagy and mTOR stimulation reduces it.[43] These mechanisms are less well known compared to the protein synthesis pathways, however, interaction with a complex of unc-51-like kinase 1 (ULK1), autophagy-related gene 13 (ATG13) and focal adhesion kinase family-interacting protein of 200 kDa (FIP200) has been shown to regulate autophagy.[44-46]

Lipid synthesis is also controlled by mTORC1 through the regulation of sterol regulatory element binding protein 1 (SREBP1) and peroxisome proliferator-activated receptor-γ (PPAR-γ), although, again, this mechanism is not entirely clear.[37, 47, 48]

Many factors contribute to the activity of mTORC1 including: ATP (energy) levels which are regulated via AMP-activated protein kinase (AMPK); oxygen levels via multiple pathways; various growth factors, such as insulin, via Ras and the canonical insulin pathway; amino acid levels via the Rag proteins; DNA stress via p53/AMPK regulated mechanisms; and inflammation via the TSC1/2 complex.[37, 38, 49-54] All these interactions are mapped in figure 1.8.

1.4.2 mTORC2

mTORC2 consists of 6 members: mTOR, Rictor (Rapamycin insensitive companion of mTOR), mSIN1 (mammalian stress activated protein kinase interacting protein, Protor-1 (protein observed with Rictor-1), mLST8 and Deptor. Many of these proteins were discovered via experimental evidence and are, thus, named arbitrarily. mTOR, mLST8 and Deptor are shared between both mTOR complexes and are thought to have similar functions.[37]

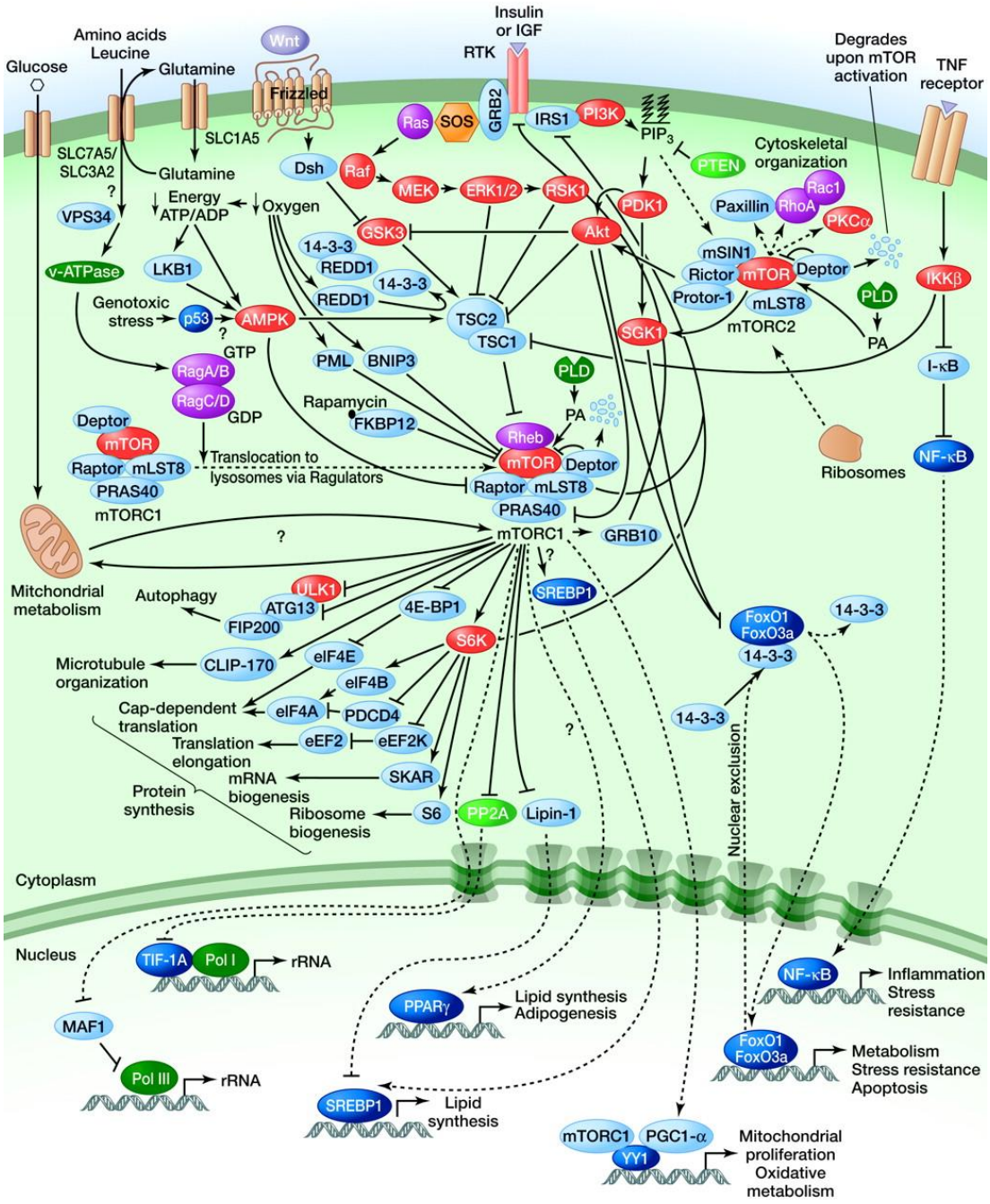

Figure 1.8: *mTOR signalling pathway. Reprinted with permission from Cold Spring Harbor Laboratory Press (2012).[53]*

Unlike mTORC1, little is known about the functions of mTORC2 or it may, simply, not play as significant a role as mTORC1. mTORC2 is not sensitive to nutrients, as mTORC1 is, but it is sensitive to some growth factors such as insulin.[36] mTORC2 is generally reported to be insensitive to Rapamycin treatment, and from a broad perspective this is mostly the case.

However, long term treatment with Rapamycin has been shown to reduce the signalling of mTORC2 in certain cell types.[40, 55]

mTORC2 has been shown to be involved in cell survival and growth through its interaction with AKT.[56] AKT is another serine/threonine kinase that is highly involved in many important pathways associated with cell metabolism, proliferation, migration, apoptosis and protein synthesis, thus, mTORC2 is also indirectly involved in these processes.[57] It has also been shown that mTORC2 is involved in regulation of the actin cytoskeleton through interaction with proteins Paxillin, RhoA, Rac1 and PKCα.[39, 40]

1.4.3 The Role of mTOR in Cancer

Since there are many examples of the importance of mTOR in cancer described in the literature, and being a 'master regulator' of cell growth, it is not surprising that faults associated with the mTOR pathway can eventually lead to cancer. Mutations of proteins upstream of mTOR such as the PI3Ks are common in many human cancers.[36] In fact, data shows that changes in expression levels of the PI3Ks, AKT and PTEN are the most common alterations found in cancers, all proteins associated with mTOR.[58] PI3K, PTEN and AKT are all upstream of mTOR (AKT is downstream of mTORC2) and so mutations in these proteins directly affect the function of mTOR, figure 1.8. 4E-BP1, downstream of mTORC1, has also been increasingly thought to be involved in cancer formation. Reduction in 4E-BP1 activity leads to the activation of cap-dependent translation which promotes cell proliferation and progression of the cell cycle.[36, 59, 60]

As mentioned previously, mTOR also controls lipid synthesis via sterol regulatory element binding protein 1 (SREBP1). An increase in lipid biosynthesis is one of the classical hallmarks of cancer as rapidly dividing cells require lipids for cell membrane production. An increase in PI3K signalling to mTORC1 results in activation of SREBP1 which causes an increase of lipid biosynthesis via the transcription target fatty acid synthase (FAS) and promotes the proliferation of cancer cells.[36, 59, 61]

Further, mTOR may have a part to play in tumour growth through involvement in autophagy. Increased activation of mTOR by mutations in upstream proteins suppress autophagy and may promote cancer growth, although, again, this mechanism is not entirely clear and the full effect autophagy plays in cancer is yet to be known.[36, 59] Additionally,

mTOR is able to promote angiogenesis through its interaction with hypoxia-inducible factor 1α (HIF1α), thereby, allowing the tumour access to fresh nutrients and oxygen.[62]

Most of the pathways discussed above feature mTORC1, however, there are increasing indications that mTORC2 also plays an important part in cancer formation and growth. AKT and SGK1 are downstream targets of mTORC2 and so, through activation, they may promote tumour growth. Also, loss of PTEN, commonly observed in a variety of cancers, promotes AKT signalling resulting in increased cell proliferation and survival.[63] Further, the mTORC2 component RICTOR is required for the growth of certain cell lines derived from PTEN deficient mice, thereby, cementing the importance of mTORC2 in cancer.[63, 64] Thus, through its interaction with AKT, PI3Ks and PTEN, mTORC2 is highly involved in cancer, arguably more so than mTORC1.

1.4.4 mTOR Inhibitors - Rapalogs

Due to the evidence led involvement of mTOR with cancer, targeting the pathway has been of great interest. Targeting mTOR for cancer treatment is relatively recent, however, with the first inhibitor being approved by the FDA in 2007. Rapamycin, also known as Sirolimus, was previously approved in 1999 for organ transplant rejection due to its observed immunosuppressant properties.

mTOR is an unusual kinase target as Rapamycin is a natural product whose phenotypic properties were discovered before any knowledge of the mTOR kinase existed and, thus, led to the discovery of the functions of mTOR itself. With a natural inhibitor already at hand, the first tested, and approved, inhibitors of mTOR for cancer treatment were analogs of Rapamycin, collectively named Rapalogs. The first approved inhibitor of mTOR for cancer treatment was Temsirolimus, approved for treatment against advanced renal cell carcinoma. Everolimus, approved in 2009 for advanced kidney cancer, and Ridaforolimus, currently unapproved but in clinical trials, soon followed suite. Their structures, as well as the structure of Rapamycin, are shown in figure 1.9.

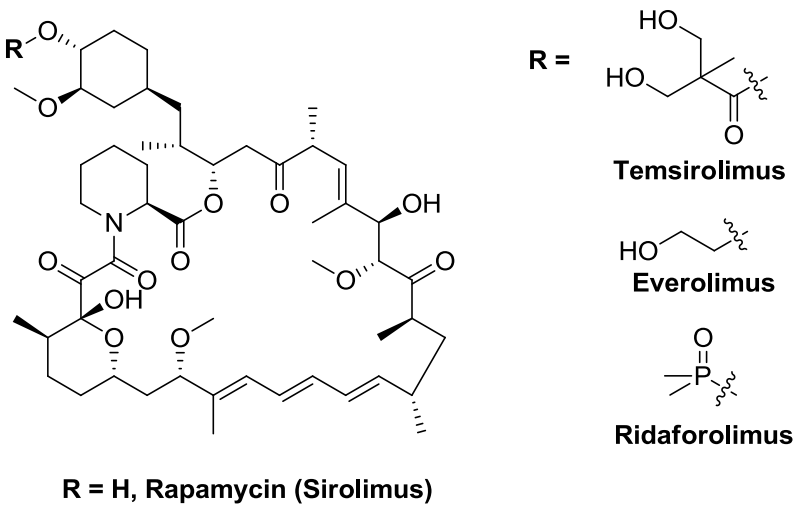

Figure 1.9: *Chemical Structure of Rapamycin (left, R = H), Temsirolmius, the first approved mTOR inhibitor for cancer therapy, Everolimus and Ridaforolimus (right).*

These rapalogs work in the same way as Rapamycin. Their modifications are mostly for improving pharmacokinetic properties. For example, the modification of Temsirolimus is to increase water solubility so it can be given by intravenous injection. Afterwards, it is converted into Rapamycin in the body which is responsible for most of its effect; therefore, it is essentially a prodrug of Rapamycin.[65] Likewise with Everolimus, however, Ridaforolimus (Deforolimus), which contains a dimethyl phosphine oxide group, is not a prodrug. The mechanisms of rapalogs are the same as Rapamycin: binding to FKBP12 prior to interaction with the FRB domain of mTOR.

Currently, Temsirolimus and Everolimus are the only two rapalogs approved for use in cancer treatment. Rapamycin, which is given orally, has a very low bioavailability limiting its usefulness in therapy.[65] Everolimus was designed to have higher bioavailability, given orally, and both Rapamycin and Everolimus are used as immunosuppressants in organ transplant patients. Temsirolimus and Ridaforolimus are both given intravenously for cancer treatment, although Ridaforolimus has yet to be approved by the FDA.

Although Rapalogs have shown promise in the lab and some success in the clinic, only moderate efficacy has been observed in a lot of tumours. This disappointing realisation has been attributed to a variety of reasons. Previous work had suggested that sensitivity to Rapalogs could be correlated with loss of PTEN.[66] However, in the clinic this was not the case and biomarkers which suggest sensitivity to rapalog treatment remain unknown.[36] mTOR, being such an important regulator of cell metabolism and growth, is linked to many

complex pathways and negative feedback mechanisms may limit the efficacy of rapalogs in a clinical setting, especially since only one of the mTOR complexes is being inhibited.

Recently, it has been discovered that the phosphorylation of 4E-BP1, downstream of mTORC1, is only partially blocked by Rapamycin treatment.[36] Due to the high involvement of 4E-BP1 in cancer progression this may explain why treatment with Rapalogs has failed to show the expected effects in the clinic. Further, mTORC2 cannot be ignored. Although, little is known about the functions of this complex, its involvement in cancer progression is apparent and by only inhibiting one of two mTOR complexes it is reasonable to see why rapalog treatment failed to hold up to the early promising results. Most importantly, Rapamycin is able to activate AKT via feedback mechanisms associated with insulin growth factors (IGFs) and mTOR/S6K inhibition.[67]

More recently, focus has been on developing ATP site inhibitors of mTOR. These inhibitors do not discriminate against mTORC1 or mTORC2 and inhibit both equally with the rationale being of overcoming the feedback mechanisms and partial inhibition of downstream targets seen with the rapalogs.

1.4.5 mTOR Inhibitors – ATP Competitive

ATP competitive inhibitors of mTOR, sometimes called second generation mTOR inhibitors, are dual inhibitors of mTORC1 and mTORC2 due to their interaction with the active site of mTOR directly. By inhibiting both complexes, the phosphorylation of all downstream targets of mTOR is reduced resulting in less negative feedback and greater effect over cell growth. In practice, these dual inhibitors have resulted in the reduced cell proliferation and greater potency in *in vivo* models, more extensively, than treatment with rapalogs.[36] By completely inhibiting the phosphorylation of downstream targets such as 4E-BP1, cap dependant translation is greatly reduced and cell growth is impaired to a much higher degree than Rapamycin treatment. Further, many transcription events are only affected with complete inhibition of mTOR and not by partial inhibition.[68] By blocking not only mTORC1 but also mTORC2, the phosphorylation of AKT and SGK1 is reduced resulting in impaired cell growth. mTORC2 inhibition also has the added benefit of reducing feedback mechanisms associated with only blocking mTORC1. mTORC2 has also been shown to be involved in angiogenesis and so, through inhibition, tumour formation may be reduced by blocking the formation of vascular systems.[69]

Many of these 2nd generation inhibitors target both mTOR and the PI3K enzymes as their kinase domains are closely related, and so, are known as dual mTOR/PI3K inhibitors.[70] Shown in figure 1.10 are the structures of some 2nd generation mTOR inhibitors. PI103 was the first potent and synthetic ATP site inhibitor of mTOR and many compounds are based around its structure, however, poor pharmacokinetic properties prevented its use in humans. The compounds AZD8055/2014, PI540, PI620, PKI402 and WAY132/354/600/687, shown in figure 1.10, all have their structures based around PI103.

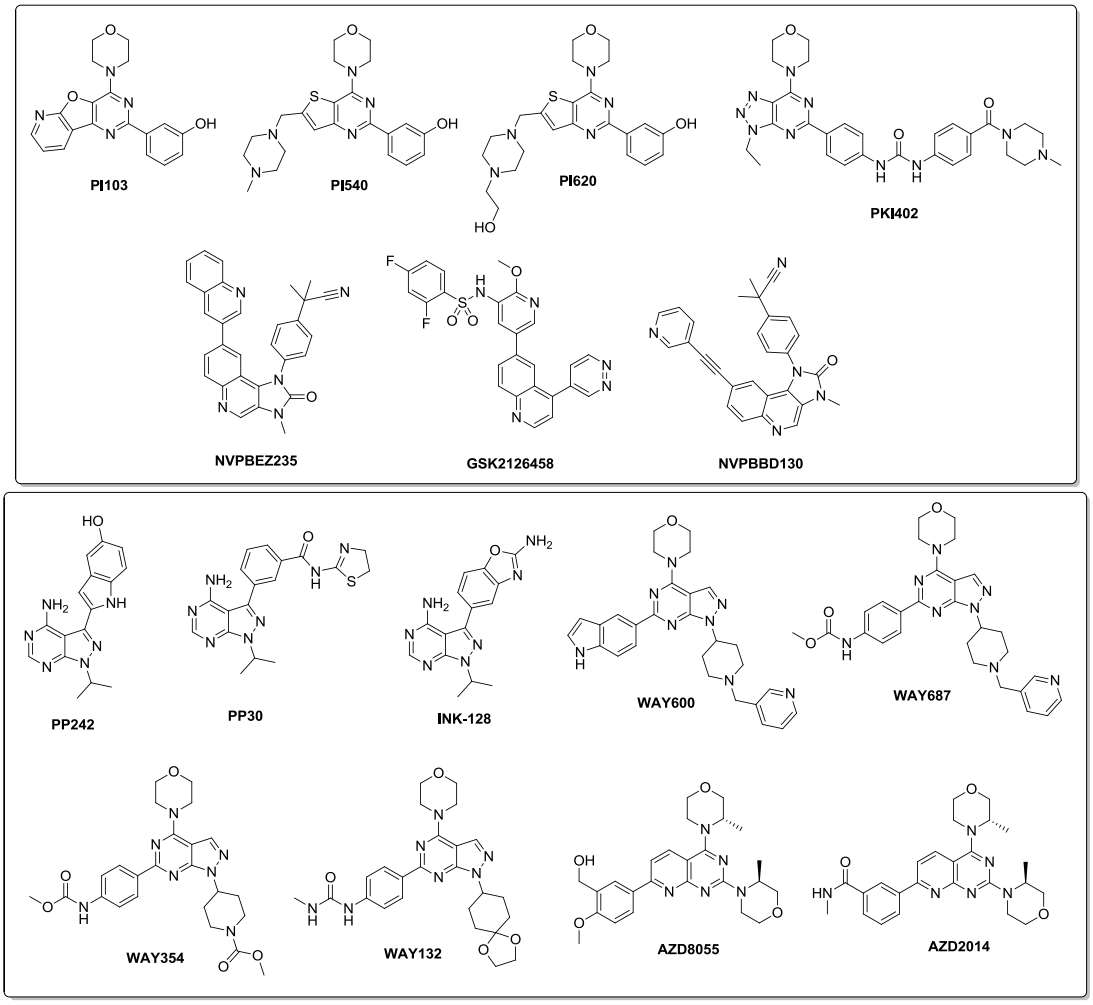

Figure 1.10: *Chemical structures of 2nd generation mTOR inhibitors targeting the ATP site. Compounds in the top box represent dual mTOR/PI3K inhibitors while compounds in the bottom box represent dual mTOR inhibitors (mTORC1/2).*

Many of the compounds shown in figure 1.10 are in clinical trials as anti-cancer drugs, however, as of now there are no 2nd generation mTOR inhibitors approved by the FDA. Many of the early dual mTOR/PI3K inhibitors shared similar structures involving 4-

morpholinylpyrimidine ring systems, whereas, the mTORC1/2 inhibitors mostly feature the pyrazolopyrimidine scaffold. With so many 2nd generation mTOR inhibitors currently in clinical trials the success of one over another may depend on other properties than mTOR inhibition such as PK properties or off-target induced toxicity.

mTOR inhibitors show great promise in cancer therapy and results in preclinical settings look promising, however, their success may be limited by a lack of sufficient biomarkers indicating patients which would benefit from therapy. Another area of concern with mTOR inhibition is the effect on the immune system. Suppression of the immune system is not something to be encouraged during chemotherapy and should be examined carefully, especially since most *in vivo* models involve immunodeficient mice.

Further, mTOR's involvement with cell metabolism should be noted as, although mTOR is upregulated in a majority of cancers, it is also found all over the body and heavy inhibition may have adverse side effects on patients. Only long term studies will tell, however, in terms of cancer therapy, these side effects may be a light penalty to pay for successful treatment.

1. Introduction

1.5 SRC

SRC is the first, and perhaps most studied, known oncogene. However, we still do not know everything about its mechanisms or its full involvement in the development of cancer. SRC was discovered over 100 years ago by Peyton Rous when he described an agent that could cause cancer in chickens. This 'agent' turned out to be a virus, now named the Rous Sarcoma Virus, and advances in molecular biology in the 1960s and 70s enabled the identification of the viral oncogene responsible for tumour transformation seen in chickens by Rous – v-SRC. Bishop and Varmus later found a proto-oncogene in cells which corresponded to the viral oncogene, v-SRC, and appropriately named it c-SRC.[32, 71] They were later rewarded with the Nobel Prize for their work in proto-oncogenes.

c-SRC encodes a non-receptor tyrosine kinase which belongs to a family of 8 kinases – BLK, FGR, FYN, HCK, LCK, LYN, SRC and YES. There are a few related 'sub-family' members such as BRK/PTK6, FRK/PTK5 and YRK.[72, 73] However, c-SRC is the one most commonly associated with cancer and, consequently, the most studied of all the members.

Resistance is a commonly observed, and troublesome, feature in cancer treatment. Therapy involving cytotoxic agents such as gemcitabine, oxaliplatin and cetuximab has led to acquired resistance involving disrupted SRC signalling.[32] As such, SRC may represent a common resistance mechanism and, thus, inhibition of SRC may re-sensitise cancers towards treatment. This creates the opportunity for combination therapies whereby SRC inhibition is combined with the drugs to which tumours have developed resistance, to provide an alternative line of therapy for patients.

The strong correlation between SRC activity and cancer progression supports the premise that SRC signifies an important target for cancer treatment. And several compounds have entered clinical trials for the treatment of various solid tumours by SRC inhibition.

1.5.1 The Structure and Function of SRC

The SRC family members all have conserved SRC homology (SH) domains and a regulatory tyrosine residue (Tyr530) at the C-terminus, figure 1.11.[32] The four SH domains are conserved across species and also in v-SRC, figure 1a, however, the C-terminal region differs. In particular, Rous Sarcoma Virus SRC (v-SRC) lacks the regulatory C-terminal domain, leading to constitutive activity and oncogenic transformation.[72] Human and chicken c-SRC, however, both possess this regulatory domain that maintains the enzyme in a constitutively inactive conformation until upstream activation. The kinase domain is found in SH1, as is a conserved tyrosine autophosphorylation site – Y419 in human and Y416 in chicken.

SRC is activated by dephosphorylation of Y530 resulting in opening of the complex and consequent access to the kinase domain, figure 1.11b. Further, autophosphorylation of Y419 in the kinase domain (Y416 in chicken) is required for full activity of SRC. Deactivation occurs via phosphorylation of Y530 which allows binding to the SH2 domain, locking the complex in a closed conformation. C-terminal SRC kinase (CSK) phosphorylates this region, thus, inactivating SRC. Certain cancers have reduced levels of CSK which leads to higher SRC activation.[74]

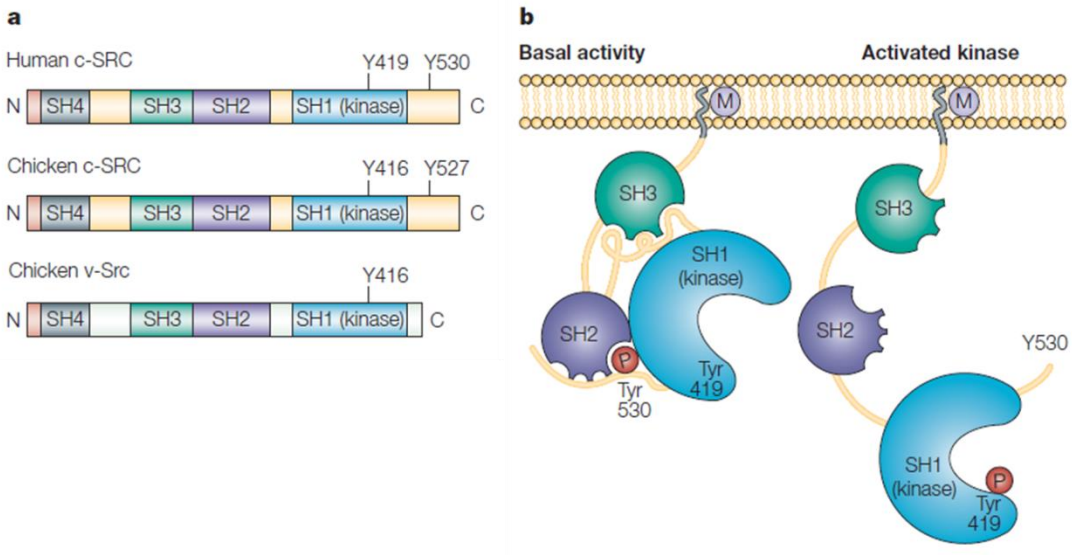

Figure 1.11: *a) Structure of human and chicken c-SRC, and chicken v-SRC showing the conserved SRC homology regions. b) Method of SRC activation/inactivation. Inactivation of SRC occurs via phosphorylation of Tyr530 which results in a closed complex with restricted access to the kinase domain. Reprinted by permission from Macmillan Publishers Ltd: [Nature Reviews] [72], copyright (2004).*

There are many other methods of SRC activation. Activation via receptor tyrosine kinases such as EGFR, PDGFR, ERBB2, fibroblast growth factor receptor, colony-stimulating factor 1 and hepatocyte growth factors represent a few.[72]

One of the major interacting proteins which binds to SRC is focal adhesion kinase (FAK) which has an important role in cell migration/invasion.[75] FAK binds to the SH2 and SH3 domains of SRC, thus, resulting in the open, active conformation. CRK-associated substrate (CAS) also binds similarly, and both FAK and CAS are key regulators of the focal adhesion complex and actin, which are essential for cell movement.[76]

1.5.2 SRC and Cancer

SRC has been shown to be important in driving certain cancers, and given that it is one of the most studied proto-oncogenes, there is considerable evidence of its role in tumour progression. The classical 'Hallmarks of Cancer' include: increased cell proliferation, ignorance of growth suppressor signals, increased cell migration and invasion, infinite replication, induction of angiogenesis and the resistance of apoptosis.[77] SRC is involved in all of these processes.[32, 72]

Increased Cell Proliferation

Evidence exists showing SRC is involved in the cell cycle to some extent, primarily the G_2 to M phase transition.[78] However, targets downstream of SRC may be more involved in control of the cell cycle rather than SRC itself.

Cell Migration and Invasion

SRC is more involved with cell-cell and cell-ECM adhesion dynamics than cell growth and so, increased activation of SRC in cancer is associated with increased cell migration and invasion leading to metastasis in the patient.[79] When activated, SRC translocates to areas of the cell membrane where the cytoskeleton is associated and interacts with the adherens junctions and focal adhesions.[80] Adherens junctions, which bind cells to cells, and focal adhesions, which bind cells to the extracellular matrix, are in a dynamic state of assembly and disassembly enabling natural cell movement, and transmission of extracellularly derived growth signals. SRC is involved in the regulation of the assembly of these components.[72]

Adherens junctions involve the binding of E-cadherin moieties located on the extracellular membranes of cells. SRC is highly involved in the complex array of proteins required to

regulate this process and increased SRC activation results in decreased E-cadherin expression.[81, 82] In turn, this leads to loss of cell-cell binding and an increase in tumour metastasis.

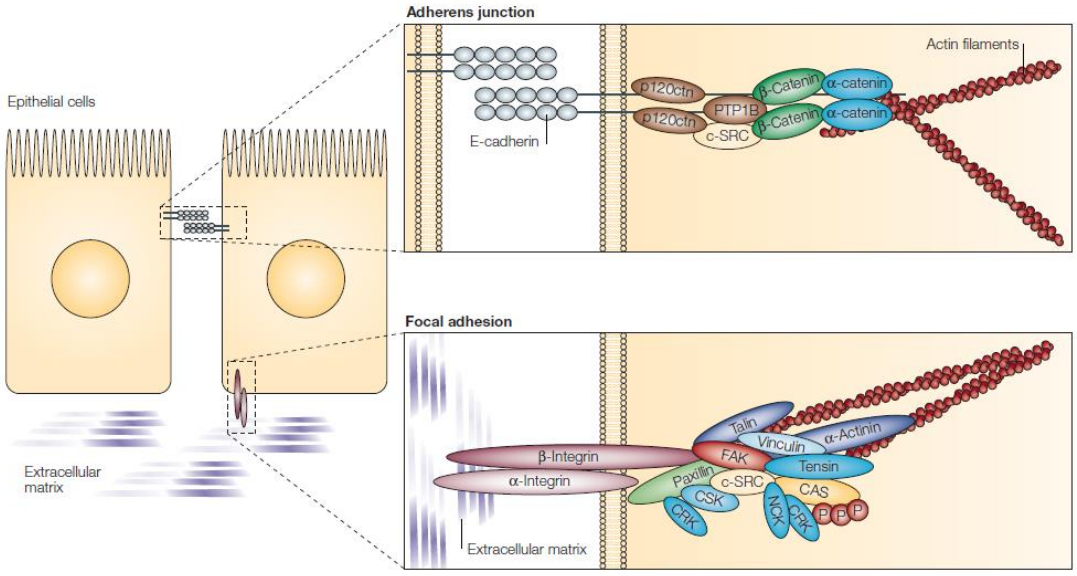

Figure 1.12: *The function of SRC in adherens junctions and focal adhesion. Reprinted by permission from Macmillan Publishers Ltd: [Nature Reviews] [72], copyright (2004).*

Similarly, SRC is involved in the mass complex of proteins involved in focal adhesion, ultimately, through integrin binding to the extracellular matrix. FAK is highly involved in this process through its interaction with SRC and together they interact with a multitude of proteins involved in focal adhesion turnover and actin remodelling.[83] Focal adhesions are involved in the control of cancer metastasis and their dysregulation results in increased patient death.[84]

Angiogenesis

Angiogenesis is a process required for tumour growth as a consequence of the need for more nutrients and oxygen. Cancer cells are able to promote angiogenesis to fulfil their energy needs. SRC has been shown to be associated with the increased expression of vascular endothelial growth factor (VEGF) via signal transducer and activator of transcription 3 (STAT3) activation.[85, 86] PP2, a non-selective SRC inhibitor, inhibits the growth of endothelial and vascular smooth muscle cells *in vivo*, thus, reducing angiogenesis.[87] The cellular migration of endothelial cells can also be reduced by SRC inhibition via VEGF.[88]

Bone Metastasis

SRC activity is also involved in bone metastasis, which represents the primary metastatic site for breast cancer and is also a site for lung, prostate and colorectal cancer. Bone remodelling is the process of bone reabsorption by osteoclasts and bone formation by osteoblasts and SRC is a key protein in the regulation of such a process. Bone metastases disrupt this balanced process and cause pain and morbidity to the patient. SRC inhibition decreases bone reabsorption by reducing osteoclast activity.[89] Thus, SRC inhibition can induce net bone formation and prevent the symptoms of bone metastases.[90]

1.5.3 SRC Inhibition

With all the evidence highlighting the role SRC plays in cancer growth and metastasis, it has become an increasingly important drug target. There are currently only three SRC inhibitors approved by the FDA for cancer therapy – Dasatinib, Bosutinib and Ponatinib – however, many are in clinical trials. All three drugs are approved for Imatinib resistant chronic myeloid leukaemia (CML). However, these drugs are considered to owe their clinical success to inhibition of the BCR-ABL fusion protein (genetic abnormality and main proliferation driver of CML) and not to SRC inhibition. Surprisingly though, given that SRC is one of the most studied oncogenes, there are relatively few examples of selective SRC inhibitors and the vast majority also inhibit c-ABL, a target which I and others have found to be have paradoxical roles in cancer.

Two of the earliest SRC inhibitors are the pyrazolo[3,4-d]pyrimidines, PP1 and PP2, figure 1.13.[91] Originally designed as inhibitors of SRC family members LCK and FYN, with IC_{50} values of 5 and 6 nM, PP1, and 4 and 5 nM, PP2, respectively, they are non-selective SRC family kinase inhibitors that are widely used as biological tools but have not made it into the clinic. PP20, figure 1.13, is a relatively recent SRC/ABL inhibitor with sub-nano molar potency. It is also non-selective and, thus, has not made it into the clinic.[92]

Many of these SRC inhibitors, particularly Dasatinib, Saracatinib and Bosutinib, have shown promising preclinical activity towards a number of solid tumours such as prostate, colon breast and lung and have been taken forward for evaluation in clinical trials, however, their preclinical successes have not translated well in the clinic.[32] Most commonly, patients did not respond to treatment, contradictory to preclinical indications.[93] Further, severe toxicity occurred in several patients causing an abrupt end to their trials.[ClinicalTrials.gov]

A reason for their lack of success in solid tumours may be due, again, to the lack of suitable biomarkers to predict patient response to the drugs. Targeted therapies usually benefit from suitable clinical biomarkers that highlight what targets are driving the patients' cancer and, thus, if they are likely to benefit from targeted drug therapy. Even similar cancers in a group of patients may respond differently to the same treatment.

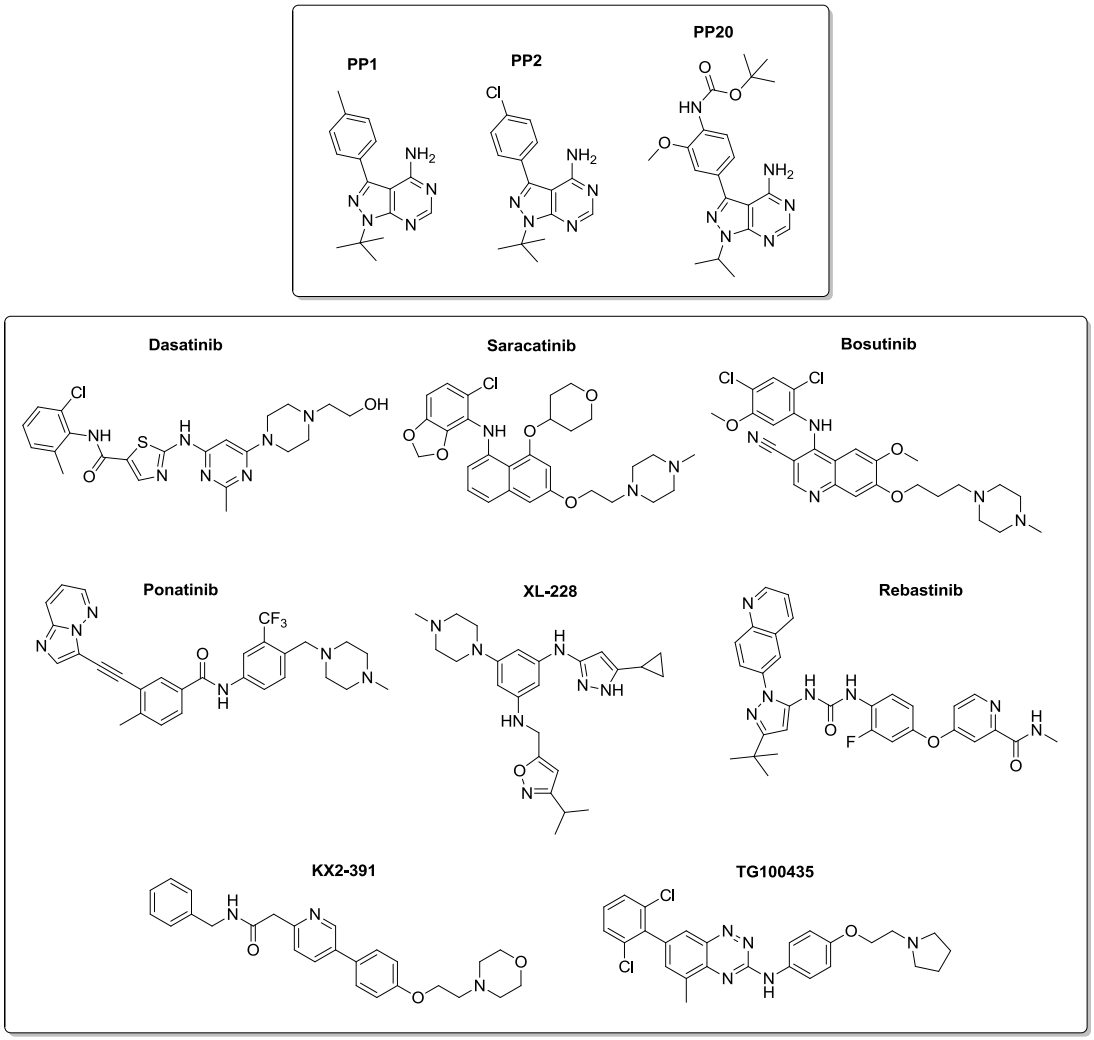

Figure 1.13: *Examples of SRC inhibitors as tools (top) and in clinical development (bottom). Remarkably, all of the inhibitors also potently target Abl. Even KX2-391 which is not an ATP-site inhibitor but a peptide substrate inhibitor inhibits ABL at an IC_{50} of between 60-75 nM.[93]*

1.5.4 SRC Inhibitors in Combination Therapy

Due to the disappointing results in single agent therapy with Dasatinib, Saracatinib and Bosutinib, and the premise that SRC is involved in a multitude of pathways within the cell, many of which drive cancer progression, several trials involving combinations of a SRC inhibitor plus a cytotoxic or targeted drug have taken place.

SRC may be involved in acquired resistance mechanisms against cytotoxic therapies such as gemcitabine and oxaliplatin.[94, 95] Combination studies *in vitro* showed that Dasatinib can increase sensitivity towards oxaliplatin and paclitaxel treatment in ovarian and colon cancer cells.[95, 96] Further, 5-FU and gemcitabine treatment against pancreatic cancer cells was shown to be more effective combined with SRC inhibition.[32] There is also evidence for the combination of a SRC inhibitor with tamoxifen for breast cancer treatment given SRC's ability to promote cell proliferation in association with the estrogen receptor (ER) and commonly seen resistance to tamoxifen therapy.[97] Similarly, combination of Dasatinib or Saracatinib with cetuximab, a monoclonal antibody against epidermal growth factor receptor (EGFR), inhibits colorectal cancer cell growth in a synergistic manner.[98]

According to ClinicalTrials.gov, there have been 255 trials involving Dasatinib, of which, 87 were combination therapies with 28 ongoing as of March 2015. Similarly, Saracatinib and Bosutinib have 30 and 34 trials, respectively, with 8 and 5 being combination therapies. These studies involve several solid tumours such as non-small cell lung cancer (NSCLC), breast, ovarian, colorectal, castration resistance prostate cancer (CRPC) and pancreatic cancer as well as leukaemia. Table 1.2 shows completed combination trials involving Dasatinib.

Overall, Dasatinib performed rather poorly. Many patients experienced severe toxicity or did not benefit from the combination over single agent therapy. However, as discussed, the issue may not be with SRC inhibition but with selecting the correct patients to benefit from such a therapy. Further, all 3 SRC inhibitors approved for use in cancer therapy inhibit ABL with the same potency, a factor which we later show to be non-beneficial or even detrimental in cancer treatment. Incredibly, during SRC's century long journey there has still not been a very potent and selective inhibitor to treat SRC driven tumours.

Combination (+ Dasatinib)	Target	Cancer	Phase	ClinicalTrials.gov Identifier
BMS-833923	SMO	Chronic myeloid leukaemia	1/2	NCT01218477
Revlimid (+Dexamethasone)	Broad MOA	Multiple myeloma	1	NCT00560391
Ixabepilone	Microtubule stabiliser	Metastatic breast cancer	1/2	NCT00924352
Daunorubicin, Cytarabine	DNA intercalator, antimetabolite	Acute myeloid leukaemia	2	NCT01238211
Fulvestrant, MK-0646	Estrogen Receptor, IGF-1 receptor	Metastatic hormone receptor-positive, HER2-negative breast cancer	1/2	NCT00903006
Bortezomib (+Dexamethasone)	Proteasome inhibitor	Multiple myeloma	1	NCT00560352
Nilutamide	Androgen receptor	Metastatic castration resistant prostate cancer		NCT00918385
Cetuximab	EGFR	Colorectal cancer	0	NCT00835679
Cediranib Maleate	VEGF	Hormone resistant prostate cancer	2	NCT01260688
Docetaxel	Anti-mitotic agent	Castration resistant prostate cancer	3	NCT00744497
Dacarbazine	DNA alkylating agent	Metastatic melanoma	1/2	NCT00597038
Docetaxel	Anti-mitotic agent	Metastatic hormone refractory prostate cancer	1/2	NCT00439270
Capecitabine	5-FU prodrug, thymidylate synthase inhibitor	Advanced breast cancer	1	NCT00452673

Table 1.2: *Completed clinical trials involving Dasatinib in combination with another agent. SMO: Smoothened receptor; MOA: Mechanism of action; IGF-1: Insulin-like growth factor 1; EGFR: Epidermal growth factor receptor; VEGF: Vascular endothelial growth factor.*

Having such an important, and well-studied, role in cancer pathophysiology, SRC is undoubtedly a relevant target for cancer therapy. Selection of relevant biomarkers will no doubt improve patient selection and increase the success of SRC inhibitors, whether it be single agent or in combination.

2. Research Aims and Rationale

Advances in combinatorial chemistry and high throughput screening have undoubtedly improved the quality of novel compounds on the basis of target potency and target selectivity. However, increasing research and development costs associated with the widespread adoption of high-throughput target directed screening strategies have not translated into increased clinical success rates. High attrition of candidate drugs during the later stages of preclinical and clinical development, and the lack of any significant improvement in the appearance of novel targets to FDA approved drugs, suggest that current drug discovery strategies are sub-optimal.[99, 100] Disappointing results in recent clinical trials with promising targeted agents underline that a major challenge to the development of successful targeted therapies for treating the majority of cancer types is overcoming heterogeneity across patients and inherent or acquired drug resistance.[8, 11, 100] Most drug discovery programs begin with a screening campaign for inhibitors against a single protein target. Subsequent chemical and target selectivity optimisation is typically based upon "on-target" potency. While this approach may be optimal for diseases caused by single-gene defects, it is, however, not appropriately tailored to health disorders with complex mechanisms and genetic heterogeneity such as cancer.[11] This reflects the fact that in most solid tumours, no single molecular event drives continued proliferation and tumour progression, and that redundancy in signalling pathways limits the efficacy of therapies targeting single molecular pathways.[8, 11]

Acknowledging the limitations of target-centric drug discovery, many research groups, including ours, are frontloading the search of robust empirical data to progress anticancer drug development programs away from classical black-and-white anticancer hypotheses. Following that paradigm, we aim to explore whether cooperative ligand-based design and phenotypic screening, complemented with biochemical assays and the use of published data (literature, patents, databases, etc.), could be effectively applied to accelerate the generation of preclinical drug candidates. The study of my thesis is founded on three wide-ranging hypotheses: (i) the use of phenotypic screening in designated models of cancer can be used to generate target-agnostic structure-bioactivity relationships and guide ligand optimisation tailored to particular cancer types/subtypes; (ii) targeting the kinase ATP pocket with compounds derived from promiscuous kinase inhibitors can enable 'rationally-biased' serendipitous discoveries; and (iii) early improvement of drug likeness on promiscuous

ligands can be concurrently used to explore pharmacodynamic diversity. By means of this pragmatic approach to anticancer kinase inhibitor discovery, target deconvolution of identified hits and leads would be largely simplified (= focused kinome screening), thereby, enabling the prompt identification of the molecular targets and anti-targets involved in the observed phenotype.

3. Design and Synthesis of Initial Library

3.1 Introduction & Aims

Protein kinases are integral components of cell-to-cell communication as regulators in signal transduction cascades, thus, governing a wide range of basic cellular functions and coordinating cellular actions. As a result, kinases are directly involved in progressive diseases including cancer and inflammation.[14, 101] The approval of a number of small molecule kinase inhibitors for the treatment of several types of cancer has shown that they can be effective drugs.[14, 101] The vast majority of kinase inhibitors target the kinase ATP site and because all kinases (>500) necessarily possess this catalytic site there is great potential for cross-reactivity. This disadvantage may, however, become a competitive advantage in anti-cancer therapy as such off-target activities may circumvent issues of molecular heterogeneity and resistance mechanisms. Indeed, a number of kinase inhibitors approved as anti-cancer agents display broad selectivity profiles (e.g. Sunitinib, Sorafenib and Dasatanib). However, the target selectivity profiles of such multi-targeting kinase inhibitors were neither selected nor optimised by rational design.

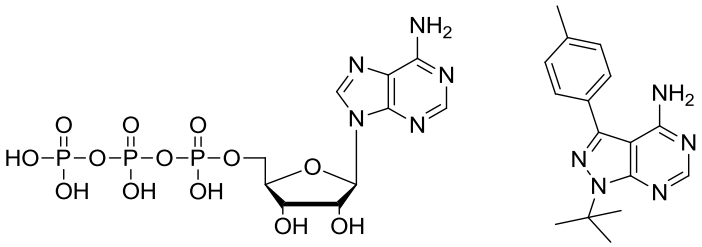

Figure 3.1: *Structure of ATP (left) and PP1 (right).*

To overcome the disadvantages of orthodox target-centric drug discovery strategies and promote a more empirical, evidence led, approach to targeted therapy, we aimed to explore a ligand-based drug design strategy, which frontloads phenotypic analysis in disease-relevant assays. Potency would be calculated across primary phenotypic endpoints from cell based assays (e.g. anti-proliferation, apoptosis, and inhibition of cell migration) and used to rapidly distil compounds according to their degree and type of anticancer activity to inform subsequent chemical design. To take advantage from prospective poly-pharmacological effects provided by small molecule inhibitors targeting the ATP binding site, novel

compounds were designed based on the ATP molecule and the promiscuous kinase inhibitor, **PP1** (4-amino-5-(4-methylphenyl)-7-(t-butyl)pyrazolo[3,4-d]pyrimidine), figure 3.1, a highly potent c-SRC family inhibitor that also targets additional tyrosine kinases such as Ret, c-Kit and Abl.[33, 102-104]

3. Design and Synthesis of Initial Library

3.2 Results

3.2.1 Library 1 Design and Synthesis

The first library of compounds was based on a core aldehyde molecule, figure 3.2, derived from ATP and PP1. A selection of various amines would then enable access to an easily synthesised library via reductive amination.

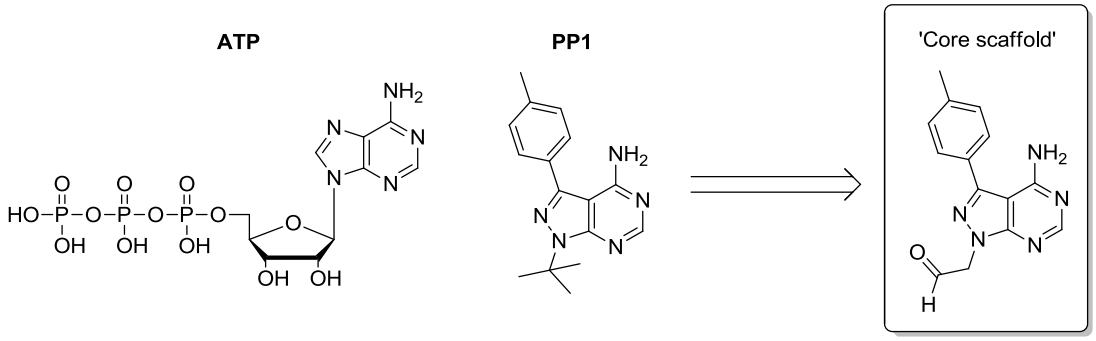

Figure 3.2: *The core aldehyde scaffold derived from ATP and PP1.*

The core aldehyde was synthesised following scheme 3.1. 5-amino-1H-pyrazole-4-carbonitrile (**1**) was heated, under microwave irradiation, in neat formamide giving core heterocycle (**2**) in excellent yield. Selective iodination was facilitated using *N*-iodosuccinimide and alkylation of **3** with bromoacetaldehyde diethyl acetal gave the protected aldehyde intermediate **4**. Suzuki reaction with p-tolylboronic acid gave compound **5** which was then deprotected to give the core aldehyde (**6**) using TFA and water (1:1). The core synthesis was overall high yielding (41.8% over 5 steps) and straightforward. No purification was attempted on compound **6** due to the reactiveness of the aldehyde. Further, compound **6** was not characterised by NMR as multiple adducts of the aldehyde (hemiacetal, geminal diol and the TFA salt) were all visualised in mass spectra resulting in complex and disordered NMR spectra.

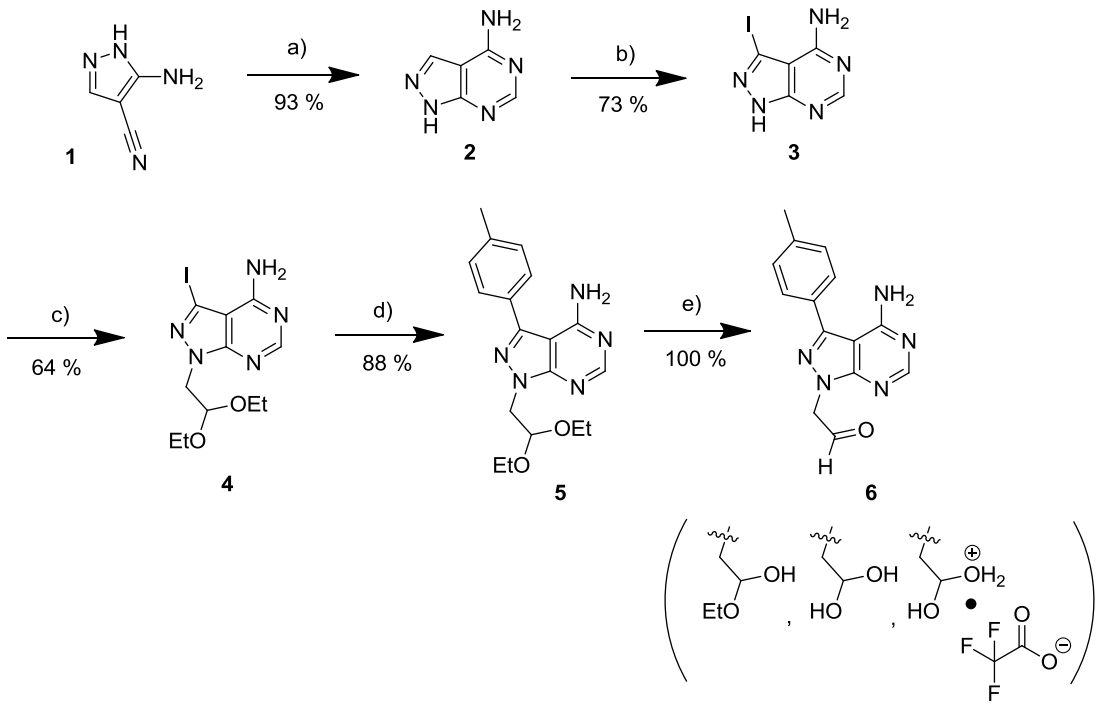

Scheme 3.1: *Core synthesis. a) Formamide, 180 °C, mw; b) NIS, 180 °C, DMF, mw; c) NaH, bromoacetaldehyde diethyl acetal, 150 °C, mw; d) p-tolylboronic acid, K_2CO_3, $Pd(OAc)_2$, PPh_3, 1,4-dioxane/water (10:1), 120 °C, mw; e) TFA/water (1:1), 100 °C, mw.*

Following on from the core synthesis, a 10 membered library was made by reductive amination, scheme 3.1. Solubility is a major factor in determining the success of a drug as many compounds with low aqueous solubility possess poor pharmacokinetic properties limiting their effectiveness in the clinic. These libraries were, therefore, designed to produce aqueous soluble compounds from the start. Chemical diversity was introduced on these water-solubilising motifs in the search for unanticipated pharmacodynamic profiles. As such, the ten amines chosen initially were substituted piperidines, piperazines and morpholine, all water solubilising moieties – scheme 3.2, compounds **7-16**.

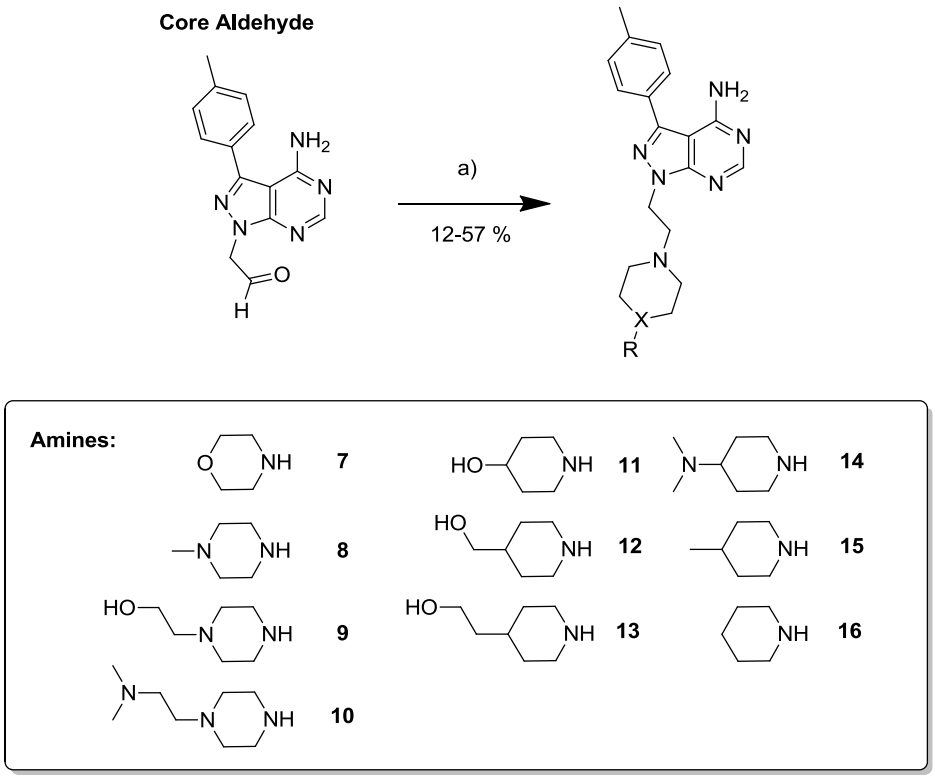

Scheme 3.2: *Synthesis of library 1 members 7-16. a) 1 eq. of amine, AcOH, $NaBH(OAc)_3$, DCM, r.t.*

3.2.2 Cell Proliferation Assay on Library 1 Compounds

To assess the anti-proliferative effect mediated by library 1 compounds in cancer cells, a single dose cell proliferation assay was set up using the IncuCyte-ZOOM™ system from Essen BioScience, figure 3.3. The IncuCyte-ZOOM™ is a microscope capable of bright field and fluorescence microscopy, situated in an incubator. This allows the real time imaging of cells across indefinite time points in a range of formats – multi-well plates, cell culture flasks/dishes etc. In addition, the software accompanying the IncuCyte is capable of calculating cell density, as percentage confluence, and so provides kinetic cell growth data. By imaging cells across the time course of an experiment, one not only obtains the optimal time points for an assay but also confirms that apparent reduced cell viability is indeed occurring due to cell death and not due to inhibition of metabolic pathways, which may occur when using a cell viability reagent.

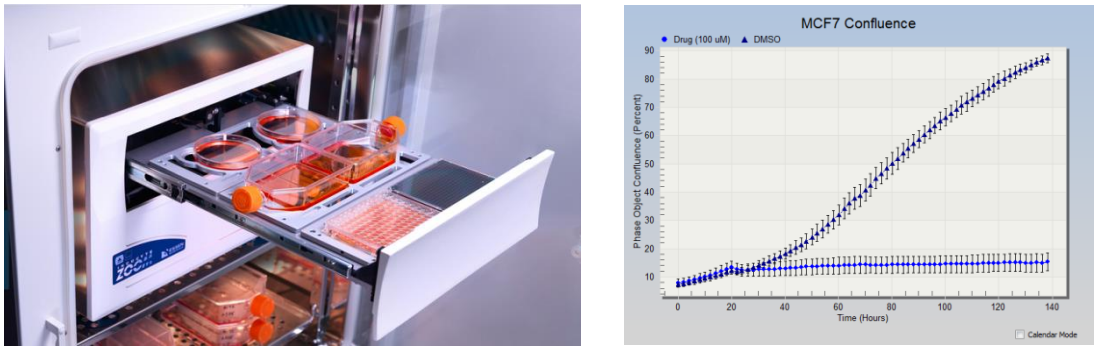

Figure 3.3: *Image of the IncuCyte-ZOOM™ system from Essen BioScience (left).Example of a cell confluence graph produced by the IncuCyte software comparing DMSO (navy blue) to drug treated cells (light blue) over 5 days treatment. The kink in the graph (20 hours) indicates at which point the drug was added (right).*

MCF7 cells, which are estrogen receptor (ER) positive breast cancer cells, were chosen as the initial cell line as they are readily available and have a strong literature presence. Of course, the choice of cell line is important and different cell lines may have led to different results, however, MCF7 cells, being a commonly used and well established breast cancer cell model, were considered as an excellent starting point to steer the drug discovery program towards breast cancer indications. Compounds were tested at a single dose of 100 µM in triplicate for 5 days with 0.1 % DMSO as negative control.

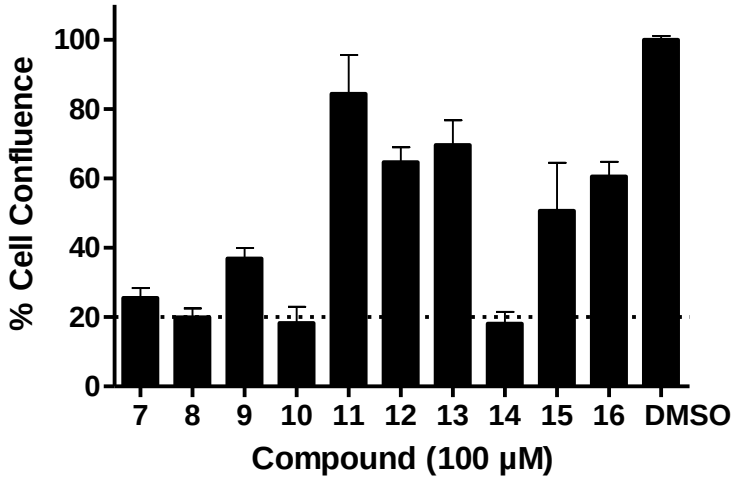

Figure 3.4: *IncuCyte single time-point analysis of MCF7 cell growth. % cell confluence normalised to DMSO on MCF7 cells after incubation with compounds* ***7-16*** *at 100 µM for 5 days. (n = 3, error bars denote standard deviation).*

The results, figure 3.4, revealed compounds **10** and **14** to be the two most potent compounds (cell confluence <20%). It was important to note, however, that 20% confluence does not correlate to 20% of the cells remaining alive as the software maps confluence based on differing contrasts between cells (or cell debris) and background (see figure 3.6), therefore, it is important to also observe the morphology of the cells and also to perform a cell proliferation assay using a reagent for measuring viability. From the structures of **10** and **14**, it was essential to make compounds **17** and **18** also, figure 3.5a, synthesised in the same way as described in scheme 3.2.

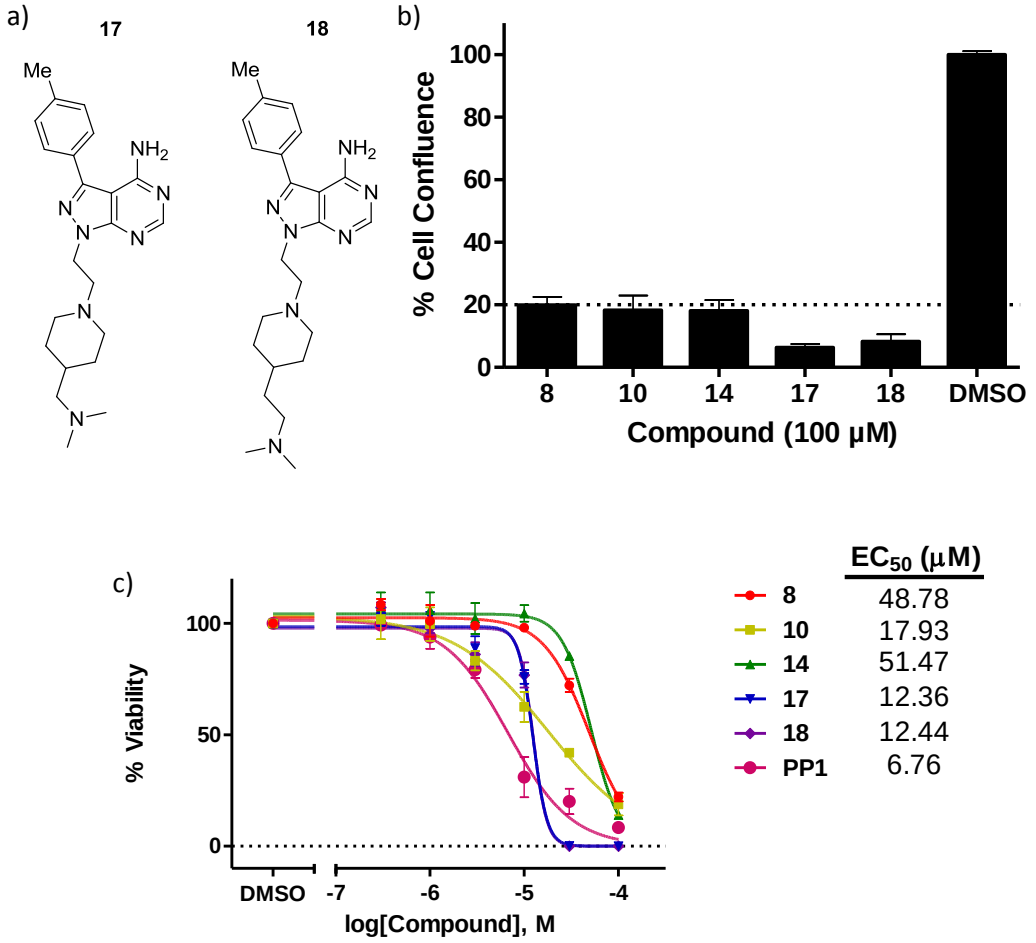

Figure 3.5: *a) Compounds **17** and **18** designed from **10** and **14.** b) IncuCyte experiment with % confluence of MCF7 cells after 5 day treatment of compounds at 100 µM, relative to DMSO (n = 3, error bars denote standard deviation). c) PrestoBlue cell viability assay - Half-log dose response assay using MCF7 cells. Curves were generated using GraphPad Prism and EC_{50} values calculated for compounds **8, 10, 14, 17, 18** and PP1. (n = 3; error bars denote standard deviation)*

Compounds **17** and **18** proved to be even slightly more potent than **10** and **14** from the IncuCyte cell confluence assay, each with confluence <10%, figure 3.5b. Following the single dose IncuCyte experiment, a cell viability assay was set up, using MCF7 cells, for compounds **8, 10, 14, 17** and **18** and PP1 as a comparison, figure 3.5c. Compounds were tested across a 10-point concentration gradient starting at 100 µM down to 0.03 µM using a half-log scale in order to obtain EC_{50} values against cell proliferation. The experiment was performed in triplicate (n = 3) using DMSO (0.1 %) as negative control and cell viability measured after 5 days of incubation with drugs using PrestoBlue® reagent.

The dose response and resulting EC_{50} values are shown in figure 3.5c. Both compound **17** and **18** share similar values of 12 µM, while analogous compound **10** had an EC_{50} of 18 µM. Due to the structural similarities between compound **18** and compound **10** it was concluded that the piperazine nitrogen at the 4-position was not essential for activity, thus, future compounds contained only piperidine moieties – 4-dimethylamino piperidines based on compounds **14, 17** and **18.**

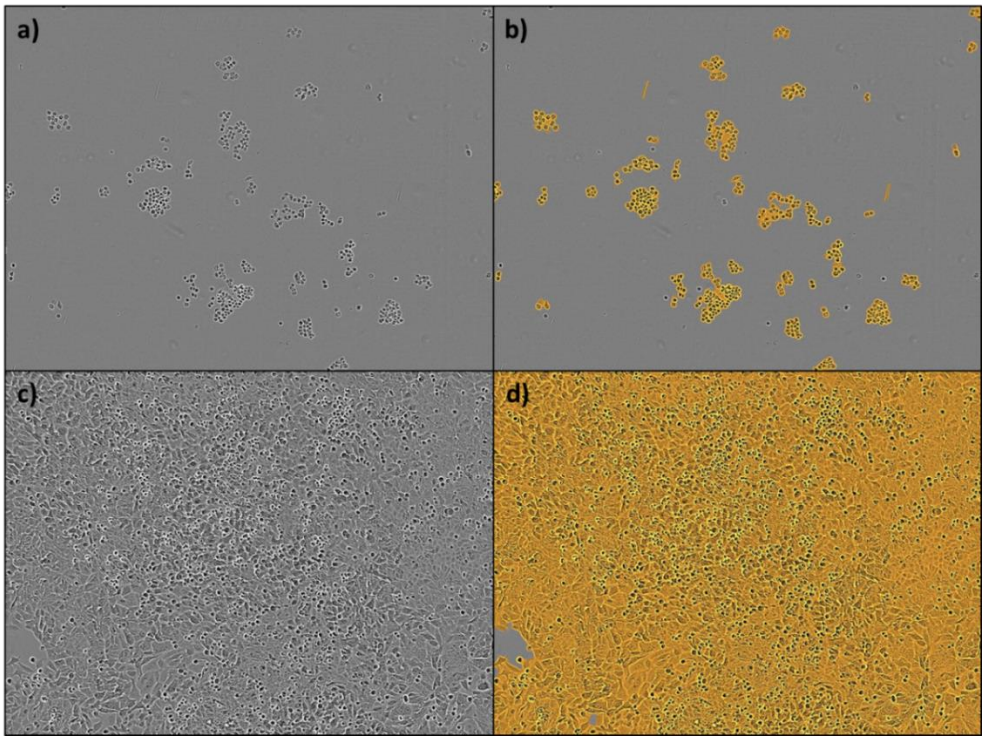

Figure 3.6: *Images obtained from IncuCyte experiment discussed above after 5 days of treatment with drug or DMSO. a) Compound **17** (100 µM) phase image. b) Compound **17** (100 µM) phase image with applied confluence mask. c) DMSO (0.1 %) phase image. d) DMSO (0.1 %) phase image with applied confluence mask.*

The above mentioned limitations of the Incucyte experiment are shown in figure 3.6. Images from the IncuCyte experiment described above with compound **17,** figure 3.5b, are shown in figure 3.6. Cells following 5 days of drug (**17**) treatment at 100 µM have shrunk, are very round and few in number indicating the induction of apoptosis, figure 3.6a. It is apparent that at this concentration, all cells undergo apoptosis and die, however, the IncuCyte's software includes them in the confluence mask, figure 3.6b, and consequently there is a 'minimum' cell confluence achievable when using this system. Figure 3.6c and 3.6d show cells in the absence of drug (0.1 % DMSO) without and with the confluence mask, respectively, for comparison.

3.2.3 Apoptosis Assay on Compounds 8, 10, 14, 17, 18 and PP1

NucView™ 488, which is a caspase-3/7 substrate, was used to detect apoptosis in MCF7 cells treated with compounds **8, 10, 14, 17, 18** and PP1**.** Upon cell damage caused by compound treatment, many pathways may be activated eventually instructing the cell to kill itself – apoptosis. However, the cascade of pathways instructing the induction of apoptosis all filter down to one final mechanism involving a group of proteases called caspases. Two types of caspases exist: initiator and effector caspases. Caspase-3 is an effector caspase and when activated by an initiator caspase it proteolytically begins to break down numerous protein substrates within the cell to cause the cell to die. NucView™ 488, being a caspase-3/7 substrate, thus, is degraded by caspase-3 or 7, binds to DNA becoming fluorescent and indicates the induction of caspase dependent apoptosis.

MCF7 cells were plated on optical imaging plates and compounds (**8, 10, 14, 17, 18** and PP1**)** added as a concentration gradient. NucView™ 488 was added at 1 µM at the time of compound addition. Cells were incubated for 5 days and imaged using the IncuCyte. Shown in figure 3.7 is an example of the images obtained from the experiment. Drug treated cells (figure 3.7a) are small and rounded indicating apoptosis which is confirmed from the NucView™ 488 fluorescence image in figure 3.7b. At this concentration (100 µM) all cells are apoptotic and dead. Similarly to cell confluence, the IncuCyte software applies a 'green mask' over the green cells, figure 3.7c, which enables the quantification of apoptotic cells. DMSO (0.1%) control is shown in figure 3.7e,f and g.

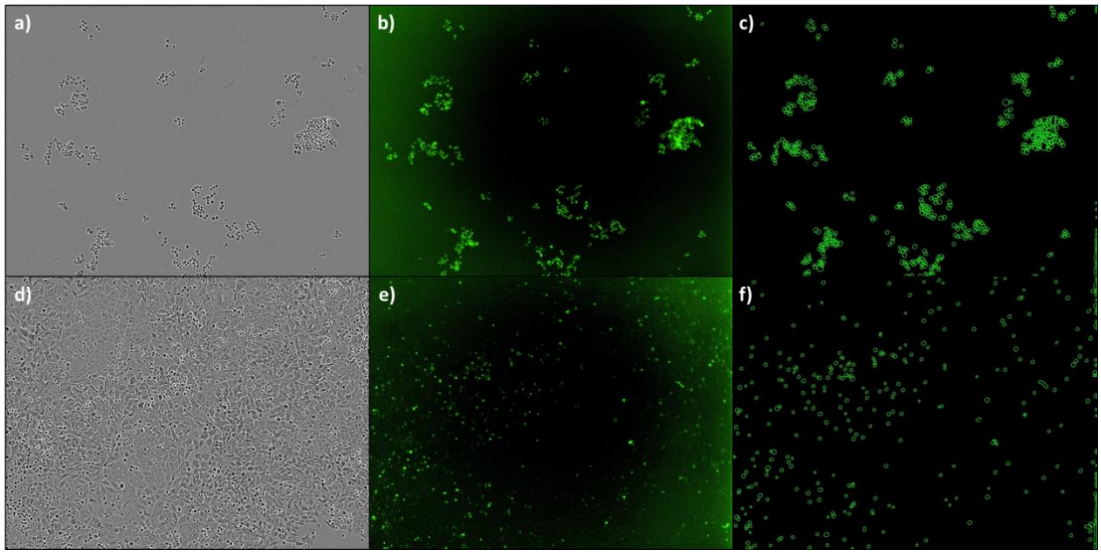

Figure 3.7: *Example phase and fluorescence images obtained from the IncuCyte apoptosis experiment discussed above after 5 days treatment with drug or DMSO and the addition of NucView™ 488 at 1 μM. a) Compound **17** (100 μM) phase image. b) Compound **17** (100 μM) green fluorescence image showing caspase-3 activity. c) Green count mask applied by IncuCyte software on image b. d) DMSO (0.1 %) phase image. e) DMSO (0.1%) green fluorescence image. f) Green count mask on image e.*

The numbers generated from the applied confluence and green (NucView) masks were divided so as to create a ratio of number of apoptotic cells to cell confluence. The data were then normalised to DMSO to account for the decreased number of cells found in higher concentrations of drug treatment. The results are shown in figure 3.8 – only values down to 10 μM are graphed as no further effect was seen below this concentration. Compound **17** showed the greatest effect on inducing apoptosis, slightly greater than compound **18**, with ratios of 31 and 27 at 100 μM compared to DMSO, respectively. This follows the same trend as in the cell viability assays. For this reason compound **17** was progressed through to the next stage, forming the basis of the library 2 compounds – section 4. So far, the target of the compounds and the mechanisms by which apoptosis and reduced viability are being induced were unknown, however, enough early structural activity relationships (SARs) were available to progress the compounds through to a second library.

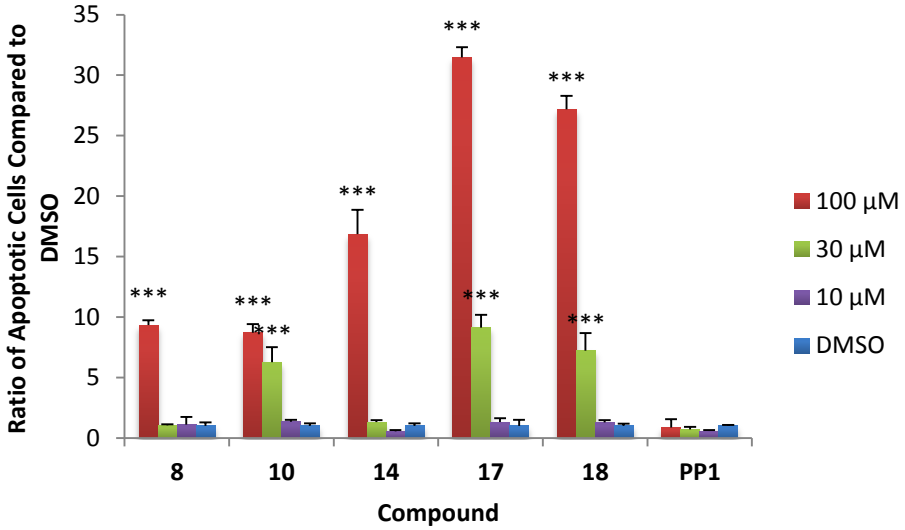

Figure 3.8: *Apoptotic ratios of MCF7 cells caused by 5 day treatment with compounds* ***8, 10, 14, 17, 18*** *and PP1 normalised to DMSO (0.1 %), ($p<0.001$, ***; n = 3; error bars denote standard deviation; t-test was used to generate significance).*

3. Design and Synthesis of Initial Library

3.3 Conclusion

In an attempt to promote a more pragmatic approach to drug discovery, the non-selective small molecule inhibitor PP1 was used as a model for the generation of a 10-membered library. Aiming to create novel kinase inhibitors, the structure of ATP was also taken into consideration when designing the library, as were major factors which determine the fate of a drug such as solubility.

Compounds **7-16** were synthesised in a 6-step process and their activity tested against HER-2 positive MCF7 breast cancer cells. Cell viability was used as a phenotypic end point in which to rank compound activity. Using the IncuCyte-ZOOM™ system from Essen BioScience, 3 compounds (**8, 10** and **14**), bearing similar structures, were identified as early 'hits' leading to the design and synthesis of a further 2 members – compounds **17** and **18**. The EC_{50} values against MCF7 cell proliferation were determined for these 5 compounds, along with PP1. Compounds **17** and **18** generated EC_{50} values of 12.36 and 12.44 μM, respectively, against proliferation.

Further, the mechanisms by which the compounds were reducing cell proliferation were determined by phase-contrast and fluorescence microscopy. The rounding up of cells upon compound treatment suggested that apoptosis was being induced and incubation with the caspase-3/7 substrate, NucView™ 488 concluded this was the case. Compounds **10, 17** and **18** were able to induce apoptosis at statistically significant levels down to 30 μM.

Given that an appropriate 'south part' of the molecules had been identified, thoughts turned to improving the compounds' potency against cell proliferation. Chapter 4 discusses the optimisation of the aryl group of the structures and investigates the mechanism of action by which they were operating.

4. The Discovery of Potent Anti-Proliferative Compounds and Target Identification

4.1 Introduction & Aims

The second library of compounds was based on the anti-proliferative hit **17**. Using the piperidinyl group of compound **17**, library 2 focuses on the modification of the aryl group of the molecule ('north' part) in order to generate more potent compounds and give some early structure activity relationships. The putative kinase targets by which the hit compounds exert their activity were also discovered via an initial 14-membered kinase panel screen by Reaction Biology Corporation.

4. The Discovery of Potent Anti-Proliferative Compounds and Target Identification

4.2 Results

4.2.1 The Design and Synthesis of Library Two

Library 2 members were synthesised in the same way as library 1 with diversity added, this time, during the Suzuki reaction step using different boronic acids/esters. 10 members were originally planned with the iodo group (compound **35**) taking the 11th place to assess the needs of an aryl group at all. The 10 aryl groups chosen are shown in scheme 4.1. These groups were chosen from examples in the literature, as they had previously shown potency against kinases, and they would also provide some structure activity relationships regarding the best aryl groups.[92, 105] PP121, shown in scheme 4.1, was used as a model compound for compounds **19** and **29** as it had previously shown good activity against a sub-set of kinases.[92] It must be noted, however, that the target of previous members, and of the projected new compounds, was still unknown so the choice of aryl group was solely to improve potency in cellular assays.

Core intermediate **4**, discussed previously in scheme 3.1, was used again for the synthesis of library 2. Suzuki reaction with **4** and corresponding commercial boronic acid/ester resulted in high to excellent yields of acetal intermediates **19-27.** Compound **28** was synthesised via a Sonogashira reaction using phenyl acetylene as the alkyne reactant. The conditions are shown as a*) in scheme 4.1, below.

Following on from the acetal intermediates, final compounds **29-35** were made via acetal deprotection using TFA/water then reduction amination with N,N-dimethyl-1-(4-piperidyl)methanamine, previously shown to be the best amine (compound **17**). Unlike the synthesis of library 1 members, however, the core aldehydes in this case were not isolated. Instead, after each deprotection reaction, the product was dried under vacuum and used immediately in the reductive amination step. This was to try and improve the yields by not storing the aldehyde.

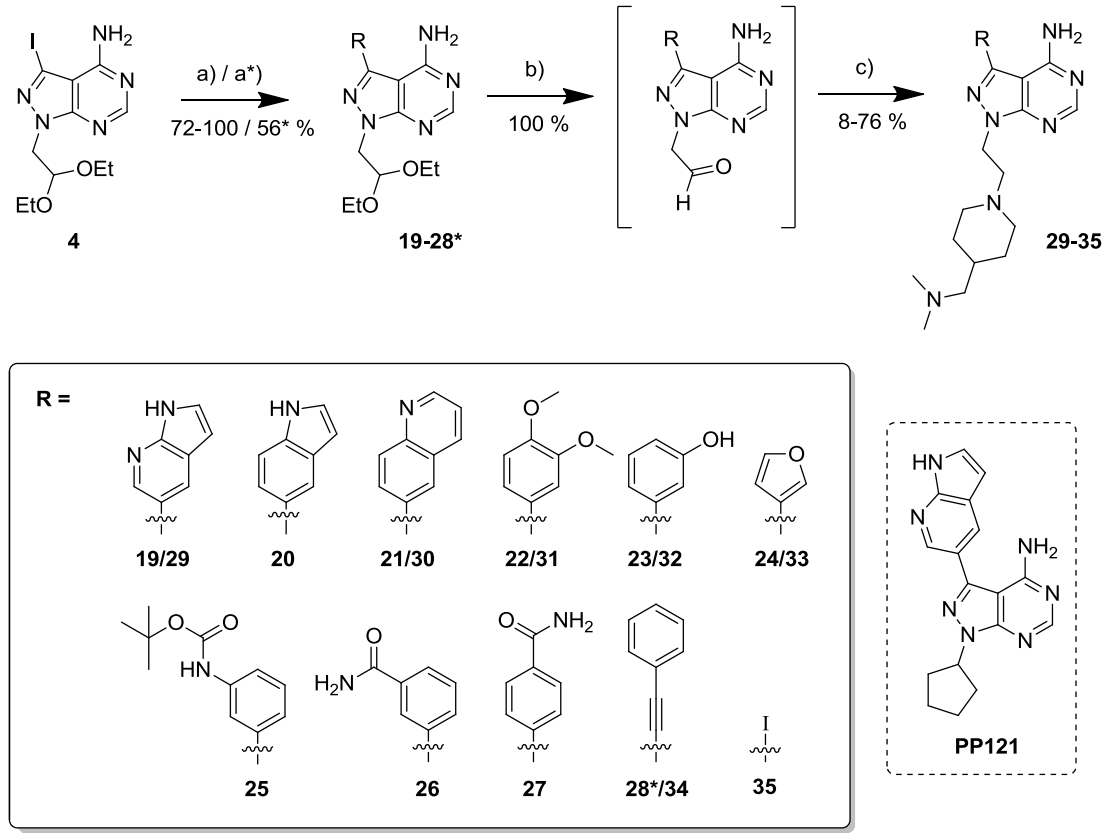

Scheme 4.1: *Library 2 synthesis. a) Boronic acid/ester, K_2CO_3, $Pd(OAc)_2$, PPh_3, 1,4-dioxane/water (10:1), 120 ^oC, mw. a*) Phenylacetylene, Et_3N, $Pd(OAc)_2$, CuI, PPh_3, THF, 70 ^oC. b) TFA/water (1:1), 100 ^oC, mw. c) N,N-dimethyl-1-(4-piperidyl)methanamine, AcOH, $NaBH(OAc)_3$, DCM, r.t. PP121 (bottom right) was used as an inspirational molecule.*

Only 7 of the projected 11 final compounds (**29-35**) were successfully synthesised, however. The yields of these reactions varied from low 8 % to high 76 %. Problems arose when deprotecting the acetal intermediates of compounds **20** and **25-27.** Upon concentration of the samples under vacuum to remove the excess TFA/water, unusual polymers appeared in the flasks which were insoluble in any of the following solvents: acetone, acetonitrile, DMF, DMSO, hexane, TFA, toluene and water; even upon boiling of the samples. As the products were insoluble, mass and NMR spectra were unobtainable and the products (likely to be some kind of polymeric structures) were discarded. It is unclear to why the polymerisation occurred but looking at the structures, all examples had either an endocyclic NH or NH_2, and so this was hypothesised to be involved. Other compounds containing OH or endocyclic NH groups, such as **32** and **29**, were successfully synthesised, although at low yields (8 and 15 %, respectively), indicating that protic groups interfered with the reductive amination process. Nonetheless, the 7 successful compounds were tested as before in MCF7 cell

viability assays to assess their potency against cell proliferation. As well as the final 7 amine compounds (**29-35**), the corresponding acetal intermediates (**19-28**), as well as core intermediate **4,** were tested also. Compound **5**, section 3.2.1, was also tested to compare the original p-toluyl group with the library 2 members. Compounds were tested along a half-log dose response in triplicate from 100 μM to 0.03 μM and compared against DMSO (0.1 %). Curves were fitted using GraphPad Prism software to generate EC_{50} values. EC_{50} values above 100 μM were estimates only and compounds were assumed non-active.

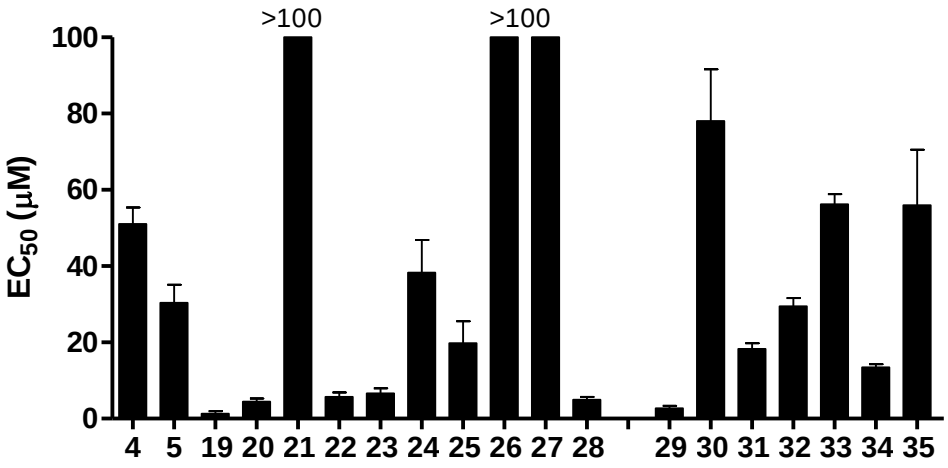

Compound	EC50 (μM)	Compound	EC50 (μM)	Compound	EC50 (μM)
4	51.04	**19**	1.32	**29**	2.69
5	30.37	**20**	4.42	**30**	78.01
		21	>100	**31**	18.27
		22	5.71	**32**	29.42
		23	6.62	**33**	56.21
		24	38.32	**34**	13.45
		25	19.81	**35**	55.98
		26	>100		
		27	>100		
		28	4.98		

Figure 4.1: *EC_{50} values against MCF7 cell proliferation of library 2 compounds (n=3, error bars denote standard deviation).*

Interestingly, compounds **19** and **29** were the most potent with EC_{50} values of 1.32 and 2.69 μM, respectively, figure 4.1. Both these compounds shared the same aryl group, the 1H-pyrrolo[2,3-b]pyridine group. Comparing compound **20** with compound **21**, the small change from an indole to a quinoline group creates a drop in potency from 4.42 μM to >100 μM highlighting the need for a hydrogen bond donor.

Even more interestingly, all the acetal compounds were more potent than their respective amine compounds i.e. the presence of a acetal at the south part of the molecule led to superior phenotypic effect than the *N*,*N*-dimethyl-1-(4-piperidyl)methanamine group, previously shown to be optimum. Indeed, this was the case with all the compounds except for the related compounds **21** and **30**. At this point, two hypotheses were considered: (i) acetal compounds could improve cell penetrability or (2) the acetal compounds and their amine equivalents were exerting a different molecular mechanism of action.

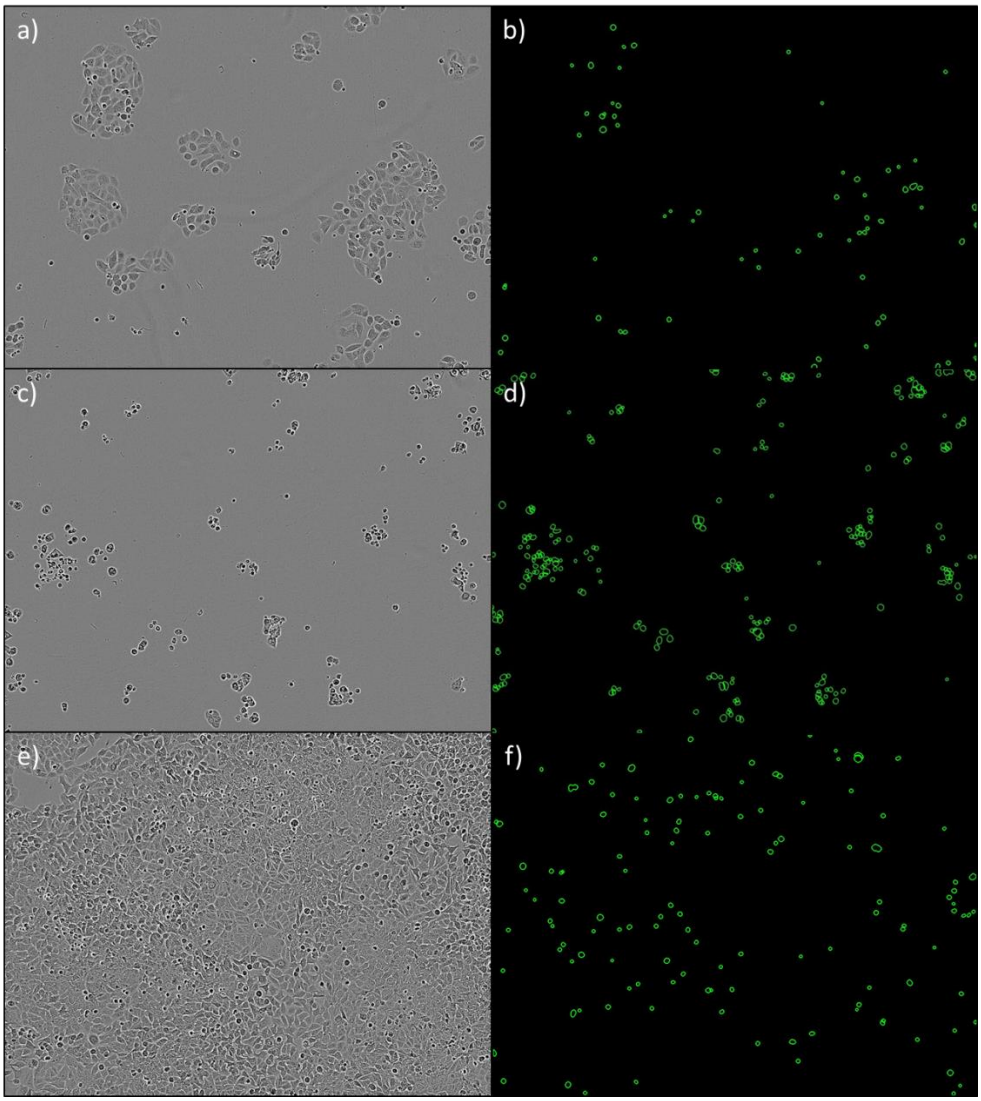

Figure 4.2: *Images from IncuCyte-ZOOM™ MCF7 cell viability experiment after 5 days of treatment with compounds **19** and **29** at 100 μM. a) Compound **19** phase image. b) Compound **19** green mask. c) Compound **29** phase image. d) Compound **29** green mask. e) DMSO control phase image. f) DMSO control green mask.*

Due to their superior potency in the MCF7 cell viability assay, compounds **19** and **29** were subjected to the IncuCyte-ZOOM™ cell growth assay discussed previously, section 3.2.2, so that the compounds' effects on cells could be observed over the incubation period. NucView™ 488 was added to cells at time of drug addition so the induction of apoptosis, if any, could be monitored.

The experiment suggested that the compounds were exerting different effects on the cells due to the different phenotypes observed after incubation. Both compounds reduced cell proliferation, however, compound **19** appeared to slow the cells' growth without causing cell death (suggesting cell cycle inhibition), whereas, compound **29** was inducing apoptosis resulting in cell death, figure 4.2. Images a) and c), figure 4.2, show MCF7 cells after 5 days of treatment with both compounds, at 100 μM. The cells in image a) look relatively healthy, whereas, the cells in image c) are very rounded indicating apoptosis and cell death. Looking at images b) and d), the green mask applied by the IncuCyte from NucView™ activity confirms that compound **29** is inducing apoptosis more so than compound **19**. There is a small amount of apoptosis seen in image b), however, cells naturally undergo apoptosis and after 5 days of treatment with a compound at high concentration this is expected - images e) and f) show comparison with DMSO as negative control. On observation of time-lapse movies created from the IncuCyte images it was clear that the cells treated with compound **29** immediately started to round up after compound addition, whereas, cells treated with compound **19** simply stopped growing.

4.2.2 Screening on a Sub-set of Kinases

To shed some light over the mechanism of action and selectivity profile of the compounds, IC_{50} values were determined for PP1, **14, 17, 18,** 19 and **29** against a selection of protein kinases known to be targeted by PP1 and based on published literature.[91, 92, 102-106] Not only would this give some insight to the mechanisms of these compounds but knowing their respective targets would also allow for further optimisation and 'tuning in' selectivity. IC_{50} values were determined from 10-point, 1:3 dilution curves starting at 100 μM down to 5.08 nM with 10μM ATP by Reaction Biology Corp. using a radioactive ATP substrate incorporation assay.

The results, shown in table 4.1, revealed that compounds **14** and **29** are moderately potent c-SRC family (BLK, FGR, FRK, FYN, HCK, LCK, LYN and SRC) inhibitors with IC_{50} values of 126 and 27 nM, respectively. Not surprising since PP121, containing the same aryl group

1H-pyrrolo[2,3-b]pyridine, is also a moderately potent SRC inhibitor (IC_{50} 14 nM). What is surprising is the difference in potency between compounds **14, 17** and **18**, however. Compound **14** was far more potent against the kinases tested than **17** or **18.** This is in contrast to their anti-proliferative properties against MCF7 cells – compounds **17** and **18** displayed EC_{50} values of around 12 μM, whereas, **14** had a value of 51 μM. These contradictory results may be explained by slight differences in physicochemical properties of the molecules, leading to variations in solubility, cell permeability or their roles in active transport mechanisms etc. On the other hand, the superior effects against cell proliferation seen with compounds **17** and **18** may be simply explained by effects on targets not tested amongst the 14 kinases shown here.

Kinase \ Hit	PP1	14	17	18	19	29
	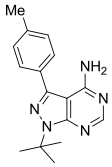	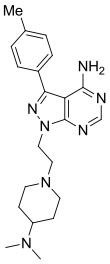	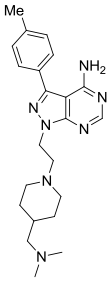	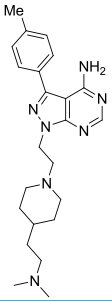	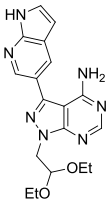	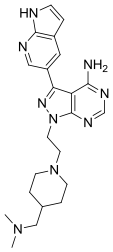
c-ABL	147.2	6323	7525	7249	1207	115.7
BLK	268.3	1545	2846	7072	$>10^5$	110.1
FGR	7.6	115	399.6	600.8	2127	45.3
FRK/PTK5	63.0	915.8	1635	3700	2691	105.6
FYN	27.5	311.1	913	1964	1226	37.8
HCK	167.4	1523	6009	11630	6774	36.1
c-KIT	1318	27360	77080	$>10^5$	$>10^5$	18850
LCK	173.8	727	1542	4344	8598	232.8
LYN	88.0	284.9	1068	2508	2298	25.2
mTOR/FRAP1	9318	$>10^5$	$>10^5$	$>10^5$	**328.4**	8565
PDGFRa	657.4	70500	$>10^5$	$>10^5$	$>10^5$	$>10^5$
RET	11.6	6584	22590	10840	598.2	288.9
c-SRC	16.6	126	302.7	1040	2453	26.9
YES/YES1	36.3	71.4	344.5	696.5	565.6	12.3

Table 4.1: *Kinase IC_{50} data (nM) for compounds PP1,* ***14, 17, 18, 19*** *and* ***29****. Data highlighted in red indicates IC_{50} values of below 100 nM. Data highlighted in green indicates mTOR inhibition below 1 μM.*

Due to the nature of phenotypic drug discovery, specific target inhibition or physicochemical properties of molecules are not independently considered, only the overall phenotypic effect resulting from the sum of all the physicochemical and pharmacological properties of each compound, which in this case is reduced cell proliferation.

All of the new compounds differentiated from PP1 in terms of selectivity towards the kinases tested. Compounds **14, 17, 18** and **29** did not inhibit c-KIT, PDGFRα or mTOR and only compound **29** showed moderate activity against RET. The piperidine moiety of compound **14, 17** and **18** was particularly effective in reducing inhibition of the RET protein leading to >500 times reduction in activity, compared to PP1. These results show that small changes to the PP1 molecule can be used to generate lead compounds with better physicochemical properties and selectivity.

Most interesting of all was compound **19,** which turned out to be a moderately potent mTOR inhibitor (328 nM), with much reduced activity against all other kinases tested. The acetal moiety was clearly the reason for this selectivity and compared to compound **29**, it is remarkable how such a small change led to such a vast difference in target selectivity, while both having similar anti-proliferative potency. This unanticipated result is in agreement, however, with the phenotypic effect mediated by **19**, as the previous IncuCyte experiment, figure 4.2, showed that compound **19** halted the growth of MCF7 cells, a common observation of mTOR inhibition due to its strong involvement in the cell cycle.[107]

Furthermore, the shared 1H-pyrrolo[2,3-b]pyridine group of compounds **19** and **29** seemed to aid the potency of both compounds against their respective targets (mTOR and SRC family), whereas, selectivity was governed through the 'south part' of the molecule through the use of the diethyl acetal or piperidine groups. PP121, on the other hand, was both a potent SRC and mTOR inhibitor, 14 and 10 nM, respectively, but was not selective for either.[92]

4. The Discovery of Potent Anti-Proliferative Compounds and Target Identification

4.3 Conclusion

Using the N,N-dimethyl-1-(4-piperidyl)methanamine moiety from compound **17**, found to be the most potent out of a series of 14 amines tested, 'chapter 1', a second library of 10 members was designed to contain varying aryl groups. The aryl groups were all commercially available, making synthesis of the library quick and straight forward, and were chosen based on their presence in recent literature, highlighting them as important groups for kinase inhibition. The acetal intermediates, compounds **19-28** were synthesised and tested also against MCF7 cell proliferation. The transformation from acetal intermediate to final compound proved troublesome for 4 out of the 10 designed compounds due to polymerisation during the TFA mediated deprotection of the acetal. As such, only 6 of the final amine containing compounds were produced. Compounds **4** and **35**, containing no aryl group but iodine only, were included in the MCF7 cell viability study.

Compounds **19** and **29**, sharing the same 1H-pyrrolo[2,3-b]pyridine group, turned out to be the most potent compounds with EC_{50} values of 1.32 and 2.69 μM, respectively. The two compounds were subjected to analysis by incubation with NucView™ 488 in the IncuCyte-ZOOM™ system revealing differing mechanisms of action of the 2 compounds.

The kinase targets, to which compounds **14, 17, 18, 19** and **29** inhibitied, were discovered via a 14-membered panel screen, based on targets inhibited by PP1. It was discovered that compound **29**, containing the amine moiety, was a potent SRC family kinase (SFK) inhibitor, whereas, compound **19**, containing the diethyl acetal, was a moderately potent mTOR inhibitor with reduced activity towards the SFKs.

This evidence led to the hypothesis that modifications on the current structures could be used to create novel and selective SRC family and mTOR inhibitors. As such, the thesis now splits into two separate chapters, one discussing the development of SRC family inhibitors and the other discussing the development mTOR selective inhibitors.

5. The Development of Novel, Potent and Selective mTOR Inhibitors

5.1 Introduction & Aims

The mini review on mTOR, chapter 1.4, highlights the increasing evidence for the involvement of mTOR in cancer. Current Rapalogs approved for cancer treatment are sub-standard owing to the lack of sufficient clinical biomarkers, partial inhibition of downstream targets, such as 4E-BP1, and inhibition of only one of the two mTOR complexes causing negative feedback resulting in the activation of AKT. Efforts have turned instead to producing selective ATP site inhibitors which inhibit both of the mTOR complexes. As such, the development of small molecule ATP site mTOR inhibitors is highly sought after and several have entered clinical trials.

Compound **19**, being a moderately potent mTOR inhibitor, created an ideal starting point for the development of a potent and more selective mTOR inhibitor than current standards and given the rational need for such therapies in cancer treatment, the progression of compound **19** seemed a logical step.

Based upon the clinical candidate INK-128, several new compounds were designed and synthesised. Their EC_{50} values against cell proliferation are discussed along with their selectivity and potency for mTOR *in vitro*. Whole kinome profiling is discussed for lead compound **41**, highlighting its excellent selectivity for mTOR, and comparing it with current gold standard, INK-128.

Further, the effects on the cell cycle by lead compounds, generated from the library of mTOR inhibitors, are analysed and discussed as is compound **41**'s effects on downstream targets of mTOR, quantified by Western blot.

5. The Development of Novel, Potent and Selective mTOR Inhibitors

5.2 Results

5.2.1 Synthesis and Testing of Analogues of Compound 19

In order to improve compound **19** in terms of potency and selectivity for mTOR, different acetal groups were tried, using the same north motif known to target mTOR potently and selectively.[35] The aryl group was based on the developmental compound INK-128, currently in Phase 1 and 2 clinical trials. INK-128 is a fairly selective mTOR kinase inhibitor with an IC_{50} of 1.4 nM and some off-target activity for PI3Kα, β, γ (152, 4700 and 165 nM, respectively) and DNA-PK (10 nM). The acetals tested were diethyl acetal, dimethyl acetal and 1,3-dioxolane.

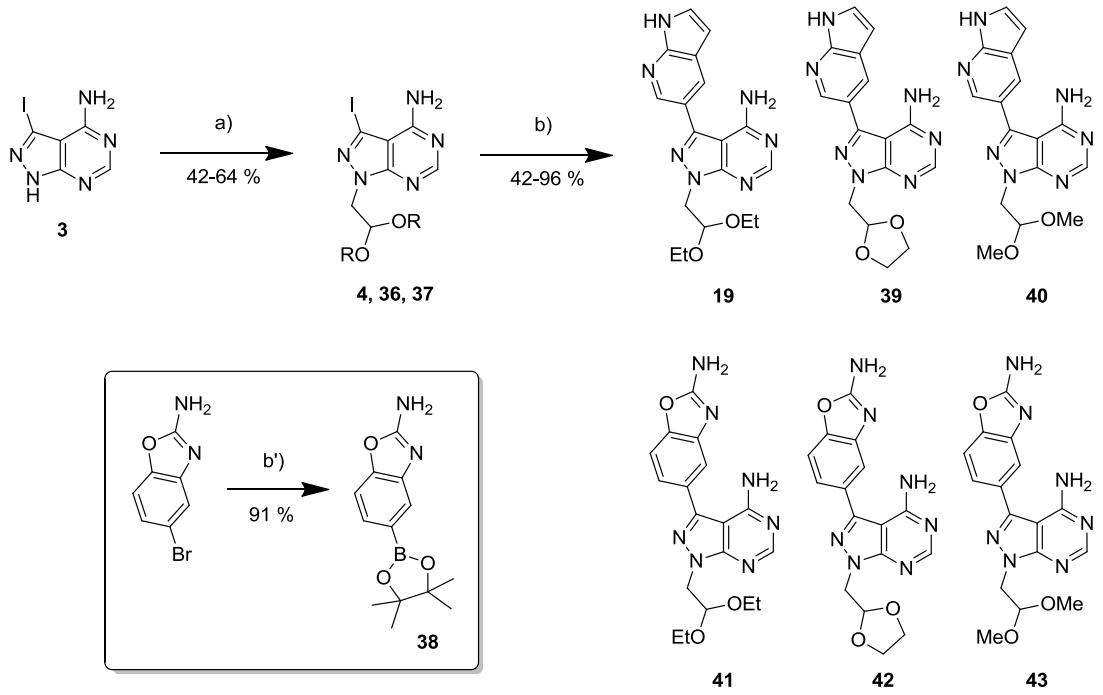

Scheme 5.1: *mTOR inhibitor optimisation. a) Bromoacetaldehyde diethyl acetal (**4**) or 2-bromomethyl-1,3-dioxolane (**36**) or bromoacetaldehyde dimethyl acetal (**37**), NaH, DMF, 150 °C, mw. b) 1H-pyrrolo[2,3-b]pyridine-5-boronic acid pinicol ester (**19, 39, 40**) or 5-(4,4,5,5-tetramethyl-1,3,2-dioxaborolan-2-yl)-1,3-benzoxazol-2-amine (**41, 42, 43**), K_2CO_3, $Pd(OAc)_2$, PPh_3, 1,4-dioxane/water (10:1), 120 °C, mw. b') Bis(pinacolato)diboron, K_2CO_3, $Pd(OAc)_2$, PPh_3, 1,4-dioxane/water (10:1), 120 °C, mw.*

Each acetal intermediate was synthesised as before: treatment of **3** with sodium hydride followed by the addition of the corresponding alkyl bromide compound gave compounds **36** and **37** in moderate yields upon heating in the microwave, scheme 5.1

The aryl group corresponding to compounds **41, 42** and **43** was non-commercially available so was synthesised from the bromo precursor, scheme 5.1, b'), in excellent yield. The following Suzuki reactions then gave the final compounds in moderate to excellent yields.

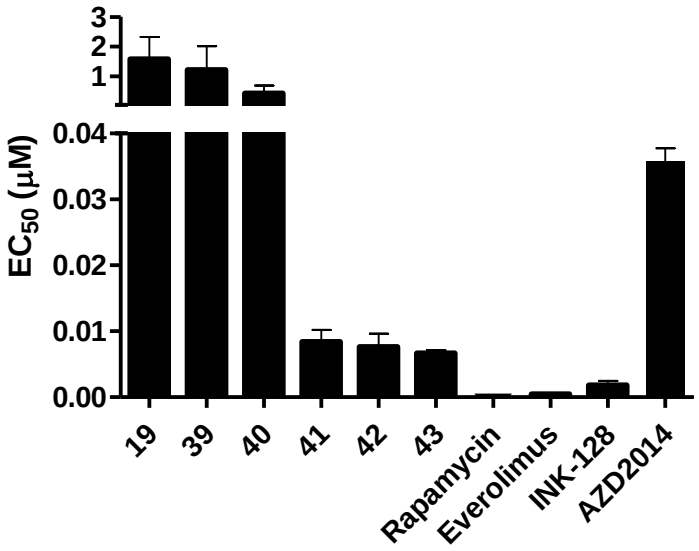

Compound	EC50 (μM)
19	1.57
39	1.22
40	0.43
41	0.0084
42	0.0076
43	0.0067
Rapamycin	0.00013
Everolimus	0.00044
INK-128	0.0018
AZD2014	0.036

Figure 5.1: *EC_{50} values of mTOR inhibitors against MCF7 cell proliferation in PrestoBlue cell viability assay (n=3, error bars denote standard deviation).*

As before, compounds were tested against MCF7 cells to assess their anti-proliferative effects. The determined EC_{50} values from the experiment are shown in figure 5.1. The 6 compounds were tested along with Rapamycin, Everolimus, INK-128 and AZD2014, all previously reported mTOR inhibitors.[35, 108] Our compounds are highly suspected to be ATP-site competitive inhibitors, like INK-128 and AZD2014, whereas, Rapamycin and Everolimus are allosteric inhibitors and inhibit only one of the two mTOR complexes.

The results reveal that although compound **40** is slightly more potent than **19**, compounds **41-43** are extremely potent against cell proliferation with EC_{50} values in the low nano-molar range. Clearly, the 2-aminobenzoxazole aryl group is driving the potency against cell viability and presumably, against mTOR. INK-128 shared a similarly low EC_{50} value of 1.8 nM which is not surprising given the similarity in their structures and the 'driving force' of the 2-aminobenoxazole group. As discussed previously, Rapalogs such as Rapamycin and Everolimus only inhibit one of the two mTOR complexes – mTORC1 – so although they

gave sub-nano-molar EC_{50} values in this assay, they are incapable of causing 100 % cell death, even at higher concentrations, as shown by the dose response curves in figure 5.2.

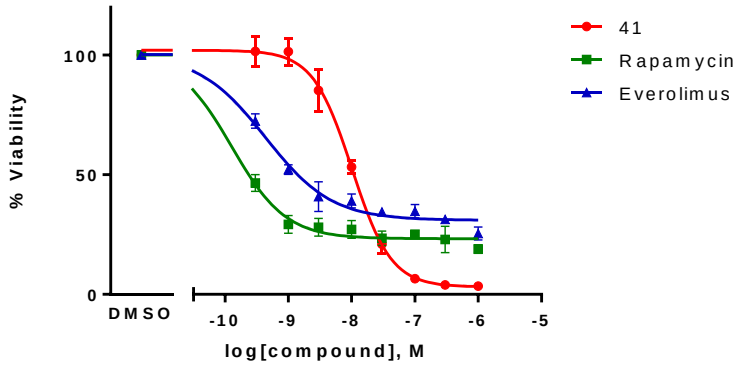

	41	Rapamycin	Everolimus
IC50	1.012e-008	1.282e-010	4.341e-010

Figure 5.2: *MCF7 cell viability dose response curves and corresponding EC_{50} values comparing compound **41**, Rapamycin and Everolimus (n=3, error bars denote standard deviation).*

5.2.2 Kinase Inhibition Data

Following the cell viability results, the IC_{50} values against the same 14 kinases tested before, and 4 new kinases, were determined for compounds **41, 42** and **43**. The new kinases were phosphoinositide 3-kinase (PI3K) alpha, beta, gamma and delta; Lipid kinases similar to, and closely associated with the mTOR pathway, and AKT. Commonly, inhibitors which target mTOR also show some off-target effects on the PI3Ks.[70]

All 3 compounds showed superior potency against mTOR with values of 15, 29 and 25 nM, respectively, table 5.1. Most interesting was the selectivity for mTOR. All of the compounds showed >130x selectivity over the previously tested kinases with the majority of kinases having no inhibition, indicated by a blank box in table 5.1. It is also interesting that the most potent compound, **41**, also showed the most selectivity over the 14 original kinases and the 4 PI3Ks. Comparing the PI3Ks, compound **41** was the weakest inhibitor of the 3 with >60x loss in potency over mTOR. Compound **43** had a moderate IC_{50} value of 98.9 nM against PI3K-γ. These results showed promise that modifications to the lower half of the molecule could be used to achieve potent mTOR and PI3K inhibitors with selectivity equal to or even greater than current standards such as INK-128.

Kinase \ Hit	19	41	42	43
	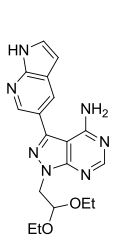	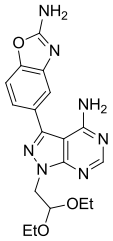	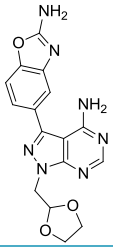	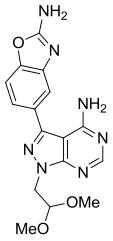
c-ABL	1207	$>10^5$	8630	9920
BLK	$>10^5$			
FGR	2127		7940	$>10^5$
FRK/PTK5	2691			
FYN	1226			
HCK	6774			
c-KIT	$>10^5$			
LCK	8598		9400	
LYN	2298			
mTOR/FRAP1	**328.4**	**15.3**	**58.9**	**25.3**
PDGFRa	$>10^5$			
RET	598.2			
c-SRC	2453			
YES/YES1	565.6		$>10^5$	
PI3K-α	ND	981	115	300
PI3K-β	ND	$>10^5$	3850	5600
PI3K-γ	ND	1340	302	98.9
PI3K-δ	ND	1840	271	505

Table 5.1: *Kinase IC_{50} data (nM) for compounds **19**, **41, 42,** and **43**. Data highlighted in red indicates IC_{50} values of below 100 nM. Data highlighted in green indicates mTOR inhibition below 1 μM. Blank boxes indicate no inhibition.*

The ethyl acetal moiety was optimum for binding to the mTOR ATP pocket over the methyl and 1,3-dioxolane and for this reason compound **41** was screened against the whole kinome to determine its kinome wide selectivity. The compound was screened against 340 wild-type kinases, 19 atypical kinases and 17 lipid kinases (listed in appendix 1a, 1b and 1c, respectively) at a single dose of 10 μM in duplicate with 10 μM of ATP by Reaction Biology Corp.

The data was then averaged and plotted as percentage enzyme activity relative to DMSO, as negative control, using DiscoverRX TREEspot™ software. Compound **41** was very selective for mTOR, even at the high concentration of 10 μM only 5 enzymes were inhibited greater than 35 % compared to DMSO, figure 5.3, which included DDR1, DNA-PK, mTOR, PI3K-

α and PI3K-γ. PI3K-α and γ previously had their IC_{50} values determined, with compound **41** showing greater than 64x and 87x selectivity for mTOR over either, respectively, table 5.1.

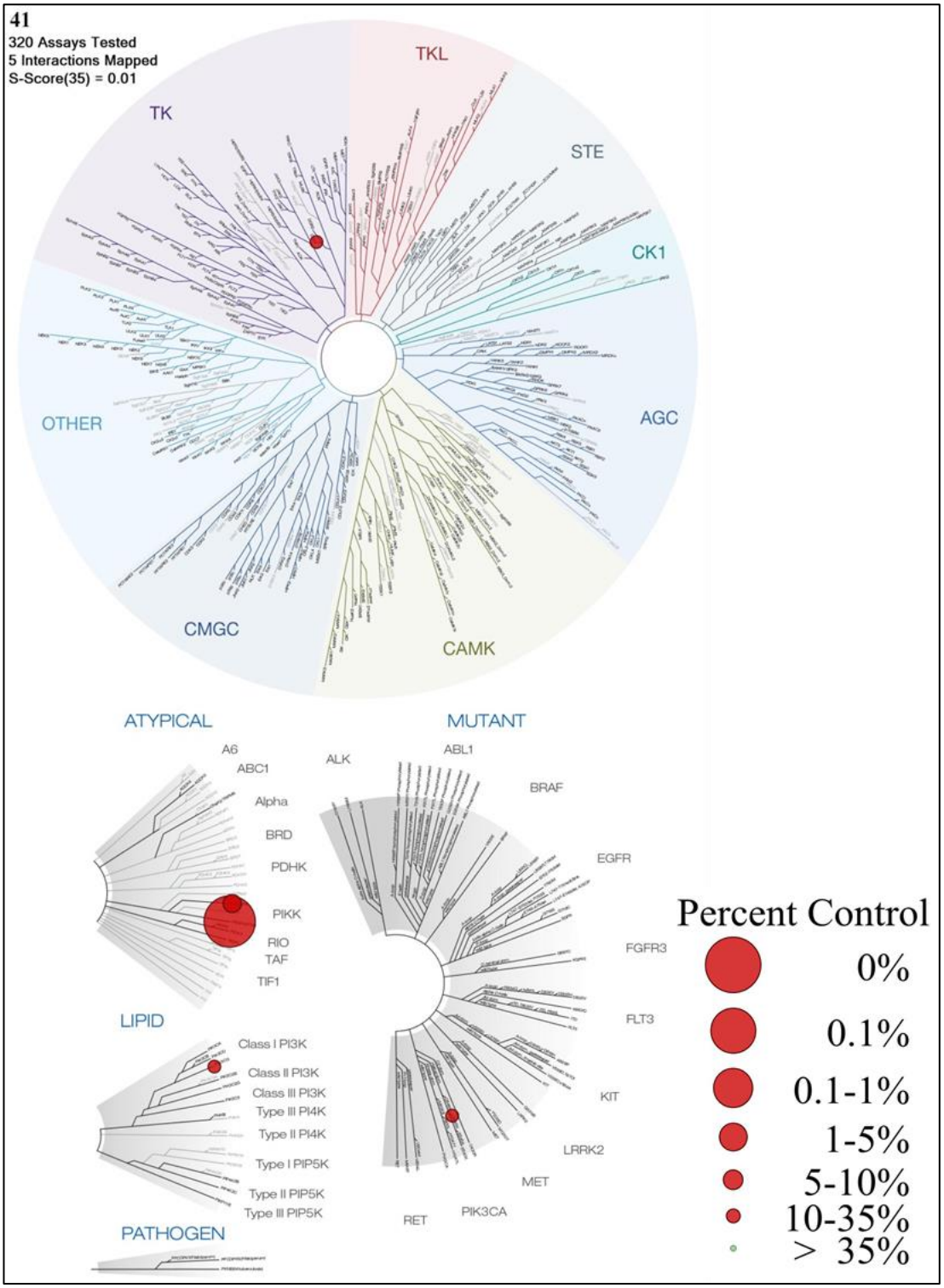

Figure 5.3: *Kinome screen tree map showing percentage enzyme activity with compound **41** at 10 μM after 35 % cut-off. The 5 interactions mapped include DDR1, DNA-PK, mTOR, PI3K-α and PI3K-γ.*

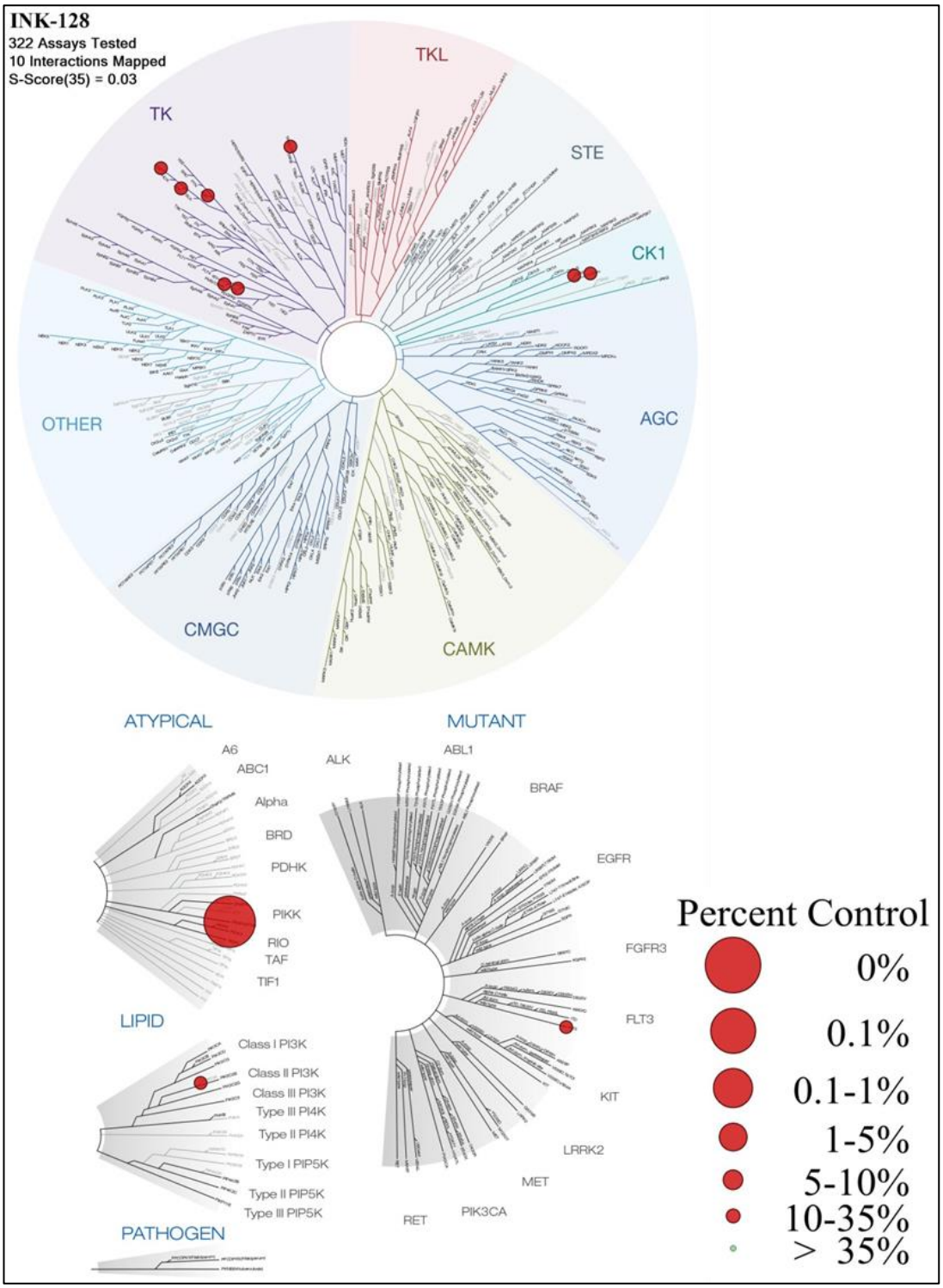

Figure 5.4: *Kinome screen tree map showing percentage enzyme activity with INK-128 at 1 μM after 35 % cut-off. The interactions mapped include CK1-δ, CK1-ε, FMS, FGR, FLT3, LCK, LYN, mTOR, TRKC and PI3KC2-α.*

DNA-PK (DNA-dependant protein kinase) is another enzyme closely related to the AKT/PI3K/mTOR family.[109] As such, it is not surprising that compound **41** had some activity. DNA-PK is a serine/threonine protein kinase that is involved in repairing damaged DNA by re-joining double strand breaks and, consequently, inhibition of DNA-PK has been shown to be beneficial to cancer treatment.[110] DDR1 (Discoidin domain receptor family, member 1) was the fifth kinase to show some inhibition in the study. DDR1 is a receptor tyrosine kinase not related to the PI3K family members so its inhibition was surprising; however, it has been shown to be over regulated in several cancers and is proposed as a therapeutic target, thus, inhibition may be helpful.[111]

As a comparison, the percentage enzyme activities for a panel of kinases was plotted in the same manner for INK-128, figure 5.4. These data were taken from Hsieh et Al.'s study described in Nature, 2012, 485, p 55-61, supplementary data page 16.[35] This study only tested 243 kinases, using the Invitrogen SelectScreen™ kinase profiling service (fluorescence based assay rather than the gold standard radioactive assay we opted for), compared to our broader panel of 340, however, the most important kinases for comparison were included (see appendix 2 for list). Even more noteworthy is the difference in concentration used. We opted for the higher concentration of 10 μM to highlight any off-target effects while 1 μM was chosen for the study of INK-128. Although INK-128 is more potent against mTOR with an IC_{50} of 1.4 nM, it also has more off-target effects, figure 5.4, with 10 interactions mapped after a 35 % cut-off, albeit, much weaker than mTOR. The interactions mapped include CK1-δ, CK1-ε, FMS, FGR, FLT3, LCK, LYN, mTOR, TRKC and PI3KC2-α. Included in this list are 3 members of the SRC family – FGR, LCK and LYN – these are not targeted at all by compound **41**. Modification of the lower half of the molecule by an ethyl acetal group enabled greater selectivity for mTOR over SRC family members and afforded a more selective inhibitor than current standards.

5.2.3 Compound 41 Stability Study

Due to similarities in the EC_{50} values of compounds **41, 42** and **43** (ethyl acetal, 1,3-dioxolane and methyl acetyl) an important hypothesis to test was whether the compounds were being hydrolysed to the corresponding aldehyde compound during the cell viability assay and whether the active compound was, in fact, the aldehyde. Treatment of compound **43** with TFA/water at 100 ^{o}C in the microwave yielded the corresponding aldehyde compound, **44**, figure 5.5a. A cell viability assay with MCF7 cells was set up and

compounds **41** and **44** tested. The results shown in figure 5.5b showed this not to be the case, however. Compound **41** gave an EC_{50} value of 9.3 nM, in agreement with the previous viability assays, whereas compound **44** was non active with only an estimated EC_{50} value of 7.9 M (this value is inaccurate, however, due to the lack of data points).

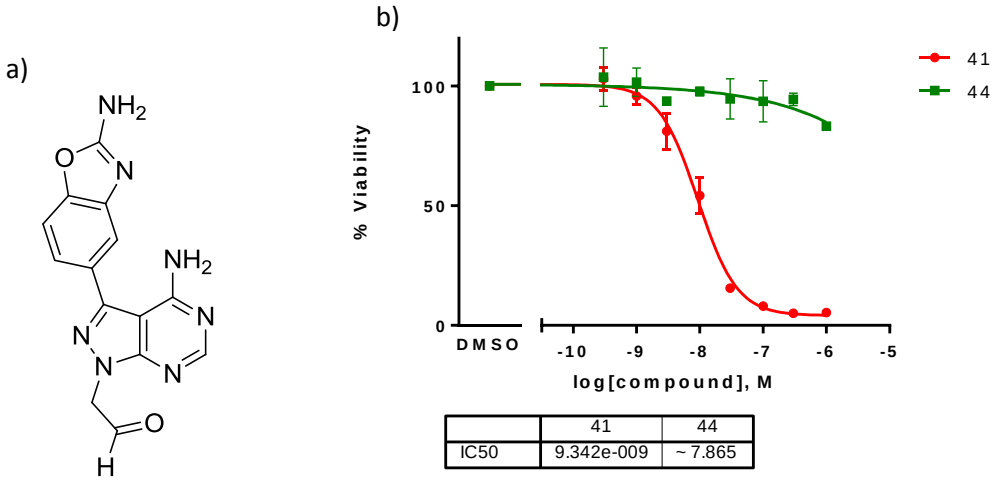

Figure 5.5: *a) Structure of compound 44. b) MCF7 cell viability dose response curves and corresponding EC_{50} values comparing compounds **41** and **44** (n=3, error bars denote standard deviation).*

To further back up the evidence that the compounds were not being hydrolysed, a non-cell conversion assay was set up where compound **41** was incubated with water at 37 ^{o}C and 0.1M HCl at 37 ^{o}C to imitate the extreme gastric acid conditions. The Eppendorfs containing the solutions were shaken on a thermoshaker and aliquots taken after 0, 0.5, 1 and 2 hours. Compound stability was determined by mass spectrometry. Shown in figure 5.6 are two mass spectra from the water only experiment at time 0 (a) and 2 h (b), respectively, each showing the unaltered compound **41** mass (M+1 = 384.2). The same was observed for the 0.1M HCl experiment, thus, confirming that no hydrolysis was occurring, even under moderately acidic conditions such as those found in the stomach.

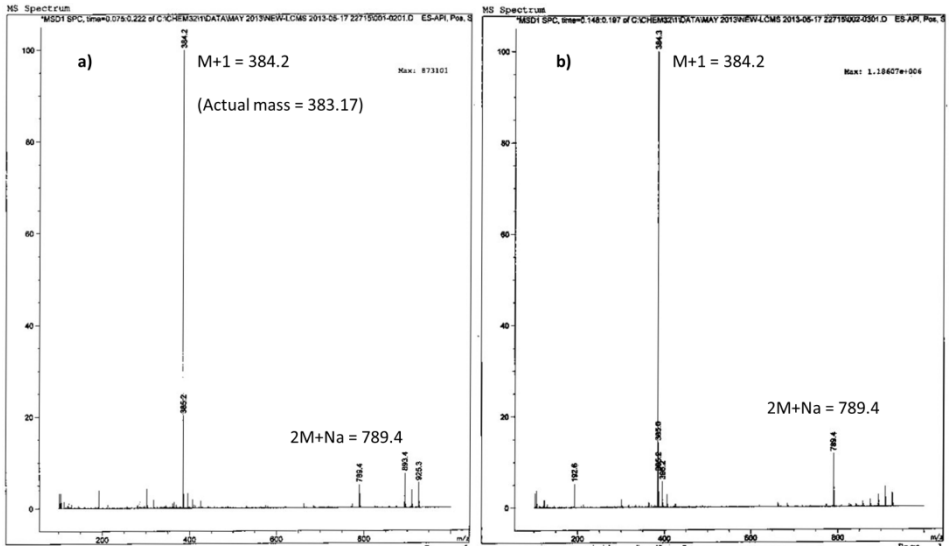

Figure 5.6: *Non-cell conversion assay of compound **41** to determine stability of acetal in water at 37 °C. a) Mass spectrum of compound **41** immediately after dissolving in water at 0.5 mg/ml. b) Mass spectrum of compound **41** after incubation in water at 37 °C for 2 hours.*

5.2.5 Further Optimisation of Compound 41 to Increase Potency Against mTOR

In order to explore some more SARs around the south part of the mTOR inhibitors, a couple of more compounds were synthesised implementing small changes to try and gain some potency over mTOR and perhaps the PI3K enzymes. Methylcyclopentyl and 2-methyltetrahydrofuran moieties were chosen for the south part of the new compounds. Their synthesis was identical to before and is shown in scheme 5.2 along with the new compounds' structures, **47** and **48**.

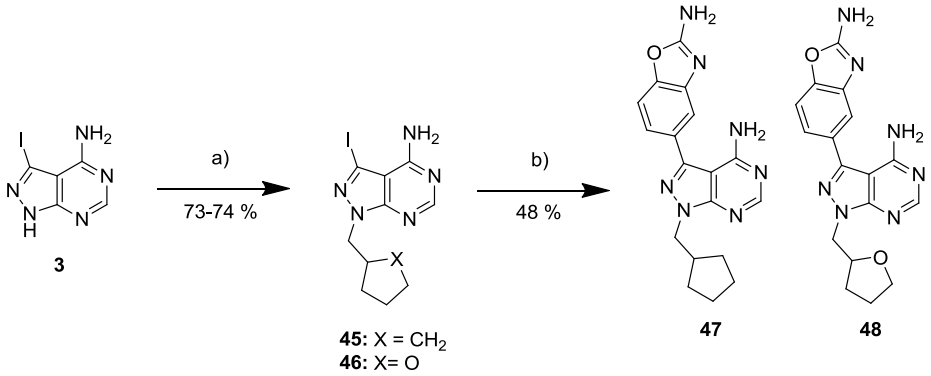

Scheme 5.2: *mTOR inhibitor further optimisation. a) (iodomethyl)cyclopentane (**47**) or 2-(bromomethyl)tetrahydrofuran (**48**), NaH, DMF, 150 °C, mw. b) 5-(4,4,5,5-tetramethyl-1,3,2-dioxaborolan-2-yl)-1,3-benzoxazol-2-amine, K_2CO_3, $Pd(OAc)_2$, PPh_3, 1,4-dioxane/water (10:1), 120 °C, mw.*

The new compounds were tested alongside compound **41** and INK-128 for comparison against MCF7, MDA-MB-231 and PC3 cell proliferation. MDA-MB-231 cells are triple negative breast cancer cells and PC3 are prostate cancer cells. The results, shown in figure 5.7, revealed compound **47** had excellent potency against all three cell types, exceeding that of the original compound, **41**, and the 'gold standard', INK-128. Compound **48** was equivalent in terms of EC_{50} values, to compound **41**. INK-128 showed EC_{50} values in agreement with literature (PC3 cells EC_{50} = 17 nM).[35]

All 4 of the compounds showed greater potency against the HER2 positive MCF7 cells than the triple negative MDA-MB-231 cells. This could suggest some preclinical indication as to which patient population would be eligible for treatment using these therapies. It was important to test their potency against the targets, in isolation, and to test in further assays, in order to determine their differences.

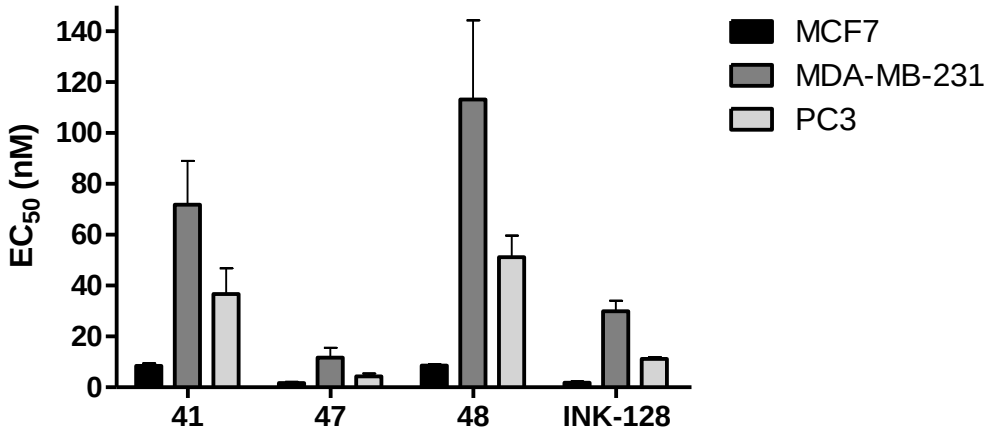

Compound\Cell Type	MCF7	MDA-MB-231	PC3
41	8.40	71.87	36.71
47	1.67	11.71	4.31
48	8.62	113.25	51.16
INK-128	1.81	29.95	11.21

Figure 5.7: *EC_{50} values (nM) against MCF7, MDA-MB-231 and PC3 cell proliferation over 5 days of compound treatment determined from half-log dose response curves. Error bars denote standard deviation; n = 3.*

5.2.6 Cell Cycle Assay

With mTOR being heavily involved in protein synthesis and the cell cycle it was important to check what effects the compounds were exerting on the cell cycle.[35] It was already previously noticed on the IncuCyte that MCF7 cells appeared to stop growing in response to treatment with compound **19** so an assay was designed to look at whether, after treatment with our compounds, stages of the cell cycle were being altered. For this purpose cells were seeded at higher density (5000 cells/well) and treated with compounds for 24 hours as a concentration gradient with DMSO (0.1 %) as negative control. The cells were then fixed with 4 % PFA in PBS and stained for DNA (DAPI or Hoechst), phospho-histone H3 (anti-pHH3 rabbit antibody with AlexaFluor®-594 goat anti-rabbit IgG) and cyclin B1 (anti-cyclin B1 antibody with AlexaFluor®-488 donkey anti-mouse IgG). Images were then taken using either the Scan^R fluorescence microscope from Olympus or the ImageXpress System from Molecular Devices and analysed using scan^R or ImageXpress software.

Cells were classified according to their DNA content into G1, S or G2 stages. Early or late mitotic cells were classified according to their cyclin B1 or phospho-histone H3 expression levels within the nuclear compartment, respectively. The compounds were tested against MCF7, MDA-MB-231 or PC3 cells as a comparison across distinct cancer cell types, figure 5.8.

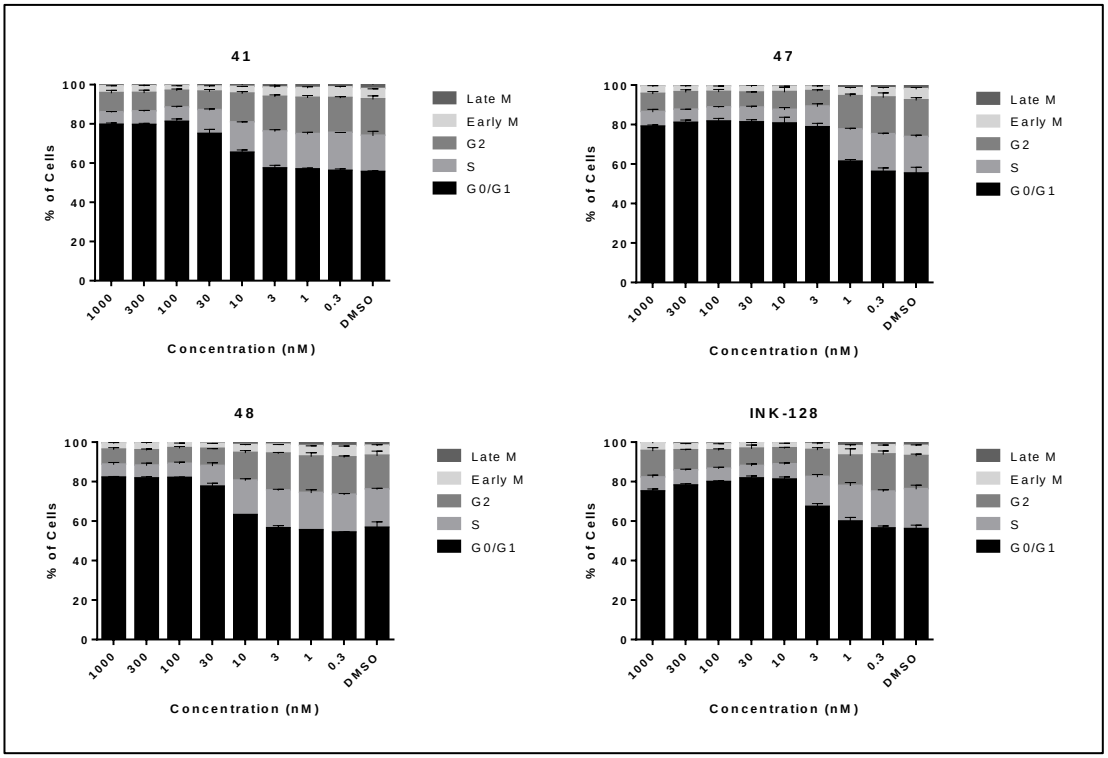

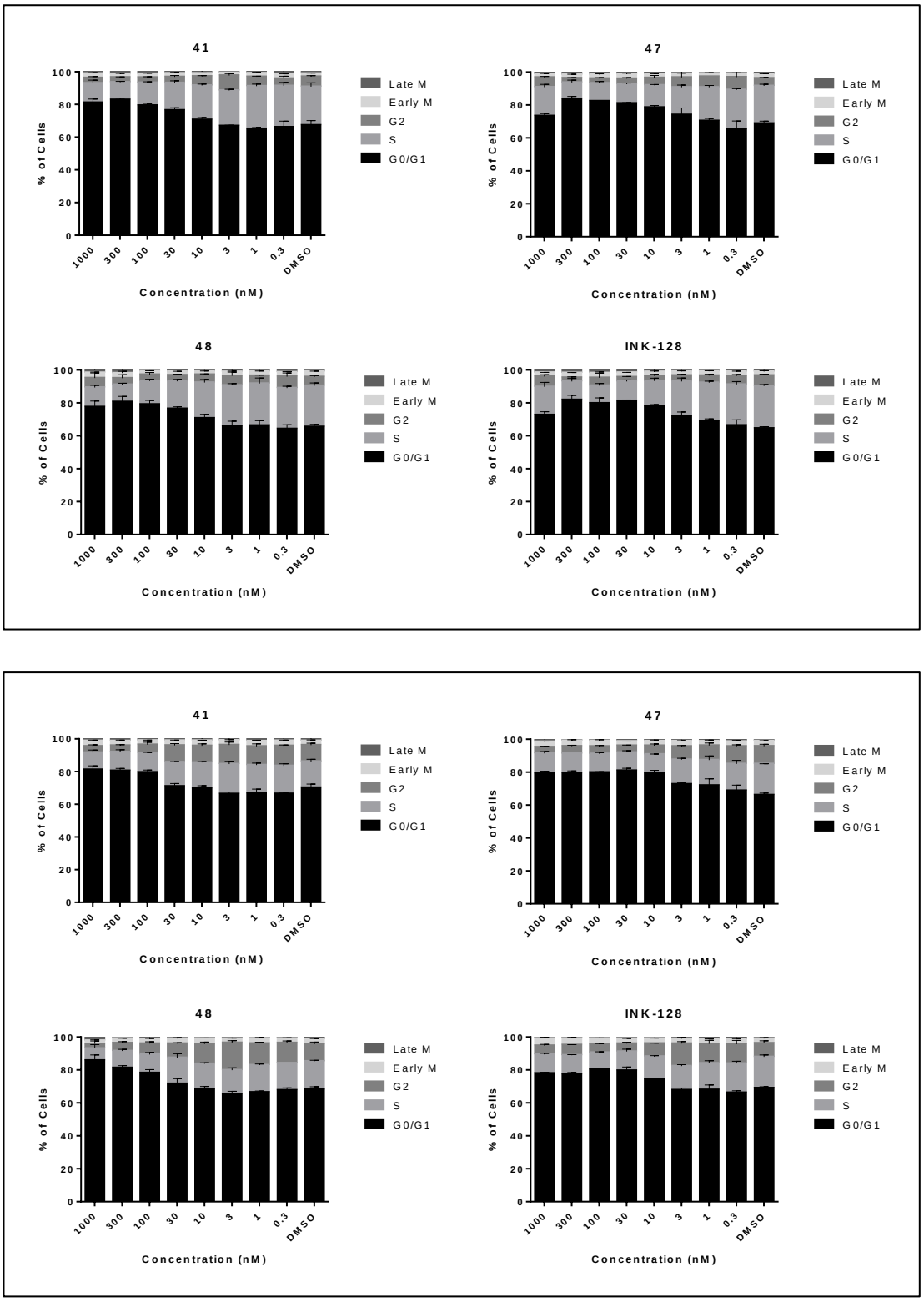

Figure 5.8: *Effects of compounds **41, 47, 48** and INK-128, across a concentration gradient, on the cell cycle of MCF7 cells (top), MDA-MB-231 cells (middle) and PC3 cells (bottom) following 24 hours treatment. Cell cycle stage was determined by DNA content and mitotic stage by cyclin B1 and phospho-histone H3 content, respectively (n=3, error bars denote standard deviation).*

All compounds, in all cell types, caused an arrest in the G0/1 stage of the cycle, the longest phase and, consequently, most abundant in cells. More likely, is that there is an increase in the number of cells in the G0 or resting phase which have simply halted the cell cycle process and are no longer dividing due to the disruption of key pathways downstream of mTOR and essential for cell growth. Consequently, there is a decrease in the number of cells in the synthesis, S, and G2 stages. Rather than the compounds decreasing the number of cells in the S and G2 stages by mTOR inhibition, these stages have, more than likely, gone down due to the lagging effect from G0/1 arrest.

The compounds follow a similar trend in terms of potency of that seen in the cell viability assay. Compounds **47** and INK-128 show the greatest effect with cell disruption occurring as low as 3 nM concentration. Compounds **41** and **48** share similar trends and generally affect the cell cycle around 10 nM. Arrest of the cell in the G0/1 phase by INK-128 is in agreement with previously published literature.[35]

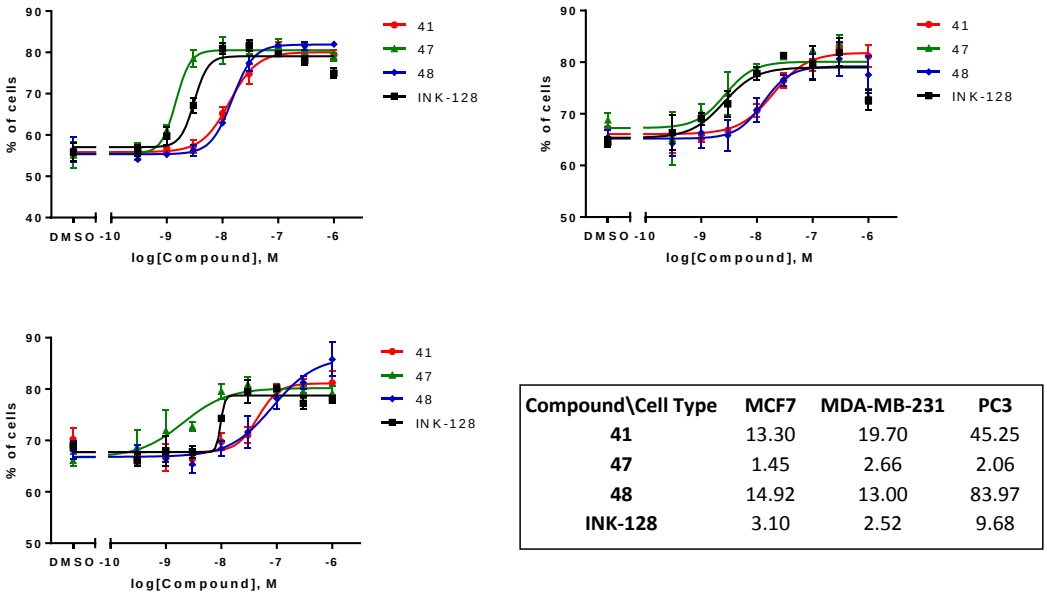

Compound\Cell Type	MCF7	MDA-MB-231	PC3
41	13.30	19.70	45.25
47	1.45	2.66	2.06
48	14.92	13.00	83.97
INK-128	3.10	2.52	9.68

Figure 5.9: *Curve fits of percentage of MCF7 (top left), MDA-MB-231 (top right) and PC3 (bottom left) cells in G0/1 stage after treatment with compounds **41, 47, 48** and **INK-128** and their corresponding EC_{50} values (nM, bottom right). (n=3, error bars denote standard deviation).*

Figure 5.9 shows the G0/1 data from the cell cycle experiment plotted as concentration against percentage of cells and the corresponding calculated EC_{50} values. This allows for a clearer comparison of compound and cell type. From these values it is evident that the

compounds are affecting MCF7 cells slightly more so than the other types. Again, this follows the same trend seen in the viability experiment. Further, compounds **41** and **48** share similar values as do **47** and **INK-128**. Structurally, these pairs are more alike which can explain their shared potency values. More than likely this pattern was arising from selectivity and potency against their kinase targets – namely mTOR, but also the PI3K enzymes, structurally similar to mTOR and known to be inhibited by INK-128.[35] It was, again, essential to calculate IC_{50} values against kinase inhibition *in vitro*.

5.2.7 Kinase Data for Compounds 41, 47, 48 and INK-128

The kinome screen had revealed that compound **41** was inhibiting DDR1, DNA-PK, PI3K-α and PI3K-γ along with mTOR and so the IC_{50} values were determined for these enzymes along with PI3K-β and PI3K-δ. Compounds **47, 48** and INK-128 were also tested against these kinases, table 5.2.

Kinase \ Hit	41	47	48	INK-128
	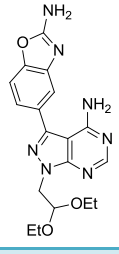	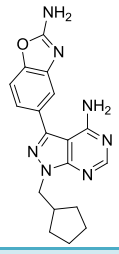	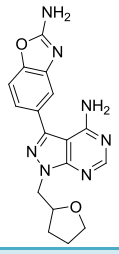	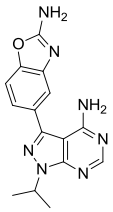
DDR1	2106	4.7	137.0	ND
DNA-PK	320.1	3.1	47.7	10.0
mTOR/FRAP1	**15.3**	**1.8**	**1.8**	**1.4**
PI3K-α	980.9	3.5	44.2	152.0
PI3K-β	$>10^5$	88.7	1118	4700
PI3K-γ	1336	4.9	76.8	156.0
PI3K-δ	1841	7.3	149.0	ND

Table 5.2: *Kinase screening data for compounds **41, 47, 48** and INK-128 (nM). INK-128 data was obtained from published data.[35] Data highlighted in green indicates mTOR inhibition below 1 μM. ND: Not determined.*

The results revealed the extent of compound **41**'s selectivity, with the next most inhibited enzyme being DNA-PK (IC_{50} of 320.1 nM) – 20 times greater than that of mTOR. All other targets tested had IC_{50} values greater than 60 times compared with mTOR, quite a

remarkable selectivity profile for a compound that was fundamentally designed by phenotypic screening.

It is noteworthy that compound **47** had gained a magnitude of potency with an IC_{50} of 1.8 nM against mTOR, compared with **41**, figure 5.10. This is in great correlation with the similar pattern observed in the cell viability and cell cycle assays. **47** was also very potent against all 7 kinases tested showing low nano-molar IC_{50} values in all but PI3K-β. This dual PI3K/mTOR inhibition is not new and, indeed, many compounds discovered previously have shown dual inhibition of these targets.[70, 92] Compared to INK-128, compound **47** is equally potent against mTOR, however, more potent against all other targets tested.

Compound **48** gave the most interesting results from this study. Although it has equal potency against cell viability as **41**, **48** was 8 times more potent against mTOR than **41** with an IC_{50} of 1.8 nM, comparable to **47**. Compound **48** also showed increased potency against all other kinases tested in this assay, compared with **41,** but still retained the same selectivity for mTOR with >20 times selectivity for mTOR over the other tested kinases. The difference in potency seen in the cell viability and cell cycle assays may, therefore, be due to the compounds' pharmacokinetic properties rather than their activities against their targets.

5.2.8 Western Blot Analysis of Compound 41

To test whether the compounds were able to inhibit mTOR to the same degree in cells as in the isolated target, a Western blot experiment was set up using MCF7 cells treated with compound **41** or INK-128. MCF7 cells were seeded at 1 x 10^6 cells per well in a 6-well plate then serum starved (0.1% FBS v/v) for 24 hours. Cells were incubated with drug for 30 minutes at varying concentration, with DMSO (0.1% v/v) as negative control, then stimulated with FBS for an hour, lysed and Western blots run as described in section 10.7.5.

To test for mTOR inhibition, antibodies corresponding to targets downstream of the mTOR complexes were incubated with the blot. mTOR is not activated via auto-phosphorylation like many other proteins found in the cell and so antibodies corresponding to mTOR phosphorylation sites would not prove that the compounds were inhibiting mTOR but only, perhaps, upstream targets.[112] That being said, by inhibiting mTOR, and therefore, its downstream targets, complex feedback mechanisms may, ultimately, result in a decrease of mTOR phosphorylation caused by other proteins upstream of the mTOR complexes.[107, 113]

It is, perhaps, easier to look at the AKT signalling pathway in order to simplify the downstream targets of mTOR, figure 5.10. There is still little known about mTORC2, however, it has been shown to activate AKT by phosphorylation at serine 473.[36] Downstream of mTORC1 are the proteins P70S6K and S6K, phosphorylated by mTOR at sites threonine 389 and serine 235/236, respectively, figure 5.10. The intensity of phosphorylation of these three proteins was determined in the Western blot.

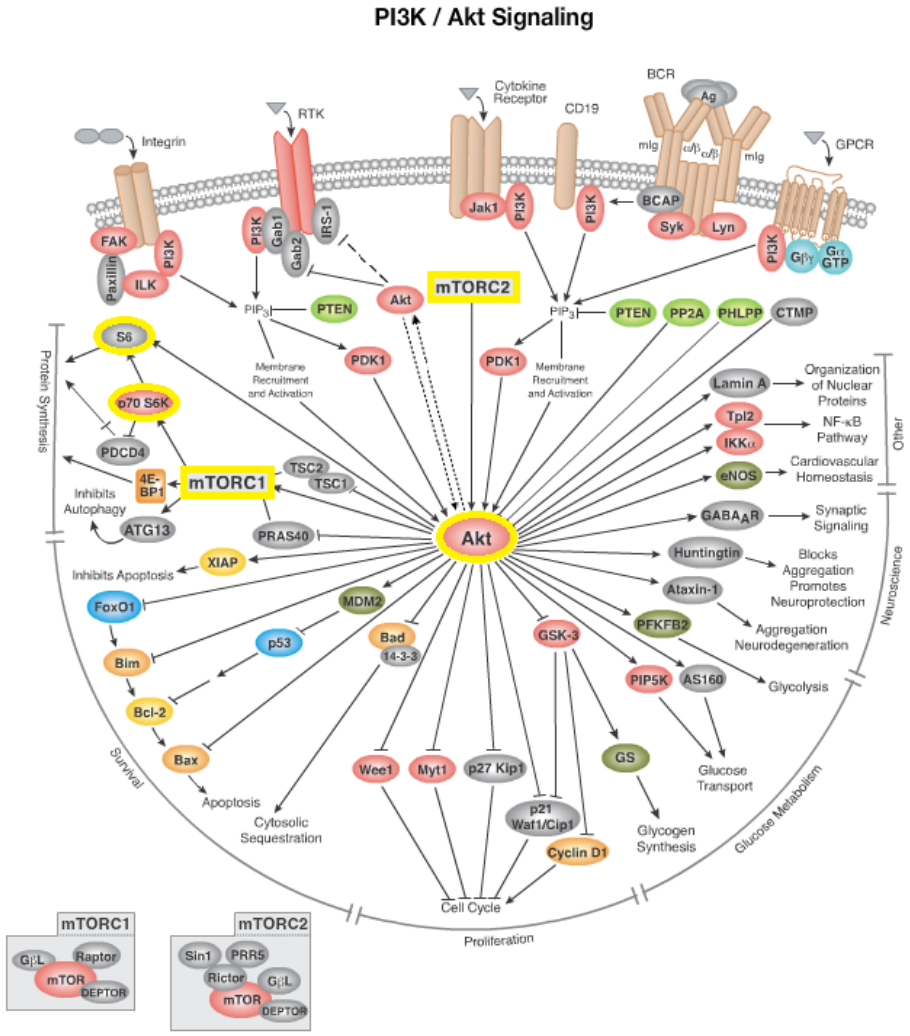

Figure 5.10: *PI3K/AKT signalling pathway. Key proteins involved in the downstream pathway of mTOR are highlighted in yellow. Illustration reproduced courtesy of Cell Signaling Technology, Inc. (www.cellsignal.com).*

The inhibition of pAKT at serine 473, along with pP70S6K and pS6K, may prove that both mTORC1 and mTORC2 are being targeted by the compounds as pAKT is only phosphorylated by mTORC2 (Rapamycin treatment, which only targets mTORC1, does not inhibit pAKT). However, it is important to take into account that PI3K activity also leads to

AKT phosphorylation. Therefore, inhibition of pAKT can result from both mTOR and PI3K inhibition. In addition, with longer treatment, feedback mechanisms and the complexity of signalling pathways may result in a reduction of the phosphorylation of AKT with Rapamycin.

To study the inhibition of mTOR by the compounds, antibodies corresponding to the phosphorylation sites of P70S6K, S6K and AKT were used. The developed blot is shown in figure 5.11, below.

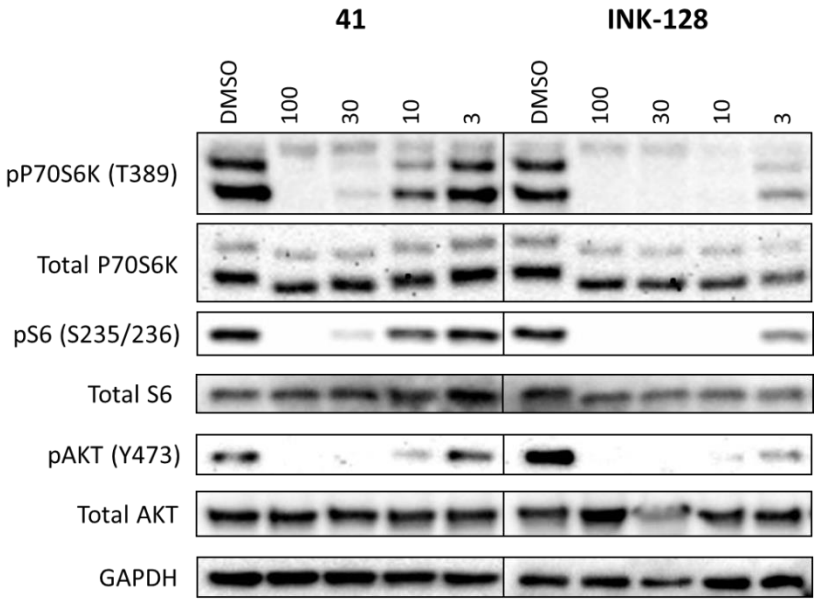

Figure 5.11: *Western blot of MCF7 cells treated with compound **41** or INK-128 at varying concentrations with DMSO (0.1% v/v) as negative control. Concentrations are in nM.*

The Western blot data are in agreement with the inhibition of mTOR at the ATP site. Compound **41** inhibits the phosphorylation of downstream targets of mTOR roughly ten times less than INK-128. This observation is in good correlation to the IC_{50} values calculated against the target in isolation. The inclusion of total P70S6K, total S6 and total AKT antibodies show that only the phosphorylation of these targets was being effected and not their overall levels of expression. This is to be expected with such a short incubation period. GAPDH was used as a loading control.

The data show that compound **41** is capable of inhibiting mTOR *in vitro* at therapeutically acceptable levels and in excellent correlation with previous phenotypic cell assay results.

5. The Development of Novel, Potent and Selective mTOR Inhibitors

5.3 Conclusion

Using the clinical candidate compound, INK-128 as a model, and varying the type of acetal group found in compound **19**, 3 new compounds were developed with low nano-molar activities against MCF7 cell proliferation. Compounds **41-43** had their inhibition against mTOR determined by kinase screening which revealed them to be very selective mTOR inhibitors with IC_{50} values of 15.3, 58.9 and 25.3 nM, respectively. The compounds showed no other inhibition over the original 14 kinases tested, however, slight inhibition was observed with compound **43** against PI3K-δ with an IC_{50} of 98.9 nM.

Lead compound **41** had its selectivity towards mTOR determined by whole kinome screen revealing it to be extremely selective towards mTOR with only DNA-PK, DDR1, PI3K-α and PI3K-γ being the other kinases inhibited. This was superior over current gold standard, INK-128. Further, compound **41** was shown to be stable in aqueous and acidic conditions concluding that the acetal group was, indeed, responsible for activity and selectivity.

Further optimisation led to compounds **47** and **48** which showed very potent inhibitory properties over cell proliferation. Cell cycle analysis showed compound **47** was capable of arresting the G0/1 stage at concentrations as low as 3 nM with **41** and **48** being slightly weaker at 10 nM.

Western blot confirmed the effects seen on the cell cycle and proliferation were in fact due to inhibition of mTOR as confirmed by decreased phosphorylation of downstream targets of mTOR.

Compound **41** represents the most selective mTOR inhibitor to date. Although only having an IC_{50} of 15.3 nM, its extreme selectivity suggests that higher concentrations may be used to achieve the desired anti-tumoral effects *in vivo*. However, due to the similarities in their structures to INK-128 (lack of freedom to operate), the progression of these series of mTOR inhibitors was not pursued any further and efforts were prioritised on developing the SRC inhibitors.

6. The Development of Novel, Potent and Selective SRC Family Kinase Inhibitors

6.1 Introduction & Aims

Compound **29** was shown to be a potent SRC family inhibitor (IC_{50} = 27 nM) and it was hypothesised that through modification of the structure the potency and selectivity towards SRC and its members could be improved over such drugs as PP1 and other SRC family inhibitors. Examples of highly selective SRC inhibitors have been reported previously, however, the most selective of which (compound 4) only inhibited SRC with an IC_{50} of 86 nM which is 3x less potent than compound **29**.[114] Further to its modest potency against SRC, compound 4 had an EC_{50} against MCF7 cell proliferation of 11 µM which is relatively high, even compared with our early 'hit' compound's (**29**) value of 2 µM.[114]

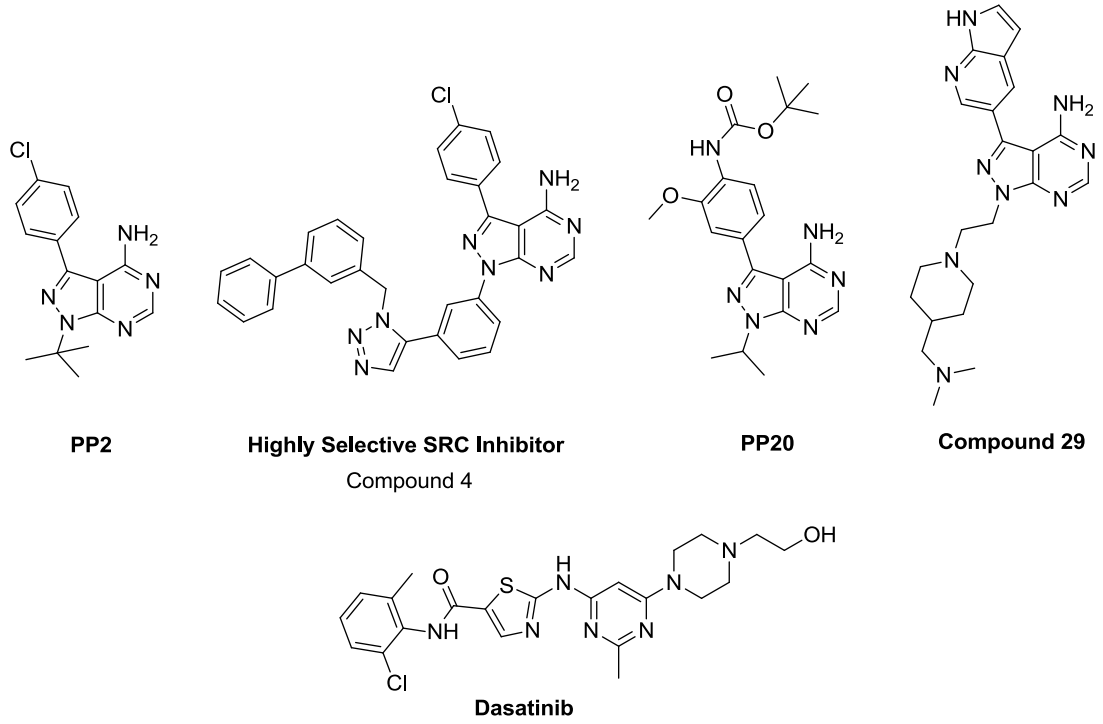

Figure 6.1: *Structure of PP2, a non-selective SRC family inhibitor similar to PP1; a highly selective, but not potent, SRC inhibitor derived from PP2; PP20, a potent SRC family inhibitor; compound **29** and Dasatinib, a potent SRC/ABL inhibitor approved for Imatinib resistance CML patients. Both PP20 and Dasatinib were used as comparisons in later assays.*

6. The Development of Novel, Potent and Selective SRC Family Kinase Inhibitors

6.2 Results

6.2.1 The Synthesis and Testing of Lead Compound 52

Looking back to compounds **14, 17** and **18** it was evident that on-target potency was favoured on the shorter amine groups over the longer chains i.e. compound **14** was >8x more potent against SRC than compound **18**, table 6.1. To corroborate this, compound **49** was synthesised, scheme 6.1, with 4-dimethylaminopiperidine, and tested against MCF7 cell proliferation then screened against the kinases tested previously, table 6.1. Compound **49** had an EC_{50} against MCF7 proliferation of 1.35 μM comparing equally to compound **29**'s value of 1.94 μM.

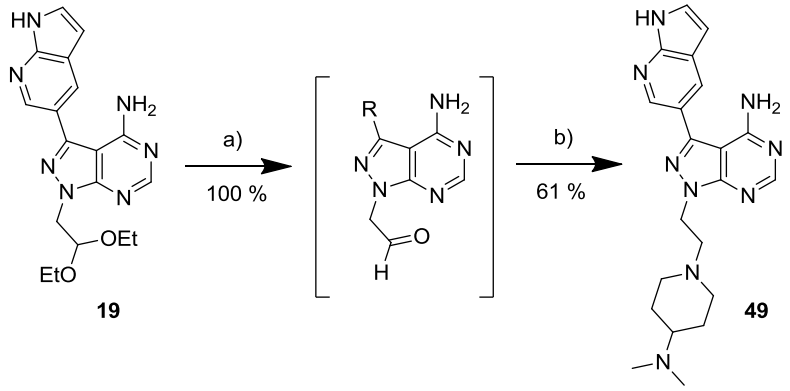

Scheme 6.1: *Compound **49** synthesis. a) TFA/water (1:1), 100 °C, mw. b) N,N-dimethylpiperidine-4-amine, AcOH, $NaBH(OAc)_3$, DCM, r.t.*

Interestingly, the kinase results showed the opposite trend as seen with compounds **14, 17** and **18** with the 4-(dimethylamino)piperidine compound (**49**) being less potent against the SRC family members than the 4-((dimethylamino)methyl)piperidine compound (**29**). Interestingly, the same reduction of potency was found for ABL.

Kinase \ Hit	14	17	18	29	49
	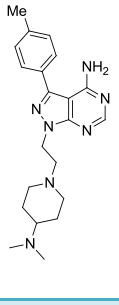	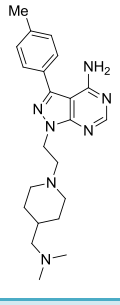	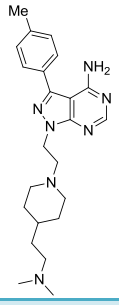	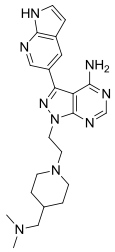	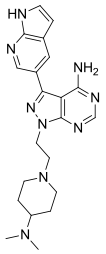
c-ABL	6323	7525	7249	115.7	283.0
BLK	1545	2846	7072	110.1	321.0
FGR	115.0	399.6	600.8	45.3	31.8
FRK/PTK5	915.8	1635	3700	105.6	147.0
FYN	311.1	913.0	1964	37.8	67.6
HCK	1523	6009	11630	36.1	1660
c-KIT	27360	77080	$>10^5$	18850	$>10^5$
LCK	727.0	1542	4344	232.8	321.0
LYN	284.9	1068	2508	25.2	85.3
mTOR/FRAP1	$>10^5$	$>10^5$	$>10^5$	8565	6700
PDGFRa	70500	$>10^5$	$>10^5$	$>10^5$	$>10^5$
RET	6584	22590	10840	288.9	465.0
c-SRC	126.0	302.7	1040	26.9	67.0
YES/YES1	71.4	344.5	696.5	12.3	28.9

Table 6.1: *IC_{50} values (nM) of compounds **14, 17** and **18** against various kinases showing decreasing potency with longer chain length against SRC. Compound **29** compared with compound **49** shows smaller amine had an opposite effect in this case. Values in red indicate an IC_{50} below 100 nM.*

In order to increase the potency of compounds **29** and **49,** thoughts turned to modifying the aryl group further as previous evidence suggested that potency was delivered from the aryl group and selectivity from the amine moiety. The breakthrough paper by Beth Aspel *et. Al.* published in Nature Chemical Biology, 2008, provided inspiration. Through their work, they discovered a series of new compounds which inhibited kinases, both selectively, and dual inhibitors of PI3Ks and tyrosine kinases.[92] As well as many other compounds, they discovered compound PP20, figure 6.1, a very potent (< 1 nM) SRC inhibitor which also targets ABL (< 1 nM), HCK (< 1 nM) and EGFR (168 nM). PP20 is also based around the pyrazolopyrimidine scaffold and was derived from two compounds (S1 and S2) which have very similar structures to PP1/2.

Based on PP20's aryl motif, compounds **51** and **52** were synthesised to represent both amine moieties found in compounds **29** and **49**, scheme 6.2. This time, in order to protect the Boc protected amine group, and avoid the polymerisation issues found with some derivatives discussed during chapter 3, the synthesis steps were reversed so that the reductive amination to introduce the amine occurred before the Suzuki reaction to introduce the aryl group.

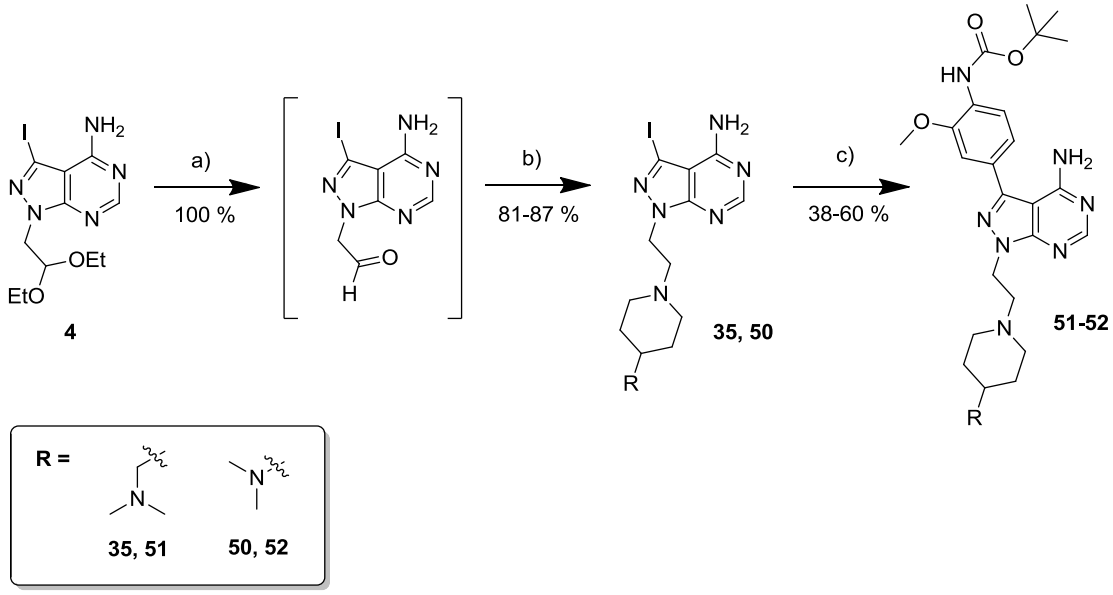

Scheme 6.2: Synthesis of c*ompounds **51** and **52**. a) TFA/water (1:1), 100 ^{o}C, mw. b) N,N-dimethylpiperidine-4-amine (**50**) or N,N-dimethyl-1-(4-piperidyl)methanamine (**35**), AcOH, $NaBH(OAc)_3$, DCM, r.t. c) [4-(tert-butoxycarbonylamino)-3-methoxy-phenyl]boronic acid, K_2CO_3, $Pd(OAc)_2$, PPh_3, 1,4-dioxane/water (10:1), 120 ^{o}C, mw*

As before, compounds **51** and **52** were tested in an MCF7 cell viability assay to assess their anti-proliferative potency. As the founding paradigm of this thesis work, compounds are only progressed after corroborating the induction of strong phenotypic effects. The compounds were also tested in another cancer cell line, MDA-MB-231, which are triple negative breast cancer cells. Dasatinib, a potent SRC/c-ABL inhibitor used for the treatment of chronic myeloid leukaemia (CML), was tested alongside compounds **51** and **52** in the viability assay. PP20 was synthesised (scheme shown in appendix 3) and tested also.

The results of the viability assay showed compound **52** to be much more potent than previous compounds with EC_{50} values of 40.35 and 10.09 nM in MCF7 and MDA-MB-231 cells, respectively. Compound **52** was also much more potent in both cell types compared with **51**. This is contradictory to the order of observed potencies against SRC kinase with

compounds **29** and **49** when comparing the 'south' amine moiety. Compared with Dasatinib, compound **52** showed superior potency in the MCF7 cells but both were equal, and much more potent, in MDA-MB-231 cells. This was an early suggestion of a possible indication area for the compounds – triple negative breast cancer is currently poorly treated and in need of much better therapies. An EC_{50} value of 10 nM is very potent in terms of cell proliferation and a very acceptable value to begin thinking about further pre-clinical development and clinical applications for the compounds, although, the properties of these compounds required much more evaluation. Regardless of their structural similarities, PP20 displayed lower anti-proliferative properties against these two cell lines, with EC_{50} values of 1843.5 and 155.0 nM, respectively. This poorly correlates with the sub-nanomolar potency against the SRC and ABL kinases *in vitro* and perhaps explains why this compound has never attracted much attention by the scientific community (there are no references of studies with PP20 apart from the original work from Aspel at Al. previously mentioned).

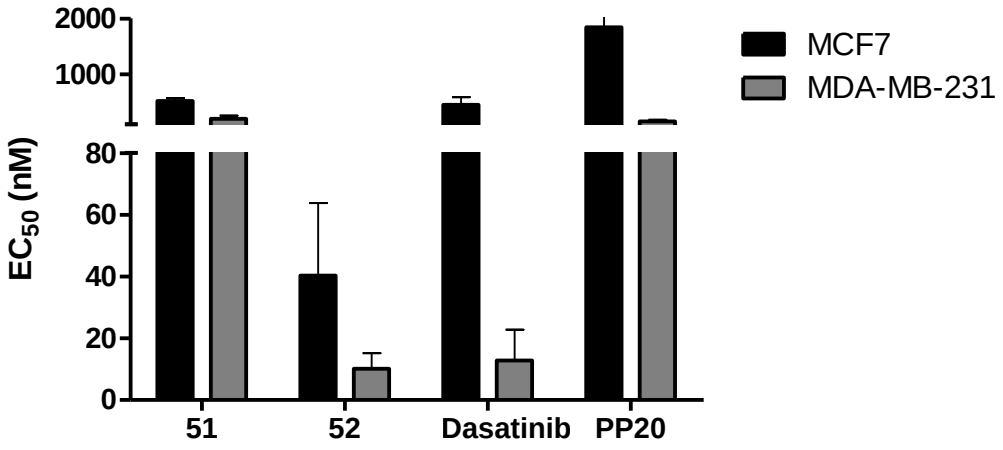

Compound\Cell Type	MCF7	MDA-MB-231
51	520.47	197.45
52	40.35	10.09
Dasatinib	451.10	12.82
PP20	1843.50	155.00

Figure 6.2: *EC_{50} values (nM) of compounds **51, 52**, Dasatinib and PP20 against MCF7 and MDA-MB-231 cell proliferation. Error bars denote standard deviation; n = 3.*

Differences in potency between compound **51** and **52** in this viability assay may be due, more so, to physicochemical properties rather than their potency against SRC. To test this

hypothesis, again, the two compounds were screened against the 14 previously tested kinases, table 6.2.

The study revealed compounds **51** and **52** to be very potent SRC inhibitors with sub-nanomolar IC_{50} values. This potency is comparable to Dasatinib and PP20. Further, the compounds were much more selective towards the SRC family members than Dasatinib with no activity against c-KIT, PDGFRa or RET. Compounds **51** and **52** were even more selective within the SRC family members with sub-nanomolar potency observed in 4 and 3, respectively, of the 9 members.

Most importantly, the compounds show low inhibition of c-ABL, highlighted in blue in table 5.2, with IC_{50} values of 189 and 479 nM, respectively. Compared with Dasatinib's sub-nanomolar value this is greater than 950-fold difference in inhibition.

Kinase \ Hit	51	52	Dasatinib	PP20
	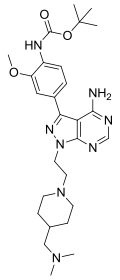	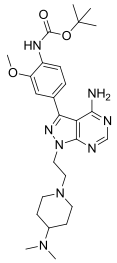	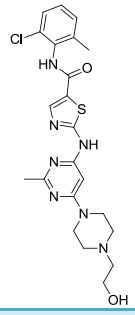	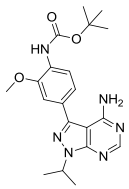
c-ABL	189.0	479.0	< 0.5	<0.5
BLK	3.3	5.4	< 0.5	NR
FGR	< 0.5	< 0.5	< 0.5	NR
FRK/PTK5	8.8	2.8	< 0.5	NR
FYN	4.6	2.0	< 0.5	NR
HCK	1.3	2.8	1.9	<0.5
c-KIT	7130	6460	39.0	NR
LCK	< 0.5	< 0.5	< 0.5	NR
LYN	2.5	0.85	< 0.5	NR
mTOR/FRAP1	$>10^5$			NR
PDGFRa	$>10^5$		9.9	NR
RET	$>10^5$		433.0	<0.5
c-SRC	< 0.5	< 0.5	< 0.5	NR
YES/YES1	< 0.5	< 0.5	< 0.5	NR

Table 6.2: *IC_{50} values (nM) of compounds **51, 52** and Dasatinib against the 14 previously tested SRC family kinases. Values in red indicate an IC_{50} below 100 nM. Values in blue indicate c-ABL inhibition. Blank boxes indicate no inhibition. NR = Not reported.*

The importance of ABL inhibition in cancer is discussed in section 6.2.2. Comparing to the 'parent' compound, PP20, the study showed that by incorporation of groups other than isopropyl or t-butyl (in the case of PP1) selective inhibition of SRC family kinases over ABL was possible, and to this date, compounds **51** and **52** represent the first sub-nanomolar inhibitors against SRC which do not inhibit ABL.

6.2.2 The Anti-Oncogenic Role of c-ABL in Cancer

Quite recently it has emerged that c-ABL may actually have paradoxical roles depending on the cancer context. Indeed, there are evidences that it is anti-oncogenic in certain cancers, particularly breast cancer.[114, 115] This means that inhibition of ABL in breast cancer can actually promote the disease rather than supress it. There is contradictory evidence on the exact role of ABL in the promotion or suppression of cancer; however, recent clinical trials involving Imatinib, a potent ABL inhibitor, have resulted in either no benefit or disease progression and toxicity.[115] To test this hypothesis, we decided to study whether the anti-proliferative activity of the highly selective SRC inhibitor **52** could be antagonised in the presence of a highly selective ABL inhibitor. Therefore, a dose ratio matrix combination assay was set up using compound **52** and GNF-2, a specific ABL allosteric site inhibitor, figure 6.3.

a)

	52								
GNF-2	**Concentration (nM\µM)**	100	30	10	3	1	0.3	0.1	0.03	DMSO
	1000	40.00	45.24	45.08	41.90	32.47	27.46	22.86	18.82	21.73
	100	56.50	61.09	59.55	56.42	46.01	41.43	34.76	27.36	27.48
	10	86.85	86.69	88.87	85.26	74.78	63.55	54.20	49.95	50.18
	1	104.75	99.67	105.82	106.12	101.73	97.51	88.11	77.26	79.75
	0.1	101.49	85.08	100.27	105.94	100.55	101.28	94.72	89.02	90.93
	DMSO	103.83	94.79	102.46	109.44	109.29	108.32	105.38	102.73	100.95

b)

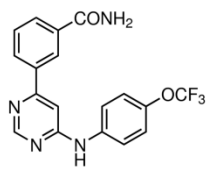

c)

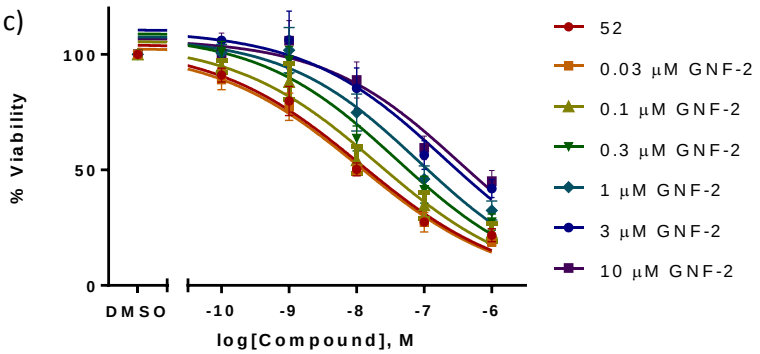

c)

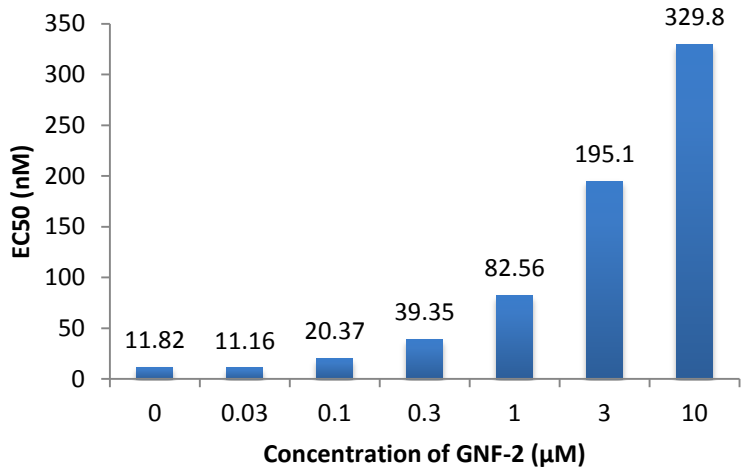

Figure 6.3: *Combination of compound **52** and GNF-2, a specific ABL inhibitor, in MDA-MB-231 cells to test the anti-oncogenic role of ABL in breast cancer. a) Combination matrix showing the percentage of viable cells compared to DMSO (0.2 % v/v). b) Structure of GNF-2. c) Concentration gradient of compound **52** with fitted curves and calculated EC_{50} values at varying concentrations of GNF-2. d) EC_{50} values of compound **52** with varying concentrations of GNF-2 plotted as a bar graph showing an exponential increase in EC_{50} with increasing concentration of GNF2.*

MDA-MB-231 cells were incubated with drug 2 days post seeding, and left for 5 days before analysing with PrestoBlue® cell viability reagent. Compound **52** was dosed along a log scale concentration gradient ranging from 1000 to 0.1 nM down the inner columns of 96-well plates. GNF-2 was dosed along a half-log scale ranging from 100 to 0.03 µM along the inner rows of 96-well plates – see the schematic in figure 6.3a. As both compounds were used in DMSO, the resulting final concentration was 0.2 % v/v DMSO in the plate. As such, all results were normalised to 0.2 % v/v DMSO.

The assay revealed an antagonistic combination between the two drugs. Compound **52** on its own gave an EC_{50} value in agreement with previous experiments, however, with increasing doses of GNF-2 (> 0.03 µM), the EC_{50} value rose from 12 nM to 330 nM at 10 µM GNF-2. This is greater than a 27-fold difference in potency through increasing ABL inhibition. Although it did not promote the growth, the effect of GNF-2 on MDA-MB-231 cells was minimal, even at 100 µM. This further reinforces the idea that ABL inhibition has no place in breast cancer therapy and that breast cancer, in particular, triple negative breast cancer, could be an ideal indication area for potent and selective SRC inhibition therapy.

Remarkably, Dasatinib and GNF-2 also resulted in an antagonistic combination, albeit to a much less pronounced effect than compound **52**, figure 6.4. This may be the result of GNF-

2's allosteric inhibition properties combined with Dasatinib's ATP-site inhibitory properties to give much reduced ABL activity and, thus, increased cell survival.

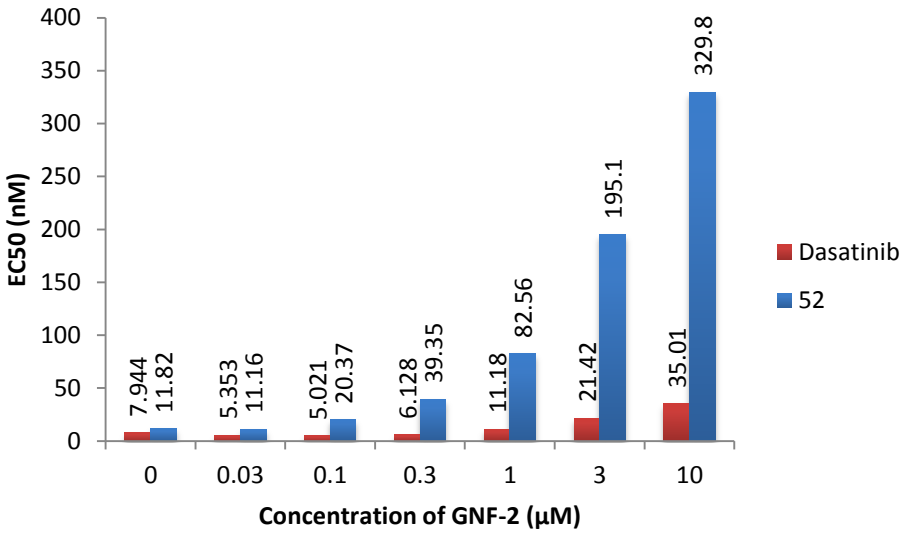

Figure 6.4: *Relative antagonistic combinations of compound **52** and Dasatinib with GNF-2. Combination of **52** and GNF-2 showed a strong antagonistic relationship while Dasatinib and GNF-2 gave a weaker effect due to Dasatinib's already potent ABL inhibitory properties.*

Due to compound **52**'s superior potency in the viability assays and its greater selectivity against ABL inhibition, it was chosen as the ideal compound for further study. Its properties against cell migration, apoptosis and kinome wide selectivity were assessed and are discussed in the next sections.

6.2.3 In Vitro Properties of Compound 52 – Whole Kinome Selectivity

Up to this point, the selectivity of compounds against targets had only been determined using the same 14 kinases, initially chosen as they were shown to be targeted by PP1. Although, proven important in determining the potency of compounds against the SRC family members and selectivity over others such as ABL, mTOR, PDGFRα and RET, it was essential to determine the inhibitory properties of compound **52** over the whole kinome to find any 'off-targets'. The kinome of an organism is the whole set of protein kinases found in a cell of which there are 518 in humans.[116] Compound **52** was screened against 340 wild type kinases by Reaction Biology Corporation – see appendix 1a for list of kinases (which represents the largest available list of kinases currently available in the market for profiling kinase inhibitor selectivity.). Percentage inhibition was determined at a single dose of 1 µM

with 10 μM of ATP in duplicate, relative to DMSO. The duplicates were averaged and plotted using TREEspot™ from DiscoveRx with a 10% cut-off value. The plotted kinome tree results are shown in figure 6.5. Red circles denote kinase inhibition greater than 90% and SRC is highlighted in blue. The interactions mapped include:

ARAF, BLK, BMX/ETK, BRK, BTK, c-SRC, CSK, ERBB4/HER4, FGR, FRK/PTK5, FYN, HCK, LCK, LYN, LYN B, TXK and YES.

Target	% Inhibition
ARAF	98.3
BMX/ETK	97.2
BRK	99.8
BTK	96.2
CSK	95.0
ERBB4/HER4	95.5
TXK	90.9

Table 6.3: *Percentage inhibition of non-SRC family kinases by compound **52** at a single dose of 1 μM, relative to DMSO.*

Of these interactions, 10 (including LYN B) belong to the SRC family which is to be expected giving the previously calculated IC_{50} values. The majority of targets inhibited sit on the SRC family branch of the kinome tree with only two falling outside - ARAF and HER4 – and only ARAF falls out with the tyrosine kinase group into the tyrosine kinase-like (TKL) group.

BRK, also known as protein tyrosine kinase 6 (PTK6) or breast tumour kinase, has recently been discovered as an important target in breast cancer.[117-119] As well as promoting cell growth via stimulation of the cell cycle, BRK has been shown to be involved in the migration and invasion of cancer cells.[117, 119] As compound **52** has been extensively tested in breast cancer cells and triple negative in particular, inhibition of BRK can been seen as an advantage in this setting rather than adverse off-target activity.

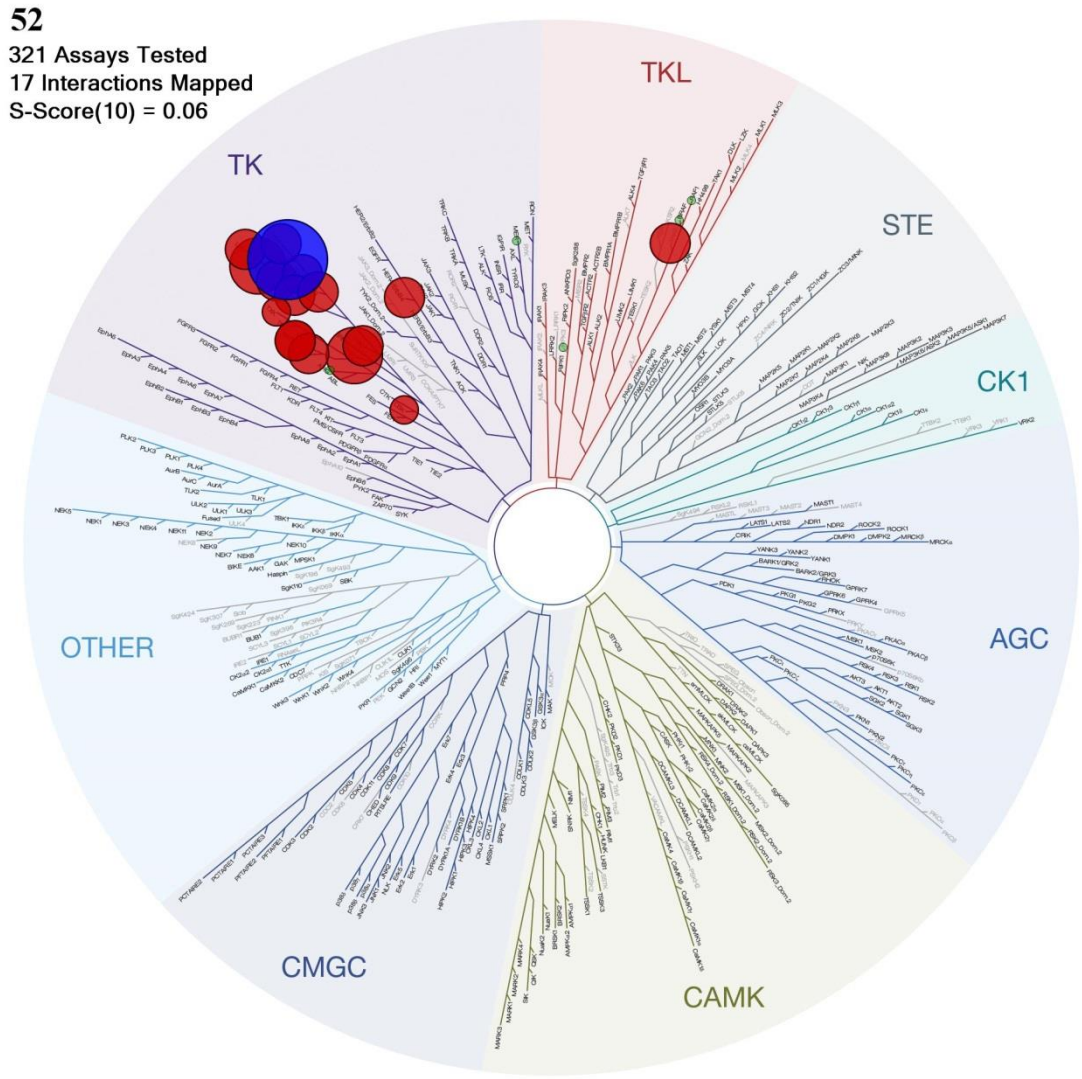

Figure 6.5: *Map of the kinome (excluding lipid, atypical and mutant kinases) showing the selectivity of compound **52** for the SRC family kinases. Red circles denote inhibition greater than 90%, SRC is coloured in blue. 17 kinases were inhibited greater than 90%, at 1 μM concentration, out of 321 tested. S-score at 10% cut-off = 0.06.*

Inhibition of a target at a single dose (1 μM) in the case of compound **52** is a good indication of target activity, however, it was important to consider the IC_{50} value of inhibition for a proper comparison against SRC. The IC_{50} value against BRK was determined for compound **52** and Dasatinib by the same conditions described before, table 6.4.

Both compounds showed good potency against BRK with IC_{50} values of 17.3 and 41.5 nM, respectively. Although neither compound showed the same potency as with SRC.

Kinase \ Hit	52	Dasatinib
	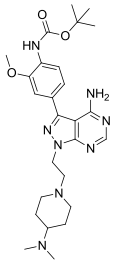	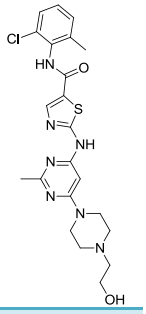
BRK/PTK6	17.3	41.5

Table 6.4: *IC_{50} values (nM) of compound **52** and Dasatinib against BRK/PTK6.*

6.2.4 Compound 52 Inhibits the Migration of MDA-MB-231 Cells in Vitro

The ability of a cell to move is very important in nature to support embryogenesis, wound healing and inflammatory response. White blood cells, for example, must find their way to a site of infection to fight off unwanted pathogens. To do this, they are able to migrate along blood vessels and then invade surrounding tissues. In cancer, however, cell mobility is an unwanted property as it is the migration of cancer cells from the primary site to other sites (metastasis) that causes the cancer to spread and ultimately, to become lethal. Single tumours are a lot easier to treat than multiple tumours spread around the body. For this purpose, drugs which inhibit cell migration and invasion are sought after.

One of the major functions of SRC in cells is the control of mobility – both migration across a 2D surface and invasion through a 3D matrix.[72] Several assays have been developed to assess the effect of a compound on the mobility of cells.[120] Perhaps the most well-known technique is the (scratch) wound healing assay where by cells are seeded at high density then a scratch created down the centre of a well and the percentage of cells migrated after a time period calculated. One of the drawbacks to this classical assay is the reproducibility of the scratch between wells and the ability to calculate accurate cell migration versus the initial scratch. To overcome this, the IncuCyte ZOOM system was used to track cell migration over a period of 24 hours. MDA-MB-231 cells were seeded at 50000 cells per well in a 96-well ImageLock™ plate from Essen BioScience, and left to adhere overnight. A 700-800 µm scratch wound was created in each well simultaneously using the WoundMaker™, which creates evenly sized wounds across a 96-well plate. The wells were then washed and fresh media containing either drug or DMSO added to each well. Images were taken every 30 minutes for 24 hours and cell migration calculated as relative wound density against time

zero by the IncuCyte ZOOM analysis software. Results were normalised to DMSO and are plotted in figure 6.6 showing cell migration at 6, 12 and 24 hours.

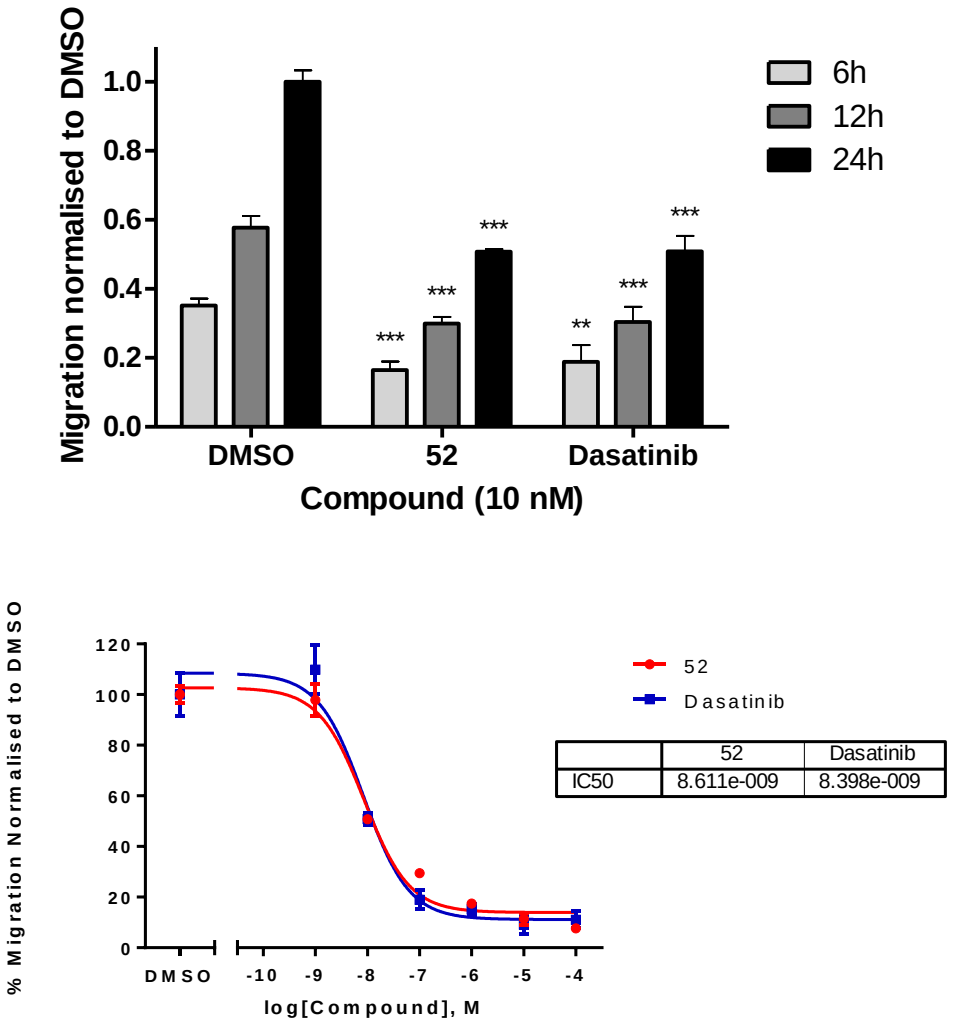

Figure 6.6: Top: *Relative migration of MDA-MB-231 cells across a scratch wound over 6, 12 and 24 hours normalised to DMSO at 24 hours. Graph shows compound **52** and Dasatinib at 10 nM concentration with statistical significance relative to DMSO; p<0.05, *; p<0.01, **; p<0.005, ***. Error bars denote standard deviation, n = 4. Bottom: Cell migration relative to DMSO after 24 hours with compound **52** and Dasatinib along a concentration gradient. Curves were plotted and EC_{50} values calculated using GraphPad Prism 6.*

Both compound **52** and Dasatinib were able to reduce migration as early as 2 hours and maintain the potency for 24 hours. Dasatinib and **52** showed very similar properties with EC_{50} values against cell migration of 8.4 and 8.6 nM, respectively.

6.2.5 Western Blot Analysis of Compound 52 and Dasatinib

To assess the level of inhibition of SRC and downstream targets *in situ* a Western blot was set up using MCF7 and MDA-MB-231 breast cancer cells. Cells were seeded in 10 cm dishes and grown until 80% confluence. Cells were then serum starved (0.1 % FBS) overnight and incubated with drug or DMSO (0.1 % v/v) for 30 minutes prior to stimulation with FBS (10 %) for an hour. The cells were then lysed and Western blotting carried out as described in method section 10.7.5.

As SRC auto-phosphorylates at tyrosine 416 upon activation, SRC activity/inhibition could be determined using an anti-phospho SRC Y416 antibody. Focal adhesion kinase, an important protein involved in cell mobility, is phosphorylated by SRC at position Y861. This antibody was used to show inhibition of downstream targets of SRC. AKT (Y326) is the primary target of BRK/PTK6 and is also phosphorylated by SRC at this position so this was included in the blot, along with pAKT (Y473), the common AKT activation site.[121, 122] Tubulin was used as a loading control. In order to determine whether pFAK, downstream of SRC, was truly being inhibited by SRC and not by off-target or direct inhibition, SYF cells (lacking expression of SRC, YES and FYN) were incubated with compound **52** and Dasatinib and phospho-FAK levels identified by Western Blot, as described previously. Figure 6.7 shows the results as scans of the photographic films used to develop the blots.

Compound **52** was able to inhibit the auto-phosphorylation of SRC down to 10 nM in both MCF7 and MDA-MB-231 cells to an equal or even greater degree than Dasatinib – a more profound difference was observed in MCF7 cells. The inhibition of FAK phosphorylation was in excellent correlation with that of SRC. Interestingly though, treatment with Dasatinib resulted in increased levels of total SRC at higher concentration (100 and 30 nM), whereas, treatment with compound **52** seemed to have a lesser effect on total SRC. This may suggest that Dasatinib is able to stabilise SRC from degradation, hence, the increased levels. Whether this results in increased levels of SRC activation is unknown, however. Interestingly, both **52** and Dasatinib seemed to increase the basal level of total FAK.

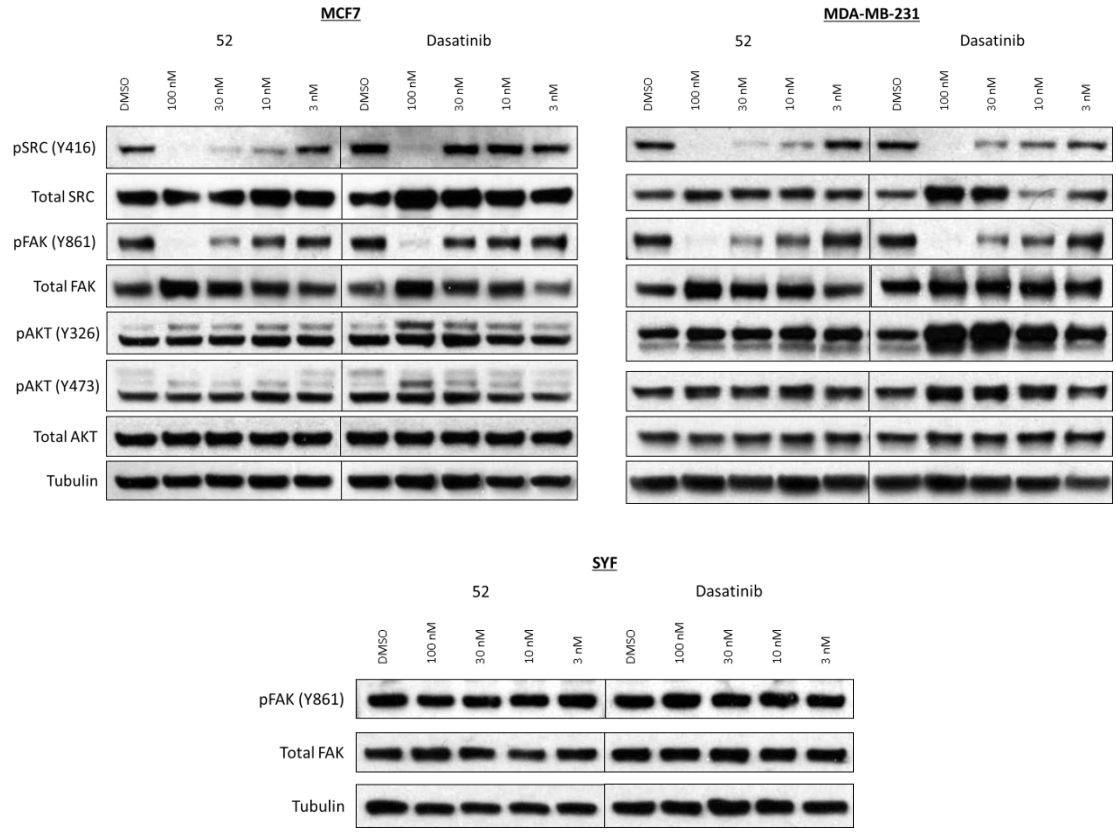

Figure 6.7: *Western Blot analysis of compound **52** and Dasatinib on SRC and downstream targets in MCF7 (top left), MDA-MB-231 (top right) and SYF cells (bottom). Compound **52** was able to inhibit the phosphorylation of SRC down to 10 nM in MCF7 and MDA-MB-231 cells and did not stabilise total SRC as Dasatinib did at higher concentrations. Tubulin was used as a loading control. SYF cells (lacking expression of SRC, YES and FYN) confirmed the inhibition of pFAK (Y861) was via pSRC inhibition and not through direct or off-target effects.*

It was hypothesised that via inhibition of BRK/PTK6, phosphorylation of AKT at Y326 would be reduced as both **52** and Dasatinib inhibit BRK at moderate levels, 17.3 and 41.5 nM IC_{50}, respectively. This was not observed, however, at the concentrations used (top dose 100 nM). Compound **52** gave constant levels of pAKT (Y326) indicating that phosphorylation at this position was via other proteins (i.e. not SRC or BRK) and basal levels of pAKT (Y326) were already high. In the case of Dasatinib, however, levels of pAKT (Y326) were increased at higher concentration of drug (100 and 30 nM – even 10 nM with MDA-MB-231 cells). This effect is more pronounced in the triple negative MDA-MB-231 cells. Again, the reason for compensatory increase in AKT signalling is unknown, however, it may lead to a negative effect in terms of cancer treatment – phosphorylation of AKT at Y326 may lead to a more stable complex with increased catalytic activity.

Looking at the results from the SYF cells, it is clear that inhibition of pFAK following compound treatment, in the MCF7 and MDA-MB-231 cells, is a result of SRC inhibition as there is no effect on pFAK seen in the SYF cells.

6.2.6 Zebrafish Cardiotoxicity and Tail Fin Cut Studies

The use of zebrafish for *in vivo* biology studies has gained increasing momentum over the past 20 years.[123, 124] Although they do not offer the same comparison to humans as mice do, their low costs, rapid growth rate, range of assays/imaging techniques available and ease of use make zebrafish a viable alternative for early *in vivo* studies. In addition, zebrafish embryos (less than 5dpf) are not subject to animal regulations. To evaluate the toxicity and *in vivo* efficacy of compound **52** and Dasatinib, both compounds were included in zebrafish embryo tail fin regeneration assays.

Zebrafish embryos are capable of regrowth of damaged tissues after amputation, in particular, amputated tails. Evidence has emerged that a member of the SRC family kinases (SFK), FYNb, is activated and involved in regeneration of the tail after tissue damage. Further, LYN acts as a sensor to detect reactive oxygen species, such as hydrogen peroxide, after injury. Activation of FYNb, was responsible for tail regeneration.[125] Yoo *et. Al.* found that incubation of the zebrafish with PP2 (a SFK inhibitor) halted the regrowth of amputated tails after only 2 hours treatment (1 hour pre, and post injury).[125] It was hypothesised that compound **52**, being a potent SFK inhibition, may give similar results. Importantly, any off-target toxicity effects would become evident since numerous kinases are essential for correct zebrafish embryo development.

Zebrafish embryos, 2 days post fertilisation (dpf), were treated with compound **52** or Dasatinib at 100μM, with DMSO as negative control, for 2 hours prior to tail amputation. The tails were then clipped from all fish at the points indicated by the red lines in figure 6.8. The fish were incubated with drug for a further 2 hours before being washed off and the fish left to develop in E3 embryo media at 28 ^{o}C for 2 days, after which, they were imaged, figure 6.8. This work was performed by Dr Liz Patton and Reece Dowling, The University of Edinburgh.

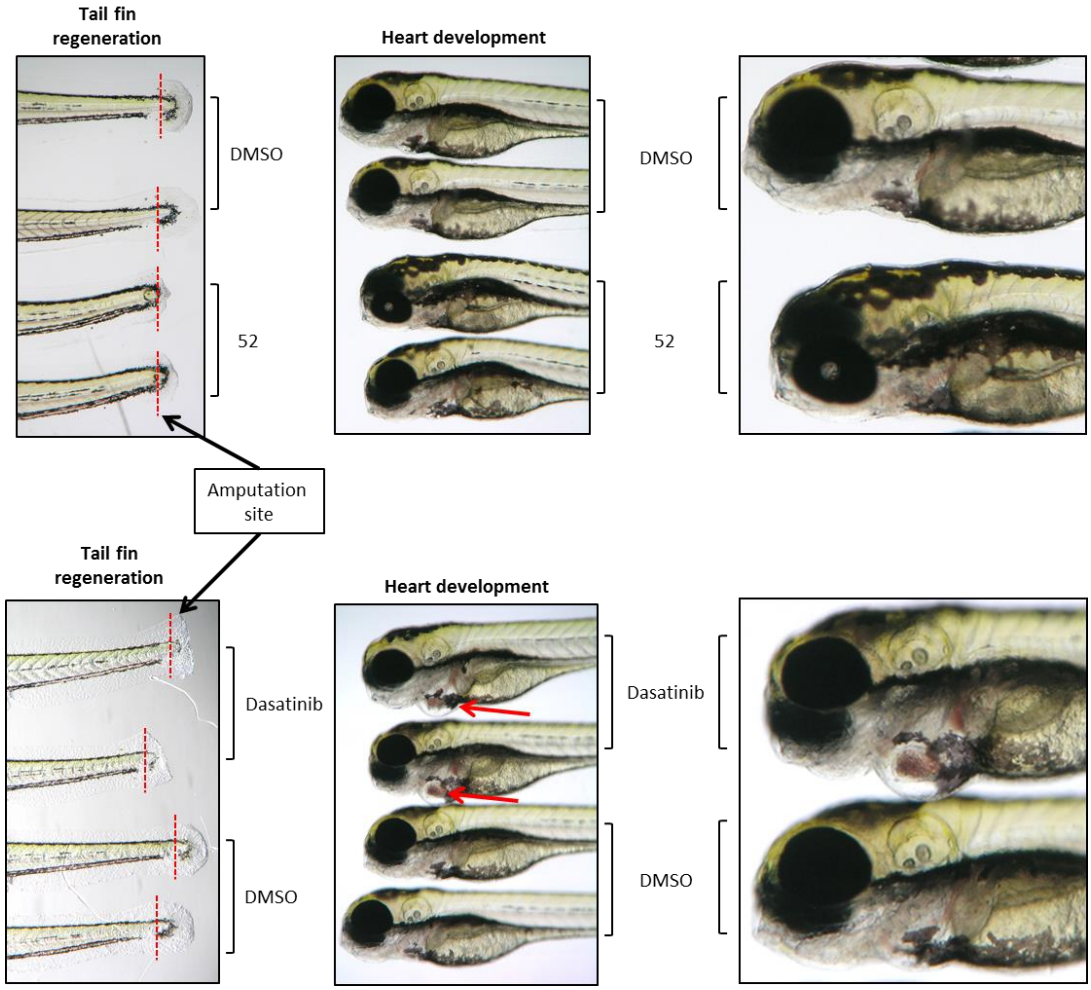

Figure 6.8: *Zebrafish embryos at 4 dpf, 2 days post tail amputation comparing compound* ***52****, Dasatinib and DMSO. Left: Full regrowth of the tail was observed with DMSO treatment, whereas, 2 hours pre and post incubation with compound* ***52*** *or Dasatinib halted the regrowth. Middle: Dasatinib treated zebrafish showed severe heart toxicity after 2 days post 4 hours incubation at 100 µM. Compound* ***52*** *and DMSO showed normal development and no toxicity. Right: Zoomed in images of heart development after 2 days post tail amputation and incubation with drug. Compound* ***52*** *shows normal growth, as seen with DMSO, while Dasatinib treatment resulted in an enlarged heart.*

2 days post amputation, zebrafish treated only with DMSO were able to completely grow back their tails as shown in figure 6.8, left, whereas, treatment with compound **52** or Dasatinib at 100 µM halted tail regeneration. This tail regeneration assay was designed as a simple proof of concept experiment to demonstrate that compound **52** was able to inhibit SFKs in a basic *in vivo* model and to assess any obvious toxicity issues associated with the drug. Even at 100 µM, zebrafish treated with compound **52** showed no signs of toxicity, figure 6.8, top middle and right, and continued to develop normally. Dasatinib, however,

caused severe cardiotoxicity as seen in figure 6.8, bottom middle and right, with the fish displaying enlarged hearts.

It was hypothesised that ABL inhibition may be the cause of the observed cardiotoxicity and indeed many groups have demonstrated the complications of ABL inhibition and the development of adverse cardiac effects.[126-129] In particular, Qui *et Al.* (PNAS, 2010) demonstrated that knock-out of c-ABL causes 'dramatically enlarged hearts' in mouse embryos which can be rescued by restoring the protein.[129] They showed that reduction in ABL activity caused an increase in cardiomyocyte proliferation, thus, resulting in the abnormally large hearts observed in the mice; the same effect seen in zebrafish treated with Dasatinib. Although their findings show that c-ABL is essential for heart development, in mammals, both Dasatinib and Imatinib (a potent ABL inhibitor approved for CML) have caused cardiotoxicity in adult patients, with fully developed hearts. These findings, along with our own evidence, further back up the premise that inhibition of c-ABL is not only harmful in breast cancer treatment but can also instigate severe toxicity in patients taking such drugs, particularly in an aging population with heart disease problems.

To further test this hypothesis, PP20, figure 6.1, was incubated with zebrafish embryos for 2 hours only, and images taken 3 days later. PP20 (dosed at 100 μM) caused severe toxicity in all zebrafish and their development was highly flawed. The embryos shown in figure 6.9a show examples of the observed growth retardation, and again, all embryos showed significantly enlarged hearts, which is the probable reason for the overall lack of development of the embryo.

PP20 proved to be even more toxic that Dasatinib at only 2 hours incubation with zebrafish embryos. Compound **52**, Dasatinib and PP20 all inhibit SRC to a similar degree, however, only **52** does not inhibit ABL. Although the properties of PP20 have not fully been explored, it is likely that the cardiotoxicity and growth retardation are due to ABL inhibition.

As a simple model of *in vivo* efficacy, tail fin regeneration assays were set up, as described above, and compound **52** compared with Dasatinib and PP20. Many assays were attempted, however, the results were generally inconsistent and statistically significant results could not be drawn. Figure 6.9b shows the results of one of the assays including a higher sample number. In this assay, zebrafish embryos were incubated with DMSO (0.1 %), Dasatinib or PP20 (100 μM) 2 hours prior to and after tail amputation and the embryos left to develop for two days in fresh E3 media before being imaged. Compound **52** was included at the higher concentration of 250 μM, firstly because it had not shown any previous toxicity, as Dasatinib

and PP20 had, but also because it inhibits FYN, the kinase responsible for regrowth, to a lesser degree than the others.

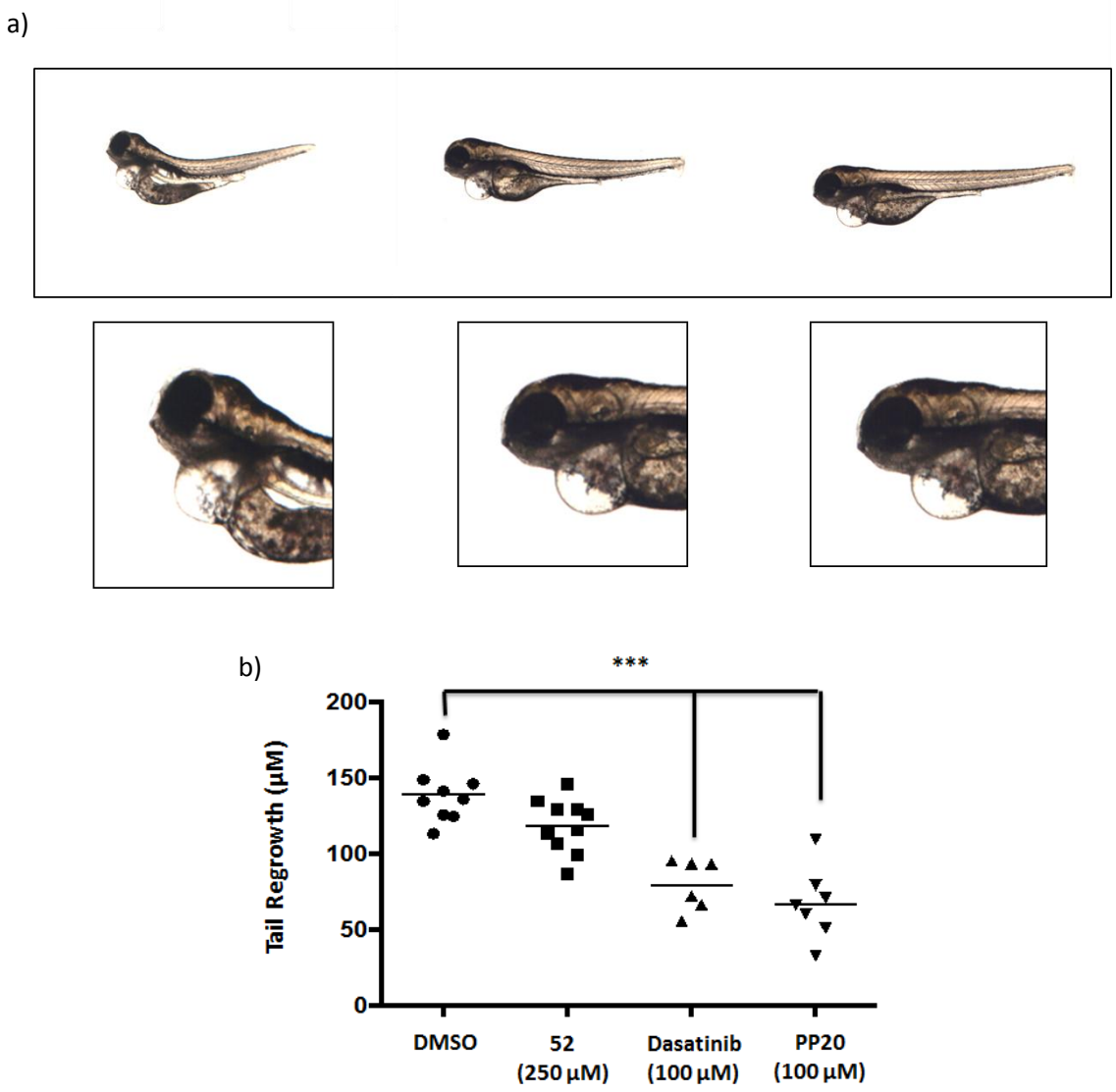

Figure 6.9: *a) Zebrafish embryos at 4 dpf after 2 hour treatment with PP20 (100 µM) at 1 dpf. All 3 fish show growth retardation and cardiotoxicity, highlighted in zoomed in images at bottom. b) Embryos were incubated with either* ***52*** *(250 µM), Dasatinib (100 µM) or PP20 (100 µM) for 2 hours prior to and after tail amputation. Tail regrowth was measured after 2 days, and plotted as a scatter plot. Performed t-tests showed both Dasatinib and PP20 were statistically significant (p<0.05, *; p<0.01, **; p<0.005, ***) but not* ***52****. *3 fish were omitted from the Dasatinib and PP20 group due to toxicity or death.*

Dasatinib and PP20 caused a statistically significant reduction in tail regrowth compared with DMSO, figure 6.9b, however, all embryos looked sick and displayed severe toxicity signs. Indeed, in both the Dasatinib and PP20 groups, 3 embryos were omitted due to death

or extreme toxicity. It is hypothesised that the reduction in tail regrowth observed with Dasatinib and PP20 was caused more so by the general toxicity than with inhibition of LYNb. **52**, on the other hand, did not show any toxicity, even at the higher concentration of 250 μM. The reduction in tail regrowth was not deemed statistically significant ($p = 0.079$), however, this result was anticipated due to its lower inhibitory properties over FYN. Most importantly, the cardiotoxicity was consistently observed with Dasatinib and PP20, but not with **52**, strongly indicating that ABL inhibition was the cause.

6. The Development of Novel, Potent and Selective SRC Family Kinase Inhibitors

6.3 Conclusion

Through the discovery of moderately potent compound **29** and modification of its aryl group, using PP20 as inspiration, lead compound **52** was generated showing extraordinary activities in cellular assays. Compound **52**, which was shown to inhibit the viability of MDA-MB-231 triple negative breast cancer cells with an EC_{50} of 10 nM, was revealed to be a sub-nanomolar potent SRC family kinase inhibitor. Most importantly, **52** did not potently inhibit the kinase c-ABL, unlike all other SRC inhibitors, either in the clinic or reported to date. Through a combination assay using the specific allosteric site ABL inhibitor GNF-2 and **52**, it was shown that ABL inhibition was detrimental in combination with SRC inhibition. This experimental evidence describing adverse effects of ABL inhibition is backed up thoroughly in the literature.[114, 115]

Not only was **52** extremely potent against SFKs, it was also very selective when tested against 341 kinases. Inhibition was generally only observed in the SRC family branch of kinases. By exploiting the properties of SFK inhibition, **52** was able to reduce the migration of MDA-MB-231 cells to the same degree as Dasatinib and was shown to potently inhibit pSRC and pFAK in MCF7 and MDA-MB-231 cells by Western Blot. Further, **52** did not show off-target effects, such as increased pAKT levels, as Dasatinib did.

Most importantly, **52** was shown to be non-toxic when incubated with zebrafish embryos and caused no growth defects. Dasatinib and PP20, on the other hand, caused severe cardiotoxicity in the embryos, which has previously been reported in the literature. Since potent and selective SRC inhibitors have not been developed until now, the study reported herein represents the first pharmacological evidence that the cardiotoxicity mediated by dual ABL/SRC inhibitors is most likely attributed to ABL inhibition.[126, 127, 129]

Currently, compound **52** represents the only sub-nanomolar SRC inhibitor that does not potently inhibit ABL. Given all the evidence of ABL's anti-oncogenic role in cancers other than CML, compound **52** represents promise for the treatment of SRC driven tumours, particularly triple negative breast cancer. The optimisation and thorough examination of the properties of **52** are discussed in the next chapters.

7. Optimisation of Lead Compound 52

7.1 Introduction & Aims

In order to develop the series of SRC inhibitors into preclinical candidates, compounds containing variations of the aryl group of compound **52** were synthesised. This allowed the creation of vital structure activity relationships to which the necessity of the current groups could be assessed. A structure activity relationship map can be drawn, figure 7.1, to show which groups should be addressed in regard to whether they are necessary for potency, stability or pharmacokinetic properties. Due to the phenotypic nature of the discovery of the previous series of inhibitors, any drugs created via modification of the lead compound were to be biased based upon phenotypic endpoints, typically cell proliferation. This would not only frontload the most potent compounds but also rule out any which possessed low permeability or solubility due to their modifications. Important issues to address regarding modifications are shown in figure 7.1. The table highlights some of the modifications made to compound **52**.

Group	Modification
Methoxy	Hydroxy, removal
Nitrogen	CH_2
Carbonyl	Removal
Oxygen	Removal, nitrogen
t-butyl	Aryl groups
Carbamate	Amide, urea, ester, alkylated amine, switch positions, (oxazole, nitrile)
Pyrimidine	Removal
Dimethyl	Pyrrolidine, piperidine

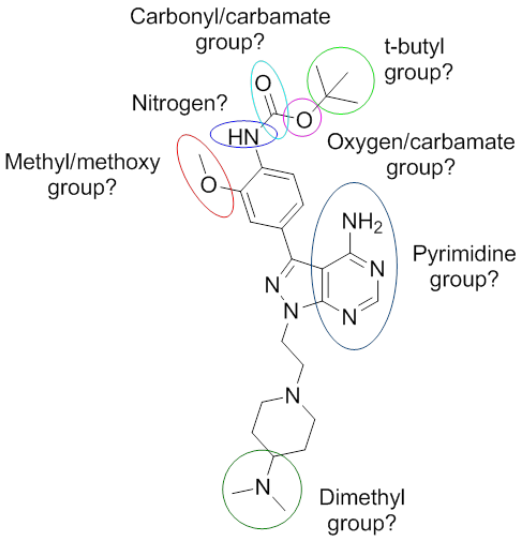

Figure 7.1: *Table showing possible modifications for groups around compound **52** (left). Structure activity relationship map of compound **52** highlighting which groups should be modified to assess their necessity (right).*

7. Optimisation of Lead Compound 52

7.2 Results

7.2.1 Design and Synthesis of Compound 55 and 56

Compound **51** showed an IC_{50} against SRC inhibition of < 0.5 nM, similar to **52**. By this reckoning, there is space in the SRC active site to accommodate larger groups to the 'south' of the molecule. Instead of lengthening the chain, as in compound **51**, two new compounds were synthesised containing pyrrolidine and piperidine groups, respectively, in order to access lipophilic pockets situated near the 'south' amine. Firstly, the two intermediates, **53** and **54**, scheme 7.1, were synthesised from the aldehyde intermediate by the same fashion as previously. Compounds **55** and **56** were then synthesised, by Suzuki reaction, from the intermediates, **53** and **54**, respectively, and [4-(tert-butoxycarbonylamino)-3-methoxy-phenyl]boronic acid.

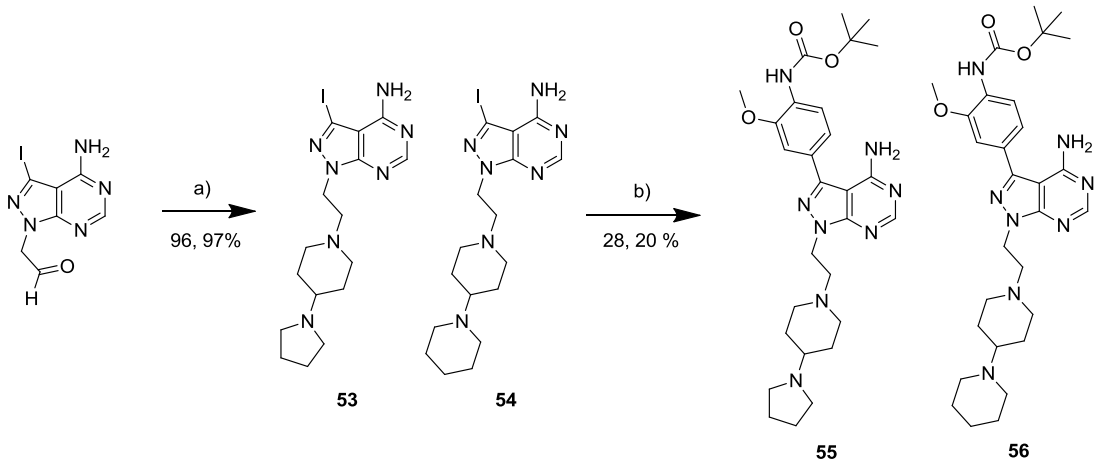

Scheme 7.1: Synthesis of c*ompounds **55** and **56**. a) 4-(1-pyrrolidinyl)piperidine (**53**) or 1,4-bipiperidine (**54**), AcOH, $NaBH(OAc)_3$, DCM, r.t. b) [4-(tert-butoxycarbonylamino)-3-methoxy-phenyl]boronic acid, K_2CO_3, $Pd(OAc)_2$, PPh_3, 1,4-dioxane/water (10:1), 120 ^oC, mw.*

Compounds **55** and **56** were tested in MCF7 and MDA-MB-231 cell viability assays, as before, to initially assess the impact of larger, more lipophilic, amine groups on cell proliferation, figure 6.2. Both compounds were less potent than **52**, however, still had EC_{50} values against both cell lines below 250 nM. Again, compounds were more potent in the triple negative MDA-MB-231 cells with the ratio of MCF7 to 231 comparing favourably with compound **52**.

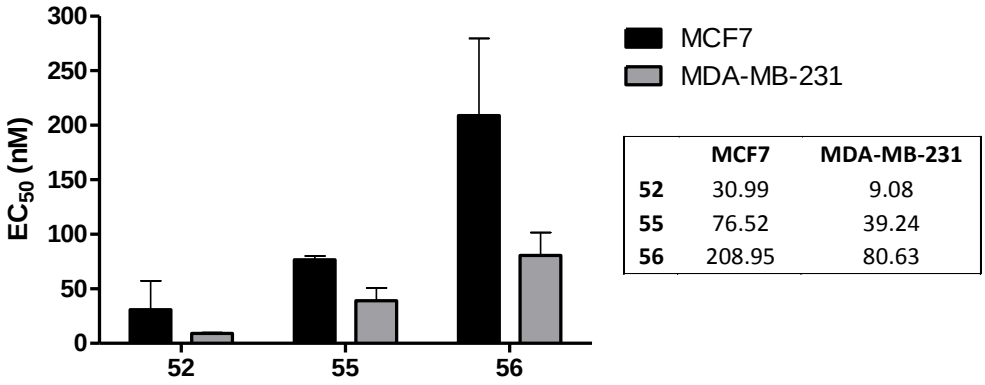

	MCF7	MDA-MB-231
52	30.99	9.08
55	76.52	39.24
56	208.95	80.63

Figure 7.2: *EC_{50} values against MCF7 and MDA-MB-231 cell proliferation plotted as an average of 3 experiments with mean values (right, nM). Error bars denote standard deviation, n = 3.*

The study suggested that increasing size and/or lipophilicity in the 'south' part of the structure was not beneficial to activity against cell proliferation and perhaps SRC inhibition. Due to this decreasing activity and the pressure of modern small drugs to comply with Lipinsk's rules (molecular weight < 500), the dimethyl amino group, found in compound **52**, was used for all further structure modifications. Other drug likeness parameters, such as ligand efficiency (LE), percentage/potency efficiency index (PEI) and binding efficiency index (BEI), also favour lower molecular weight compounds, given similar potencies.

7.2.2 Aryl Group Modifications – Synthesis and Biological Testing

To fulfil some of the questions raised from the structure activity map in figure 7.1, a series of varying aryl groups were synthesised to satisfy concerns over the optimal aryl group for SRC inhibition and pharmacokinetic properties. The first group synthesised was aiming to determine whether the oxygen, and therefore, carbamate, was required and whether the t-butyl group could be replaced with a phenyl group. For this purpose, a set of boronic esters (**57-62**) were synthesised from the common precursor 4-Amino-3-methoxyphenylboronic acid pinacol ester and various commercially available acetyl chlorides, chloroformates or t-butylisocyante, compound **58**, scheme 7.2.

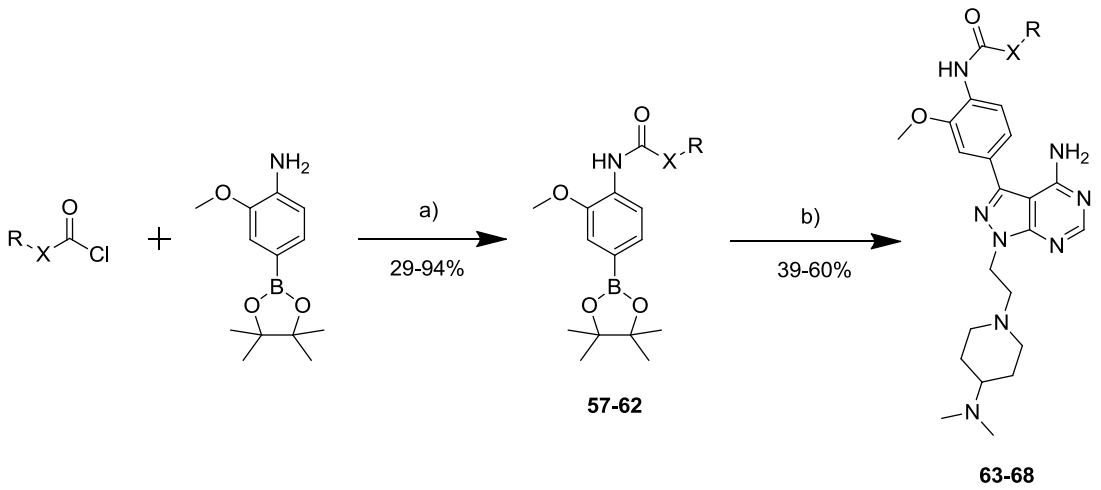

Compound	X =	R=	Compound	X =	R=
57	CH_2	t-butyl	**63**	CH_2	t-butyl
58	NH	t-butyl	**64**	NH	t-butyl
59	O	Phenyl	**65***	O	Phenyl
60*	O	Benzyl	**66***	O	Benzyl
61	CH_2	Phenyl	**67**	CH_2	Phenyl
62	CH_2	Benzyl	**68**	CH_2	Benzyl

Scheme 7.2: *Synthesis of intermediate boronic esters **57-62** and compounds **63-68**. a) t-butylacetal chloride; t-butylisocyanate; phenyl chloroformate; benzyl chloroformate; phenylacetyl chloride or hydrocinnamoyl chloride, 4-amino-3-methoxyphenylboronic acid pinacol ester, NEt_3, DCM, r.t. b) 1-[2-[4-(dimethylamino)-1-piperidyl]ethyl]-3-iodo-pyrazolo[3,4-d]pyrimidin-4-amine, K_2CO_3, $Pd(OAc)_2$, PPh_3, 1,4-dioxane/water (10:1), 120 ^oC, mw. * Product was not as desired.*

Boronic esters **57** and **58** contained an amide and a urea group instead of a carbamate, thereby, challenging the requirement of a hydrogen bond acceptor (-O-) with a non-hydrogen bonding atom (-CH_2-) and a hydrogen bond donor (-NH-). The synthesis of both boronic esters and corresponding final compounds, **63** and **64**, proceeded in good yield with the conditions described in scheme 7.2.

Boronic ester **59** was designed to challenge the presence of the t-butyl group with a phenyl group and, similarly, **60**, with a benzyl group. **59** was synthesised successfully, however, the product of reaction between 4-amino-3-methoxyphenylboronic acid pinacol ester and benzyl chloroformate was the unexpected, benzylated product, **60***, figure 7.3a, rather than the desired boronic acid. The rearrangement depicted in figure 7.3a is one possible explanation for the by-product. Nonetheless, **60*** was isolated and purified, and used to create compound

66*, hereby named **66**, by Suzuki reaction. Further complications arose when attempting to synthesise compound **65** from intermediate **59**. Following the Suzuki reaction using the standard protocol, desired product **65** was not detected but the free amino compound instead, figure 7.3b. The reaction was repeated under the same conditions but the outcome was the same with the phenyl formate group of the boronic ester intermediate missing. Perhaps the phenyl carbamate was unstable at higher temperatures and degraded during the Suzuki reaction. Regardless, the free amino derivate, **65***, hereby known as **65**, was isolated and purified, and later used in biological testing.

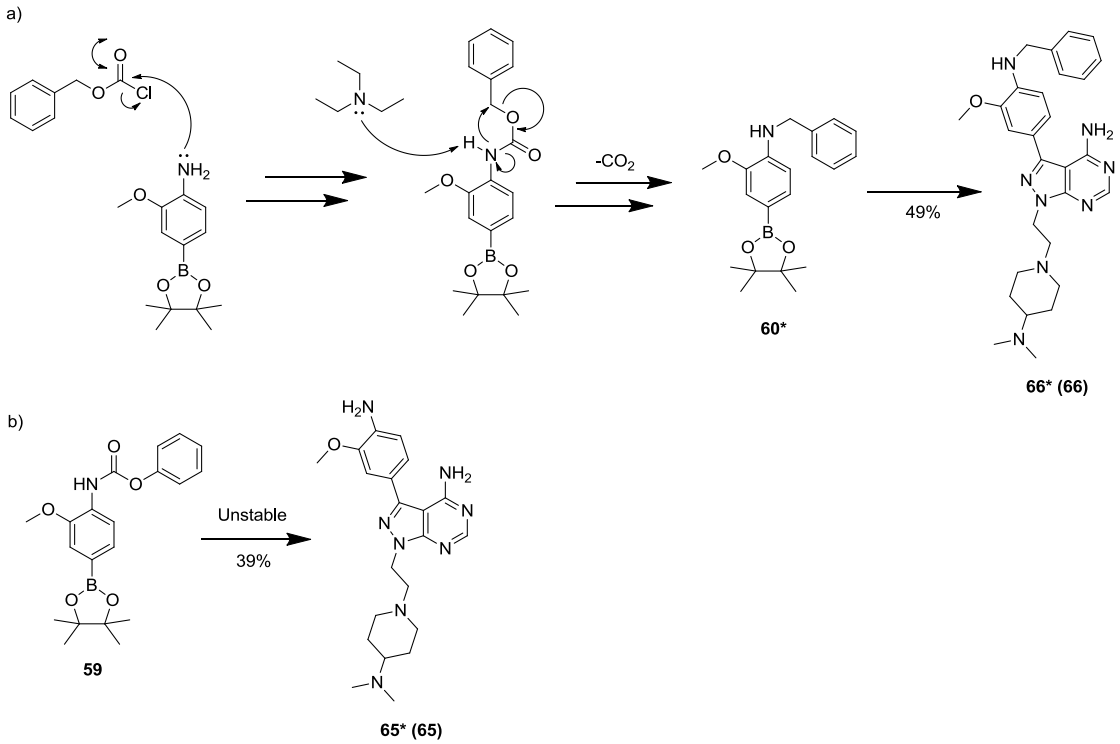

Figure 7.3: *a) Possible rearrangement mechanism during reaction of 4-amino-3-methoxybenzeneboronic acid pinacol ester and benzyl chloroformate to create **60*** and corresponding final compound, **66*** (**66**). b) Loss of phenyl formate during Suzuki reaction created by-product **65*** (**65**).*

Boronic esters **61** and **62** were similar to **59** and **60** in that they have phenyl and benzyl groups, respectively, instead of t-butyl. In this case, however, the oxygen was replaced by a CH_2. This was designed to provide a direct comparison between carbamate and amide groups, giving important information on the structural requirements of the hydrogen bond acceptor. Due to the complications that arose during the synthesis of final compounds **65** and **66**, however, this direct comparison was could not be carried out. Both intermediates **61** and

62, and their corresponding final compounds, **67** and **68** were synthesised following the procedure described in scheme 7.2, successfully, and in good yield.

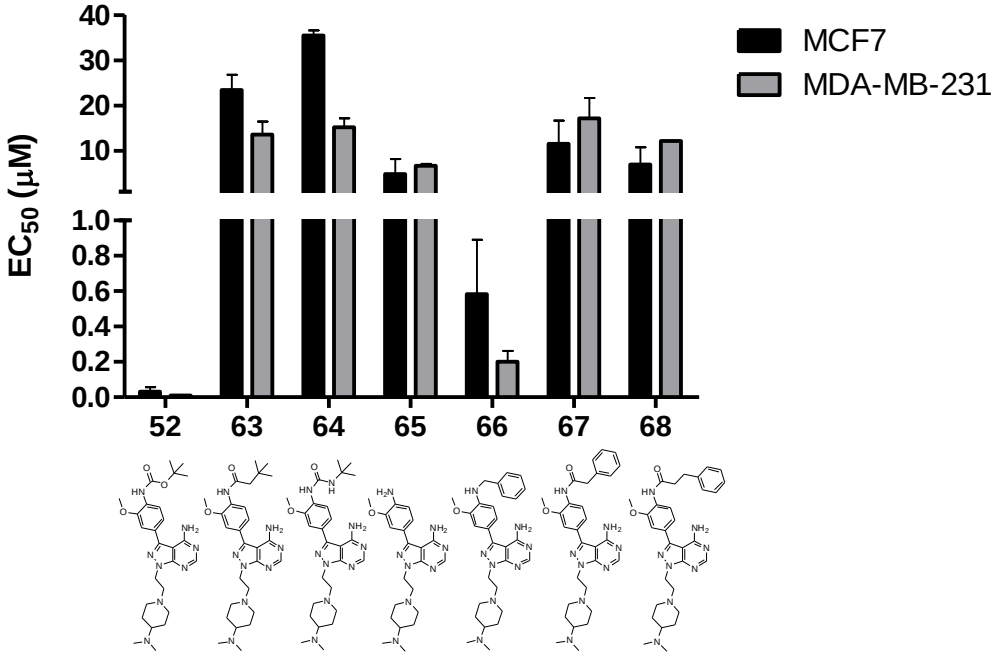

Compound\Cell Type	MCF7	MDA-MB-231
52	0.031	0.0091
63	23.44	13.59
64	35.47	15.23
65	4.93	6.72
66	0.58	0.20
67	11.59	17.21
68	7.04	12.18

Figure 7.4: *Plotted EC_{50} values (μM) against MCF7 and MDA-MB-231 cell proliferation comparing lead compound **52** with aryl modified compounds **63-68**. Structures are included below the x-axis for convenience. Error bars denote standard deviation, n = 3.*

Compounds were tested in MCF7 and MDA-MB-231 cell viability assays, as before, and the calculated EC_{50} values plotted in a bar graph, figure 7.4. Surprisingly, the only compound to show sub-micro molar potency was **66**, the benzyl amine containing derivative from the unexpectedly synthesised boronic acid **60***. Compound **66** had an EC_{50} value of 583 and 202 nM against MCF7 and MDA-MB-231 cell proliferation, respectively. Though not as potent as lead compound **52**, these values represent acceptable potency for further consideration.

Even more surprising were compounds **63** and **64**. The modification from a carbamate group to an amide or urea reduced the compounds' potency >750x relative to lead 52, strongly indicating that a hydrogen bond acceptor is essential for activity at this position. It is curious as to why compound **66** was more potent given the lack of any hydrogen bond acceptors on the aryl groups. However, as **66** is notably different from the other compounds, it may be that other targets than SRC were being inhibited.

7.2.3 Further Optimisation of the Aryl Group - Pyridines

Given the unexpected success of compound **66**, two more compounds were designed and synthesised based upon its structure. Compounds **71** and **72**, based around a pyridine ring instead of phenyl, were synthesised from boronic ester intermediates, **69** and **70**, scheme 6.3, from 4-amino-3-methoxyphenylboronic acid pinacol ester. The more polar pyridine group was designed to mimic compound **66** but featured a hydrogen bond acceptor extended further to the extremities of the structure.

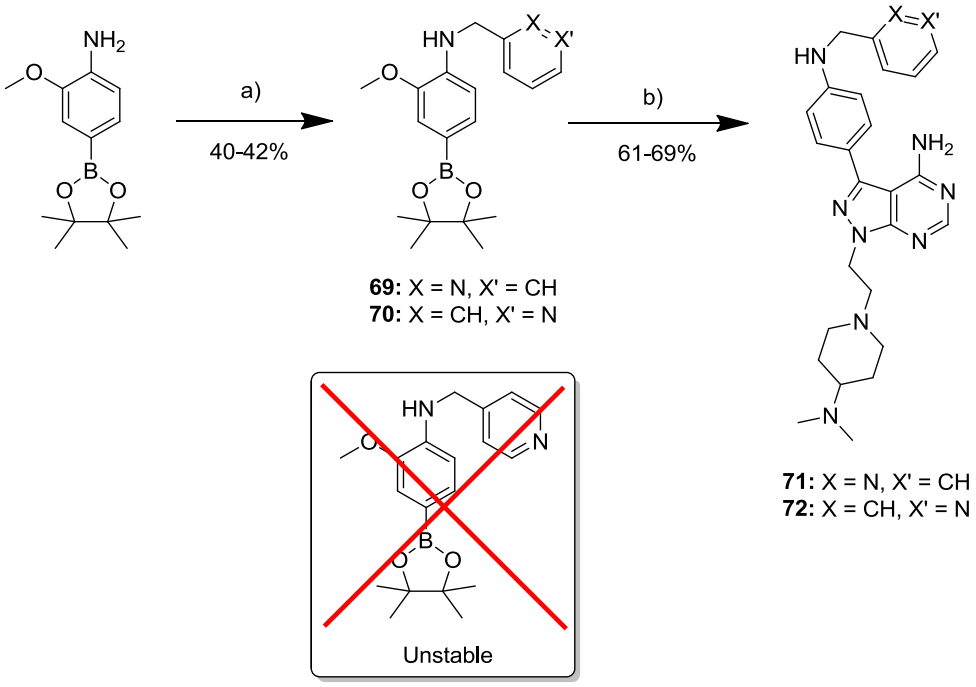

Scheme 7.3: *Synthesis of compounds **71** and **72** from boronic ester intermediates **69** and **70**. a) 2-(bromomethyl)pyridine hydrobromide or 3-(bromomethyl)pyridine hydrobromide, NEt_3, DCM, r.t. b) **69** or **70**, 1-[2-[4-(dimethylamino)-1-piperidyl]ethyl]-3-iodo-pyrazolo[3,4-d]pyrimidin-4-amine (**50**), K_2CO_3, $Pd(OAc)_2$, PPh_3, 1,4-dioxane/water (10:1), 120 ^oC, mw. The 4-(methyl)pyridine equivalent boronic ester was not able to be synthesised. It was thought to be unstable in the presence of light like its precursor, 4-amino-3-methoxyphenylboronic acid pinacol ester.*

The synthesis of the 4-(methyl)pyridine boronic ester equivalent was unsuccessful. The starting compound, 4-amino-3-methoxybenzeneboronic acid pinacol ester, was sensitive to light and although reactions were carried out in the dark, very little product was isolated from the reaction with 4-(bromomethyl)pyridine hydrobromide. Nonetheless, compounds **71** and **72** were successful and taken forward for biological testing.

The compounds, synthesised in good yields, were tested in a cell viability assay with MDA-MB-231 cells. Due to the greater effect of compound **52** in the triple negative breast cancer cells, all subsequent compound ranking and importance were decided based upon the EC_{50} values gathered against MDA-MB-231 cell proliferation. Compound **71** and **72** gave EC_{50} values of 40.20 and 4.14 μM, respectively. Comparing with compound **66**'s value of 0.20 μM, compounds **71** and **72** were much weaker and the more polar pyridine group was not tolerated.

7.2.4 Further Optimisation of the Aryl Group – Phenyl Modifications

With the optimum 'south' part of the molecule determined, section 7.2.1, and compound **52** still remaining the best compound in terms of potency against cell proliferation, efforts were focused on altering the aryl group associated with **52** to answer some more of the questions raised in the SAR map in figure 7.1. More appropriately, was the methoxy group or the -NH- from the aryl moiety required for potency?

To answer these questions, again, a series of boronic acids/esters were synthesised, or were commercially available, and were cross-coupled to intermediate **50** by Suzuki reaction, scheme 7.4. The table below describes the final compounds synthesised, in which way they differ from compound **52,** and which issues they will address in terms of SARs.

Compound	Modification	SAR
75	Methoxy to hydroxy	H bond acceptor to donor
76	Methoxy removal	Removal of H bond acceptor
77	Methoxy removal and N-boc at 2-position	Determine optimum position for N-boc
78	Methoxy to pyridine	Bring H bond acceptor closer to ring
79	Methoxy to CH as an indole	Fill space with neutral group and force carbamate to assume flat position
81	Methoxy to 3-position, N-boc to 2-position	Challenge optimum group position
84	Carbamate to ester	Removal of H bond donor
86	Methoxy removal and carbamate	Removal of H bond donor and acceptor

	to ester	
87	Methoxy removal and carbamate to acid	Charged group instead of neutral
90	Carbamate to amide	Switch nitrogen position
94	Carbamate to oxazole	Locked position involving aromatic group
95	Methoxy removal and carbamate to nitrile	Removal of all groups with extended H bond acceptor

Table 7.1: *Compound modifications relative to **52** and the SARs they will address.*

All final compounds were synthesised from their respective intermediates in moderate to excellent yields with no complications. Boronic acid/ester synthesis, where appropriate, involved starting from either commercially available amino phenyl compounds to which the amine was protected with a Boc group or phenyl acetic acid precursors with the conversion to acid chlorides using thionyl chloride. Subsequent substitution then proceeded in low to good yield.

All 12 final compounds were assessed in MDA-MB-231 cell viability assays to determine their potency relative to compound **52**. The results, figure 7.5, varied greatly from totally inactive, compounds **87, 90** and **95**, to very potent, compounds **84** and **86**, with EC_{50} values comparable to **52**.

Compounds **87**, **90** and **95** were completely inactive, which is not surprising given their drastic changes relative to **52**. **87**, which features a carboxylic acid moiety, is a highly charged molecule, expected to be found in zwitterion form at physiological pH (negatively charged on the north of the molecule and positively charged on the south). Although the introduction of zwitterions can aid solubility in large or lipophilic compounds, they present significant problems with cell permeation unless transported through the cell membrane by active transport or other means. It is highly likely that compound **87** struggled to penetrate the cell. It is shown in section 7.2.6 that **87** has no effect on SRC family inhibition. Based on the target potency data, in this case, I cannot confirm whether cell permeability is also an issue, however, the charges associated with the molecule most likely do present the problem.

Compound **90**, which features a 'reverse amide' relative to the nitrogen position in the carbamate in compound **52**, indicates that the nitrogen is not tolerated in this position or the restriction in movement in the lipophilic region of the pyrrolidine, presented by the amide, is not fulfilling the needs of the kinase active site.

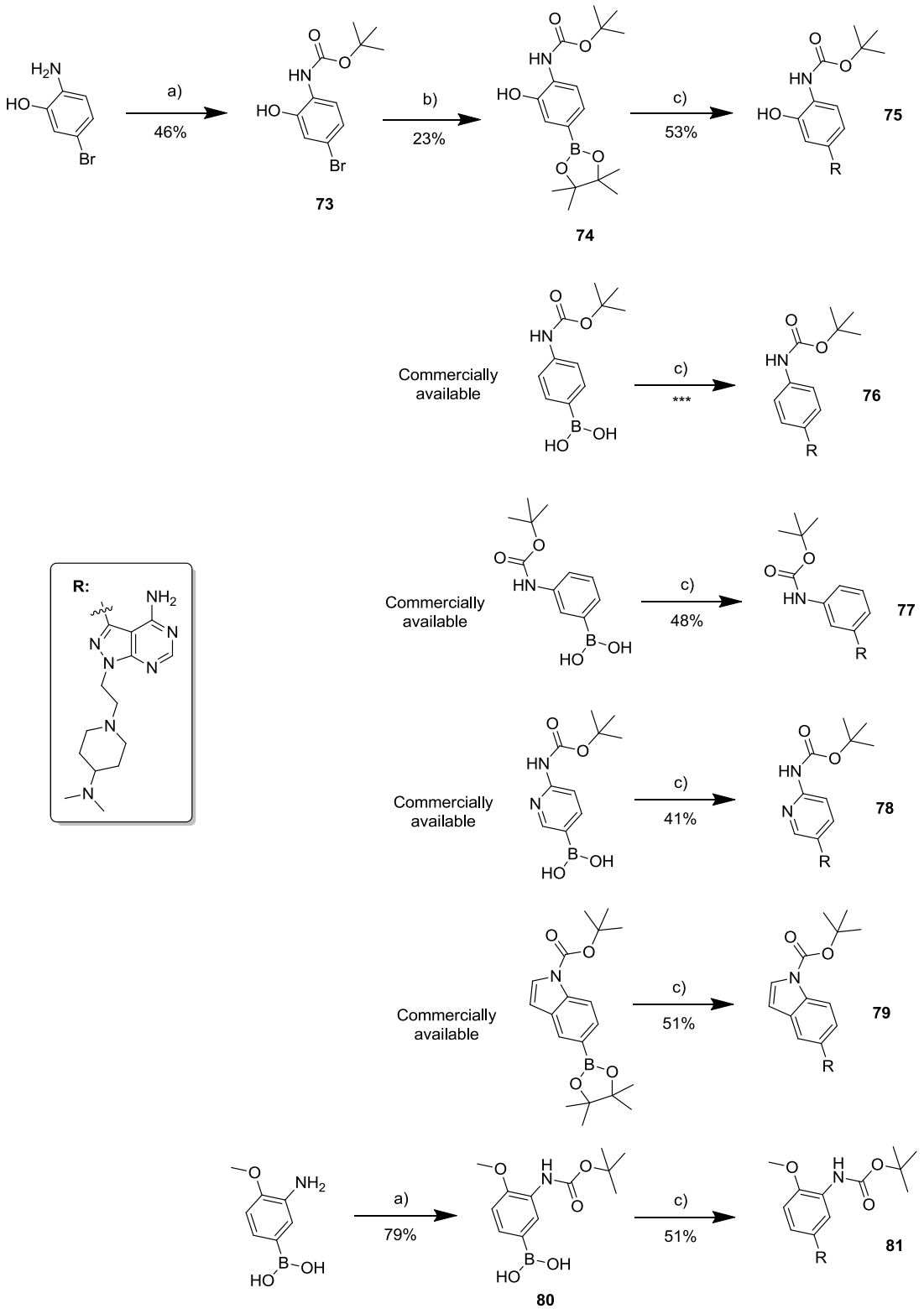

Scheme 7.4: *Synthesis of compounds **73**-**81**. a) Di-tertbutyldicarbonate, DMAP, DCM, r.t. b) bis(pinacolato)diboron, $Pd(OAc)_2$, PPh_3, 1,4-dioxane/water (10:1), 120 ^oC, mw. c) 1-[2-[4-(dimethylamino)-1-piperidyl]ethyl]-3-iodo-pyrazolo[3,4-d]pyrimidin-4-amine (**50**), K_2CO_3, $Pd(OAc)_2$, PPh_3, 1,4-dioxane/water (10:1), 120 ^oC, mw.*

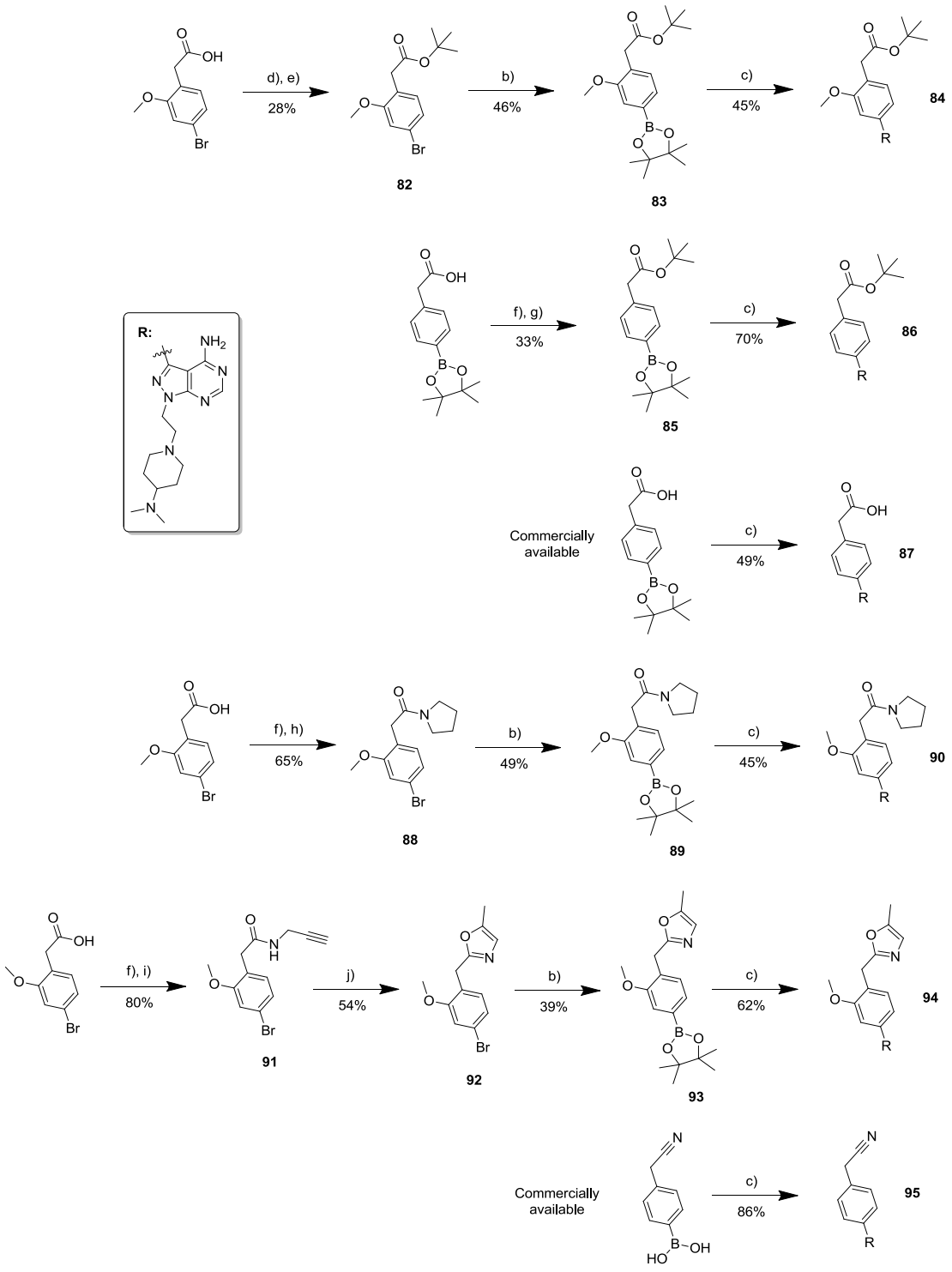

Scheme 7.4 cont.: *Synthesis of compounds **82**-**95**. b) bis(pinacolato)diboron, $Pd(OAc)_2$, PPh_3, 1,4-dioxane/water (10:1), 120 °C, mw. c) 1-[2-[4-(dimethylamino)-1-piperidyl]ethyl]-3-iodo-pyrazolo[3,4-d]pyrimidin-4-amine (**50**), K_2CO_3, $Pd(OAc)_2$, PPh_3, 1,4-dioxane/water (10:1), 120 °C, mw. d) Thionyl chloride, DMF (cat.), THF, 80 °C. e) t-butyl alcohol, NEt_3, THF, r.t. f) Thionyl chloride, DMF (cat.), toluene, 120 °C. g) t-butyl alcohol, NEt_3, toluene, r.t. h) Pyrrolidine, NEt_3, toluene, r.t. i) Propargylamine, NEt_3, toluene, r.t. j) $FeCl_3$, 1,2-dichloroethane, 150 °C.*

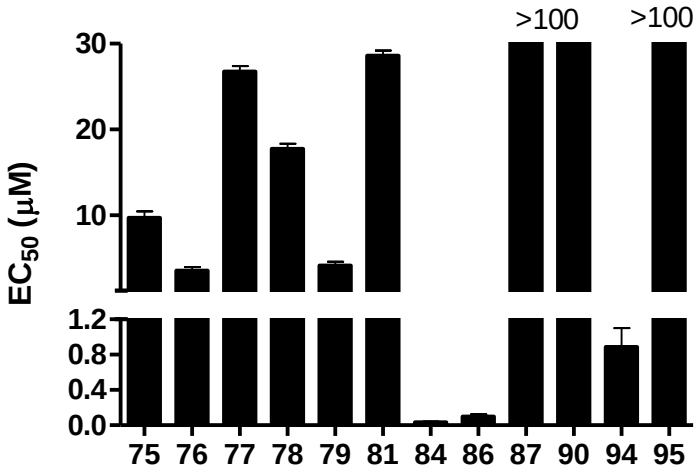

Compound	75	76	77	78	79	81	84	86	87	90	94	95
EC_{50} (μM)	9.71	3.57	26.77	17.74	4.15	28.59	0.036	0.10	>100	>100	0.89	>100

Figure 7.5: *Calculated EC_{50} values (μM) plotted as a bar graph for compounds **75**-**95** against MDA-MB-231 cell proliferation. Error bars denote standard deviation, n = 3.*

Compound **95**, featuring a nitrile group instead of the carbamate and the methoxy group removed, also showed no activity against cell proliferation. This compound is drastically different from lead compound **52** and features no lipophilic moiety which appears to be required for activity.

Compounds **84** and **86** gave EC_{50} values of 36 and 100 nM, respectively. This indicates that the nitrogen and, hence, carbamate group of **52** is not required for activity but its presence does not hinder activity and gives, roughly 3x, greater potency against cell proliferation. Whether this difference is down to pharmacokinetics or kinase inhibition is discussed in section 7.2.6. Remarkably, the loss of the nitrogen and the methoxy group still produced a potent compound (**86**) indicating that, although beneficial for activity, the methoxy group is not essential to produce a potent compound against MDA-MB-231 cell proliferation, at least. Comparing with compound **76**, which contains the t-butyl carbamate without the methoxy group, compound **86** is 35x more potent. This is surprising given that the only difference is the substitution from nitrogen to a CH_2.

Compound **94** also gave a sub-micro molar potency with an EC_{50} of 0.89 μM. At first, an oxazole might seem a significantly different group from those in **52**, however, by looking at an overlay of **94** with **84**, one can see how related the structures are and how they might sit

in the SRC active site, thus, explaining the reasons for compound **94**'s activity. Indeed oxazoles are known bioisosteres of ester groups used to increase biochemical stability.

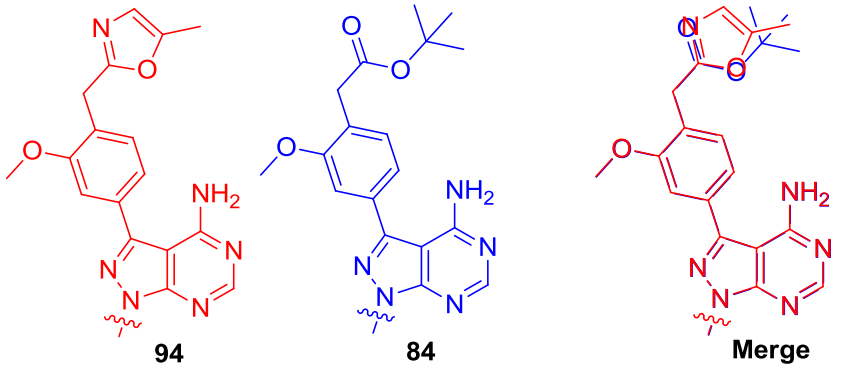

Figure 7.6: *Compounds **84** and **94** merged together to show the similarities in their 2D structures.*

Compounds **75-81** all gave micro molar EC_{50} values against MDA-MB-231 cell proliferation. From these low values, important SARs can be derived:

75: A hydroxyl group and, therefore, a hydrogen bond donor, is not tolerated.
76: Results suggest that the methoxy is required; however, compound **85** suggests it is not.
77: The carbamate group is optimum at the para position of the phenyl group.
78: A pyridine instead of phenyl ring is not well tolerated.
79: A lipophilic group instead of methoxy, represented by an indole, is not tolerated.
81: The methoxy and carbamate groups are optimum at meta and para, respectively.

Given all the data gathered from the compounds it can be summarised that the carbamate group must be in the para (4) position but substitution for an ester, by substitution of the -NH- for a -CH_2-, is well tolerated. The methoxy group is not required *if* an ester is present instead of the carbamate, however, adds an extra degree of potency when present. Furthermore, the methoxy group *is* required when the carbamate is present. This can perhaps be explained by considering the intramolecular interactions between the NH and methoxy group, figure 7.7.

The use of the indole group not only challenged the requirement of the methoxy but also forced the carbamate group to adopt a more rigid position. Further, the introduction of

pyridine, indole and nitrile groups are not tolerated, neither is having an amide instead of ester. An oxazole is also a good and stable substitution for the ester group.

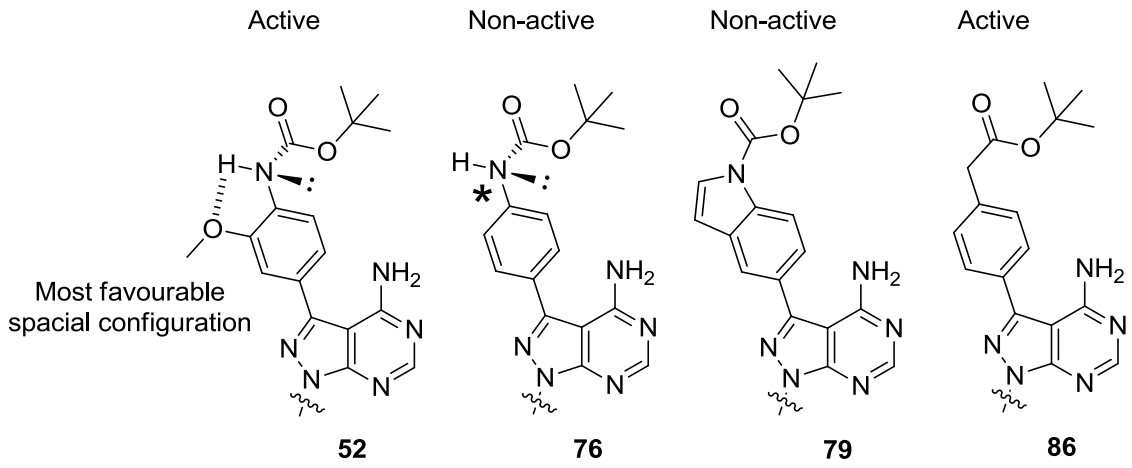

Figure 7.7: *Compounds **52, 76, 79** and **86** highlighting the spatial requirements for activity.*Perhaps the lone-pair of electrons on the nitrogen are forced perpendicular to the phenyl ring to accommodate bonding with the aromatic pi system.*

7.2.5 Synthesis of Compounds 99, 100 and 101 to Complete SAR on 'South' of Structure

Through all structural modifications in section 7.2.4, compound **52** remained the most potent compound against cell proliferation. As a final nail in the coffin for the optimisation of the 'south' amine part of the structure, 3 more compounds were designed and synthesised, scheme 7.5. Previously, in section 3.2.2, compound **8** was shown to be one of the most potent of the library one compounds featuring a 4-methylpiperizine group. In contrast, compound **11** was non-active, featuring a 4-hydroxypiperidine group. By modifying this group to a 4-methoxypiperidine, the properties of the group are changed from a hydrogen bond donor to an acceptor which appears to be favourable in these group of inhibitors. The 3 new compounds designed featured 4-methylpiperizine, 4-methoxypiperidine and 3-dimethylaminopiperidine groups, thus, challenging the position of the key nitrogen in the 'south' of the molecule.

The compounds were synthesised as previously by reduction amination using aldehyde **6** and one of three amines then Suzuki reaction with [4-(tert-butoxycarbonylamino)-3-methoxy-phenyl]boronic acid, scheme 7.5, in excellent yield.

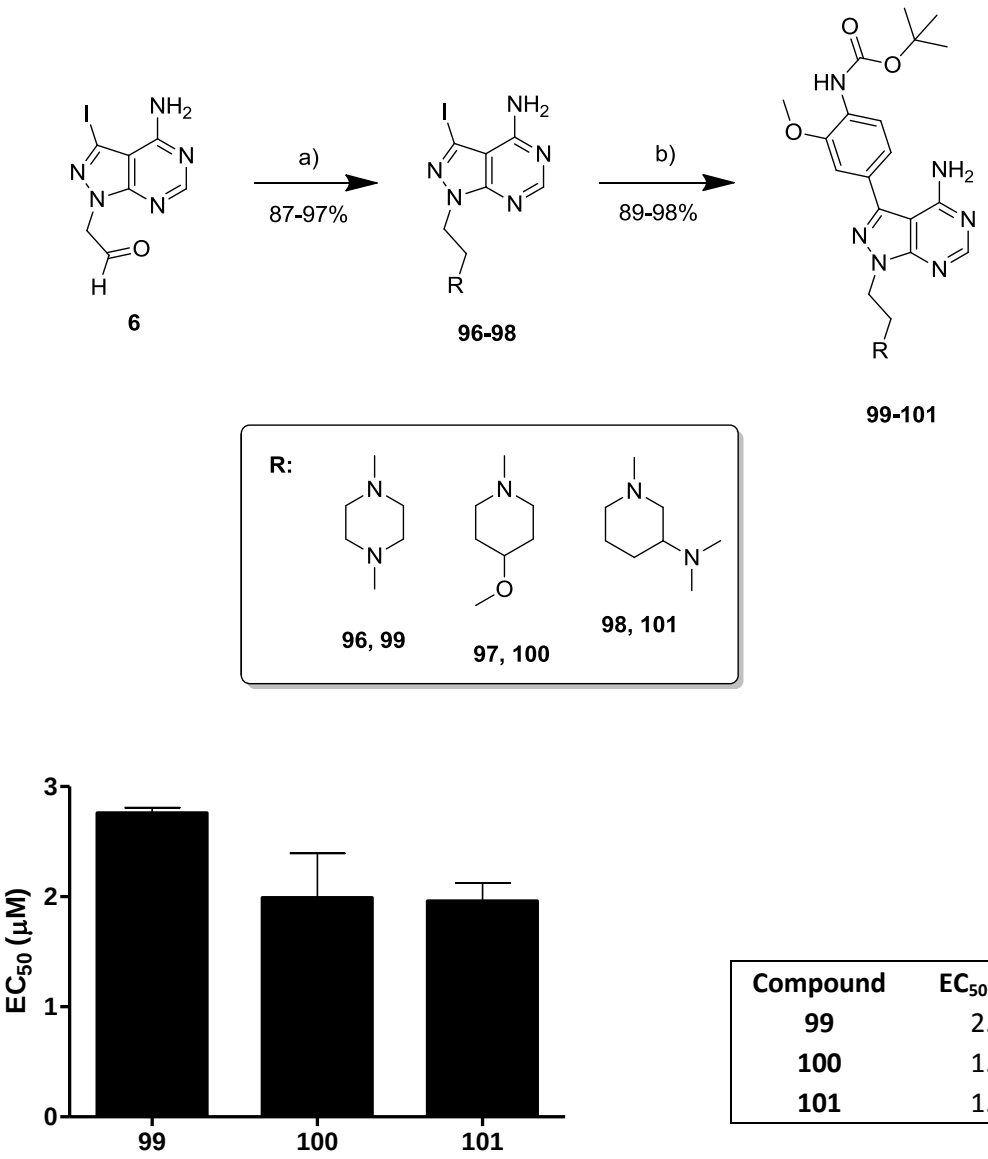

Compound	EC_{50} (μM)
99	2.76
100	1.99
101	1.96

Figure 7.8: Scheme 7.5, top: *Synthesis of intermediates **96-98** and final compounds **99-101**. a) 4-methylpiperizine (**96, 99**); 4-methoxypiperidine (**97, 100**); or 3-dimethylaminopiperidine, AcOH, $NaBH(OAc)_3$, DCM, r.t. b) [4-(tert-butoxycarbonylamino)-3-methoxy-phenyl]boronic acid, K_2CO_3, $Pd(OAc)_2$, PPh_3, 1,4-dioxane/water (10:1), 120 ^oC, mw. Bottom: Plotted EC_{50} values against MDA-MB-231 cell proliferation. Error bars denote standard deviation, n=3.*

The compounds were tested in cell viability assays using MDA-MB-231 cells. EC_{50} values calculated from curves plotted in GraphPad Prism are shown in figure 7.8, plotted as a bar graph. All 3 compounds gave supra-micromolar EC_{50} values. Compared with lead compound **52**'s value of ~10 nM these compounds were 200x less potent. This drastic difference in potency from such a subtle change highlights how sensitive enzymes truly are with regard to their inhibitors. Furthermore, this data provides great confidence that the original 4-

dimethylaminopiperidine group is optimum for SRC inhibition and/or compound penetration into cells to reduce their proliferation.

Such is the beauty of phenotypic drug discovery, even the most potent enzyme inhibitor is not considered a drug unless it possesses the correct physical properties to enable it to pass through the cell membrane and exert its effects. Phenotypic drug discovery supports the unearthing of these properties simultaneously, and quickly divides the good from the poor compounds by providing rapid proof-of-concepts in functional cell based assays. From a critical point of view, however, using this strategy, compounds with interesting binding activities but poor cell penetrability may be discarded as inactive. Those discarded compounds, which have the potential to be physicochemically improved in further medicinal chemistry campaigns, represent the real collateral damage of this pragmatic approach of drug discovery.

7.2.6 Kinase Activity of Compounds 55, 56, 66, 76, 84, 86, 87, 94 and 99

All compounds that gave EC_{50} values of less than 1 μM were tested against the SRC family kinases to determine their on-target potency and selectivity. Compounds **76** and **87** were included in this study to gain a greater insight into why they were less potent than their ester equivalents, **86**, as was compound **99** to see how SRC inhibition differed by placing the nitrogen into the ring. Compounds were tested against the same 14 kinases as before as well as BRK/PTK6, previously shown to be inhibited by compound **52**. The study was conducted by Reaction Biology Corp. as described in section 10.7.15.

The IC_{50} values against the 15 kinases are shown in table 7.2. Comparing all compounds with the same north of the molecule (compounds **55**, **56** and **99**) with **52,** compound **99** is the weakest of the three with an IC_{50} of 20.9 nM against SRC. This is in good agreement with its reduced anti-proliferative effects against MDA-MB-231 cells and provides good confirmation that the nitrogen of the 4-dimethylamino group is in the optimum position in the other compounds. Nonetheless, **99** is still a very potent inhibitor against SRC family members with excellent selectivity over ABL. Compounds **55** and **56**, which showed excellent potency against cell proliferation, are both very potent SFK inhibitors. Compound **55** is slightly more potent, leaving **56** to be slightly more selective against ABL. These data are in good agreement with their EC_{50} values, section 7.2.1.

Kinase \ Hit	55	56	63	64	66	76	84	86	87	94	99
	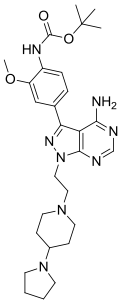	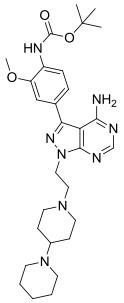	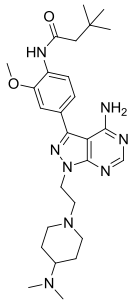	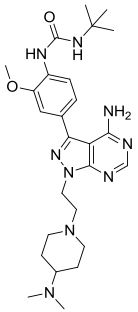	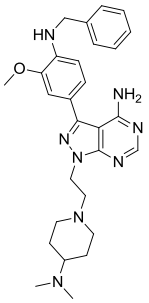	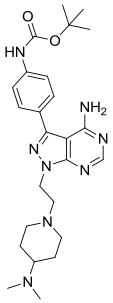	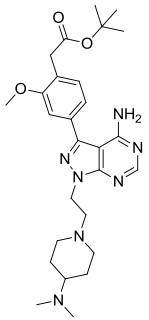	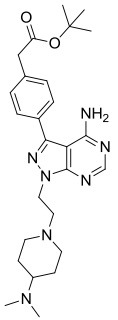	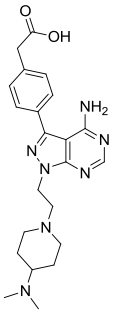	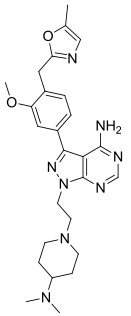	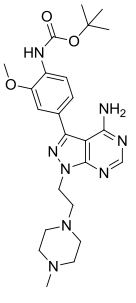
ABL1	406.7	808.2		9440.0	1204.0		370.0	2950.0		3460.0	4690.0
BLK	2.7	8.5	452.8	307.0	7.0	378.0	3.7	15.4		49.4	118.0
BRK/PTK6	22.0	30.4	206.0	198.0	36.5	242.0	20.9	37.3		43.9	34.0
FGR	<0.5	<0.5	53.7	74.00	1.1	9.490	<0.5	<0.5		3.4	1.2
FRK/PTK5	3.1	7.3	1267.0	1680.0	166.9	730.0	5.1	30.5		192.0	30.7
FYN	0.8	4.1	787.2	749.0	4.3	342.0	3.1	6.4		156.0	29.8
HCK	2.3	4.8	344.2	492.0	7.4	308.0	2.5	10.3		102.0	10.0
c-KIT	4041.0	6302.0		5820.0	514.3	22200.0					
LCK	<0.5	3.1	63.0	87.9	1.5	30.8	0.5	1.3		6.9	1.3
LYN	<0.5	1.6	298.8	444.0	5.7	259.0	0.7	5.0		44.9	12.1
mTOR											
PDGFRa		9886.0			6666.0						
RET					7496.0						
c-SRC	<0.5	0.9	113.6	194.0	3.5	71.30	1.0	1.0		46.3	20.9
YES/YES1	<0.5	0.6	30.3	36.4	0.6	7.9	<0.5	<0.5		1.5	0.8

Table 7.2: *IC_{50} values (nM) against 15 kinases. Values below 100 nM are highlighted in red. Empty boxes indicate no inhibition.*

Compounds **63** and **64** are much weaker SFK inhibitors, not surprising given their high EC_{50} values against cell proliferation, which, again, strongly suggests that a hydrogen bond acceptor is essential closer to the t-butyl position. Compound **66**, which turned out to be a potent SFK inhibitor, remains a mystery as to why it is so potent. It does not possess an oxygen to act as a hydrogen bond acceptor as previous results suggest necessary. However, perhaps its mode of binding differs from the other compounds and the phenyl ring has access to a lipophilic pocket. Structural studies would be needed to support any hypotheses.

Compounds **76**, **84**, **86** and **87** had IC_{50} values which corresponded greatly to their respective potencies against cell proliferation. **87** was completely non-active against all kinases tested, most likely due to its highly charged nature, explaining its zero effect when tested in cells. Again, **76**, **84** and **86** follow the same trend seen with the cell viability assay. Compound **76** is only a moderately potent SFK inhibitor whereas, **84** and **86** are very potent inhibitors, with **84** being slightly more potent, however, sacrificing on the selectivity over ABL. Both these compounds represent leads due to their excellent potency against cell proliferation, inhibition of the SFKs, and lower molecular weight (509 and 479, respectively).

7.2.7 Synthesis of Pyrazole Compound 104

There are many examples in the literature of the binding modes of pyrazolopyrimidine based kinase inhibitors through x-ray crystal structures and computational models.[92, 109, 130, 131] All of these examples show important binding between the NH_2 and one of the pyrimidine nitrogen's with the enzyme – with glutamic acid commonly binding to the NH_2. As the pyrazolopyrimidine mimics the adenine of ATP, it is understandable to see why such important binding occurs between the amino-pyrimidine ring and the active site. Nonetheless, compound **104** was synthesised to prove that the pyrimidine was essential for activity from 3-iodo-1H-pyrazole following the route in scheme 7.6. If it turned out that compound **104** was equally as active, this would provide a great opportunity to reduce the molecular weight of the compounds, thus, increasing their ligand efficiency.

The compound was synthesised in good yield and tested in a MDA-MB-231 cell viability assay. The resulting EC_{50} against cell proliferation was 32.6 μM, conclusively proving that the pyrimidine was essential for compound activity. Given the essential role of this group, this result further corroborates that the compounds described in this thesis do bind to the ATP site of the protein.

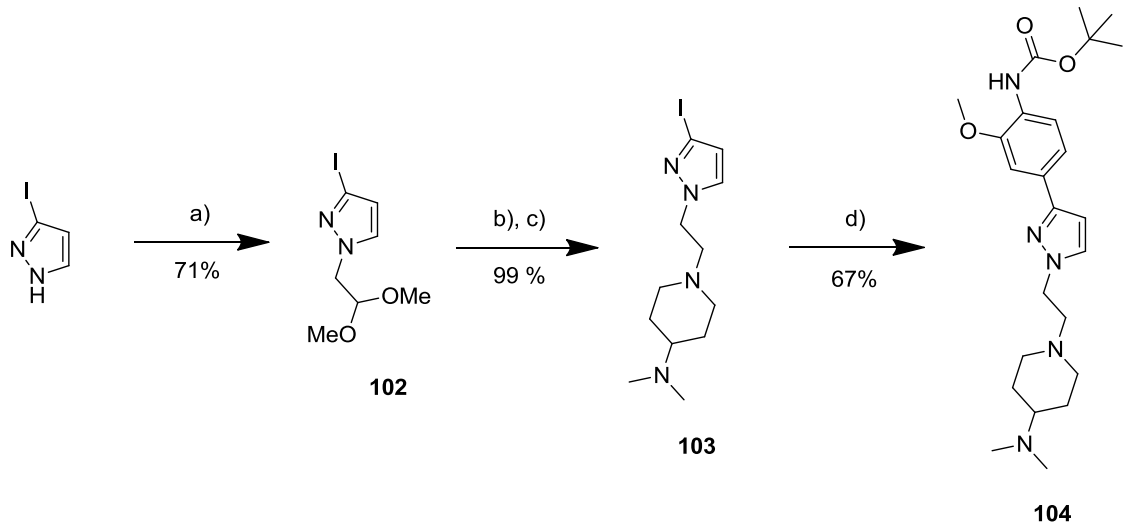

Scheme 7.6: *Synthesis of intermediates **102** and **103**, and final compound **104**. a) Bromoacetaldehyde dimethyl acetal, NaH, DMF, 150 °C, mw. b) TFA/H_2O (1:1), 100 °C, mw. c) 4-dimethylaminopiperidine, AcOH, $NaBH(OAc)_3$, DCM, r.t. d) [4-(tert-butoxycarbonylamino)-3-methoxy-phenyl]boronic acid, K_2CO_3, $Pd(OAc)_2$, PPh_3, 1,4-dioxane/water (10:1), 120 °C, mw.*

7. Optimisation of Lead Compound 52

7.3 Conclusion

The SAR map, figure 7.1, was created to question which groups, and their positions, were essential for compound activity, and whether alteration would improve or supress activity. As such, 25 compounds were synthesised to search for the ideal and optimum positions of groups belonging to lead compound **52**. The 'answered' map is shown in figure 7.8 with the structure activity relationships of **52** highlighted.

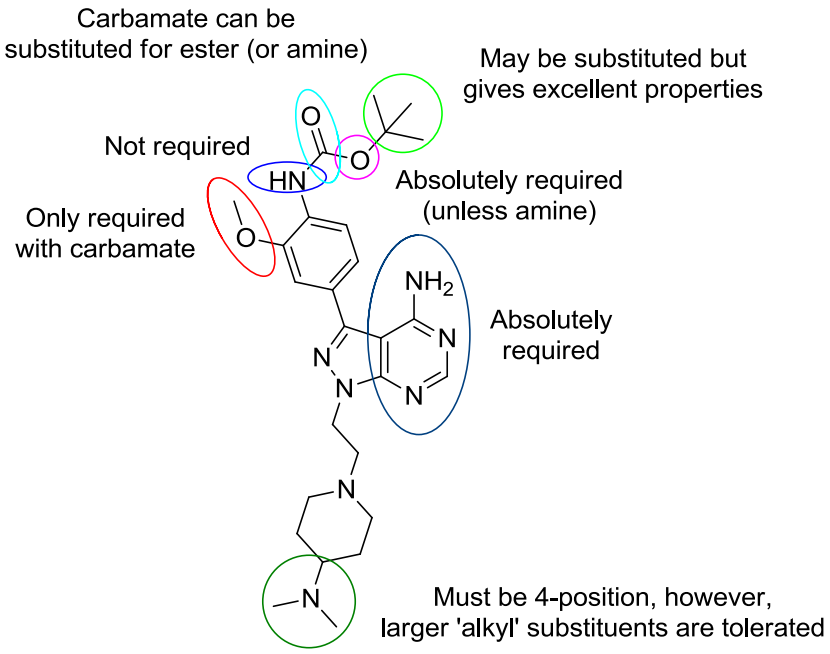

Figure 7.8: *Structure activity relationships of compound **52**.*

Exploration of the aryl group of lead compound **52** and final optimisation of the amine moiety of the structure has unveiled a total of 6 compounds with lead-to-candidate drug properties. Compounds **52**, **55**, **56**, **66**, **84** and **86** all showed excellent potency against triple negative breast cancer, MDA-MB-231, cell proliferation and sub-nano molar inhibition of one or more of the SFKs with generally excellent selectivity over ABL and other related kinases such as c-KIT, PDGFRa and RET. Their properties are summarised in table 7.3.

Up until this point, the physicochemical properties of the compounds have been ignored, owing to the adaptability of phenotypic drug screening to discriminate between those compounds with good or bad properties. However, advancing a compound to the preclinical or clinical stage requires thought to such properties, as such, they are also listed in table 7.3.

Compound	52	55	56	66	84	86
	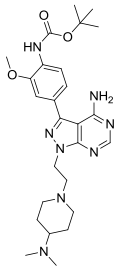	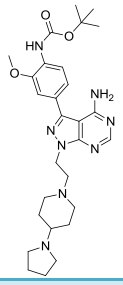	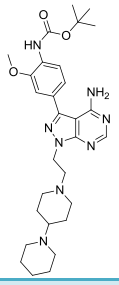	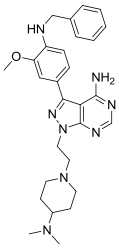	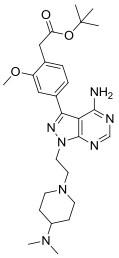	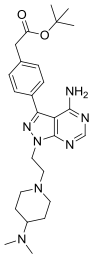
MW	510.63	536.67	550.7	500.64	509.64	479.62
clogP	2.693	3.096	3.601	3.057	3.027	3.043
TPSA	123.675	123.675	123.675	97.37	111.648	102.414
H-bond Donor	2	2	2	2	1	1
H-bond Acceptor	9	9	9	7	9	8
EC_{50} - 231 (nM)	9.08	39.24	80.63	201.77	35.85	100.27
EC_{50} - MCF7 (nM)	30.99	76.52	208.95	583.2	414.9	2581.7
IC_{50} - ABL (nM)	479.0	406.7	808.2	1204.0	370.0	2950.0
IC_{50} - SRC (nM)	< 0.5	< 0.5	< 0.5	3.5	1.0	1.0
Ratio ABL:SRC	958	813	1616	344	370	2950

Table 7.3: *Summary of key properties of 6 lead compounds. MW: molecular weight. clogP: Calculated logP (Molinspiration Cheminformatics). TPSA: Topological polar surface area (Molinspiration Cheminformatics). *For compounds with <0.5 nM IC_{50}, the ratio of ABL to SRC was calculated using 0.5 as a value for SRC.*

All compounds possess properties which conform to Lipinski's rule of five (MW <500, logP <5, H-bond donor <5 and H-bond acceptor <10), albeit the molecular weight is slightly above the Lipinski's limit of 500.[132] However, the rule of five should be taken as a rough guide and not as an absolute necessity. Furthermore, these 'rules' are more appropriate when designing drugs from scratch and not when optimising drugs already shown to be effective, as in the compounds above. The polar surface areas of all 6 drugs are below the 'upper' limit of 140 Å, which is a good predictor for the permeation of compounds through membranes.[133, 134] The ratio between ABL and SRC inhibition is also listed in table 7.3. This highlights the excellent selectivity between the two kinases, something that was unprecedented to date.

8. Pre-clinical Testing of Lead Compounds

8.1 Introduction & Aims

Pre-clinical testing of a drug involves determining whether a compound has the potential, and safety aspect, required for use in humans, using biological techniques. Drug metabolism and pharmacokinetics (DMPK) is commonly used to describe such studies. Here the absorption, distribution, metabolism, excretion and toxicology (ADMET) of a compound is assessed to predict its safety and usefulness as a drug. It is important to assess these properties of a drug prior to clinical testing. Contrary to the lab, drugs *in vivo* may act differently and the best compound in the lab may simply be too poorly absorbed or metabolised too quickly, to be useful as a drug. It is at this point that properties other than efficacy are more important. Perhaps a less potent drug has the better ADMET properties and is the best choice for clinical evaluation. Dosing schemes can also be predicted or determined by looking at the metabolism and clearance of a drug vs. its bioavailability – absorption and distribution. These studies are not only undertaken pre-clinically but remain important when the drug is finally dosed in human.

Firstly, it is important to assess a drug's toxicity, in particular, any potential cardiotoxicity. QT (the time taken from the start of the Q to the end of the T wave in the heart's electrical cycle) prolongation is a potentially fatal condition in which the QT interval is elongated during the heart's electric cycle. These cardiac arrhythmias can be brought on by inhibition of one of the potassium channels in the heart known as human ether-a-go-go or hERG, which a surprising number of drugs are able to inhibit. Inhibition of the hERG channel has become a major obstacle for drug development, particularly in industry, due to its connection with QT interval prolongation.[135, 136] For this reason, it is important to assess the effect of any new drugs in development against hERG in order to modify, or rule out, any potential compounds likely to cause future complications.[137] Compounds which possess a basic amine with aromatic/lipophilic groups surrounding are prone to hERG inhibition and common pharmacophores have been identified to try and predict hERG liabilities.[138-140] Figure 8.1 shows some drugs that are known to clinically induce QT prolongation. Here the common pharmacophores can be identified: all compounds possess substituted piperidines and lipophilic aromatic groups, a feature common to the 6 lead compounds described in section 7.

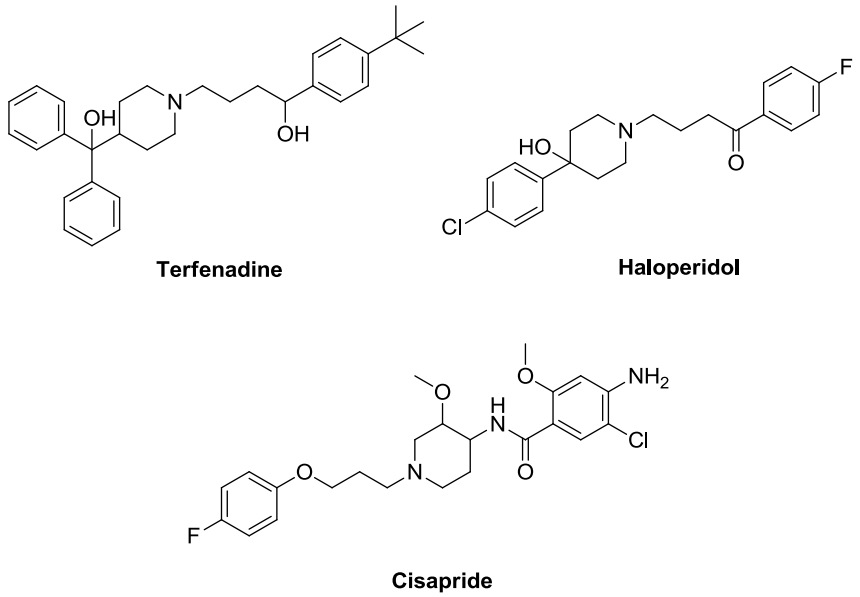

Figure 8.1: *Three drugs known to clinically induce QT prolongation via inhibition of hERG. Substituted piperidines and lipophilic aromatic groups are common to all three structures, highlighting a pharmacophore model for hERG inhibition.[141]*

Whether drugs are administered orally or intravenously, or otherwise, they must enter the blood stream (unless topical medicines) to enable transport around the body and reach the site of action. Firstly, this requires soluble and permeable compounds stable to the acidic conditions of the stomach, if taken orally. Secondly, an important factor to consider is a drug's stability and binding properties in the blood itself. Proteins are able to bind to drugs in the blood, appropriately called plasma protein binding (PPB). Too highly bound could mean drugs are unable to reach their targets, thus, limiting their effectiveness, and too weakly bound could mean the drugs are cleared from the body quickly, thus, limiting their half-life. Further, some drugs may be unstable in blood plasma alone. There are an abundance of enzymes in the blood, including many esterases, capable of metabolising drugs. For this purpose, plasma stability assays are carried out to determine a drug's stability over a time period in blood plasma.

The main site of metabolism in the body is the liver. Although essential for the proper clearance of toxic substances from the body, fast metabolism of drugs limits their effectiveness and lowers convenience for the patient as higher or more frequent doses are required to maintain a steady concentration of active drug. Most metabolisms in the liver occur from cytochrome P450 (CYPs) enzymes found in the endoplasmic reticulum (ER). In the lab, these CYPs can be concentrated into small vesicles known as microsomes by cell

centrifugation. The microsomes, containing parts of the ER with CYPs, are then incubated alongside drugs to assess their stability in a given time period. Similarly, stability can be assessed by incubation with whole liver hepatocyctes over a time period. This is, arguably, more representative of natural bodily functions than CYPs or microsomes in isolation.

Along with CYPs conducting essential (and sometimes troublesome) metabolism of drugs, they also conduct the metabolism of some endogenous hormones and are even involved in the synthesis of cholesterol.[142] Therefore, CYPs play an important role in the body. Some drugs are capable of inhibiting CYPs, rather than acting as substrates. This causes problems for the metabolism of other compounds/drugs so potentially dangerous overdoses may occur when more than one drug is taken. This is known as drug-drug interactions. To test for this, compounds can be incubated with various CYPs, in isolation, to determine if they inhibit or induce the enzymes. CYPs 1A2, 2A6, 2C8, 2C9, 2C19, 2D6, 2E1 and 3A4 are the isoforms generally used to determine drug-drug interactions.[143]

Although *in vitro* testing gives some insights into the more important issues of pre-clinical testing, it is often hard to predict how a drug will actually behave in a whole organism. For this purpose, pharmacokinetic (PK) studies can be carried out in mice or rats to determine oral bioavailability and the half-life of a compound.

The excretion of a drug is less commonly studied as it generally requires radio labelled compounds and the collection of urine and faeces from an organism. It is difficult to assess a drug's excretion *in vitro* and so experiments are generally more expensive. As long as the drug, or its metabolites, do not accumulate in the body, excretion is generally not a problem.

Although the chemistry around the lead structures could go on indefinitely, the 6 compounds, described in section 6.3, possessed the properties of leads suitable for pre-clinical evaluation. The considerations discussed above highlight some of the most common tests taken pre-clinically to assess whether a drug is suitable/safe for clinical studies.

8. Pre-clinical Testing of Lead Compounds

8.2 Results

8.2.1 hERG Liability Study

The 6 lead compounds all possess a basic amine (2, in fact) and an aromatic (though not lipophilic, except **66**) group commonly associated with hERG inhibition so it was essential to test their activity against the hERG channel before advancing any further. Compounds were added to mammalian cells expressing the hERG channel in a 384-well plate across a concentration range (8nM to 25 µM). The percentage change in hERG tail-current was then calculated by whole-cell voltage-clamping and IC_{50} values calculated from the data. The study was performed by Cyprotex, see section 10.7.8 for methods.

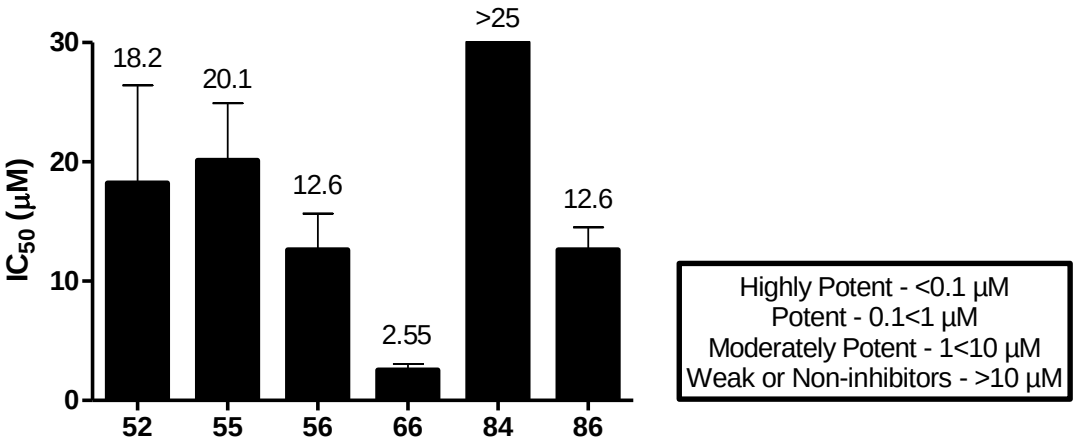

Figure 8.1: *IC_{50} values against hERG inhibition plotted as a bar graph for 6 lead compounds. Replicates ranged from n=11 to n=18. Error bars denote standard error. Compound **84** showed 25 % inhibition of hERG at the top concentration of 25 µM so an accurate IC_{50} could not be calculated. Curve fit estimates suggest ~140 µM.*

The study revealed that all compounds inhibit hERG above 1 µM. Only one compound, **66**, was considered a moderately potent hERG inhibitor with the other 5 being weak or non-inhibitors, in the case of **84**. This correlates well with the pharmacophore model which suggests more lipophilic aromatic groups inhibit hERG to a greater extent. This excellent result allowed the progressing of compounds towards assessing their stability and other ADME properties. With **86** being less potent than the other compounds in the viability assays, and the cost of screening taken into consideration, it was disregarded going forward

and only the other 5 compounds were tested for CYP inhibition. Although **66** was a moderately potent hERG inhibitor, and was less potent, both against SRC and MDA-MB-231 cell proliferation, it was included in the next study due to its structural difference over the other 5 inhibitors.

8.2.2 Cytochrome P450 Enzyme Inhibition Assay

As discussed above, inhibition of the cytochrome P450 enzymes can result in a potentially dangerous drug overdose due to the reduced metabolism of another drug. To test for this, compounds **52, 55, 56, 66** and **84** were screened at 10 μM in duplicate against 5 of the most commons CYPs to cause drug-drug interactions – CYPs 1A2, 3A4, 2C9, 2D6 and 2C19 – table 8.1. This work was undertaken by Dr Scott Webster, The University of Edinburgh, see section 10.7.9 for methods.

Compound	CYP1A2	CYP3A4	CYP2C9	CYP2D6	CYP2C19
52	24.54	0	0	0	0
55	6.86	0	0	0	0
56	0	0	0	0	0
66	8.25	3.05	0	0	26.80
84	4.33	5.59	0	0	0
Naphthoflavone (1A2, 2C19)	99.82				99.29
Ketaconozole (3A4)		92.62			
Sulphenazole (2C9)			95.57		
Quinidine (2D6)				88.09	

Table 8.1: *Inhibition of cytochrome P450 enzymes by compounds **52, 55, 56, 66** and **84**. Experiments were performed in duplicate and average values calculated. Appropriate controls are highlighted towards the bottom of the table. Blank spaces indicate non-tested. 0 indicates zero or negative values.*

The study revealed that the compounds had very little inhibition over the 5 CYPs. CYP1A2 was the most inhibited enzyme with 24.5% inhibition observed from compound **52** and compound **66** caused the most inhibition with 3 CYPs being inhibited from 3-27%. Overall, the compounds caused very little CYP inhibition at a moderately high concentration of 10 μM. This was an excellent result, giving rise to confidence that the drugs should not cause significant drug-drug interactions *in vivo*, although, it would be essential to test against all the known isoforms, and get IC_{50} values, for full reassurance.

8.2.3 Plasma Protein Binding Study

Compounds **52, 55, 56, 66** and **84** were subjected to plasma protein binding (PPB) assays to assess to which extent they were likely to remain bound to plasma in the blood. This plays an important role on the clearance of a drug from the body and also may determine which dose to give to a patient. Compounds were incubated with human or rat plasma at 37 ^{o}C for 24 hours then the percentage unbound determined by LC-MS/MS. Compounds were tested in duplicate with Warfarin (99-100% bound) and Quinidin (81-87% bound) as controls.[144] This work was undertaken by Dr Scott Webster, The University of Edinburgh, see section 10.7.10 for methods.

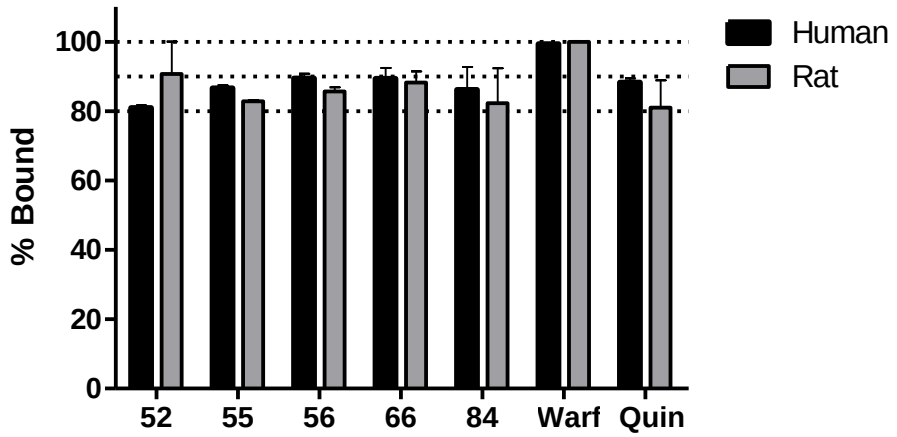

Figure 8.2: *Average bound fraction of compounds **52**, **55, 56, 66** and **84** plotted as a percentage of starting concentration in human and rat plasma. All compounds were between 80 and 90% bound to plasma proteins which are widely accepted values. Warf = warfarin; Quin = quinidine. Error bars denote standard deviation, n = 2.*

All compounds were between 80 and 90 % bound to plasma proteins in both the human and rat plasma. The ideal value of bound drug is widely disputed, however, even though > 90% bound is considered to be high, 30% of drugs approved between 2003 and 2013 had > 95% PPB and 5% had > 99% PPB.[145] A value between 80 and 90% is a generally accepted value.

8.2.4 Human Liver Microsome Stability Assay

The bioavailability of a compound is dependent on many factors with one of them being the first-pass metabolism by the liver. To get an idea for metabolism by CYPs, human liver microsomes (HLM) were incubated alongside the 5 compounds for 30 minutes, at 37 ^{o}C, and the percentage remaining compound determined, relative to the parent compound at the start of the assay. The results, figure 8.3, show generally excellent stability across all compounds. Unfortunately, the data for compound **56** was inconsistent due to problems with the MS so it has been excluded from the study. This work was undertaken by Dr Scott Webster, The University of Edinburgh, see section 10.7.11 for methods.

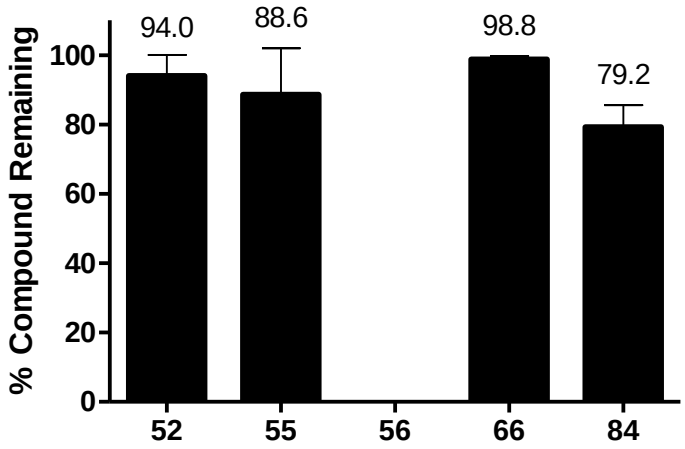

Figure 8.3: *Percentage compound remaining after 30 min incubation with human liver microsomes relative to time 0. All compounds showed values >75 % remaining, thus, indicating they are highly stable in the presence of liver microsomes. Error bars denote standard deviation, n = 2.*

Given that compound **84** is an ester, rather than a carbamate, it is understandable that is should be less stable in the presence of microsomes containing CYPs. Nonetheless, 79% of the parent compound was still detectable after 30 minutes incubation. Further, the most likely metabolite of **84** is the carboxylic acid derivative, compound **86**, which is completely non-active against the SFK or cells. That means the primary metabolite of **84** is likely to be non-active and non-toxic in the body, and cleared very quickly due to its charged nature. Predictable metabolisation pathways aid the anticipation of the formation of toxic metabolites and, if necessary, aid the optimisation of drugs with less toxic metabolites.

8.2.5 Stability in Human, Mouse and Rat Plasma

Compounds **52, 55** and **84**, which excelled in the hERG, CYP, PPB and HLM study, had their stability in human, mouse and rat plasma tested. Due to costs, compound **56** and **66** were excluded as they had shown greater potency towards hERG, and were generally less potent than the other compounds. As the blood is the main transport system for carrying drugs around the body, their stability in plasma is critical to their effectiveness as a treatment. Compounds **52, 55** and **84** were incubated at 1 µM with plasma from either human, mouse or rat for 2 hours at 37 ^{o}C. The percentage of compound remaining after 15, 30, 60 and 120 minutes was determined by LC-MS/MS and reported relative to time 0. Studies were performed by Cyprotex, see section 10.7.12 for methods.

Compounds were stable in all 3 plasmas with > 90% recovery after 2 hours incubation, figure 7.4. Compound **84**, which contains an ester rather than a carbamate, was also stable in all 3 plasmas. This is an excellent result given that esters are generally less stable than carbamates, more so, in plasma, which contains a cocktail of enzymes including esterases.

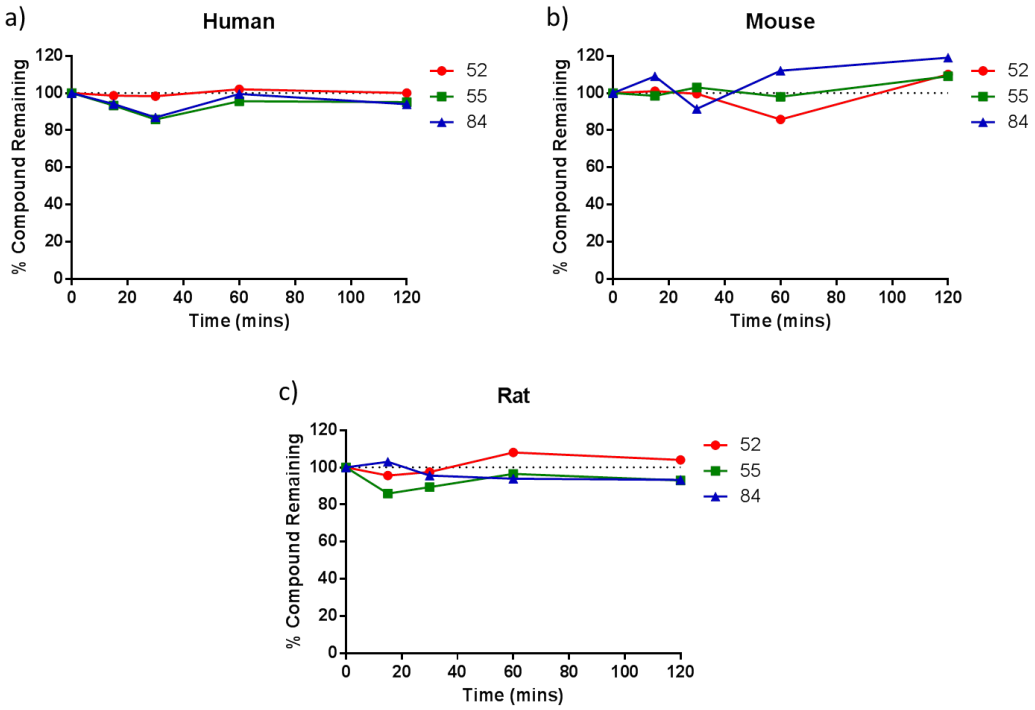

Figure 8.4: *Compound stability in a) human, b) mouse or c) rat plasma over 2 hours. All compounds showed >90% recovery after 2 hours incubation.*

8.2.6 Hepatocyte Stability of Compounds 52 and 84

Compounds **52, 55** and **84** were stable in human, mouse and rat plasma, however, most metabolism occurs in the liver and, although the compounds were previously tested with human liver microsomes, more robust assessment of their stability was required before proceeding to *in vivo* studies. Compounds, **52** and **84** were incubated with mouse and human hepatocytes, which contain the CYP enzymes necessary for metabolism, to assess their stability.

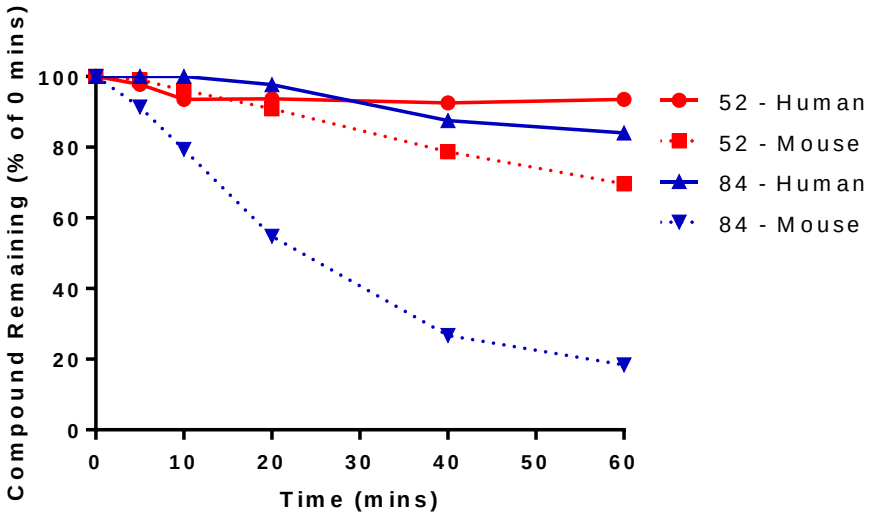

Compound	CL_{int} (µL/min/10^6 cells)	SE CL_{int}	$t_{1/2}$ (min)
52 - Human	1.84	0.989	751
52 - Mouse	12.5	0.447	110
84 - Human	6.82	0.853	203
84 - Mouse	67.9	3.08	20.4

Figure 8.5: *Compound stability in human and mouse hepatocytes over 60 minute incubation. Calculated factors from hepatocyte study - intrinsic clearance (CL_{int}) with standard error (SE) and half-life ($t_{1/2}$).*

Compounds **52** and **84,** at 3 µM, were incubated with hepatocytes over 60 minutes and samples taken at 0, 5, 10, 20, 40 and 60 mins and analysed by LCMS/MS. Data is presented relative to compound concentration at time 0 and intrinsic clearance and half-life calculated from the values obtained. Verapamil and umbelliferone are used as control compounds. Studies were performed by Cyprotex, see section 10.7.13 for methods.

As expected, and in correlation with the human liver microsome study, 8.2.4, compound **84** was less stable than **52**, figure 8.5. This can be attributed to the less stable ester in **84** compared to the carbamate in **52**. Compound **84** is rather unstable in mouse hepatocyctes with a half-life of only 20.4 minutes. However, incubation with human heptocytes gave a $t_{1/2}$ value of 203 minutes, 10x longer than in mouse. Importantly, the same trend was observed for compound **52** in human and mouse hepatocytes (7.5x difference in half-life). This emphasises the importance of cross species testing, more importantly, it highlights that data obtained from mice experiments cannot translate similarly in humans but consistent differences between values in different species from structurally related compounds can help to estimate the expected human half-life after corroboration of *in vivo* PK.

Compound **52** showed significantly to be more stable in human hepatocytes than mouse, and gave a $t_{1/2}$ of 751 minutes and intrinsic clearance value of 1.84 µL/min/10^6 cells. These represent very encouraging values indicating that the compounds are stable enough for therapeutic dosing.

8.2.7 Pharmacokinetic Data of Compounds 52 and 84

Given that compound **52** is the superior compound in terms of SFK inhibition, and against cell viability, it was chosen to undergo mouse PK studies to determine its oral bioavailability and half-life, *in vivo*. Both compounds **55** and **84** showed similar potencies regarding kinase inhibition and cell proliferation, however, compound **84** was superior in the hERG assay meaning that a higher dose could be accepted in the clinic without causing toxicity, at least due to hERG inhibition. **84** is also of lower molecular weight (509.64 vs 539.67) than **55** which makes it the more efficient ligand and more compliant to Lipinski's rules. The presence of an ester, rather than a carbamate, does make **84** less stable than **55**, as demonstrated by the HLM study, however, it would result in a nice comparison in PK values with **52** *in vivo*. Further, compound **52** and **84** both showed excellent-to-good stability when incubated with human hepatocytes. This work was performed by Cyprotex, see section 10.7.14 for methods.

Female CD1 mice were given 10 mg/kg (0.25 mg/25 g mouse) of compound **52** or **84** orally (as a solution in nanopure water) or via IV injection (as a saline solution) and compound concentration measured over 8 hours. Shown in figure 8.6 are the concentration curves over 8 hours of both compounds after oral and IV administration, respectively. The consequent half-life and bioavailability values are shown in table 8.1.

Compound	$T_{1/2}$ (hrs)	Bioavailability
52	2.94	25.3 %
84	2.14	52.1 %

Table 8.1: *In vivo half-life and bioavailability based on the PK data for compounds **52** and **84**.*

The half-life values of 2.94 and 2.14 hours for compounds **52** and **84**, respectively, are moderate and acceptable values as is, however, the hepatocyte studies strongly suggest that the compounds would be more stable in humans than in mice. The bioavailability values of 25.3 and 52.1 % for **52** and **84**, respectively, are reasonable values, again suggesting that both compounds could be suitable as orally available drugs.

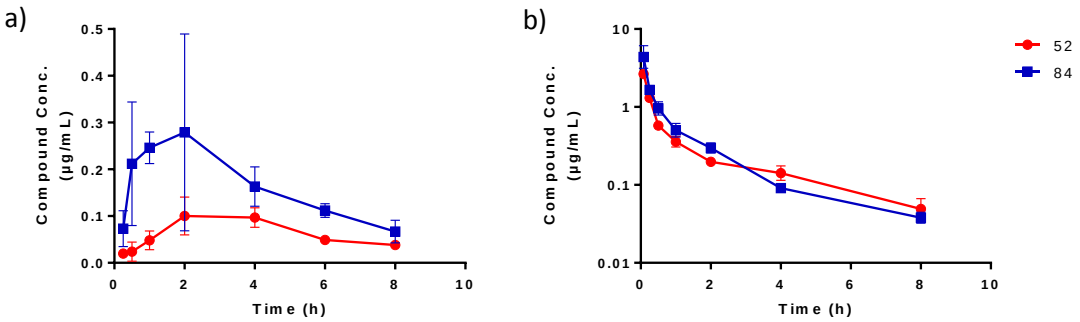

Figure 8.6: *In vivo pharmacokinetic data of compounds **52** and **84**. Average compound concentration over 8 hours following, a) oral administration and, b) IV administration.*

8. Pre-clinical Testing of Lead Compounds

8.3 Conclusion

Compounds **52, 55, 56, 66, 84** and **86,** optimised via a mechanism informed phenotypic drug discovery route, previously presented properties suggestive of a preclinical candidate. As such, they were progressed through assays designed to test hERG inhibition, cytochrome P450 enzyme inhibition, plasma protein binding, human liver microsome stability and stability in human, mouse and rat plasma. Compounds **52** and **84**, which excelled in all the assays described, had their pharmacokinetic properties in mice tested leading to a prediction of bioavailability and compound half-life.

Compounds **52** and **84** represent suitable candidates for further investigation and studies are currently on-going regarding their *in vivo* efficacy and toxicity in tumour xenograft mouse models.

9. Discussion

Cancer survival rates have undoubtedly improved over the last 40 years.[146] In the 1970s, only 25 % of patients diagnosed with cancer survived over ten years and, nowadays, this figure has risen to 50 %. This can be attributed to both the development of better therapies and increased knowledge and detection of cancers. These numbers are highly generalised, however, and survival depends implicitly on the type of cancer. For example, men with cancer of the testis show a 98 % survival rate over ten years, whereas, a mere 1% of patients with pancreatic cancer can expect to live over ten years.

Breast cancer remains the most common cancer in females, accounting for 30 % of cases; however, survival is generally quite high (78 %) due to the ease of detection and consequent surgical removal of the breast.[146, 147] Nonetheless, due to its high incidence, breast cancer still remains one of the most lethal cancers, accounting for 7% of cancer deaths in 2012 in the UK. In particular, triple negative breast cancer, which accounts for around 15-20% of all breast cancers, is aggressive and still poorly treated.[148] Evidently, even with the increase in survival over the last 40 years, a lot more research is required to improve the treatment options for cancer, particularly to improve efficacy and response duration across multiple patient subgroups, and particularly, those cancer sub-types which are poorly served by current therapies such as triple negative breast cancer.

Using an agile ligand based, mechanism informed, phenotypic approach to drug discovery, the identification of a series of potent and selective inhibitors towards targets strongly implicated in cancer has been discovered, and is discussed in this thesis.

Using PP1 and ATP as models, the generation and evaluation of an initial 10-membered library led to the design of a further two compounds with interesting anti-proliferative effects (EC_{50} values of 12 μM). Probing into the compounds' mechanisms of action led to the conclusion that the early 'hit' compounds **17** and **18** were affecting cell viability by the induction of apoptosis.

Further optimisation by pseudo-rational ligand-based design, and careful examination of the literature, led to the discovery of compounds **19** and **29,** which were found to affect cell viability differently, by two distinct mechanisms. Compound **19**, which was halting the growth of the cells without causing death, was revealed to be a moderately potent mTOR

inhibitor with an IC_{50} of 328 nM. Compound **29**, on the other hand, which was inducing apoptosis and causing cell death, was a potent SRC family kinase inhibitor. This enabled the classification of compounds into two different categories for exploration of selective mTOR and SRC family inhibitors, respectively.

Through optimisation of compound **19**, a series of extremely potent and selective mTOR inhibitors were produced. The most selective of which, **41**, was screened against 342 kinases - a significant portion of the kinome - and had selectivity for mTOR greater than current competitors. Its properties were thoroughly examined *in vitro* and to date, **41** represents the most selective mTOR inhibitor discovered, to the best of my knowledge. Due to its structure bearing strong similarities with INK-128, however, intellectual property for this compound, and the series, would never be granted, and such is the sad reality of the world we live in today, without intellectual property, and proper investment, a compound cannot be progressed to clinical stage. As such, the optimisation of the mTOR inhibitors has temporarily stopped until novel chemical space with freedom-to-operate is found.

Optimisation of the early SRC inhibitor, compound **29**, led to the discovery of lead compound **52**. **52** demonstrated excellent phenotypic properties in *in vitro* experiments against cell proliferation (40 and 10 nM EC_{50} against MCF7 and MDA-MB-231, respectively) and cell migration (8.6 nM EC_{50}, MDA-MB-231 cells) and was, importantly, non-toxic during incubation with zebrafish embryos. Most importantly, **52** inhibited SRC with an IC_{50} of <0.5 nM and did not potently inhibit ABL, unlike all other clinical SRC inhibitors reported. Simultaneous inhibition of ABL with an allosteric inhibitor was shown to be non-beneficial and drastically reduced the effectiveness of SRC inhibition against triple negative breast cancer cell proliferation. Further, **52** was shown to be extremely selective to the SRC family kinase branch of kinases, even at the high concentration of 1 μM. This level of selectivity allows for more predictive results in the clinic and enables the selection of patients by SRC driven biomarkers. Combination treatment involving compounds with this level of selectivity also allows for a more fine-tuned treatment while reducing the susceptibility to acquired drug resistance and adverse effects.

The development of a further 5 lead compounds was mediated by the synthesis and testing of 26 compounds, all designed to challenge the structural requirements of compound **52**. These 6 lead compounds had their properties compared in cell viability and kinase assays and possessed the characteristics suitable for pre-clinical testing.

Due to the strong attrition rate of drugs in the clinic, it is of upmost importance to thoroughly test drugs pre-clinically, to the best of one's ability. Of course, biological assays will never match the complexity and unpredictability of the human body but, nonetheless, a comprehensive investigation of their properties is sought after.

Since 1996, when the biological impact of the hERG channel was beginning to be explored, there have been 8 drugs withdrawn from the market due to observed QT prolongation.[141] However, only 1 of these drugs, propoxyphene, was removed after 2005 with the other 7 occurring before. Increasing knowledge of the hERG channel has led to robust testing of drugs, pre-clinically, to ensure that they are not later rejected in the clinic. As such, it has become paramount to test drugs for hERG inhibition prior to progression. Failure to do so could result in a costly withdrawal later on.

All 6 lead compounds were tested for hERG inhibition and were found to be non-inhibitors, in general, with only 1, compound **66**, containing an unsubstituted benzylamino group, giving an IC_{50} of 2.55 μM - a value relating to a moderately potent hERG inhibitor. It is important to note, however, that the difference between the on-target (SRC) IC_{50} and hERG's is around 1,000 fold. This large gap makes the hERG liability less of a concern. Compound **84** excelled with an estimated IC_{50} of 140 μM - completely non-active.

Compounds **52** and **85** showed little cytochrome P450 inhibition, were bound to human and rat plasma proteins between 80 and 90 %, were relatively stable during incubation with human liver microsomes, and were stable in human, mouse and rat plasma over 120 minutes. As such, they were taken forward to have their pharmacokinetic properties assessed in mice. Compound **52** had a plasma half-life of 2.94 hours and an oral bioavailability of 25.3 %. **84** had a plasma half-life of 2.14 hours and oral bioavailability of 52.1 %. Initially, these figures seemed far from optimum, however, when comparing with the clinical SRC inhibitor Dasatinib, which has a half-life of only 0.79 hours, in mice, and oral bioavailability between 14-34%, compounds **52** and **84** possess sufficient pharmacokinetic properties to allow progression.[149] Importantly, the difference in stability between mouse and human hepatocytes (>7.5x) also supports the hypothesis that the compounds would have longer half-lives in patients.

The pre-clinical testing of compounds **52** and **84** are on-going. Owing to the previously discussed properties of the two compounds, *in vivo* pharmacodynamic and efficacy models are being organised and the development of the series of compounds is in continuation.

To summarise, this thesis describes the development of a series of novel mTOR and SRC family kinase inhibitors using a ligand-based phenotypic drug discovery approach. In the relatively short time of 3 years, and low cost of approximately £100k (materials, labour and outsourcing costs), a series of compounds have been discovered possessing properties suitable for clinical evaluation. These compounds inhibit targets strongly shown to correlate with cancer progression and as such, are valuable assets to the fight against cancer. Comparing with industrial standards, the work described in this thesis is at a tiny fraction of the cost expected to produce such a potent and promising series of compounds. It is evident that, despite the identification of a plethora of new drug targets in the post-genomic era, productivity within the pharmaceutical industry is slowing, and perhaps the 'classical model' of targeted drug discovery should be thoughtfully examined and new approaches considered.

Not only does the work described in this thesis challenge the way that industry conducts its research but it also highlights that, although multi-target inhibitors may circumvent problems associated with drug acquired resistance, their off-target inhibition may present counter intuitive solutions to cancer therapy. Such is the case with ABL inhibition. The majority of SRC inhibitors, and indeed all of the clinically approved SRC inhibitors, inhibit ABL to the same or greater degree than their 'primary' target. The work described in section 6.2.2 suggests that inhibition of ABL is detrimental to cancer treatment and there is increasing evidence in the literature to support this premise, particularly regarding cardiotoxicity. [114, 115, 126, 127, 129]

Compounds **52, 55, 56, 66, 84** and **86**, to the best of my knowledge, represent the first and only sub-nano molar SRC inhibitors that do not inhibit ABL, with selectivity ranging from 344x (**66**) to 2950x (**86**), assuming a SRC inhibition value of 0.5 nM (actual value is <0.5 nM). These compounds possess properties as good as, or better than, competitors, which represent approved drugs, or clinical candidates undergoing clinical development, and could represent the basis of a valid therapy for cancer treatment, providing further investigation. The speed and cost of the discovery of these compounds represent a perfect example of the advantages of phenotypic drug discovery over traditional targeted discovery. The development of these compounds is on-going and they will, hopefully, one day represent the gold standard in SRC targeted cancer treatment.

From a critical point of view, however, it is likely that one or more of the 78 novel compounds generated and tested during this thesis could possess interesting potency and/or selectivity over targets that did not play a role on the highly proliferative nature of the cancer

cell lines used in the phenotypic screens. On the other hand, some compounds might have shown poor phenotypic effect due to low cell penetrability. These "false negatives" are indeed the main weakness of this approach. With this last comment, I would like to emphasise that the strategy proposed herein is far from perfect. Consequently, all drug discovery approaches have their place, and their validity, in the fight against cancer, and many complement each other. This modest contribution describes just another possible pathway for exploration.

10. Experimental

10.1 General Information

All experiments were performed in a Biotage Initiator microwave synthesiser or conventially under an inert atmosphere of nitrogen using commercially available anhydrous solvents.

10.1.1 Chemicals

All commercially available chemicals were obtained from Fisher Scientific, Matrix Scientific, Sigma-Aldrich or VWR International Ltd and were used without purification.

10.1.2 Chromatography

Thin layer chromatography was run on Merck TLC Silica gel 60 F254 plates; typically 5 cm x 10 cm. Detection was achieved using a 254 nm UV source or permanganate stain. Purification of compounds was achieved through manual column chromatography using commercially available silica gel (220 – 440 mesh, Sigma-Aldrich) and solvents.

10.1.3 Nuclear Magnetic Resonance

All NMR spectra were recorded at ambient temperature on a 500 MHz Bruker Avance III spectrometer at the School of Chemistry, The University of Edinburgh. Samples were dissolved in deuterated solvents commercially available from Sigma-Aldrich.

^{1}H NMR spectra: chemical shifts are reported in parts per million (ppm) relative to tetramethylsilane. The data is presented as follows: chemical shift, integration, multiplicity (s = singlet, d = doublet, t = triplet, q = quartet, m = multiplet), coupling constants (in Hertz, Hz) and interpretation. ^{13}C NMR spectra were referenced to the solvent carbon peak. The data is presented as follows: chemical shift and assignment; and were confirmed by DEPT90, DEPT135, 2D-HSQC and 2D-COSY spectra. The spectra were interpreted using MestReNova.

10.1.4 Mass Spectrometry

Low Resolution Mass Spectra (LRMS) were obtained using a Microsaic Systems 4000 MiD system under electron spray ionisation (ESI) conditions. High Resolution Mass Spectra (HRMS) were obtained using a Bruker 3.0 T Apex II Spectrometer at the School of Chemistry, The University of Edinburgh.

10. Experimental

10.2 Experimental for Chapter 2

10.2.1 Synthesis of Compounds 2-6

Synthesis of 1H-pyrazolo[3,4-d]pyrimidin-4-amine (2):

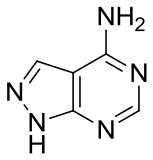

5-amino-1H-pyrazole-4-carbonitrile (3 g, 27.77 mmol) and formamide (15 ml) were added to a 20 ml microwave vial and the mixture heated at 180 ^{o}C for 2 hours using microwave radiation. The precipitate formed on cooling was filtered off and washed with water (50 ml) and allowed to dry giving the product as a cream solid (3.5 g, 25.92 mmol, 93 %). **^{1}H NMR** (500 MHz, DMSO) δ 13.34 (s, 1H), 8.13 (s, 1H), 8.07 (s, 1H), 7.69 (br. m, 2H); **^{13}C NMR** (126 MHz, DMSO) δ 158.19 (CH), 156.03 (C), 154.98 (C), 132.79 (CH),99.83 (C); **MS** (ES +ve) $[M+H]^{+}$: 136.0, 157.9 (+Na), (ES -ve) $[M-H]^{-}$: 133.9.

Synthesis of 3-iodo-1H-pyrazolo[3,4-d]pyrimidin-4-amine (3):

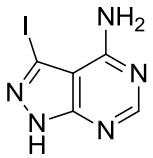

1H-pyrazolo[3,4-d]pyrimidin-4-amine (1.5 g, 11.11 mmol) was suspended in 15 ml of DMF and N-iodosuccinimide (1.2 eq., 3.0 g, 13.34 mmol) added. The mixture was heated at 180 ^{o}C in the microwave for an hour. EtOH (80 ml) was added to the reaction and a precipitate began to form, which was aided by sonication. The precipitate was filtered and washed with EtOH (x3, 20 ml) and allowed to dry in an oven at 40^{o}C overnight to give a sand coloured solid (2.115 g, 8.105 mmol, 73.0 %). **^{1}H NMR** (500 MHz, DMSO) δ 13.80 (s, 1H), 8.16 (s, 1H), 7.79 - 6.44 (m, 2H); **^{13}C NMR** (126 MHz, DMSO) δ 157.60 (C), 156.08 (CH), 155.04 (C), 102.50 (C), 89.82 (C); **MS** (ES +ve) $[M+H]^{+}$: 283.9 (+Na), (ES -ve) $[M-H]^{-}$: 259.9, 287.8 (+Na).

Synthesis of 1-(2,2-diethoxyethyl)-3-iodo-pyrazolo[3,4-d]pyrimidin-4-amine (4):

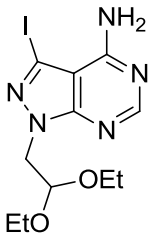

To a solution of 3-iodo-1H-pyrazolo[3,4-d]pyrimidin-4-amine (500 mg, 1.92 mmol) in DMF (15 ml) was added sodium hydride (1.5 eq., 2.88 mmol, 60 % dispersion in mineral oil, 115.2 mg) and the solution allowed to stir for 30 mins until the gas evolution had subsided. Bromoacetaldehyde diethyl acetal (1.5 eq. 2.88 mmol, 0.435 ml) was then added dropwise and the mixture heated at 150 ^{o}C in the microwave for 40 mins. EtOAc and water (50 ml) were added to the mixture and the organics separated. The aqueous layer was washed with EtOAc (50 ml, x3) and the organics combined and washed with water (x3, 30 ml), dried over $MgSO_4$ and concentrated in vacuo. The crude product was purified by column chromatography MeOH/DCM (0-5 %) to give a light orange solid (461 mg, 1.22 mmol, 63.7 %). **^{1}H NMR** (500 MHz, DMSO) δ 8.21 (s, 1H), 7.90 - 6.30 (m, 2H), 4.93 (t, J = 5.7, 1H), 4.33 (d, J = 5.8, 2H), 3.62 (dq, J = 9.4, 6.9, 2H), 3.40 (dq, J = 9.6, 7.0, 2H), 0.98 (t, J = 7.0, 6H); **^{13}C NMR** (126 MHz, DMSO) δ 157.86 (C), 156.30 (CH), 154.03 (C), 103.18 (CH), 99.50 (C), 89.51 (C), 61.39 (CH_2), 48.76 (CH_2), 15.39 (CH_3); **MS** (ES +ve) $[M+H]^+$: 377.8, 400.0 (+Na), (ES -ve) $[M-H]^-$: 376.0.

Synthesis of 1-(2,2-diethoxyethyl)-3-(p-tolyl)pyrazolo[3,4-d]pyrimidin-4-amine (5):

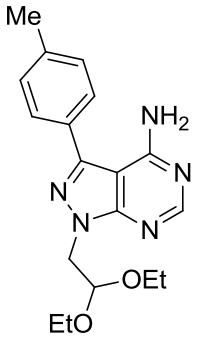

To a solution of 1-(2,2-diethoxyethyl)-3-iodo-pyrazolo[3,4-d]pyrimidin-4-amine (1.135 g, 3.01 mmol) in dioxane/water (10 ml/1 ml) was added p-tolylboronic acid (1.5 eq., 614 mg, 4.52 mmol), potassium carbonate (1.5 eq., 624.7 mg, 4.52 mmol) followed by palladium acetate (5 mol %, 33.8 mg) and the mixture heated in the microwave at 120 ^{o}C for an hour. EtOAc and water (50 ml) were added to the mixture and the organic layer separated, dried

over $MgSO_4$ and concentrated in vacuo. The crude product was purified by column chromatography, MeOH/DCM (0-5 %) to give a light brown solid (902 mg, 2.64 mmol, 87.8 %). **^{1}H NMR** (500 MHz, $CDCl_3$) δ 8.42 (s, 1H), 7.58 (d, J = 8.0, 2H), 7.34 (d, J = 7.8, 2H), 5.12 (t, J = 5.8, 1H), 4.58 (d, J = 5.8, 2H), 3.78 (dq, J = 9.4, 7.0, 2H), 3.52 (dq, J = 9.4, 7.0, 2H), 2.44 (s, 3H), 1.12 (t, J = 7.0, 6H); **^{13}C NMR** (126 MHz, $CDCl_3$) δ 158.28 (C), 156.43 (C), 155.55 (CH), 145.25 (C), 139.76 (C), 131.90 (CH), 128.93 (CH), 100.49 (CH), 62.46 (CH_2), 49.53 (CH_2), 21.09 (CH_3), 15.78 (CH_3); **MS** (ES +ve) $[M+1]^+$: 341.19, (ES -ve) $[M-1]^-$: 340.0.

Synthesis of 2-[4-amino-3-(p-tolyl)pyrazolo[3,4-d]pyrimidin-1-yl]acetaldehyde (6):

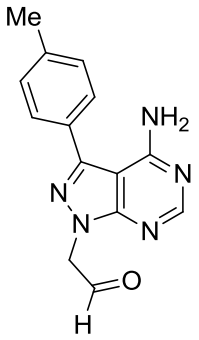

To a suspension of 1-(2,2-diethoxyethyl)-3-(p-tolyl)pyrazolo[3,4-d]pyrimidin-4-amine (400 mg, 1.17 mmol) in 5 ml of water was added 5 ml of TFA and the mixture heated to 100 ^oC for 30 mins in the microwave. The mixture was transferred to a RBF, washed with DCM and concentrated in vacuo. The product was washed with DCM and Et_2O and dried in vacuo to give a light brown solid (assuming quantitative yield). NMR spectra were not obtained for this compound as different salts of the product led to messy spectra.

10.2.2 Synthesis of Compounds 7-18

To a suspension of 2-[4-amino-3-(p-tolyl)pyrazolo[3,4-d]pyrimidin-1-yl]acetaldehyde (40 mg, 0.105 mmol) in DCM (1 ml) was added either morpholine, 1-methylpiperazine, 2-piperazin-1-ylethanol, N,N-dimethyl-2-piperazin-1-yl-ethanamine, piperidin-4-ol, 4-piperidylmethanol, 2-(4-piperidyl)ethanol, N,N-dimethylpiperidin-4-amine, 4-methylpiperidine, or piperidine (**7-16**, 1 eq., 0.105 mmol), respectively, and a drop of AcOH and the mixture allowed to stir for 10 mins. Sodium triacetoxyborohydride (22.2 mg, 0.105 mmol) was then added and the mixture stirred until complete (~ 1hr). The reaction mixture was concentrated *in vacuo* and purified without any further work up due to the high solubility of the product in the aqueous layer.

1-(2-morpholinoethyl)-3-(p-tolyl)pyrazolo[3,4-d]pyrimidin-4-amine (7):

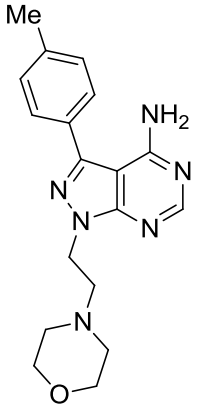

Purified by column chromatography (MeOH/DCM 0-5 %) to give a pale yellow solid (17 mg, 0.05 mmol, 47.9 %). **^{1}H NMR** (500 MHz, MeOD) δ 8.27 (s, 1H), 7.60 (d, *J* = 8.1, 2H), 7.42 (d, *J* = 7.8, 2H), 4.58 (t, *J* = 6.5, 2H), 3.67 – 3.61 (m, 4H), 2.97 (t, *J* = 6.5, 2H), 2.61 (s, 4H), 2.47 (s, 3H); **^{13}C NMR** (126 MHz, $CDCl_3$) δ 158.60 (C), 156.29 (CH), 155.24 (C), 145.23 (C), 138.81 (C), 130.95 (C), 130.35 (CH), 129.05 (CH), 99.05 (C), 67.59 (2x CH_2), 58.02 (CH_2), 54.16 (CH_3), 44.93 (CH_2), 22.12 (2x CH_2); **MS** (ES +ve) $[M+1]^+$: 339.1, 361.0 (+Na), (ES -ve) $[M-1]^-$: 377.0; **HRMS** (ES +ve), $C_{18}H_{22}N_6O$ $[M+H]^+$: calculated 339.19279, found 339.193067.

1-[2-(4-methylpiperazin-1-yl)ethyl]-3-(p-tolyl)pyrazolo[3,4-d]pyrimidin-4-amine (8):

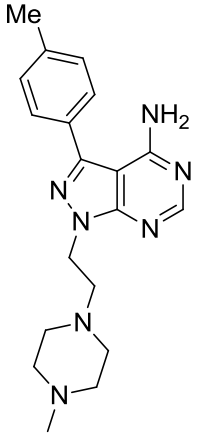

Purified by column chromatography (MeOH/DCM 0-10% - 10% MeOH with 3 drops of NH_3 aq. per 20 ml) to give a pale orange solid (20 mg, 0.057 mmol, 54.2 %) **^{1}H NMR** (500 MHz, MeOD) δ 8.27 (s, 1H), 7.60 (d, *J* = 8.1, 2H), 7.41 (d, *J* = 7.8, 2H), 4.57 (t, *J* = 6.5, 2H), 2.97 (t, *J* = 6.5, 2H), 2.53 (m, 8H), 2.47 (s, 3H), 2.37 (s, 3H).; **^{13}C NMR** (126 MHz, $CDCl_3$) δ 158.02 (C), 155.87 (CH), 154.77 (C), 144.58 (C), 139.25 (C), 130.45 (C), 130.14

(CH), 128.50 (CH), 98.59 (C), 56.89 (CH_2), 54.91 (CH_2), 52.50 (CH_2), 45.59 (CH_3), 44.60 (CH_2), 21.47 (CH_3); **MS** (ES +ve) $[M+1]^+$: 352.0, 374.2 (+Na), (ES -ve) $[M-1]^-$: 350.2; **HRMS** (ES +ve), $C_{19}H_{26}N_7$ $[M+H]^+$: calculated 352.22442, found 352.224816.

2-[4-[2-[4-amino-3-(p-tolyl)pyrazolo[3,4-d]pyrimidin-1-yl]ethyl]piperazin-1-yl]ethanol (9):

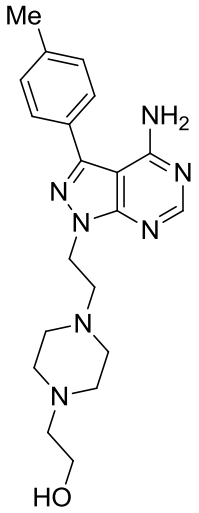

Purified by column chromatography (MeOH/DCM 5-10% - 10% MeOH with 10-30 drops of NH_3 aq. per 100 ml) to give a pale orange solid (15 mg, 0.039 mmol, 37.5 %). **^{1}H NMR** (500 MHz, MeOD) δ 8.27 (s, 1H), 7.60 (d, *J* = 8.0, 2H), 7.41 (d, *J* = 7.9, 2H), 4.57 (t, *J* = 6.4, 2H), 3.73 (t, *J* = 5.7, 2H), 2.99 (t, *J* = 6.4, 2H), 2.74 (m, 10H), 2.46 (s, 3H); **^{13}C NMR** (126 MHz, $CDCl_3$) δ 157.70 (C), 155.50 (CH), 154.57 (C), 144.39 (C), 139.07 (C), 130.26 (C), 129.93 (CH), 128.24 (CH), 98.28 (C), 59.13 (CH_2), 57.16 (CH_2), 56.58 (CH_2), 52.80 (CH_2), 52.04 (CH_2), 44.34 (CH_2), 21.23 (CH_3); **MS** (ES +ve) $[M+1]^+$: 382.0, 404.2 (+Na), (ES -ve) $[M-1]^-$: 379.9; **HRMS** (ES +ve), $C_{20}H_{28}N_7O$ $[M+H]^+$: calculated 382.23499, found 382.234597.

1-[2-[4-(2-dimethylaminoethyl)piperazin-1-yl]ethyl]-3-(p-tolyl)pyrazolo[3,4-d]pyrimidin-4-amine (10):

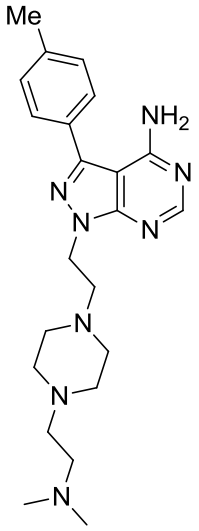

Purified by column chromatography (MeOH/DCM 5-10 % - 10 % MeOH with 25 drops of NH_3 aq. per 100 ml) to give a pale orange solid (5 mg, 0.0312 mmol, 11.7 %). **^{1}H NMR** (500 MHz, MeOD) δ 8.27 (s, 1H), 7.59 (d, *J* = 8.0, 2H), 7.41 (d, *J* = 8.0, 2H), 4.56 (t, *J* = 6.6, 2H), 2.96 (t, *J* = 6.6, 2H), 2.89 (t, *J* = 6.6, 2H), 2.76 – 2.60 (m, 6H), 2.60 (s, 6H), 2.51 (m, 4H), 2.46 (s, 3H); **^{13}C NMR** (126 MHz, MeOD) δ 158.50 (C), 155.39 (CH), 154.14 (C), 145.16 (C), 139.21 (C), 129.83 (C), 129.60 (CH), 128.10 (CH), 97.76 (C), 56.40 (CH_2), 54.64 (CH_2), 53.51 (CH_2), 52.56 (CH_2), 52.24 (CH_2), 43.79 (CH_2), 43.36 (CH_3), 19.97 (CH_3); **MS** (ES +ve) $[M+1]^+$: 409.3, 431.2 (+Na); **HRMS** (ES +ve), $C_{22}H_{33}N_8$ $[M+H]^+$: calculated 409.28227, found 409.282102.

1-[2-[4-amino-3-(p-tolyl)pyrazolo[3,4-d]pyrimidin-1-yl]ethyl]piperidin-4-ol (11):

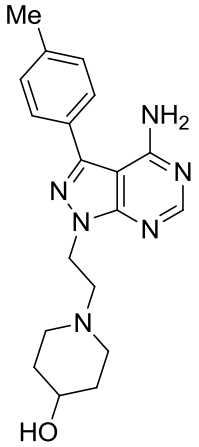

Purified by column chromatography (MeOH/DCM 5-10 % - 10 % MeOH with 10 drops of NH_3 aq. per 50 ml) to give a light brown solid (8 mg, 0.023 mmol, 21.6 %). **^{1}H NMR** (500 MHz, MeOD) δ 8.33 (s, 1H), 7.63 (d, *J* = 8.1, 2H), 7.43 (d, *J* = 7.8, 2H), 4.82 (t, *J* = 5.9, 2H), 3.96 (s, 1H), 3.66 (s, 2H), 3.53 (s, 2H), 3.32 – 3.16 (m, 2H), 2.47 (s, 3H), 2.03 (s, 2H), 1.82 (s, 2H); **^{13}C NMR** (126 MHz, $CDCl_3$) δ 157.59 (C), 154.87 (CH), 154.55 (C), 145.87 (C), 139.77 (C), 130.28 (CH), 129.74 (C), 128.37 (CH), 98.57 (C), 55.54 (CH_2), 53.57 (CH_2), 48.95 (CH_2), 42.60 (CH_2), 31.59 (CH_2), 21.45 (CH_3); **MS** (ES +ve) $[M+1]^+$: 353.2, 375.1 (+Na); **HRMS** (ES +ve), $C_{19}H_{25}N_6O$ $[M+H]^+$: calculated 353.20844, found 353.208248.

[1-[2-[4-amino-3-(p-tolyl)pyrazolo[3,4-d]pyrimidin-1-yl]ethyl]-4-piperidyl]methanol (12):

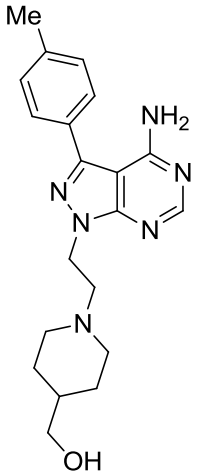

Purified by column chromatography (MeOH/DCM 5-10 % - 10 % MeOH with 10 drops of NH_3 aq. per 100 ml) to give a light brown solid (7 mg, 0.019 mmol, 18.2 %). **^{1}H NMR** (400 MHz, MeOD) δ 8.28 (s, 1H), 7.61 (d, *J* = 8.1, 2H), 7.42 (d, *J* = 7.8, 2H), 4.61 (t, *J* = 6.7, 2H), 3.42 – 3.36 (m, 4H), 3.16 (s, 2H), 3.03 (s, 2H), 2.47 (s, 3H), 2.23 (s, 2H), 1.77 (d, *J* = 11.9, 2H), 1.56 – 1.49 (m, 1H), 1.26 (m, 2H); **^{13}C NMR** (126 MHz, $CDCl_3$) δ 157.69 (C), 155.74 (CH), 154.38 (C), 144.35 (C), 139.05 (C), 130.27 (C), 129.99 (CH), 128.30 (CH), 98.40 (C), 67.76 (CH_2), 57.10 (CH_2), 53.31 (CH_2), 44.67 (CH_2), 38.26 (CH), 28.56 (CH_2), 21.29 (CH_3); **MS** (ES +ve) $[M+1]^+$: 367.3, 338.9 (+Na); **HRMS** (ES +ve), $C_{20}H_{27}N_6O$ $[M+H]^+$: calculated 367.22409, found 367.223856.

2-[1-[2-[4-amino-3-(p-tolyl)pyrazolo[3,4-d]pyrimidin-1-yl]ethyl]-4-piperidyl]ethanol (13):

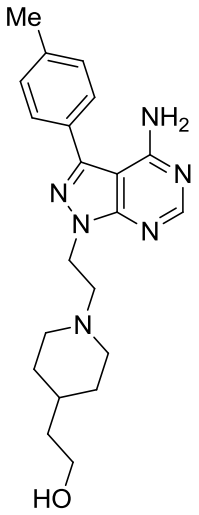

Purified by column chromatography (MeOH/DCM 5-10 % - 10 % MeOH with 2 drops of NH_3 aq. per 10 ml) to give a light orange solid (13 mg, 0.034 mmol, 32.6 %). **^{1}H NMR** (500 MHz, $CDCl_3$) δ 8.36 (s, 1H), 7.58 (d, J = 8.1, 2H), 7.37 (d, J = 7.8, 2H), 5.94 (br. s, 2H), 4.79 (t, J = 6.4, 2H), 3.74 - 3.67 (m, 2H), 3.49 (m, 4H), 2.56 (br. s, 2H), 2.46 (s, 3H), 1.85 (d, J = 11.0, 2H), 1.58 (m, 5H); **^{13}C NMR** (126 MHz, $CDCl_3$) δ 158.02 (C), 155.80 (CH), 154.96 (C), 145.91 (C), 139.94 (C), 130.55 (CH), 130.13 (C), 128.65 (CH), 118.15 (C), 115.83 (C), 98.92 (CH), 60.29 (CH_2), 51.28 (CH_2), 42.73 (CH_2), 38.56 (CH_2), 31.34 (CH_2), 30.08 (CH_2), 21.76 (CH_3); **MS** (ES +ve) $(M+1)^+$: 381.1, (ES -ve) $[M-1]^-$: 378.7; **HRMS** (ES +ve), $C_{21}H_{29}N_6O$ $[M+H]^+$: calculated 381.23974, found 381.239592.

1-[2-[4-(dimethylamino)-1-piperidyl]ethyl]-3-(p-tolyl)pyrazolo[3,4-d]pyramidin-4-amine (14):

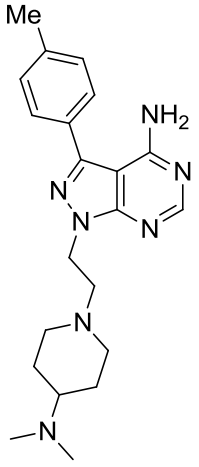

Purified by column chromatography (MeOH/DCM 10 % - 10 % MeOH with 20 drops of NH_3 aq. per 50 ml) to give a light brown solid (13 mg, 0.034 mmol, 32.7 **%). ^{1}H NMR** (500 MHz, $CDCl_3$) δ 8.35 (s, 1H), 7.56 (d, J = 8.0, 2H), 7.33 (d, J = 7.8, 2H), 5.68 (s, 2H), 4.54 (t, J = 7.0, 2H), 3.08 (d, J = 11.8, 2H), 2.93 (t, J = 7.0, 2H), 2.43 (s, 3H), 2.41 (m, 1H), 2.40 (s, 6H), 2.10 (dd, J = 11.8, 9.9, 2H), 1.84 (d, J = 12.3, 2H), 1.52 (qd, J = 12.1, 3.7, 2H); **^{13}C NMR** (126 MHz, $CDCl_3$) δ 158.16 (C), 156.04 (CH), 154.87 (C), 144.69 (C), 139.38 (C), 130.60 (C), 130.32 (CH), 128.57 (CH), 98.70 (C), 62.72 (CH), 56.96 (CH_2), 52.86 (2x CH_2), 45.13 (CH_2), 41.01 (2x CH_3), 27.71 (CH_2), 21.61 (CH_3); **MS** (ES +ve) $[M+1]^+$: 380.2, 402.1 (+Na); **HRMS** (ES +ve), $C_{21}H_{30}N_7$ $[M+H]^+$: calculated 380.25572, found 380.255345.

1-[2-(4-methyl-1-piperidyl)ethyl]-3-(p-tolyl)pyrazolo[3,4-d]pyrimidin-4-amine (15):

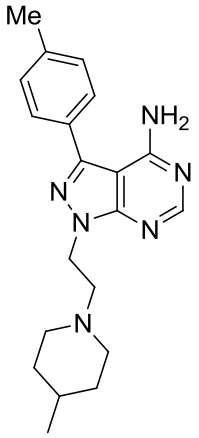

Purified by column chromatography (MeOH/DCM 0-8 %) to give a light brown solid (16 mg, 0.046 mmol, 43.5 %). **^{1}H NMR** (500 MHz, $CDCl_3$) δ 8.35 (s, 1H), 7.57 (d, J = 8.0, 2H), 7.37 (d, J = 7.8, 2H), 4.85 (t, J = 6.3, 2H), 3.64 (m, 2H), 3.40 (d, J = 12.7, 2H), 2.87 (dd, J = 12.8, 10.2, 2H), 2.46 (s, 3H), 1.83 (d, J = 13.2, 2H), 1.64 (m, 1H), 1.52 (td, J = 14.6, 3.9, 2H), 1.02 (d, J = 6.5, 3H); **^{13}C NMR** (126 MHz, $CDCl_3$) δ 157.55 (C), 155.04 (CH), 154.44 (C), 145.98 (C), 139.71 (C), 130.20 (2x CH), 129.48 (C), 128.27 (2x CH), 98.51 (C), 53.44 (CH_2), 43.99 (2x CH_2), 41.68 (CH_2), 30.36 (2x CH_2), 29.13 (CH), 21.37 (CH_3), 21.28 (CH_3); **MS** (ES +ve) $[M+1]^+$: 351.1; **HRMS** (ES +ve), $C_{20}H_{27}N_6$ $[M+H]^+$: calculated 351.22917, found 351.229656.

1-[2-(1-piperidyl)ethyl]-3-(p-tolyl)pyrazolo[3,4-d]pyrimidin-4-amine (16):

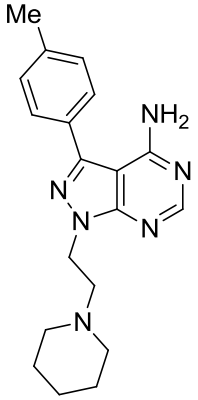

Purified by column chromatography (MeOH/DCM 0-10 %) to give a light brown solid (20 mg, 0.059 mmol, 56.7 %). **^{1}H NMR** (601 MHz, MeOH) δ 8.31 (s, 1H), 7.61 (d, J = 8.0, 2H), 7.42 (d, J = 7.8, 2H), 4.75 (t, J = 6.3, 2H), 3.45 (m, 2H), 3.18 – 3.14 (m, 2H), 2.47 (s, 3H), 1.83 – 1.70 (m, 6H), 1.63 (s, 2H). **^{13}C NMR** (151 MHz, MeOH) δ 177.66 (C), 155.72 (CH), 145.87 (C), 139.30 (C), 129.64 (2x CH), 128.04 (2x CH), 109.85 (C), 97.95 (C), 56.01 (CH_2), 53.55 (CH_2), 44.34 (CH_2), 23.69 (CH_2), 22.38 (CH_2), 21.64 (2x CH_2), 19.95 (CH_3).; **MS** (ES +ve) $[M+1]^+$: 337.0; **HRMS** (ES +ve), $C_{19}H_{24}N_6$ $[M+H]^+$: calculated 337.21352, found 337.213381.

Synthesis of 1-[2-[4-(dimethylaminomethyl)-1-piperidyl]ethyl]-3-(p-tolyl)pyrazolo[3,4-d]pyrimidin-4-amine (17):

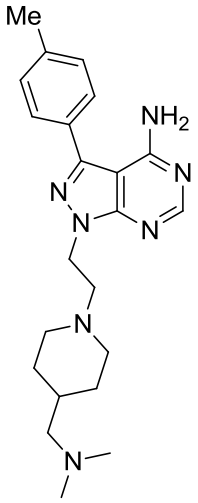

To a suspension of 2-[4-amino-3-(p-tolyl)pyrazolo[3,4-d]pyrimidin-1-yl]acealdehyde (100 mg, 0.374 mmol) in DCM (2 ml) was added N,N-Dimethyl-1-piperidin-4-ylmethanamine (1 eq. 53.2 mg, 0.374 mmol) and a drop of AcOH and the mixture allowed to stir for 10 mins. Sodium triacetoxyborohydride (79.3 mg, 0.374 mmol) was then added and the mixture

allowed to stir for 18 hours. The mixture was reduced in vacuo and purified, without a work up, by column chromatography MeOH/DCM (0-10 % - 10 % with 10 drops NH_3 aq. per 100 ml) to give a light orange solid (48 mg, 0.122 mmol, 32.6 %). **^{1}H NMR** (500 MHz, $CDCl_3$) δ 8.30 (s, 1H), 7.55 (d, J = 8.1, 2H), 7.32 (d, J = 7.8, 2H), 4.54 (t, J = 6.8, 2H), 3.04 (d, J = 11.6, 2H), 2.95 (t, J = 6.8, 2H), 2.57 (s, 6H), 2.41 (s, 3H), 2.11 (t, J = 10.9, 2H), 1.74 (d, J = 12.6, 2H), 1.63 (s, 2H), 1.26 (m, 3H); **^{13}C NMR** (126 MHz, $CDCl_3$) δ 158.06 (C), 155.40 (CH), 154.56 (C), 144.79 (C), 139.23 (C), 130.36 (C), 130.16 (CH), 128.40 (CH), 98.53 (C), 64.32 (CH_2), 56.97 (CH_2), 53.15 (CH_2), 44.52 (CH_2), 44.42 (CH_3), 32.62 (CH), 30.14 (CH_2), 21.44 (CH_3); **MS** (ES +ve) $[M+1]^+$: 394.3, 416.2 (+Na); **HRMS** (ES +ve), $C_{22}H_{32}N_7$ $[M+H]^+$: calculated 394.27137, found 394.271595.

Synthesis of 1-[2-[4-(2-dimethylaminoethyl)-1-piperidyl]ethyl]-3-(p-tolyl)pyrazolo[3,4-d]pyrimidin-4-amine (18):

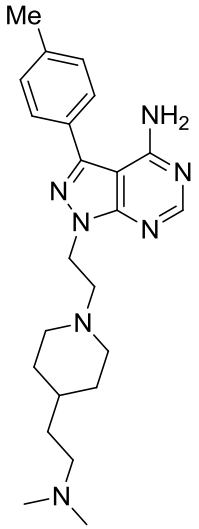

To a suspension of 2-[4-amino-3-(p-tolyl)pyrazolo[3,4-d]pyrimidin-1-yl]acealdehyde (100 mg, 0.374 mmol) in DCM (2 ml) was added dimethyl-(2-piperidin-4-yl-ethyl)-amine (1 eq. 58.4 mg, 0.374 mmol) and a drop of AcOH and the mixture allowed to stir for 10 mins. Sodium triacetoxyborohydride (79.3 mg, 0.374 mmol) was then added and the mixture allowed to stir for 18 hours. The mixture was reduced in vacuo and purified, without a work up, by column chromatography MeOH/DCM (0-10 % - 10 % with 0-10 drops NH_3 aq per 100 ml) to give a light yellow solid (69.8 mg, 0.171 mmol, 45.8 %)**. ^{1}H NMR** (500 MHz, MeOD) δ 8.25 (s, 1H), 7.59 – 7.55 (m, 2H), 7.38 (d, *J* = 7.8, 2H), 4.58 (t, *J* = 6.6, 2H), 3.14 (d, *J* = 11.8, 2H), 3.09 – 2.99 (m, 4H), 2.79 (s, 6H), 2.43 (s, 3H), 2.23 (t, *J* = 11.0, 2H), 1.74 (d, *J* = 12.9, 2H), 1.65 – 1.57 (m, 2H), 1.44 – 1.36 (m, 1H), 1.27 (dd, *J* = 21.1, 11.8, 2H); **^{13}C NMR** (126 MHz, MeOD) δ 158.50 (C). 155.45 (CH), 154.14 (C), 145.30 (C), 139.23 (C),

129.79 (C), 129.60 (CH), 128.09 (CH), 97.83 (C), 56.50 (CH_2), 55.70 (CH_2), 52.99 (2x CH_2), 43.45 (CH_2), 42.14 (2x CH_3), 32.84 (CH), 30.88 (2x CH_2), 30.64 (CH_2), 19.97 (CH_3); **MS** (ES +ve) $[M+1]^+$: 408.1; **HRMS** (ES +ve), $C_{23}H_{34}N_7$ $[M+H]^+$: calculated 408.28702, found 408.286812.

10. Experimental

10.3 Experimental for Chapter 3

10.3.1 Synthesis of Compounds 19-27

To a solution of 1-(2,2-diethoxyethyl)-3-iodo-pyrazolo[3,4-d]pyrimidin-4-amine, **4**, (100 mg, 0.265 mmol) in dioxane/water (4.5 ml/0.5 ml) was added either 1H-pyrrolo[2,3-b]pyridine-5-boronic acid pinicol ester, 6-indolylboronicacid, 5-isoquinolineboronicacid, 3,4-dimethoxyphenylboronicacid, 3-hydroxyphenylboronicacid, furan-3-boronicacid, 3-(N-Boc-amino)phenylboronic, 3-aminocarbonylphenylboronicacid or 4-aminocarbonylphenylboronic acid (1.5 eq., 0.397 mmol), potassium carbonate (1.5 eq., 54.8 mg, 0.397 mmol), triphenylphosphine (20 mol %, 20.8 mg) and palladium acetate (5 mol %, 4.5 mg) and the mixture heated in the microwave at 120 ^{o}C for an hour. EtOAc (50 ml) and water (50 ml) were added to the mixture and the organic layer separated, washed with brine (50 ml), dried over $MgSO_4$ and concentrated in vacuo.

1-(2,2-diethoxyethyl)-3-(1H-pyrrolo[2,3-b]pyridin-5-yl)pyrazolo[3,4-d]pyrimidin-4-amine (19):

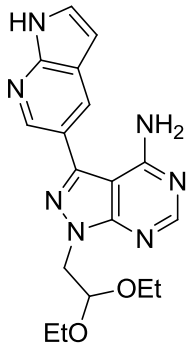

Purified by column chromatography, MeOH/DCM (0-6 %) to give a white solid (93 mg, 0.253 mmol, 95.6 %). **^{1}H NMR** (500 MHz, CDCl3) δ 9.53 (s, 1H), 8.62 (d, J = 1.9, 1H), 8.41 (s, 1H), 8.24 (d, J = 2.0, 1H), 7.45 (d, J = 3.4, 1H), 6.62 (d, J = 3.5, 1H), 6.29 – 5.86 (br. s, 2H), 5.14 (t, J = 5.7, 1H), 4.62 (d, J = 5.7, 2H), 3.79 (dq, J = 9.4, 7.0, 2H), 3.55 (dq, J = 9.4, 7.0, 2H), 1.14 (t, J = 7.0, 6H); **^{13}C NMR** (126 MHz, CDCl3) δ 156.75 (C), 154.58 (C), 153.42 (CH), 148.87 (C), 143.78 (C), 142.83 (CH), 128.83 (CH), 126.85 (CH), 121.30 (C), 120.46 (C), 101.80 (CH), 99.93 (CH), 98.47 (C), 62.17 (2x CH_2), 49.33 (CH_2), 15.34 (2x CH_3); **MS** (ES +ve) $[M+H]^+$: 368.2, 390.2 (+Na), (ES –ve) $[M-H]^-$: 366.2; **HRMS** (ES +ve), $C_{18}H_{22}N_7O_2$ $(M+H)^+$: calculated 368.18295, found 368.18090.

1-(2,2-diethoxyethyl)-3-(1H-indol-5-yl)pyrazolo[3,4-d]pyrimidin-4-amine (20):

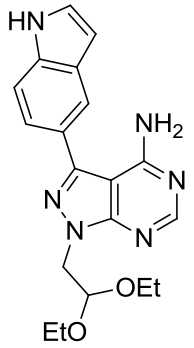

Purified by column chromatography, MeOH/DCM (0-4 %) to give a deep red solid (86 mg, 0.253 mmol, 95.6 %). **^{1}H NMR** (500 MHz, CDCl3) δ 8.51 (s, 1H), 8.40 (s, 1H), 7.79 (d, J = 8.1, 1H), 7.72 (s, 1H), 7.41 (dd, J = 8.1, 1.4, 1H), 7.35 – 7.29 (m, 1H), 6.63 (t, J = 2.1, 1H), 5.62 (s, 2H), 5.15 (t, J = 5.8, 1H), 4.59 (d, J = 5.8, 2H), 3.78 (dq, J = 9.4, 7.0, 2H), 3.53 (dq, J = 9.4, 7.0, 2H), 1.12 (t, J = 7.0, 6H); **^{13}C NMR** (126 MHz, CDCl3) δ 157.68 (C), 155.02 (CH), 146.56 (C), 136.51 (C), 129.02 (C), 126.69 (C), 126.35 (CH), 122.17 (CH), 120.38 (CH), 111.69 (CH), 103.20 (CH), 100.35 (C), 98.73 (CH), 62.39 (2x CH_2), 49.44 (CH_2), 15.60 (2x CH_3); **MS** (ES +ve) [M+H]+: 367.2, 389.2 (+Na).

1-(2,2-diethoxyethyl)-3-(6-quinolyl)pyrazolo[3,4-d]pyrimidin-4-amine (21):

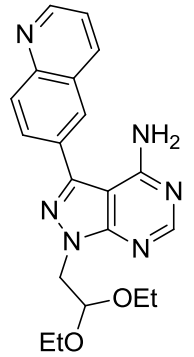

Purified by column chromatography, MeOH/DCM (0-5 %) to give a pale orange solid (86 mg, 0.227 mmol, 85.8 %). **^{1}H NMR** (400 MHz, CDCl3) δ 9.39 (s, 1H), 8.59 (d, J = 6.0, 1H), 8.47 (s, 1H), 8.16 (d, J = 8.2, 1H), 7.93 (dd, J = 7.1, 1.2, 1H), 7.84 (d, J = 6.0, 1H), 7.79 (dd, J = 8.2, 7.2, 1H), 5.18 (t, J = 5.7, 1H), 4.68 (d, J = 5.8, 2H), 3.83 (dq, J = 9.4, 7.0, 2H), 3.58 (dq, J = 9.4, 7.0, 2H), 1.21 – 1.13 (m, 6H); **^{13}C NMR** (126 MHz, CDCl3) δ 157.36 (C), 155.87 (CH), 154.77 (C), 152.99 (CH), 144.34 (CH), 141.21 (C), 134.32 (C), 132.29 (CH), 129.43 (CH), 129.32 (C), 128.98 (C), 127.01 (CH), 118.25 (CH), 99.92 (C), 99.80 (CH), 61.94 (2x CH_2), 49.18 (CH_2), 15.23 (2x CH_3); **MS** (ES +ve) $[M+H]^+$: 379.2, 401.2 (+Na),

(ES –ve) $[M-H]^-$: 377.2; **HRMS** (ES +ve), $C_{20}H_{23}N_6O_2$ $(M+H)^+$: calculated 379.18770, found 379.18660.

1-(2,2-diethoxyethyl)-3-(3,4-dimethoxyphenyl)pyrazolo[3,4-d]pyrimidin-4-amine (22):

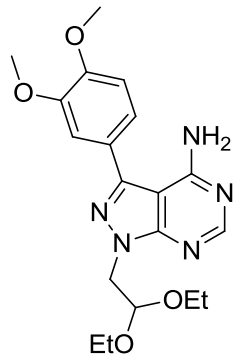

Purified by column chromatography, MeOH/DCM (0-2%) to give a pale yellow solid (97 mg, 0.251 mmol, 94.5%). **^{1}H NMR** (500 MHz, CDCl3) δ 8.38 (s, 1H), 7.23 – 7.19 (m, 2H), 7.02 (d, J = 8.7, 1H), 5.94 (s, 2H), 5.12 (t, J = 5.7, 1H), 4.57 (d, J = 5.8, 2H), 3.97 (d, J = 9.8, 6H), 3.78 (dq, J = 9.4, 7.0, 2H), 3.53 (dq, J = 9.4, 7.0, 2H), 1.13 (t, J = 7.0, 6H); **^{13}C NMR** (126 MHz, CDCl3) δ 157.59 (C), 155.28 (CH), 154.78 (C), 149.94 (C), 149.69 (C), 144.70 (C), 125.68 (C), 120.81 (CH), 111.61 (CH), 111.56 (CH), 99.82 (CH), 98.32 (C), 61.81 (2x CH_2), 56.06 (2x CH_3), 48.88 (CH_2), 15.19 (2x CH_3); **MS** (ES +ve) $[M+H]^+$: 388.2, (ES –ve) $[M-H]^-$: 368.2; **HRMS** (ES +ve), $C_{19}H_{26}N_5O_4$ $(M+H)^+$: calculated 388.19793, found 388.19620.

3-[4-amino-1-(2,2-diethoxyethyl)pyrazolo[3,4-d]pyrimidin-3-yl]phenol (23):

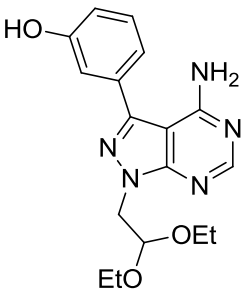

Purified by column chromatography, MeOH/DCM (0-3%) to give a cream solid (80 mg, 0.233 mmol, 88.0 %). **^{1}H NMR** (500 MHz, CDCl3) δ 8.45 (s, 1H), 7.38 (t, J = 7.9, 1H), 7.20 (d, J = 7.5, 1H), 7.12 (s, 1H), 6.95 (d, J = 8.1, 1H), 5.89 (s, 2H), 5.10 (t, J = 5.7, 1H), 4.57 (d, J = 5.7, 2H), 3.76 (tt, J = 14.1, 7.0, 2H), 3.52 (tt, J = 14.1, 7.0, 2H), 1.11 (t, J = 7.0, 6H); **^{13}C NMR** (126 MHz, CDCl3) δ 157.10 (C), 155.85 (CH), 153.86 (C), 152.23 (C), 145.53 (C),

133.41 (C), 131.04 (CH), 120.31 (CH), 117.10 (CH), 115.15 (CH), 99.75 (CH), 97.78 (C), 62.16 (2x CH_2), 49.22 (CH_2), 15.17 (2x CH_3); **MS** (ES +ve) $[M+H]^+$: 344.2, 366.2 (+Na), (ES –ve) $[M-H]^-$: 342.2; **HRMS** (ES +ve), $C_{17}H_{22}N_5O_3$ $(M+H)^+$: calculated 344.17172, found 344.17000.

1-(2,2-diethoxyethyl)-3-(3-furyl)pyrazolo[3,4-d]pyrimidin-4-amine (24):

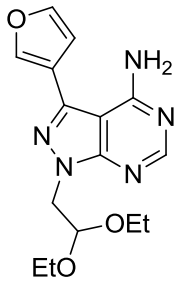

Purified by column chromatography, MeOH/DCM (0-2 %) to give a cream coloured solid, (66.8 mg, 0.211 mmol, 79.5 %). **^{1}H NMR** (500 MHz, CDCl3) δ 8.38 (s, 1H), 7.83 (dd, J = 1.4, 0.9, 1H), 7.61 (t, J = 1.7, 1H), 6.77 (dd, J = 1.8, 0.8, 1H), 5.82 (s, 2H), 5.09 (t, J = 5.8, 1H), 4.55 (d, J = 5.8, 2H), 3.76 (dq, J = 9.4, 7.0, 2H), 3.52 (dq, J = 9.4, 7.0, 2H), 1.11 (t, J = 7.0, 6H); **^{13}C NMR** (126 MHz, CDCl3) δ 156.93 (C), 154.38 (C), 154.12 (CH), 144.66 (CH), 141.11 (CH), 136.98 (C), 118.52 (C), 110.29 (CH), 99.73 (CH), 98.61 (C), 61.92 (2x CH2), 49.04 (CH2), 15.17 (2x CH3); **MS** (ES +ve) $[M+H]^+$: 318.2, 340.2(+Na), 657.2 (2M+Na), (ES –ve) $[M-H]^-$: 317.2; **HRMS** (ES +ve), $C_{15}H_{20}N_5O_3$ $(M+H)^+$: calculated 318.15607, found 318.15400.

t-butyl-N-[3-[4-amino-1-(2,2-diethoxyethyl)pyrazolo[3,4-d]pyrimidin-3-yl]phenyl]carbamate (25):

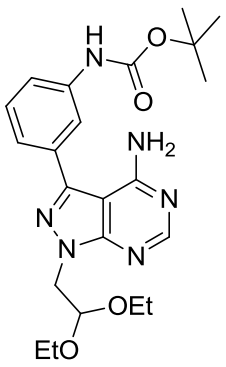

Purified by column chromatography, MeOH/DCM (0-2%) to give a light brown sold (118 mg, 0.268 mmol, 100 %). **^{1}H NMR** (500 MHz, CDCl3) δ 8.40 (s, 1H), 7.85 (s, 1H), 7.52 – 7.45 (m, 2H), 6.66 (s, 1H), 6.42 (s, 2H), 5.14 (t, J = 5.7, 1H), 4.61 (d, J = 5.8, 2H), 3.80 (dq,

J = 9.4, 7.0, 2H), 3.55 (dq, J = 9.4, 7.0, 2H), 1.56 (s, 9H), 1.15 (t, J = 7.0, 6H); **^{13}C NMR** (126 MHz, CDCl3) δ 156.33 (C), 154.37 (C), 153.16 (C), 152.61 (CH), 145.15 (C), 139.02 (C), 133.26 (C), 130.27 (CH), 123.17 (CH), 119.83 (CH), 119.30 (CH), 99.83 (CH), 97.91 (C), 81.30 (C), 62.09 (2x CH2), 49.25 (CH2), 28.32 (3x CH3), 15.20 (2x CH3); **MS** (ES +ve) $[M+H]^+$: 443.2, 465.2 (+Na), (ES –ve) $[M-H]^-$: 441.2; **HRMS** (ES +ve), $C_{22}H_{31}N_6O_4$ $(M+H)^+$: calculated 443.24013, found 443.23840.

3-[4-amino-1-(2,2-diethoxyethyl)pyrazolo[3,4-d]pyrimidin-3-yl]benzamide (26):

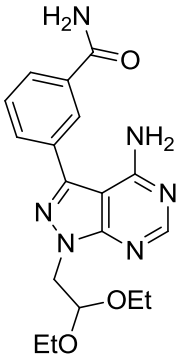

Purified by column chromatography, MeOH/DCM (0-8 %) to give a cream/light rose coloured solid (71 mg, 0.192 mmol, 72.4 %). **^{1}H NMR** (500 MHz, MeOD) δ 8.34 (s, 1H), 8.24 (t, J = 1.6, 1H), 8.03 (d, J = 8.3, 1H), 7.93 – 7.89 (m, 1H), 7.69 (t, J = 7.7, 1H), 5.09 (t, J = 5.7, 1H), 4.55 (d, J = 5.7, 2H), 3.76 (dq, J = 9.5, 7.1, 2H), 3.52 (dq, J = 9.5, 7.0, 2H), 1.10 (t, J = 7.0, 6H); **^{13}C NMR** (126 MHz, MeOD) δ 170.18 (C), 153.90 (C), 152.52 (C), 152.85 (CH), 145.20 (C), 134.81 (C), 132.54 (C), 131.37 (CH), 129.26 (CH), 128.06 (CH), 127.51 (CH), 100.11 (CH), 97.34 (C), 62.42 (2x CH2), 49.09 (CH2), 14.11 (2x CH3); **MS** (ES +ve) $[M+H]^+$: 371.2, 393.2 (+Na), (ES –ve) $[M-H]^-$: 369.2; **HRMS** (ES +ve), $C_{18}H_{23}N_6O_3$ $(M+H)^+$: calculated 371.18262, found 371.18130

4-[4-amino-1-(2,2-diethoxyethyl)pyrazolo[3,4-d]pyrimidin-3-yl]benzamide (27):

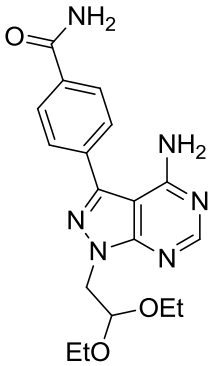

Purified by column chromatography, MeOH/DCM (0-6 %) to give a cream solid (90 mg, 0.243 mmol, 91.7 %). **^{1}H NMR** (500 MHz, MeOD) δ 8.33 (s, 1H), 8.10 – 8.05 (m, 2H), 7.85 – 7.80 (m, 2H), 5.09 (t, J = 5.7, 1H), 4.55 (d, J = 5.7, 2H), 3.76 (dq, J = 9.5, 7.0, 2H), 3.52 (dq, J = 9.5, 7.0, 2H), 1.09 (t, J = 7.0, 6H); **^{13}C NMR** (126 MHz, MeOD) δ 170.27 (C), 157.12 (C), 154.16 (C), 153.44 (CH), 144.76 (C), 135.58 (C), 134.35 (C), 128.30 (4x CH), 100.11 (CH), 97.50 (C), 62.39 (2x CH2), 49.05 (CH2), 14.10 (2x CH3); **MS** (ES +ve) $[M+H]^+$: 371.2, 393.2 (+Na), (ES –ve) $[M-H]^-$: 369.2; **HRMS** (ES +ve), $C_{18}H_{23}N_6O_3$ $(M+H)^+$: calculated 371.18262, found 371.17970.

10.3.2 Synthesis of Compound 28

1-(2,2-diethoxyethyl)-3-(2-phenylethynyl)pyrazolo[3,4-d]pyrimidin-4-amine (28):

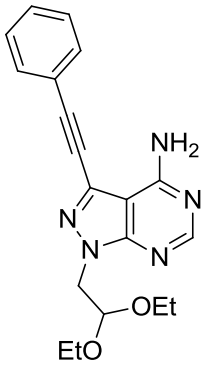

To a solution of 1-(2,2-diethoxyethyl)-3-iodo-pyrazolo[3,4-d]pyrimidin-4-amine (100 mg, 0.265 mmol) in THF (5 ml) was added phenylacetylene (1.5 eq., 0.397mmol, 40.5 mg, 37.7 µl), triethylamine (1.5 eq., 0.397 mmol, 29.1 µl), palladium acetate (5 mol %, 4.5 mg), triphenylphosphine (20 mol %, 20.8 mg) and copper iodide (5 mol%, 2.5 mg). The mixture was heated conventially at 70^{o}C for 2 hours. EtOAc and water were added to the mixture and the organic layer separated, dried over $MgSO_4$ and concentrated *in vacuo*. The crude product was purified by column chromatography, MeOH/DCM (0-2%) to give a light yellow solid (52 mg, 0.148 mmol, 55.9 %). **^{1}H NMR** (500 MHz, CDCl3) δ 8.90 – 8.35 (m, 1H), 7.59 (dd, J = 7.7, 1.7, 2H), 7.45 – 7.36 (m, 3H), 6.20 (s, 2H), 5.09 (t, J = 5.6, 1H), 4.53 (d, J = 5.7, 2H), 3.74 (dq, J = 9.3, 7.0, 2H), 3.50 (dq, J = 14.4, 7.2, 2H), 1.10 (t, J = 7.0, 6H); **^{13}C NMR** (126 MHz, CDCl3) δ 153.88 (CH), 131.82 (2x CH), 129.58 (CH), 128.67 (2x CH), 121.45 (C), 99.81 (CH), 94.33 (C), 80.63 (C), 62.07 (2x CH_2), 49.41 (CH_2), 15.16 (2x CH_3); **MS** (ES +ve) $[M+H]^+$: 352.2, 725.2 (2M +Na), (ES –ve) $[M-H]^-$: 350.2; **HRMS** (ES +ve), $C_{19}H_{22}N_5O_2$ $(M+H)^+$: calculated 352.17680, found 352.17680.

10.3.3 Synthesis of Compounds 29-35

Synthesis of 1-[2-[4-(dimethylaminomethyl)-1-piperidyl]ethyl]-3-(1H-pyrrolo[2,3-b]pyridin-5-yl)pyrazolo[3,4-d]pyrimidin-4-amine (29):

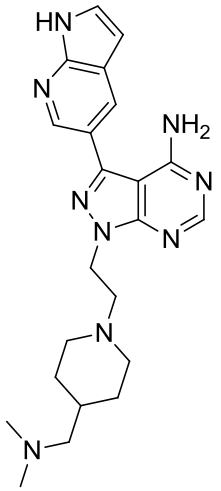

60 mg, 0.163 mmol, of 1-(2,2-diethoxyethyl)-3-(1H-pyrrolo[2,3-b]pyridin-5-yl)pyrazolo[3,4-d]pyrimidin-4-amine was added to a 20 ml microwave vial. 5 ml of water was added followed by 5 ml of TFA and the mixture heated conventially at 100^{o}C for an hour. The mixture was concentrated *in vacuo* to leave a light brown oil which was used without further purification 0.163 mmol of 2-[4-amino-3-(1H-pyrrolo[2,3-b]pyridin-5-yl)pyrazolo[3,4-d]pyrimidin-1-yl]acetaldehyde was dissolved in 2 ml of DCM. N,N-dimethyl-1-(4-piperidyl)methanamine (1.5 eq., 0.245 mmol, 34.8 mg) was added followed by a drop of acetic acid. The mixture was allowed to stir for 10 mins then sodium triacetoxyborohydride (1.5 eq., 0.245 mmol, 51.9 mg) added and the mixture allowed to stir for 2 hours. The mixture was concentrated *in vacuo* and the product purified by column chromatography, MeOH/DCM (5-10% then 10% with 5-20 drops of NH_3 aq. Per 100 ml) to give a light orange solid, (15.3 mg, 0.0365 mmol, 14.9 %). **^{1}H NMR** (500 MHz, MeOD) δ 8.52 (s, 1H), 8.29 (d, J = 2.0, 1H), 8.28 (s, 1H), 7.52 (d, J = 3.5, 1H), 6.62 (d, J = 3.5, 1H), 4.64 (t, J = 6.4, 2H), 3.25 (d, J = 11.7, 2H), 3.13 (t, J = 6.3, 2H), 2.96 (d, J = 7.2, 2H), 2.84 (s, 6H), 2.37 (t, J = 11.4, 2H), 1.88 (m, 1H), 1.80 (d, J = 13.1, 2H), 1.36 – 1.31 (m, 2H); **^{13}C NMR** (126 MHz, MeOD) δ 161.79 (C), 158.65 (C), 155.54 (CH), 154.33 (C), 148.16 (C), 143.72 (C), 141.84 (CH), 128.67 (CH), 127.12 (CH), 120.73 (C), 100.63 (CH), 98.19 (C), 62.67 (CH_2), 56.31 (CH_2), 52.22 (2x CH_2), 43.41 (CH_2), 42.72 (2x CH_3), 30.93 (CH), 28.39 (2x CH_2); **MS** (ES +ve) $[M+H]^+$: 420.2; **HRMS** (ES +ve), $C_{22}H_{29}N_9$ $[M+H]^+$: calculated 420.25404, found 420.254249.

Synthesis of 1-[2-[4-(dimethylaminomethyl)-1-piperidyl]ethyl]-3-(6-quinolyl)pyrazolo[3,4-d]pyrimidin-4-amine (30):

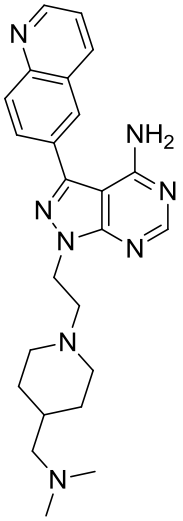

60 mg, 0.159 mmol of 1-(2,2-diethoxyethyl)-3-(6-quinolyl)pyrazolo[3,4-d]pyrimidin-4-amine was added to a 20 ml microwave vial. 5 ml of water was added followed by 5 ml of TFA and the mixture heated conventially at 100°C for an hour. The mixture was concentrated *in vacuo* to give a brown oil which was used without further purification. 0.159 mmol of 2-[4-amino-3-(6-quinolyl)pyrazolo[3,4-d]pyrimidin-1-yl]acetaldehyde was dissolved in 2 ml of DCM. N,N-dimethyl-1-(4-piperidyl)methanamine (1.5 eq., 0.238 mmol, 33.9 mg) was added followed by a drop of acetic acid and the mixture allowed to stir for 10 mins. Sodium triacetoxyborohydride (1.5 eq., 0.238 mmol, 50.4 mg) was added and the mixture allowed to stir for 17 hours. The mixture was concentrated *in vacuo* and purified by column chromatography, MeOH/DCM (5-10% then 20 drops NH_3 aq per 100 ml) to give a fluorescent yellow coloured solid, 48.9 mg, 0.122 mmol, 70.6 %. **^{1}H NMR** (500 MHz, MeOD) δ 9.37 (s, 1H), 8.47 (d, J = 6.0, 1H), 8.31 (m, 2H), 7.99 (dd, J = 7.1, 1.2, 1H), 7.90 – 7.84 (m, 2H), 4.65 (t, J = 6.7, 2H), 3.09 (d, J = 11.7, 2H), 2.99 (t, J = 6.7, 2H), 2.28 (s, 6H), 2.27 (m, 2H), 2.18 – 2.11 (m, 2H), 1.75 (d, J = 12.4, 2H), 1.57 (ddd, J = 11.3, 7.4, 3.9, 1H), 1.24 – 1.12 (m, 2H); **^{13}C NMR** (126 MHz, MeOD) δ 158.26 (C), 155.67 (CH), 154.06 (C), 152.47 (CH), 142.47 (CH), 141.58 (C), 134.67 (C), 132.89 (CH), 129.35 (CH), 129.21 (c), 129.11 (C), 127.33 (CH), 118.82 (CH), 99.55 (C), 65.35 (CH_2), 56.79 (CH_2), 53.22 (2x CH_2), 44.34 (2x CH_3), 44.05 (CH_2), 33.06 (CH), 30.04 (2x CH_2); **MS** (ES +ve) $[M+H]^+$: 431.2; **HRMS** (ES +ve), $C_{24}H_{30}N_9$ $[M+H]^+$: calculated 431.25879, found 431.258695.

Synthesis of 3-(3,4-dimethoxyphenyl)-1-[2-[4-(dimethylaminomethyl)-1-piperidyl]ethyl]pyrazolo[3,4-d]pyrimidin-4-amine (31):

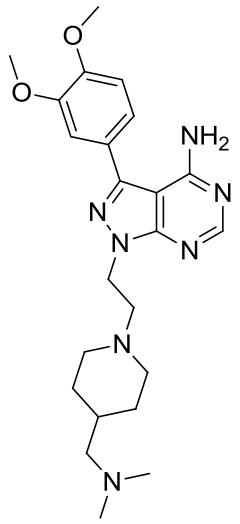

70 mg, 0.181 mmol of 1-(2,2-diethoxyethyl)-3-(3,4-dimethoxyphenyl)pyrazolo[3,4-d]pyrimidin-4-amine was added to a 20 ml microwave vial. 5 ml of water was added followed by 5 ml of TFA and the mixture heated conventially at 100°C for an hour. The mixture was concentrated *in vacuo* to leave a light brown oil which was used without further purification. 0.181 mmol of 2-[4-amino-3-(3,4-dimethoxyphenyl)pyrazolo[3,4-d]pyrimidin-1-yl]acetaldehyde was dissolved in 4 ml of DCM. N,N-dimethyl-1-(4-piperidyl)methanamine (1.5 eq., 0.271 mmol, 38.5 mg) was added followed by a drop of acetic acid and the mixture allowed to stir for 10 mins. Sodium triacetoxyborohydride (1.5 eq., 0.271 mmol, 57.4 mg) was added and the mixture allowed to stir for 17 hours. The mixture was concentrated *in vacuo* and the product purified by column chromatography, MeOH/DCM (5-10 % then 10 drops of NH_3 aq per 100 ml) to give a light yellow solid (14.5 mg, 0.033 mmol, 20.8 %). **^{1}H NMR** (500 MHz, MeOD) δ 8.26 (s, 1H), 7.27 (s, 1H), 7.25 (d, J = 8.2, 1H), 7.14 (d, J = 8.2, 1H), 4.63 (t, J = 6.3, 2H), 3.91 (s, 6H), 3.18 (s, 2H), 2.98 (d, J = 7.2, 2H), 2.85 (s, 6H), 2.45 (m, 2H), 1.92 (m, 1H), 1.83 (d, J = 13.2, 2H), 1.35 (dd, J = 22.2, 11.5, 2H); **^{13}C NMR** (126 MHz, MeOD) δ 158.58 (C), 155.51 (CH), 154.22 (C), 150.22 (C), 149.67 (C), 145.44 (C), 125.19 (C), 120.91 (CH), 111.94 (CH), 111.73 (CH), 97.82 (C), 62.49 (CH_2), 56.18 (CH_2), 55.13 (2x CH_3), 52.16 (2x CH_2), 43.08 (CH_2), 42.69 (2x CH_3), 30.70 (CH), 28.13 (2x CH_2); **MS** (ES +ve) $[M+H]^+$: 440.2; **HRMS** (ES +ve), $C_{23}H_{33}N_7O_2$ $[M+H]^+$: calculated 440.26902, found 440.268379.

Synthesis of 3-[4-amino-1-[2-[4-(dimethylaminomethyl)-1-piperidyl]ethyl]pyrazolo[3,4-d]pyrimidin-3-yl]phenol (32):

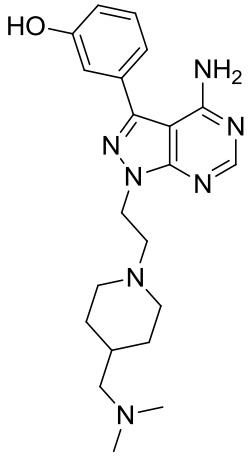

60 mg, 0.175 mmol of 3-[4-amino-1-(2,2-diethoxyethyl)pyrazolo[3,4-d]pyrimidin-3-yl]phenol was added to a 20 ml microwave vial. 5 ml of water was added followed by 5 ml of TFA and the mixture heated conventially at 100^{o}C for an hour. The mixture was concentrated *in vacuo* to leave a light brown oil which was used without further purification. 0.175 mmol of 2-[4-amino-3-(3-hydroxyphenyl)pyrazolo[3,4-d]pyrimidin-1-yl]acetaldehyde was dissolved in 4 ml of DCM. N,N-dimethyl-1-(4-piperidyl)methanamine (1.5 eq., 0.262 mmol, 37.2 mg) was added followed by a drop of acetic acid and the mixture allowed to stir for 10 mins. Sodium triacetoxyborohydride (1.5 eq., 0.262 mmol, 55.5 mg) was added and the mixture allowed to stir for 20 hours. The mixture was concentrated *in vacuo* and the product purified by column chromatography, MeOH/DCM (10 % then 0-20 drops of NH_3 aq per 100 ml) to give a dark orange solid (5.5 mg, 0.0139 mmol, 8.0 %). **^{1}H NMR** (500 MHz, MeOD) δ 8.26 (s, 1H), 7.39 (t, J = 7.9, 1H), 7.17 – 7.09 (m, 2H), 6.95 (dd, J = 7.8, 2.1, 1H), 4.57 (t, J = 6.7, 2H), 3.08 (d, J = 11.7, 2H), 2.96 (t, J = 6.7, 2H), 2.47 (m, 8H), 2.16 (t, J = 11.0, 2H), 1.74 (d, J = 12.9, 2H), 1.64 (m, 1H), 1.21 (dd, J = 21.1, 12.0, 2H); **^{13}C NMR** (126 MHz, MeOD) δ 158.44 (C), 158.06 (C), 155.42 (CH), 154.06 (C), 145.17 (C), 133.97 (C), 130.16 (CH), 119.09 (CH), 115.96 (CH), 114.92 (CH), 97.73 (C), 64.57 (CH_2), 56.66 (CH_2), 52.78 (2x CH_2), 43.83 (2x CH_3), 43.77 (CH_2), 32.46 (CH), 29.58 (2x CH_2). **MS** (ES +ve) $[M+H]^+$: 396.4; **HRMS** (ES +ve), $C_{21}H_{29}N_7O$ $[M+H]^+$: calculated 396.24281, found 396.242971.

Synthesis of 1-[2-[4-(dimethylaminomethyl)-1-piperidyl]ethyl]-3-(3-furyl)pyrazolo[3,4-d]pyrimidin-4-amine (33):

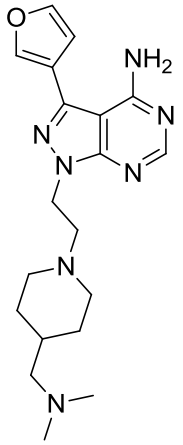

52 mg, 0.164 mmol of 1-(2,2-diethoxyethyl)-3-(3-furyl)pyrazolo[3,4-d]pyrimidin-4-amine was added to a 20 ml microwave vial. 5 ml of water was added followed by 5 ml of TFA and the mixture heated conventially at 100^{o}C for an hour. The mixture was concentrated *in vacuo* to leave a light brown oil which was used without further purification**.** 0.164 mmol of 2-[4-amino-3-(3-furyl)pyrazolo[3,4-d]pyrimidin-1-yl]acetaldehyde was dissolved in 4 ml of DCM. N,N-dimethyl-1-(4-piperidyl)methanamine (1.5 eq., 0.246 mmol, 35.0 mg) was added followed by a drop of acetic acid and the mixture allowed to stir for 10 mins. Sodium triacetoxyborohydride (1.5 eq., 0.246 mmol, 52.1 mg) was added and the mixture allowed to stir over the weekend. The mixture was concentrated *in vacuo* and the product purified by column chromatography, MeOH/DCM (5-10 % then 10-20 drops of NH_3 aq per 100 ml) to give a dark golden brown solid (45.7 mg, 0.124 mmol, 75.5 %). **^{1}H NMR** (500 MHz, MeOD) δ 8.23 (s, 1H), 7.96 (dd, J = 1.4, 0.9, 1H), 7.71 (t, J = 1.7, 1H), 6.82 (dd, J = 1.8, 0.8, 1H), 4.53 (t, J = 6.7, 2H), 3.08 (d, J = 11.7, 2H), 2.94 (t, J = 6.7, 2H), 2.62 (d, J = 6.6, 2H), 2.57 (s, 6H), 2.16 (dd, J = 11.8, 10.0, 2H), 1.72 (d, J = 12.9, 2H), 1.68 (m, 1H), 1.26 – 1.18 (m, 2H); **^{13}C NMR** (126 MHz, MeOD) δ 158.57 (C), 155.45 (CH), 153.98 (C), 144.34 (CH), 141.47 (CH), 137.22 (C), 118.30 (C), 109.73 (CH), 98.17 (C), 63.97 (CH_2), 56.59 (CH_2), 52.62 (2x CH_2), 43.73 (CH_2), 43.43 (2x CH_3), 32.02 (CH), 29.27 (2x CH_2); **MS** (ES +ve) $[M+H]^+$: 370.2; **HRMS** (ES +ve), $C_{19}H_{27}N_7O$ $[M+H]^+$: calculated 370.22716, found 370.227049.

Synthesis of 1-[2-[4-(dimethylaminomethyl)-1-piperidyl]ethyl]-3-(2-phenylethynyl)pyrazolo[3,4-d]pyrimidin-4-amine (34):

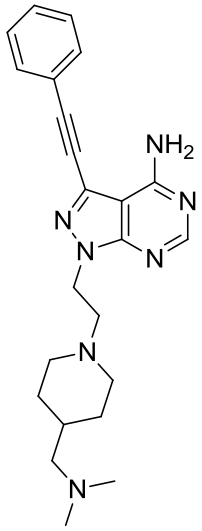

50 mg, 0.142 mmol of 1-(2,2-diethoxyethyl)-3-(2-phenylethynyl)pyrazolo[3,4-d]pyrimidin-4-amine was added to a 20 ml microwave vial. 5 ml of water was added followed by 5 ml of TFA and the mixture heated conventially at 100^{o}C for an hour. The mixture was concentrated *in vacuo* to leave a dark brown oil which was used without further purification. 0.142 mmol of 2-[4-amino-3-(2-phenylethynyl)pyrazolo[3,4-d]pyrimidin-1-yl]acetaldehyde was suspended in 4 ml of DCM. N,N-dimethyl-1-(4-piperidyl)methanamine (1.5 eq., 0.213 mmol, 30.3 mg) was added followed by a drop of acetic acid and the mixture allowed to stir for 10 mins. Sodium triacetoxyborohydride (1.5 eq., 0.213 mmol, 45.1 mg) was added and the mixture allowed to stir for an hour. The mixture was concentrated *in vacuo* and the product purified by column chromatography, MeOH/DCM (5-10 % then 5-10 drops of NH_3 aq per 100 ml) to give a dark orange solid, (23.4 mg, 0.058 mmol, 40.7 %). **^{1}H NMR** (500 MHz, MeOD) δ 8.23 (s, 1H), 7.69 – 7.61 (m, 2H), 7.46 – 7.40 (m, 3H), 4.51 (t, J = 6.7, 2H), 3.02 (d, J = 11.7, 2H), 2.90 (t, J = 6.7, 2H), 2.29 (s, 6H), 2.28 – 2.25 (m, 2H), 2.10 (td, J = 11.8, 2.3, 2H), 1.71 (d, J = 12.8, 2H), 1.54 (dtd, J = 14.6, 7.5, 3.7, 1H), 1.15 (qd, J = 12.5, 3.7, 2H); **^{13}C NMR** (126 MHz, MeOD) δ 158.22 (C), 156.07 (CH), 153.13 (C), 131.48 (CH x2), 129.25 (CH), 128.38 (CH x2), 126.72 (C), 121.47 (C), 100.98 (C), 93.76 (C), 79.88 (C), 65.21 (CH_2), 56.68 (CH_2), 52.96 (CH_2 x2), 44.27 (CH_3 x2), 44.22 (CH_2), 32.94 (CH), 29.92 (CH_2 x2); **MS** (ES +ve) $[M+H]^+$: 404.3; **HRMS** (ES +ve), $C_{23}H_{29}N_7$ $[M+H]^+$: calculated 404.24790, found 404.247888.

Synthesis of 1-[2-[4-(dimethylaminomethyl)-1-piperidyl]ethyl]-3-iodo-pyrazolo[3,4-d]pyrimidin-4-amine (35):

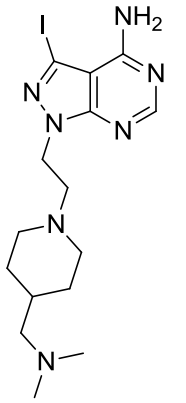

75 mg, 0.199 mmol of 1-(2,2-diethoxyethyl)-3-iodo-pyrazolo[3,4-d]pyrimidin-4-amine was added to a 10 ml microwave tube. 2.5 ml of water and 2.5 ml of TFA were added and the mixture heated to 100°C for an hour. The mixture was concentrated *in vacuo* to give a white solid which was used without further purification. 0.199 mmol of 2-(4-amino-3-iodo-pyrazolo[3,4-d]pyrimidin-1-yl)acetaldehyde was suspended in 3 ml of DCM. N,N-dimethyl-1-(4-piperidyl)methanamine (1.5 eq., 0.299 mmol, 42.2 mg) was added followed by a drop of acetic acid and the mixture allowed to stir for 10 mins. Sodium triacetoxyborohydride (1.5 eq., 0.299 mmol, 63.4 mg) was added and the mixture allowed to stir for 17 hours. The mixture was concentrated *in vacuo* and purified by column chromatography, MeOH/DCM (0-10 % then 5-15 drops of NH_3 aq. per 100 ml) to give a light yellow coloured solid (63.6 mg, 0.148 mmol, 74.5 %). **^{1}H NMR** (500 MHz, MeOD) δ 8.20 (s, 1H), 4.49 (t, *J* = 6.7, 2H), 3.01 (d, *J* = 11.7, 2H), 2.87 (t, *J* = 6.7, 2H), 2.28 (s, 6H), 2.27 (d, 2H), 2.10 (td, *J* = 11.8, 2.3, 2H), 1.72 (d, *J* = 13.0, 2H), 1.55 (ddt, *J* = 15.0, 7.6, 3.8, 1H), 1.15 (qd, *J* = 12.3, 3.7, 2H); **^{13}C NMR** (126 MHz, MeOD) δ 158.05 (C), 155.63 (CH), 153.58 (C), 103.66 (C), 86.95 (C), 65.27 (CH_2), 56.73 (CH_2), 52.96 (2x CH_2), 44.30 (2x CH_3), 44.15 (CH_2), 32.97 (CH), 30.09 (2x CH_2); **MS** (ES +ve) $[M+H]^+$: 430.2.

10. Experimental

10.4 Experimental for Chapter 4

10.4.1 Synthesis of Compounds 36-43

Synthesis of 1-(1,3-dioxolan-2-ylmethyl)-3-iodo-pyrazolo[3,4-d]pyrimidin-4-amine (36):

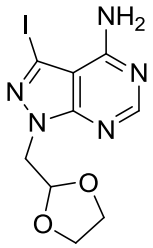

To a solution of 3-iodo-1H-pyrazolo[3,4-d]pyrimidin-4-amine (1 g, 3.83 mmol) in DMF (15 ml) was added sodium hydride (1 eq., 3.83 mmol, 60% dispersion in mineral oil, 153.5 mg) and the suspension allowed to stir for 30 mins until gas evolution had subsided. 2-Bromomethyl-1,3-dioxolane (1 eq. 3.83 mmol, 635.6 g, 0.39 ml) was then added dropwise and the mixture heated to 150 ^{o}C in the microwave for an hour. EtOAc and water (50 ml) were added to the mixture and the organics separated. The aqueous layer was washed with EtOAc (x5, 50 ml) and organics combined. The combined organics were then washed with water (x3, 30 ml) to remove any residual DMF and the organics combined, dried over $MgSO_4$ and concentrated *in vacuo*. The product was purified by column chromatography, MeOH/DCM (0-5 %) to give a light yellow solid (695.6 mg, 2.005 mmol, 52.3 %). **^{1}H NMR** (500 MHz, CDCl3) δ 8.33 (s, 1H), 6.07 (s, 2H), 5.36 (t, *J* = 4.5, 1H), 4.52 (d, *J* = 4.5, 2H), 4.00 – 3.92 (m, 2H), 3.90 – 3.83 (m, 2H); **^{13}C NMR** (126 MHz, CDCl3) δ 157.01 (C), 155.66 (CH), 154.45 (C), 103.95 (C), 101.51 (CH), 87.00 (C), 65.27 (2x CH_2) , 49.97 (CH_2); **MS** (ES +ve) $[M+H]^+$: 348.0

Synthesis of 1-(1,3-dioxolan-2-ylmethyl)-3-iodo-pyrazolo[3,4-d]pyrimidin-4-amine (37):

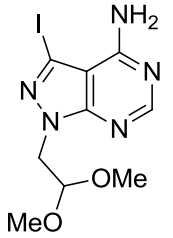

To a solution of 3-iodo-1H-pyrazolo[3,4-d]pyrimidin-4-amine (750 mg, 2.87 mmol) in DMF (10 ml) was added sodium hydride (1.5 eq., 4.31 mmol, 60% dispersion in mineral oil, 172.4 mg) and the suspension allowed to stir for 30 mins until the gas evolution had subsided. Bromoacetaldehyde dimethyl acetal (1.5 eq. 4.31 mmol, 724.0 mg, 0.506 ml) was then added dropwise and the mixture heated in the microwave for 30 mins at 150 ^{o}C. EtOAc and water (50 ml) were added to the mixture and the organic layer separated. The aqueous layer was washed with EtOAc (x3, 20 ml) and the organic layers combined, dried over $MgSO_4$ and concentrated *in vacuo.* The product was purified by column chromatography, MeOH/DCM (0-3 %) to give a light cream coloured solid (638.9 mg, 1.83 mmol, 63.8 %). **^{1}H NMR** (500 MHz, CDCl3) δ 8.35 (s, 1H), 6.11 (s, 2H), 4.94 (t, *J* = 5.7, 1H), 4.50 (d, *J* = 5.7, 2H), 3.38 (s, 6H); **^{13}C NMR** (126 MHz, CDCl3) δ 156.94(c), 155.42 (CH), 154.20 (C), 103.87 (C), 101.22 (CH), 86.79 (C), 53.51 (CH_3), 48.40 (CH_2); **MS** (ES +ve) $[M+H]^+$: 349.0

Synthesis of 5-(4,4,5,5-tetramethyl-1,3,2-dioxaborolan-2-yl)-1,3-benzoxazol-2-amine (38):

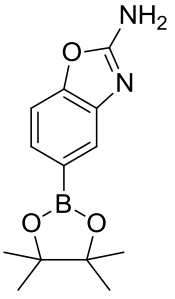

To a solution of 5-bromo-1,3-benzoxazol-2-amine (500 mg, 2.359 mmol) in dioxane/water (9 ml/1 ml) was added bis(pinacolato)diboron (1.5 eq., 899 mg, 3.538 mmol), potassium carbonate (1.5 eq., 489 mg, 3.538 mmol) and triphenylphosphine (20 mol %, 185.6 mg) followed by palladium acetate (5 mol %, 39.7 mg) and the mixture heated in the microwave at 120 ^{o}C for 30 mins. EtOAc and water (50 ml) were added to the mixture and the organics separated. The aqueous layer was washed with EtOAc (x2, 50 ml) and the organics

combined. The combined organics were then washed with brine, dried over $MgSO_4$ and concentrated *in vacuo*. The product was purified by column chromatography, MeOH/DCM (0-3 %) to give a red/orange solid (556.1 mg, 2.137 mmol, 90.6 %). **^{1}H NMR** (500 MHz, MeOD) δ 7.63 (s, 1H), 7.49 (dd, *J* = 8.0, 1.1, 1H), 7.29 (d, *J* = 8.0, 1H), 1.37 (s, 12H); **^{13}C NMR** (126 MHz, MeOD) δ 163.38 (C), 150.64 (C), 142.08 (C), 127.70 (CH), 121.07 (CH), 116.08 (C), 107.88 (CH), 83.65 (2x C), 23.78 (4x CH_3); **MS** (ES +ve) $[M+H]^+$: 261.4.

Synthesis of 1-(1,3-dioxolan-2-ylmethyl)-3-(1H-pyrrolo[2,3-b]pyridin-5-yl)pyrazolo[3,4-d]pyrimidin-4-amine (39):

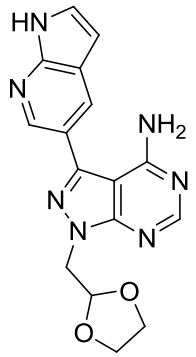

To a solution of 1-(1,3-dioxolan-2-ylmethyl)-3-iodo-pyrazolo[3,4-d]pyrimidin-4-amine (100 mg, 0.288 mmol) in dioxane/water (4.5 ml/0.5 ml) was added 1H-pyrrolo[2,3-b]pyridine-5-boronic acid pinicol ester (1.5 eq., 70.3 mg, 0.576 mmol), potassium carbonate (1.5 eq., 59.7 mg, 0.576 mmol) and triphenylphosphine (20 mol %, 22.6 mg) followed by palladium acetate (5 mol %, 4.2 mg) and the mixture heated in the microwave at 120 ^oC for an hour. EtOAc (50 ml) and water (50 ml) were added to the mixture and the organic layer separated. The aqueous layer was washed with EtOAc (20 ml, x2) and the organics combined dried over $MgSO_4$ and concentrated in vacuo. The crude product was purified by column chromatography, MeOH/DCM (0-10 %) to give a white solid (65.6 mg, 0.195 mmol, 67.6 %). **^{1}H NMR** (500 MHz, DMSO) δ 11.81 (s, 1H), 8.45 (d, *J* = 2.0, 1H), 8.24 (s, 1H), 8.17 (d, *J* = 1.7, 1H), 7.56 – 7.52 (m, 1H), 6.55 (dd, *J* = 3.4, 1.9, 1H), 5.34 (t, *J* = 4.8, 1H), 4.44 (d, *J* = 4.8, 2H), 3.96 – 3.86 (m, 2H), 3.86 – 3.75 (m, 2H); **^{13}C NMR** (126 MHz, MeOD) δ 158.69 (C), 155.72 (CH), 154.66 (C), 148.21 (C), 143.81 (C), 141.90 (CH), 128.77 (CH), 127.06 (CH), 120.73 (C), 120.63 (C), 101.42 (CH), 100.66 (CH), 98.16 (C), 64.80 (2x CH_2), 49.19 (CH_2); **MS** (ES +ve) $[M+H]^+$: 338.9; **HRMS** (ES +ve), $C_{16}H_{16}N_7O_2$ $(M+H)^+$: calculated 338.13600, found 338.13690.

Synthesis of 1-(2,2-dimethoxyethyl)-3-(1H-pyrrolo[2,3-b]pyridin-5-yl)pyrazolo[3,4-d]pyrimidin-4-amine (40):

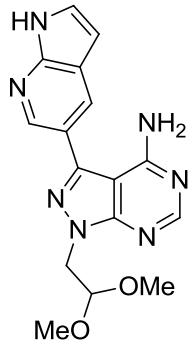

To a solution of 1-(1,3-dioxolan-2-ylmethyl)-3-iodo-pyrazolo[3,4-d]pyrimidin-4-amine (100 mg, 0.287 mmol) in dioxane/water (4.5 ml/0.5 ml) was added 1H-pyrrolo[2,3-b]pyridine-5-boronic acid pinicol ester (1.5 eq., 70.3 mg, 0.430 mmol), potassium carbonate (1.5 eq., 59.7 mg, 0.430 mmol) and triphenylphosphine (20 mol %, 22.6 mg) followed by palladium acetate (5 mol %, 4.2 mg) and the mixture heated in the microwave at 120 ^{o}C for an hour. EtOAc (50 ml) and water (50 ml) were added to the mixture and the organic layer separated. The aqueous layer was washed with EtOAc (20 ml, x2) and the organics combined, dried over $MgSO_4$ and concentrated *in vacuo*. The crude product was purified by column chromatography, MeOH/DCM (0-5 %) to give a white solid (67.5 mg, 0.199 mmol, 69.3 %). **^{1}H NMR** (500 MHz, CDCl3) δ 9.22 (s, 1H), 8.68 (s, 1H), 8.46 (s, 1H), 8.29 (d, *J* = 1.8, 1H), 7.49 (d, *J* = 10.6, 1H), 6.66 (s, 1H), 5.71 (s, 2H), 5.09 (t, *J* = 5.7, 1H), 4.64 (d, *J* = 5.7, 2H), 3.46 (s, 6H); **^{13}C NMR** (126 MHz, CDCl3) δ 157.21 (C), 154.80 (CH), 148.64 (C), 143.34 (C), 143.18 (C), 143.08 (CH), 128.76 (CH), 126.40 (CH), 121.56 (C), 120.19 (C), 101.81 (CH), 101.31 (CH), 98.63 (C), 53.44 (2x CH_3), 48.11 (CH_2); **MS** (ES +ve) $[M+H]^+$: 340.2, 379.2 (+K), (ES –ve) $[M-H]^-$: 338.2; **HRMS** (ES +ve), $C_{16}H_{18}N_7O_2$ $(M+H)^+$: calculated 340.15165, found 340.15190.

5-[4-amino-1-(2,2-diethoxyethyl)pyrazolo[3,4-d]pyrimidin-3-yl]-1,3-benzoxazol-2-amine (41):

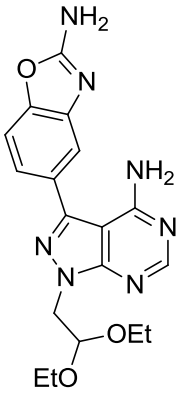

To a solution of 1-(2,2-diethoxyethyl)-3-iodo-pyrazolo[3,4-d]pyrimidin-4-amine (50 mg, 0.133 mmol) in dioxane/water (4.5 ml/0.5 ml) was added 5-(4,4,5,5-tetramethyl-1,3,2-dioxaborolan-2-yl)-1,3-benzoxazol-2-amine (1.5 eq., 51.8 mg, 0.199 mmol), potassium carbonate (1.5 eq., 27.2 mg, 0.199 mmol) and triphenylphosphine (20 mol %, 10.4 mg) followed by palladium acetate (5 mol %, 2.25 mg) and the mixture heated in the microwave at 120 ^{o}C for 30 mins. The reaction was repeated to double the product. EtOAc (50 ml) and water (50 ml) were added to the mixture and the organic layer separated. The aqueous layer was washed with EtOAc (20 ml) and the organics combined, dried over $MgSO_4$ and concentrated *in vacuo*. The crude product was purified by column chromatography, MeOH/DCM (0-8 %) to give a pale orange/red solid (54.6 mg, 0.142 mmol, 53.7 %). **^{1}H NMR** (500 MHz, MeOD) δ 8.25 (s, 1H), 7.51 (d, *J* = 1.4, 1H), 7.46 (d, *J* = 8.2, 1H), 7.35 (dd, *J* = 8.2, 1.7, 1H), 5.06 (t, *J* = 5.7, 1H), 4.49 (d, *J* = 5.7, 2H), 3.75 (dq, *J* = 9.5, 7.1, 2H), 3.49 (dq, *J* = 9.5, 7.0, 2H), 1.08 (t, *J* = 7.0, 6H); **^{13}C NMR** (126 MHz, MeOD) δ 164.34 (C), 158.52 (C), 155.52 (CH), 154.38 (C), 149.00 (C), 145.43 (C), 143.61 (C), 128.63 (C), 121.13 (CH), 114.96 (CH), 109.00 (CH), 100.27 (CH), 97.73 (C), 62.43 (2x CH_2), 48.85 (CH_2), 14.12 (2x CH_3); **MS** (ES +ve) $[M+H]^+$: 384.8; **HRMS** (ES +ve), $C_{18}H_{22}N_7O_3$ $(M+H)^+$: calculated 384.17786, found 384.1771.

Synthesis of 5-[4-amino-1-(1,3-dioxolan-2-ylmethyl)pyrazolo[3,4-d]pyrimidin-3-yl]-1,3-benzoxazol-2-amine (42):

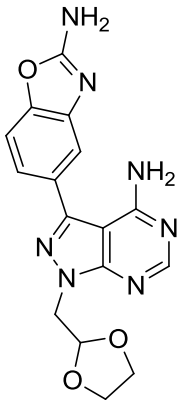

To a solution of 1-(1,3-dioxolan-2-ylmethyl)-3-iodo-pyrazolo[3,4-d]pyrimidin-4-amine (100 mg, 0.288 mmol) in dioxane/water (4.5 ml/0.5 ml) was added 5-(4,4,5,5-tetramethyl-1,3,2-dioxaborolan-2-yl)-1,3-benzoxazol-2-amine (1.5 eq., 111.4 mg, 0.432 mmol), potassium carbonate (1.5 eq., 59.7 mg, 0.432 mmol) and triphenylphosphine (20 mol %, 22.6 mg) followed by palladium acetate (5 mol %, 4.2 mg) and the mixture heated in the microwave at 120 ^{o}C for an hour. EtOAc (50 ml) and water (50 ml) were added to the mixture and the organic layer separated. The aqueous layer was washed with EtOAc (20 ml, x2) and the organics combined dried over $MgSO_4$ and concentrated *in vacuo*. The crude product was purified by column chromatography, MeOH/DCM (0-10 %) to give a peach coloured solid (43.36 mg, 0.123 mmol, 42.6 %). **^{1}H NMR** (500 MHz, DMSO) δ 8.24 (s, 1H), 7.53 (s, 2H), 7.47 (d, *J* = 8.1, 1H), 7.40 (d, *J* = 1.5, 1H), 7.23 (dd, *J* = 8.1, 1.7, 1H), 5.34 (t, *J* = 4.8, 1H), 4.43 (d, *J* = 4.8, 2H), 3.97 – 3.90 (m, 2H), 3.85 – 3.78 (m, 2H); **^{13}C NMR** (126 MHz, DMSO) δ 163.92 (C), 158.62 (C), 156.32 (CH), 155.19 (C), 148.84 (C), 145.03 (C), 144.89 (C), 128.84 (C), 120.91 (CH), 115.45 (CH), 109.37 (CH), 101.49 (CH), 97.76 (C), 64.86 (2x CH_2), 49.28 (CH_2); **MS** (ES +ve) $[M+H]^+$: 354.9; **HRMS** (ES +ve), $C_{16}H_{16}N_7O_3$ $(M+H)^+$: calculated 354.13091, found 354.13140.

Synthesis of 5-[4-amino-1-(2,2-dimethoxyethyl)pyrazolo[3,4-d]pyrimidin-3-yl]-1,3-benzoxazol-2-amine (43):

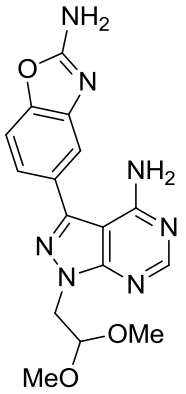

To a solution of 1-(1,3-dioxolan-2-ylmethyl)-3-iodo-pyrazolo[3,4-d]pyrimidin-4-amine (100 mg, 0.287 mmol) in dioxane/water (4.5 ml/0.5 ml) was added 5-(4,4,5,5-tetramethyl-1,3,2-dioxaborolan-2-yl)-1,3-benzoxazol-2-amine (1.5 eq., 112.1 mg, 0.431 mmol), potassium carbonate (1.5 eq., 59.7 mg, 0.431 mmol) and triphenylphosphine (20 mol %, 22.6 mg) followed by palladium acetate (5 mol %, 4.2 mg) and the mixture heated in the microwave at 120 ^{o}C for an hour. EtOAc (50 ml) and water (50 ml) were added to the mixture and the organic layer separated. The aqueous layer was washed with EtOAc (20 ml, x2) and the organics combined dried over $MgSO_4$ and concentrated *in vacuo*. The crude product was purified by column chromatography, MeOH/DCM (0-10 %) to give a peach coloured solid (60.22 mg, 0.169 mmol, 59.1 %). **^{1}H NMR** (500 MHz, MeOD) δ 8.28 (s, 1H), 7.55 (d, *J* = 1.3, 1H), 7.48 (d, *J* = 8.2, 1H), 7.38 (dd, *J* = 8.2, 1.7, 1H), 4.98 (t, *J* = 5.7, 1H), 4.53 (d, *J* = 5.7, 2H), 3.41 (s, 6H); **^{13}C NMR** (126 MHz, MeOD) δ 164.33 (C), 158.53 (C), 155.53 (CH), 154.33 (C), 149.00 (C), 145.49 (C), 143.60 (C), 128.63 (C), 121.04 (CH), 114.98 (CH), 108.98 (CH), 101.82 (CH), 97.72 (C), 52.94 (2x CH_3), 47.79 (CH_2); **MS** (ES +ve) $(M+H)^+$: 356.7; **HRMS** (ES +ve), $C_{16}H_{18}N_7O_3$ $(M+H)^+$: calculated 356.14656, found 356.14530.

10.4.2 Synthesis of Compound 44

Synthesis of 2-[4-amino-3-(2-amino-1,3-benzoxazol-5-yl)pyrazolo[3,4-d]pyrimidin-1-yl]acetaldehyde (44):

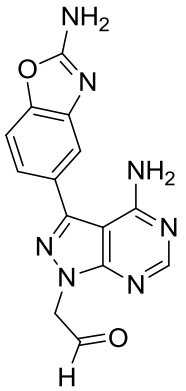

5-[4-amino-1-(2,2-dimethoxyethyl)pyrazolo[3,4-d]pyrimidin-3-yl]-1,3-benzoxazol-2-amine, **43**, (9.0 mg, 25.3 umol) was added to a 2ml microwave tube. 1 ml of water and 1 ml of TFA were added and the mixture heated to 100^{o}C in the microwave for 30 mins. The product was transferred to a flask and concentrated *in vacuo* giving the product without further purification in quantitative yield.

10.4.3 Synthesis of Compounds 45-48

Synthesis of 1-(cyclopentylmethyl)-3-iodo-pyrazolo[3,4-d]pyrimidin-4-amine (45):

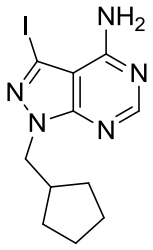

To a solution of 3-iodo-1H-pyrazolo[3,4-d]pyrimidin-4-amine (200 mg, 0.766 mmol) in DMF (2 ml) was added sodium hydride (1.5 eq., 1.149 mmol, 60% dispersion in mineral oil, 45.9 mg) and the suspension allowed to stir for 30 mins until gas evolution had subsided. (iodomethyl)cyclopentane (1.5 eq. 1.149 mmol, 312.9 mg, 0.195 ml) was then added dropwise and the mixture heated at 150 ^{o}C in the microwave for an hour. EtOAc and water (50 ml) were added to the mixture and the organic layer separated. The aqueous layer was washed with EtOAc (x1, 50 ml) and organics combined. The combined organics were then

washed with brine (30 ml) to remove any residual DMF and the organics dried over $MgSO_4$ and concentrated *in vacuo*. The product was purified by column chromatography, MeOH/DCM (0-1.5 %) to give a white solid (190.44 mg, 0.555 mmol, 72.5 %). **^{1}H NMR** (500 MHz, MeOD) δ 8.21 (s, 1H), 4.28 (d, *J* = 7.6, 2H), 2.55 (dt, *J* = 14.8, 7.4, 1H), 1.76 – 1.64 (m, 4H), 1.63 – 1.54 (m, 2H), 1.34 (dd, *J* = 12.9, 5.7, 2H); **^{13}C NMR** (126 MHz, MeOD) δ 158.11 (C), 155.61 (CH), 153.23 (C), 103.43 (C), 86.40 (C), 51.63 (CH_2), 40.09 (CH), 29.57 (2x CH_2), 24.56 (2x CH_2); **MS** (ES +ve) $[M+H]^+$: 343.5.

Synthesis of 3-iodo-1-(tetrahydrofuran-2-ylmethyl)pyrazolo[3,4-d]pyrimidin-4-amine (46):

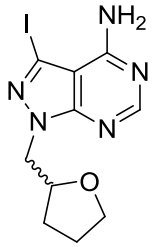

To a solution of 3-iodo-1H-pyrazolo[3,4-d]pyrimidin-4-amine (200 mg, 0.766 mmol) in DMF (2 ml) was added sodium hydride (1.5 eq., 1.149 mmol, 60% dispersion in mineral oil, 45.9 mg) and the suspension allowed to stir for 30 mins until gas evolution had subsided. 2-(bromomethyl)tetrahydrofuran (1.5 eq. 1.149 mmol, 188.4 mg) was then added dropwise and the mixture heated at 150 ^oC in the microwave for 30 mins. EtOAc and water (50 ml) were added to the mixture and the organic layer separated. The aqueous layer was washed with EtOAc (x2, 50 ml) and organics combined. The combined organics were then washed with brine (30 ml) to remove any residual DMF and the organics dried over $MgSO_4$ and concentrated *in vacuo*. The product was purified by column chromatography, MeOH/DCM (0-2 %) to give a white solid (177.05 mg, 0.564 mmol, 73.6 %). **^{1}H NMR** (500 MHz, MeOD) δ 8.22 (s, 1H), 4.47 – 4.36 (m, 2H), 4.33 (dd, *J* = 12.9, 3.9, 1H), 3.91 – 3.83 (m, 1H), 3.78 – 3.69 (m, 1H), 2.05 (dt, *J* = 12.4, 6.7, 1H), 1.98 – 1.86 (m, 2H), 1.83 – 1.74 (m, 1H); **^{13}C NMR** (126 MHz, MeOD) δ 158.10 (C), 155.70 (CH), 153.70 (C), 103.55 (C), 87.00 (C), 77.13 (CH), 67.73 (CH_2), 50.74 (CH_2), 28.43 (CH_2), 24.89 (CH_2); **MS** (ES +ve) $[M+H]^+$: 354.5.

Synthesis of 5-[4-amino-1-(cyclopentylmethyl)pyrazolo[3,4-d]pyrimidin-3-yl]-1,3-benzoxazol-2-amine (47):

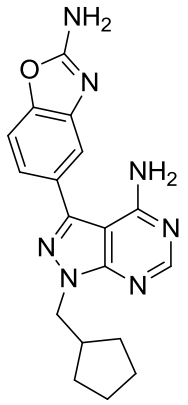

To a solution of 1-(cyclopentylmethyl)-3-iodo-pyrazolo[3,4-d]pyrimidin-4-amine (100 mg, 0.292 mmol) in dioxane/water (4.5 ml/0.5 ml) was added 5-(4,4,5,5-tetramethyl-1,3,2-dioxaborolan-2-yl)-1,3-benzoxazol-2-amine (1.5 eq., 113.9 mg, 0.438 mmol), potassium carbonate (1.5 eq., 60.5 mg, 0.438 mmol) and triphenylphosphine (20 mol %, 15.3 mg) followed by palladium acetate (5 mol %) and the mixture heated in the microwave at 120 ^{o}C for an hour. EtOAc (50 ml) and water (50 ml) were added to the mixture and the organic layer separated. The aqueous layer was washed with EtOAc (20 ml) and the organics combined dried over $MgSO_4$ and concentrated *in vacuo*. The crude product was purified by column chromatography, MeOH/DCM (0-6 %) to give a light cream solid (48.91 mg, 0.140 mmol, 48.0 %). **^{1}H NMR** (500 MHz, MeOD) δ 8.26 (s, 1H), 7.54 (d, *J* = 1.4, 1H), 7.48 (d, *J* = 8.2, 1H), 7.37 (dd, *J* = 8.2, 1.7, 1H), 4.35 (d, *J* = 7.6, 2H), 2.63 (dt, *J* = 14.9, 7.5, 1H), 1.84 – 1.66 (m, 4H), 1.61 (m, 2H), 1.43 (m, 2H); **^{13}C NMR** (126 MHz, MeOD) δ 164.32 (C), 158.56 (C), 155.37 (CH), 153.70 (C), 148.96 (C), 144.95 (C), 143.59 (C), 128.74 (C), 121.17 (CH), 114.99 (CH), 108.94 (CH), 97.59 (C), 51.23 (CH_2), 40.14 (CH), 29.69 (2x CH_2), 24.61 (2x CH_2); **MS** (ES +ve) $[M+H]^+$: 350.2, 721.4 (2M+Na), (ES -ve) $[M-H]^-$: 348.2; **HRMS** (ES +ve), $C_{18}H_{20}N_7O_1$ $(M+H)^+$: calculated 350.17239, found 350.17260.

Synthesis of 5-[4-amino-1-(tetrahydrofuran-2-ylmethyl)pyrazolo[3,4-d]pyrimidin-3-yl]-1,3-benzoxazol-2-amine (48):

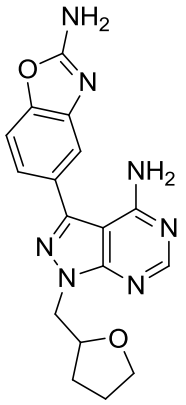

To a solution of 3-iodo-1-(tetrahydrofuran-2-ylmethyl)pyrazolo[3,4-d]pyrimidin-4-amine (100 mg, 0.299 mmol) in dioxane/water (4.5 ml/0.5 ml) was added 5-(4,4,5,5-tetramethyl-1,3,2-dioxaborolan-2-yl)-1,3-benzoxazol-2-amine (1.5 eq., 113.9 mg, 0.438 mmol), potassium carbonate (1.5 eq., 60.5 mg, 0.438 mmol) and triphenylphosphine (20 mol %, 15.3 mg) followed by palladium acetate (5 mol %) and the mixture heated in the microwave at 120 ^{o}C for an hour. EtOAc (50 ml) and water (50 ml) were added to the mixture and the organic layer separated. The aqueous layer was washed with EtOAc (20 ml) and the organics combined dried over $MgSO_4$ and concentrated *in vacuo*. The crude product was purified by column chromatography, MeOH/DCM (0-10 %) to give a light rose coloured solid (50.09 mg, 0.143 mmol, 47.7 %). **^{1}H NMR** (500 MHz, MeOD) δ 8.27 (s, 1H), 7.55 (d, *J* = 1.5, 1H), 7.48 (d, *J* = 8.2, 1H), 7.38 (dd, *J* = 8.2, 1.7, 1H), 4.50 (dq, *J* = 13.1, 7.0, 2H), 4.40 (dd, *J* = 13.0, 3.9, 1H), 3.91 (dd, *J* = 14.7, 6.8, 1H), 3.76 (dd, *J* = 14.1, 7.6, 1H), 2.08 (dt, *J* = 12.3, 6.6, 1H), 2.02 – 1.89 (m, 2H), 1.89 – 1.79 (m, 1H); **^{13}C NMR** (126 MHz, MeOD) δ 164.32 (C), 158.52 (C), 155.46 (CH), 154.21 (C), 148.97 (C), 145.32 (C), 143.56 (C), 128.69 (C), 121.19 (CH), 115.02 (CH), 108.97 (CH), 97.75 (C), 77.22 (CH), 67.76 (CH_2), 50.41 (CH_2), 28.54 (CH_2), 24.94 (CH_2); **MS** (ES +ve) $[M+H]^+$: 352.2, 725.3 (2M+Na); **HRMS** (ES +ve), $C_{17}H_{18}N_7O_2$ $(M+H)^+$: calculated 352.15165, found 352.15220.

10. Experimental

10.5 Experimental for Chapter 5

10.5.1 Synthesis of Compound 49

Synthesis of 1-[2-[4-(dimethylamino)-1-piperidyl]ethyl]-3-(1H-pyrrolo[2,3-b]pyridin-5-yl)pyrazolo[3,4-d]pyrimidin-4-amine (49):

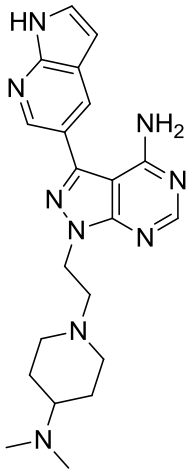

40 mg, 0.109 mmol of 1-(2,2-diethoxyethyl)-3-(1H-pyrrolo[2,3-b]pyridin-5-yl)pyrazolo[3,4-d]pyrimidin-4-amine was added to a 10 ml microwave tube. 2.5 ml of water and 2.5 ml of TFA were then added and the mixture heated to 100 ^{o}C for 30 mins in the microwave. The solvents were removed *in vacuo* to give a dark brown oil which was used without further purification. 0.109 mmol of 2-[4-amino-3-(1H-pyrrolo[2,3-b]pyridin-5-yl)pyrazolo[3,4-d]pyrimidin-1-yl]acetaldehyde was dissolved in 3 ml of THF. N,N-dimethylpiperidine-4-amine (1.5 eq., 0.1635 mmol, 20.9 mg) was added and the mixture was allowed to stir for 5 mins. Sodium triacetoxyborohydride (1.5 eq., 0.1635 mmol, 34.7 mg) was then added and the mixture allowed to stir for an hour. The reaction mixture was concentrated *in vacuo* and purified by column chromatography, MeOH/DCM (10 % then 5-40 drops of NH_3 aq. per 50 ml) to give a light yellow solid (26.9 mg, 0.0664 mmol, 60.9 %). **^{1}H NMR** (500 MHz, MeOD) δ 8.50 (d, *J* = 1.9, 1H), 8.28 (d, *J* = 2.0, 1H), 8.27 (s, 1H), 7.51 (d, *J* = 3.5, 1H), 6.62 (d, *J* = 3.5, 1H), 4.56 (t, *J* = 6.4, 2H), 3.19 (d, *J* = 12.1, 2H), 3.06 (tt, *J* = 12.0, 3.9, 1H), 2.97 (t, *J* = 6.4, 2H), 2.77 (s, 6H), 2.18 (t, *J* = 11.1, 2H), 2.00 (d, *J* = 12.4, 2H), 1.58 (qd, *J* = 12.3, 3.9, 2H); **^{13}C NMR** (126 MHz, MeOD) δ 158.64 (C), 155.49 (CH), 154.32 (C), 148.16 (C), 143.50 (C), 141.84 (CH), 128.66 (CH), 127.12 (CH), 120.78 (C), 120.73 (C), 100.63 (CH),

98.08 (C), 63.37 (CH), 55.82 (CH_2), 51.54 (2xCH_2), 44.11 (CH_2), 39.16 (2xCH_3), 26.18 (2xCH_2); **MS** (ES +ve) $(M+H)^+$: 406.6; **HRMS** (ES +ve), $C_{21}H_{28}N_9$ $(M+H)^+$: calculated 406.24622, found 406.24490.

10.5.2 Synthesis of Compounds 50-52

Synthesis of 1-[2-[4-(dimethylamino)-1-piperidyl]ethyl]-3-iodo-pyrazolo[3,4-d]pyrimidin-4-amine (50):

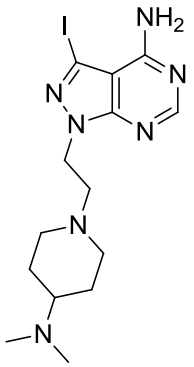

150 mg, 0.398 mmol, of 1-(2,2-diethoxyethyl)-3-iodo-pyrazolo[3,4-d]pyrimidin-4-amine was added to a 10 ml microwave tube. 2.5 ml of water and 2.5 ml of TFA were added and the mixture heated to 100^oC for an hour. The mixture was concentrated *in vacuo* to give a white solid which was used without further purification. 0.398 mmol of 2-(4-amino-3-iodo-pyrazolo[3,4-d]pyrimidin-1-yl)acetaldehyde was suspended in 3 ml of DCM. N,N-dimethylpiperidine-4-amine (1.5 eq., 0.598 mmol, 76.6 mg) was added followed by a drop of acetic acid and the mixture allowed to stir for 10 mins. Sodium triacetoxyborohydride (1.5 eq., 0.598 mmol, 126.8 mg) was added and the mixture allowed to stir for 17 hours overnight. The mixture was concentrated *in vacuo* and the product purified by column chromatography, MeOH/DCM (0-10 % then 5-20 drops of NH_3 aq. per 100 ml) to give a light orange/brown solid (163.8 mg, 0.405 mmol, 99.1 %). **^{1}H NMR** (500 MHz, MeOD) δ 8.22 (s, 1H), 4.49 (t, *J* = 6.4, 2H), 3.32 (s, 3H), 3.15 (d, *J* = 12.1, 2H), 2.96 (ddd, *J* = 16.0, 8.0, 4.0, 1H), 2.91 (t, *J* = 6.4, 2H), 2.72 (s, 6H), 2.15 (td, *J* = 12.0, 2.0, 2H), 2.04 – 1.96 (m, 2H), 1.54 (qd, *J* = 12.2, 3.9, 2H); **^{13}C NMR** (126 MHz, MeOD) δ 158.07 (C), 155.67 (CH), 153.70 (C), 103.59 (C), 86.97 (C), 63.18 (CH), 55.86 (CH_2), 51.38 (2x CH_2), 44.37 (CH_2), 39.31 (2x CH_3), 26.42 (2x CH_2); **MS** (ES +ve) $[M+H]^+$: 416.2.

Synthesis of tert-butyl N-[4-[4-amino-1-[2-[4-(dimethylaminomethyl)-1-piperidyl]ethyl]pyrazolo[3,4-d]pyrimidin-3-yl]-2-methoxy-phenyl]carbamate (51):

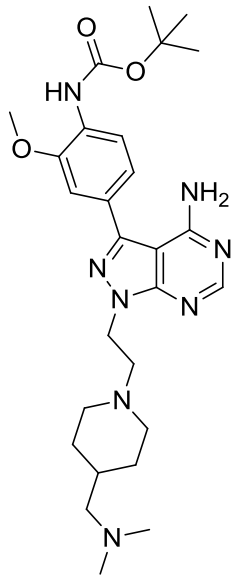

To a solution of 1-[2-[4-(dimethylaminomethyl)-1-piperidyl]ethyl]-3-iodo-pyrazolo[3,4-d]pyrimidin-4-amine (50 mg, 0.1165 mmol) in dioxane/water (4.5 ml/0.5 ml) was added [4-(tert-butoxycarbonylamino)-3-methoxy-phenyl]boronic acid (1.5 eq., 46.7 mg, 0.175 mmol), potassium carbonate (1.5 eq., 24.2 mg, 0.175 mmol) and triphenylphosphine (20 mol %, 9.2 mg) followed by palladium acetate (5 mol %) and the mixture heated in the microwave at 120 ^{o}C for 45 mins. EtOAc (50 ml) and water (50 ml) were added to the mixture and the organic layer separated. The aqueous layer was washed with EtOAc (20 ml, x3) and the organics combined dried over $MgSO_4$ and concentrated *in vacuo*. The crude product was purified by column chromatography, MeOH/DCM (0-10 % then 5-20 drops of NH_3 aq. per 100 ml) to give a dark brown solid (36.5 mg, 0.0696 mmol, 59.7 %). **^{1}H NMR** (500 MHz, MeOD) δ 8.27 (s, 1H), 8.08 (d, *J* = 8.2, 1H), 7.30 (d, *J* = 1.8, 1H), 7.26 (dd, *J* = 8.2, 1.8, 1H), 4.58 (t, *J* = 6.8, 2H), 3.98 (s, 3H), 3.08 (d, *J* = 11.7, 2H), 2.96 (t, *J* = 6.8, 2H), 2.34 (s, 6H), 2.32 (d, *J* = 7.2, 2H), 2.16 (dd, *J* = 11.8, 9.6, 2H), 1.76 (d, *J* = 12.3, 2H), 1.63 – 1.58 (m, 1H), 1.57 (s, 9H), 1.24 – 1.16 (m, 2H); **^{13}C NMR** (126 MHz, MeOD) δ 158.52 (C), 155.40 (CH), 154.07 (C), 153.46 (C), 149.24 (C), 145.04 (C), 128.77 (C), 127.39 (C), 120.43 (CH), 119.56 (CH), 110.29 (CH), 97.78 (C), 80.18 (C), 65.19 (CH_2), 56.76 (CH_2), 55.08 (CH_3), 52.96 (2x CH_2), 44.24 (2x CH_3), 43.79 (CH_2), 32.92 (CH), 29.89 (2x CH_2), 27.22 (3x CH_3); **MS** (ES +ve) $[M+H]^+$: 525.4, (ES –ve) $[M-H]^-$: 523.3; **HRMS** (ES +ve), $C_{27}H_{41}N_8O_3$ $(M+H)^+$: calculated 525.32961, found 525.32890.

Synthesis of tert-butyl N-[4-[4-amino-1-[2-[4-(dimethylamino)-1-piperidyl]ethyl]pyrazolo[3,4-d]pyrimidin-3-yl]-2-methoxy-phenyl]carbamate (52):

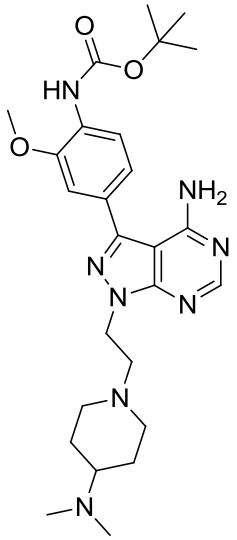

To a solution of 1-[2-[4-(dimethylamino)-1-piperidyl]ethyl]-3-iodo-pyrazolo[3,4-d]pyrimidin-4-amine (50 mg, 0.1205 mmol) in dioxane/water (4.5 ml/0.5 ml) was added [4-(tert-butoxycarbonylamino)-3-methoxy-phenyl]boronic acid (1.5 eq., 48.3 mg, 0.181 mmol), potassium carbonate (1.5 eq., 25.0 mg, 0.181 mmol) and triphenylphosphine (20 mol %, 9.5 mg) followed by palladium acetate (5 mol %) and the mixture heated in the microwave at 120 ^{o}C for an hour. EtOAc (50 ml) and water (50 ml) were added to the mixture and the organic layer separated. The aqueous layer was washed with EtOAc (20 ml, x2) and the organics combined dried over $MgSO_4$ and concentrated *in vacuo*. The crude product was purified by column chromatography, MeOH/DCM (0-10 % then 5-20 drops of NH_3 aq. per 100 ml) to give a light brown solid (23.1 mg, 0.0453 mmol, 37.6 %). **^{1}H NMR** (500 MHz, MeOD) δ 8.27 (s, 1H), 8.08 (d, *J* = 8.2, 1H), 7.30 (d, *J* = 1.8, 1H), 7.26 (dd, *J* = 8.2, 1.9, 1H), 4.56 (t, *J* = 6.7, 2H), 3.98 (s, 3H), 3.14 (d, *J* = 11.9, 2H), 2.94 (t, *J* = 6.7, 2H), 2.39 (m, 7H), 2.14 (dd, *J* = 12.0, 10.0, 2H), 1.90 (d, *J* = 12.5, 2H), 1.57 (s, 9H), 1.49 (qd, *J* = 12.1, 3.6, 2H); **^{13}C NMR** (126 MHz, MeOD) δ 158.53 (C), 155.40 (CH), 154.12 (C), 153.46 (C), 149.24 (C), 145.02 (C), 128.78 (C), 127.38 (C), 120.43 (CH), 119.56 (CH), 110.28 (CH), 97.73 (C), 80.18 (C), 62.29 (CH), 56.22 (CH_2), 55.07 (CH_3), 52.20 (2x CH_2), 44.00 (CH_2), 40.06 (2x CH_3), 27.24 (2x CH_2), 27.21 (3x CH_3); **MS** (ES +ve) $[M+H]^+$: 511.3; **HRMS** (ES +ve), $C_{26}H_{38}N_8O_3$ $[M+H]^+$: calculated 511.31396, found 511.3151.

10. Experimental

10.6 Experimental for Chapter 6

10.6.1 Synthesis of Compounds 53-56

Synthesis of 3-iodo-1-[2-(4-pyrrolidin-1-yl-1-piperidyl)ethyl]pyrazolo[3,4-d]pyrimidin-4-amine (53):

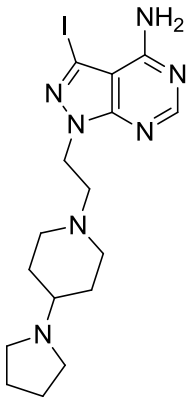

300 mg, 0.8646 mmol of 1-(1,3-dioxolan-2-ylmethyl)-3-iodo-pyrazolo[3,4-d]pyrimidin-4-amine was added to a 10 ml microwave tube. 2.5 ml of water and 2.5 ml of TFA were added and the mixture heated to 100^{o}C for 3 hours. The product was concentrated *in vacuo* and used without further purification. 0.432 mmol of 2-(4-amino-3-iodo-pyrazolo[3,4-d]pyrimidin-1-yl)acetaldehyde was suspended in 3 ml of DCM. 4-(1-pyrrolidinyl)piperidine (1.5 eq., 0.648 mmol, 99.9 mg) was added followed by a drop of acetic acid and the mixture allowed to stir for 10 mins. Sodium triacetoxyborohydride (1.5 eq., 0.648 mmol, 137.3 mg) was added and the mixture allowed to stir for 17 hours. The mixture was concentrated *in vacuo* and purified by column chromatography, MeOH/DCM (0-10 %) to give a green/brown solid, (183.1 mg, 0.415 mmol, 96.1 %). **^{1}H NMR** (500 MHz, MeOD) δ 8.22 (s, 1H), 4.50 (t, J = 6.3, 2H), 3.34 (m, 4H), 3.12 (d, J = 12.0, 2H), 3.06 (dd, J = 13.9, 9.7, 1H), 2.90 (t, J = 6.3, 2H), 2.21 – 2.00 (m, 8H), 1.52 (td, J = 12.1, 8.1, 2H); **MS** (ES +ve) $(M+H)^{+}$: 442.2

Synthesis of 3-iodo-1-[2-[4-(1-piperidyl)-1-piperidyl]ethyl]pyrazolo[3,4-d]pyrimidin-4-amine (54):

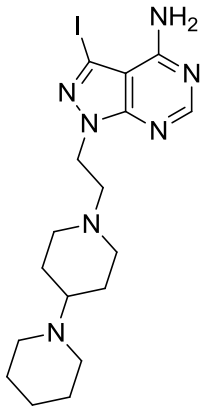

300 mg, 0.8646 mmol of 1-(1,3-dioxolan-2-ylmethyl)-3-iodo-pyrazolo[3,4-d]pyrimidin-4-amine was added to a 10 ml microwave tube. 2.5 ml of water and 2.5 ml of TFA were added and the mixture heated to 100^{o}C for 3 hours. The product was concentrated *in vacuo* and used without further purification. 0.432 mmol of 2-(4-amino-3-iodo-pyrazolo[3,4-d]pyrimidin-1-yl)acetaldehyde was suspended in 3 ml of DCM. 1,4-bipiperidine (1.5 eq., 0.648 mmol, 108.9 mg) was added followed by a drop of acetic acid and the mixture allowed to stir for 10 mins. Sodium triacetoxyborohydride (1.5 eq., 0.648 mmol, 137.3 mg) was added and the mixture allowed to stir for 17 hours. The mixture was concentrated *in vacuo* and purified by column chromatography, MeOH/DCM (0-10 %) to give a dark green/brown thick oil, (191.6 mg, 0.421 mmol, 97.5%). ^{1}**H NMR** (601 MHz, DMSO) δ 8.21 (s, 1H), 4.38 (t, J = 6.6, 2H), 2.85 (broad m, 9H), 1.98 (m, 2H), 1.54 (broad m, 10H); **MS** (ES +ve) $(M+H)^{+}$: 456.2

Synthesis of tert-butyl N-[4-[4-amino-1-[2-(4-pyrrolidin-1-yl-1-piperidyl)ethyl]pyrazolo[3,4-d]pyrimidin-3-yl]-2-methoxy-phenyl]carbamate (55):

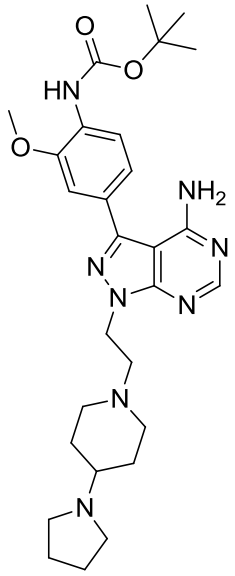

To a solution of 3-iodo-1-[2-(4-pyrrolidin-1-yl-1-piperidyl)ethyl]pyrazolo[3,4-d]pyrimidin-4-amine (50 mg, 0.113 mmol) in dioxane/water (4.5 ml/0.5 ml) was added [4-(tert-butoxycarbonylamino)-3-methoxy-phenyl]boronic acid (1.5 eq., 45.4 mg, 0.170 mmol), potassium carbonate (1.5 eq., 23.5 mg, 0.170 mmol) and triphenylphosphine (20 mol %, 8.9 mg) followed by palladium acetate (5 mol %) and the mixture heated in the microwave at 120 ^{o}C for an hour. EtOAc (50 ml) and water (50 ml) were added to the mixture and the organic layer separated. The aqueous layer was washed with EtOAc (20 ml, x2) and the organics combined and washed with brine then dried over $MgSO_4$ and concentrated *in vacuo*. The crude product was purified by column chromatography, MeOH/DCM (0-10 % then 5-25 drops of NH_3 aq. per 100 ml) to give a light orange solid (16.69 mg, 31.12 µmol, 27.5 %). **^{1}H NMR** (500 MHz, MeOD) δ 8.27 (s, 1H), 8.08 (d, *J* = 8.2, 1H), 7.30 (d, *J* = 1.8, 1H), 7.25 (dd, *J* = 8.2, 1.8, 1H), 4.56 (t, *J* = 6.6, 2H), 3.98 (s, 3H), 3.12 (d, *J* = 12.0, 2H), 2.94 (m, 6H), 2.53 (m, 1H), 2.15 (t, *J* = 11.1, 2H), 2.01 (d, *J* = 12.2, 2H), 1.93 (dd, *J* = 8.3, 5.0, 4H), 1.57 (s, 9H), 1.55 – 1.48 (m, 2H); **^{13}C NMR** (126 MHz, MeOD) δ 158.52 (C), 155.40 (CH), 154.15 (C), 153.45 (C), 149.24 (C), 145.00 (C), 128.80 (C), 127.36 (C), 120.43 (CH), 119.55 (CH), 110.27 (CH), 97.69 (C), 80.19 (C), 62.00 (CH), 56.16 (CH_2), 55.08 (CH_3), 51.62 (2x CH_2), 51.22 (2x CH_2), 44.01 (CH_2), 29.65 (2x CH_2), 27.22 (3x CH_3), 22.49 (2x CH_2); **MS** (ES +ve) $[M+H]^+$: 537.4, (ES -ve) $[M-H]^-$: 535.3; **HRMS** (ES +ve), $C_{28}H_{40}N_8O_3$ $[M+H]^+$: calculated 537.32961, found 537.3281.

Synthesis of tert-butyl N-[4-[4-amino-1-[2-[4-(1-piperidyl)-1-piperidyl]ethyl]pyrazolo[3,4-d]pyrimidin-3-yl]-2-methoxy-phenyl]carbamate (56):

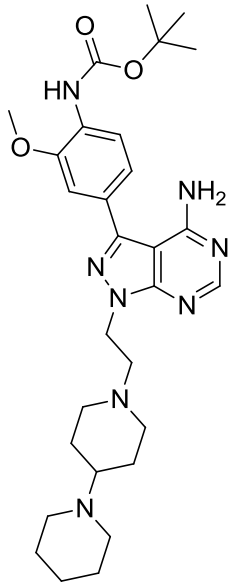

To a solution of 3-iodo-1-[2-[4-(1-piperidyl)-1-piperidyl]ethyl]pyrazolo[3,4-d]pyrimidin-4-amine (50 mg, 0.110 mmol) in dioxane/water (4.5 ml/0.5 ml) was added [4-(tert-butoxycarbonylamino)-3-methoxy-phenyl]boronic acid (1.5 eq., 44.0 mg, 0.165 mmol), potassium carbonate (1.5 eq., 22.8 mg, 0.165 mmol) and triphenylphosphine (20 mol %, 5.8 mg) followed by palladium acetate (5 mol %) and the mixture heated in the microwave at 120 ^{o}C for an hour. EtOAc (50 ml) and water (50 ml) were added to the mixture and the organic layer separated. The aqueous layer was washed with EtOAc (20 ml, x2) and the organics combined, dried over $MgSO_4$ and concentrated *in vacuo*. The crude product was purified by column chromatography, MeOH/DCM (0-10 % then 5-15 drops of NH_3 aq. per 100 ml) to give a light brown solid (12.3 mg, 22.35 µmol, 20.3 %). **^{1}H NMR** (500 MHz, MeOD) δ 8.27 (s, 1H), 8.08 (d, *J* = 8.2, 1H), 7.30 (d, *J* = 1.7, 1H), 7.26 (dd, *J* = 8.2, 1.8, 1H), 4.55 (t, *J* = 6.6, 2H), 3.96 (s, 3H), 3.15 (d, *J* = 11.8, 2H), 2.93 (t, *J* = 6.6, 2H), 2.74 (br. s, 4H), 2.51 (br. s, 1H), 2.13 (t, *J* = 11.1, 2H), 1.91 (d, *J* = 12.0, 2H), 1.72 – 1.62 (m, 4H), 1.55 (m, 13H); **^{13}C NMR** (126 MHz, MeOD) δ 158.52 (C), 155.40 (CH), 154.13 (C), 153.45 (C), 149.24 (C), 145.02 (C), 128.79 (C), 127.37 (C), 120.43 (CH), 119.56 (CH), 110.28 (CH), 97.73 (C), 80.19 (C), 62.69 (CH), 56.21 (CH_2), 55.08 (CH_3), 52.43 (2x CH_2), 49.83 (2x CH_2), 44.00 (CH_2), 27.22 (3x CH_3), 26.78 (2x CH_2), 24.68 (2x CH_2), 23.34 (CH_2); **MS** (ES +ve) $[M+H]^+$: 551.2; **HRMS** (ES +ve), $C_{29}H_{42}N_8O_3$ $[M+H]^+$: calculated 551.34526, found 551.3469.

10.6.2 Synthesis of Compounds 57-68

Synthesis of N-[2-methoxy-4-(4,4,5,5-tetramethyl-1,3,2-dioxaborolan-2-yl)phenyl]-3,3-dimethyl-butanamide (57):

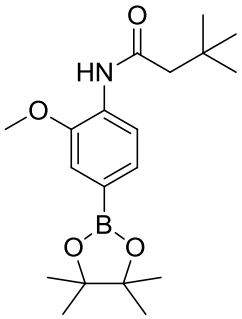

To a solution of 4-Amino-3-methoxybenzeneboronic acid, pinacol ester (150 mg, 0.602 mmol) in DCM (2 ml) was added triethylamine (1.2 eq., 0.722 mmol, 73.1 mg, 100.76 µl) followed by t-butylacetal chloride (1.2 eq., 0.722 mmol, 96.8 mg, 99.9 µl) and the mixture allowed to stir for 20 hours. Water was added to the mixture and the organic layer separated, dried over $MgSO_4$ and concentrated *in vacuo*. The product was purified by column chromatography, MeOH/DCM (0-3%) to give a brown solid (195.7 mg, 0.564 mmol, 93.6 %). **^{1}H NMR** (500 MHz, CDCl3) δ 8.44 (d, *J* = 8.0, 1H), 7.83 (s, 1H), 7.47 (dd, *J* = 8.0, 1.0, 1H), 7.32 – 7.29 (m, 1H), 3.95 (s, 3H), 2.31 – 2.27 (m, 2H), 1.36 (s, 12H), 1.13 (s, 9H); **^{13}C NMR** (126 MHz, CDCl3) δ 170.06 (C), 169.99 (C), 146.89 (C), 130.52 (C), 128.54 (CH), 118.61 (CH), 115.22 (CH), 83.75 (2x C), 55.86 (CH_3), 52.08 (CH_2), 31.22 (C), 29.81 (3x CH_3), 24.86 (4x CH_3); **MS** (ES +ve) $[M+H]^+$: 348.6, 370.6 (+Na).

Synthesis of 1-tert-butyl-3-[2-methoxy-4-(4,4,5,5-tetramethyl-1,3,2-dioxaborolan-2-yl)phenyl]urea (58):

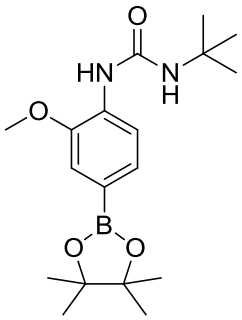

To a solution of 4-Amino-3-methoxybenzeneboronic acid, pinacol ester (150 mg, 0.602 mmol) in DCM (3 ml) was added t-butylisocyanate (20 eq., 12.04 mmol, 1.19 g) and the mixture left to stir at for 72 hours. DCM and water were added to the mixture and the organic layer separated, dried over $MgSO_4$ and concentrated *in vacuo*. The product was purified by column chromatography, MeOH/DCM (0-2%) to give a dark brown solid, (40.9 mg, 0.117 mmol, 19.5 %). **^{1}H NMR** (500 MHz, CDCl3) δ 8.09 (d, *J* = 8.0, 1H), 7.44 (dd, *J* = 8.0, 1.2, 1H), 7.27 (d, *J* = 1.0, 1H), 6.88 (s, 1H), 3.92 (s, 3H), 1.42 (s, 9H), 1.37 (d, *J* = 3.9, 12H); **^{13}C NMR** (126 MHz, CDCl3) δ 153.97 (C), 146.81 (C), 131.78 (C), 128.70 (CH), 117.77 (CH), 115.36 (CH), 83.65 (CH), 55.74 (C), 50.97 (CH_3), 29.36 (C), 29.09 (3x CH_3), 24.87 (4x CH_3); **MS** (ES +ve) $[M+H]^+$: 349.7, 371.6 (+Na)

Synthesis of Phenyl N-[2-methoxy-4-(4,4,5,5-tetramethyl-1,3,2-dioxaborolan-2-yl)phenyl]carbamate (59):

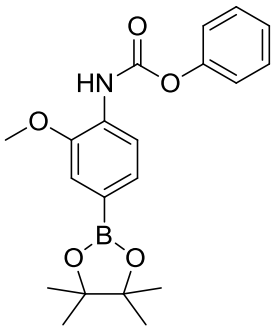

To a solution of 4-Amino-3-methoxybenzeneboronic acid, pinacol ester (150 mg, 0.602 mmol) in DCM (2 ml) was added triethylamine (1.2 eq., 0.722 mmol, 73.1 mg, 100.76 µl) followed by phenyl chloroformate (1.2 eq., 0.722 mmol, 112.6 mg, 90.25 µl) and the mixture allowed to stir for 20 hours. Water was added to the mixture and the organic layer separated, dried over $MgSO_4$ and concentrated *in vacuo*. The product was purified by column chromatography, (100% DCM) to give a clear white solid (190.8 mg, 0.517 mmol, 85.9 %). **^{1}H NMR** (500 MHz, CDCl3) δ 8.16 (d, *J* = 7.6, 1H), 7.74 (s, 1H), 7.49 (dd, *J* = 8.0, 1.1, 1H), 7.46 – 7.40 (m, 2H), 7.33 (d, *J* = 1.0, 1H), 7.29 – 7.20 (m, 3H), 3.99 (s, 3H), 1.38 (s, 12H); **^{13}C NMR** (126 MHz, CDCl3) δ 151.36 (C), 150.61 (C), 146.98 (C), 129.97 (C), 129.41 (2x CH), 128.61 (CH), 125.68 (CH), 125.05 (C), 121.74 (2x CH), 117.30 (CH), 115.41 (CH), 83.80 (2x C), 55.96 (CH_3), 24.92 (4x CH_3); **MS** (ES +ve) $[M+H]^+$: 370.5, 392.5 (+Na).

Synthesis of N-benzyl-2-methoxy-4-(4,4,5,5-tetramethyl-1,3,2-dioxaborolan-2-yl)aniline (60*):

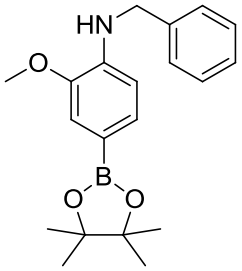

To a solution of 4-Amino-3-methoxybenzeneboronic acid, pinacol ester (150 mg, 0.602 mmol) in DCM (2 ml) was added triethylamine (1.2 eq., 0.722 mmol, 73.1 mg, 100.76 µl) followed by benzyl chloroformate (1.2 eq., 0.722 mmol, 123.2 mg, 103.07 µl) and the mixture allowed to stir for 18 hours. The product was concentrated *in vacuo* and purified by column chromatography (100% DCM), to give a light brown thick oil, (65.9 mg, 0.172 mmol, 28.6 %). Only after characterisation was it discovered that the alkylated product (shown) had been produced instead. **^{1}H NMR** (600 MHz, CDCl3) δ 7.43 – 7.26 (m, 8H), 6.68 (d, *J* = 7.6, 1H), 4.41 (s, 2H), 3.91 (s, 3H), 1.35 (s, 12H); **^{13}C NMR** (126 MHz, MeOD) δ 158.39 (C), 146.09 (C), 141.18 (C), 139.78 (C), 128.82 (CH), 128.08 (CH), 126.76 (CH), 126.52 (CH), 114.34 (CH), 108.93 (CH), 83.13 (CH_2), 54.55 (CH_3), 46.58 (C), 23.73 (4x CH_3); **MS** (ES +ve) $[M+H]^+$: 340.6.

Synthesis of N-[2-methoxy-4-(4,4,5,5-tetramethyl-1,3-dioxolan-2-yl)phenyl]-2-phenyl-acetamide (61):

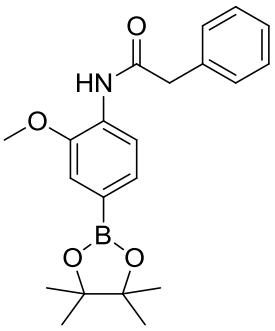

To a solution of 4-Amino-3-methoxybenzeneboronic acid, pinacol ester (150 mg, 0.602 mmol) in DCM (2 ml) was added triethylamine (1.2 eq., 0.722 mmol, 73.1 mg, 100.76 µl) followed by phenylacetyl chloride (1.2 eq., 0.722 mmol, 111.2 mg, 95.1 µl) and the mixture allowed to stir for 18 hours. The mixture was concentrated *in vacuo* and purified by column

chromatography, MeOH/DCM (0-1.5 %) to give a cream solid, (200.9 mg, 0.547 mmol, 90.9 %). **^{1}H NMR** (500 MHz, CDCl3) δ 8.40 (d, J = 8.0, 1H), 7.95 (s, 1H), 7.43 (ddd, J = 11.3, 6.6, 1.6, 3H), 7.39 – 7.33 (m, 3H), 7.22 (d, J = 1.0, 1H), 3.78 (s, 5H), 1.35 (s, 12H); **^{13}C NMR** (126 MHz, CDCl3) δ 168.92 (C), 168.84 (C), 147.04 (C), 134.50 (C), 130.31 (C), 129.61 (2x CH), 129.05 (2x CH), 128.51 (CH), 127.47 (CH), 118.43 (CH), 115.31 (CH), 83.76 (C), 55.88 (CH_3), 45.24 (CH_2), 24.86 (4x CH_3); **MS** (ES +ve) $[M+H]^+$: 368.7, 390.6 (+Na)

Synthesis of N-[2-methoxy-4-(4,4,5,5-tetramethyl-1,3,2-dioxaborolan-2-yl)phenyl]-3-phenyl-propanamide (62):

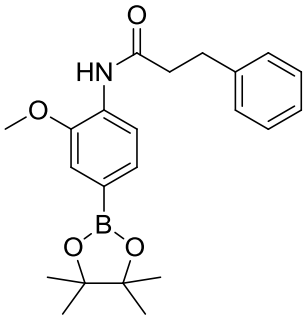

To a solution of 4-Amino-3-methoxybenzeneboronic acid, pinacol ester (150 mg, 0.602 mmol) in DCM (2 ml) was added triethylamine (1.2 eq., 0.722 mmol, 73.1 mg, 100.76 µl) followed by hydrocinnamoyl chloride (1.2 eq., 0.722 mmol, 121.3 mg, 106.9 µl) and the mixture allowed to stir for 23 hours. The mixture was concentrated *in vacuo* and purified by column chromatography, MeOH/DCM (0-2 %) to give a brown solid, (240.0 mg, 0.629 mmol, 100 %). **^{1}H NMR** (500 MHz, CDCl3) δ 8.44 (d, J = 8.0, 1H), 7.83 (s, 1H), 7.47 (d, J = 8.0, 1H), 7.35 – 7.30 (m, 2H), 7.28 – 7.21 (m, 4H), 3.90 (s, 3H), 3.14 – 3.04 (m, 2H), 2.79 – 2.72 (m, 2H), 1.37 (s, 12H); **^{13}C NMR** (126 MHz, CDCl3) δ 170.25 (C), 170.17 (C), 146.82 (C), 140.70 (C), 130.40 (C), 128.56 (CH), 128.52 (CH), 128.40 (CH), 126.34 (CH), 118.68 (CH), 115.21 (CH), 83.78 (2x C), 55.84 (CH_3), 39.72 (CH_2), 31.42 (CH_2), 24.87 (4x CH_3); **MS** (ES +ve) $[M+H]^+$: 382.7, 390.6 (+Na)

Synthesis of N-[4-[4-amino-1-[2-[4-(dimethylamino)-1-piperidyl]ethyl]pyrazolo[3,4-d]pyrimidin-3-yl]-2-methoxy-phenyl]-3,3-dimethyl-butanamide (63):

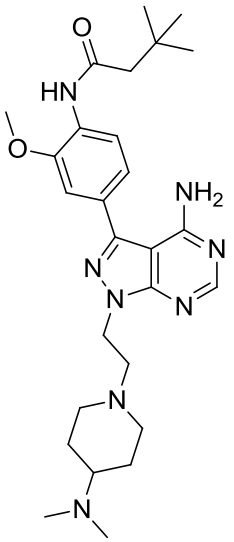

To a solution of 1-[2-[4-(dimethylamino)-1-piperidyl]ethyl]-3-iodo-pyrazolo[3,4-d]pyrimidin-4-amine (50 mg, 0.1205 mmol) in dioxane/water (4.5 ml/0.5 ml) was added N-[2-methoxy-4-(4,4,5,5-tetramethyl-1,3,2-dioxaborolan-2-yl)phenyl]-3,3-dimethyl-butanamide (1.5 eq., 63.1 mg, 0.181 mmol), potassium carbonate (1.5 eq., 25.0 mg, 0.181 mmol) and triphenylphosphine (20 mol %, 9.5 mg) followed by palladium acetate (5 mol %) and the mixture heated in the microwave at 120 ^{o}C for 30 mins. The product was concentrated *in vacuo* and purified by column chromatography, MeOH/DCM (5-10% then 0-30 drops of triethylamine per 100 ml) to give a sand coloured solid, (34.3 mg, 0.0675 mmol, 56.0 %). **^{1}H NMR** (500 MHz, MeOD) δ 8.28 (s, 1H), 8.10 (d, *J* = 8.1, 1H), 7.35 (d, *J* = 1.8, 1H), 7.28 (dd, *J* = 8.1, 1.8, 1H), 4.57 (t, *J* = 6.7, 2H), 3.99 (s, 3H), 3.15 (m, 2H), 2.95 (t, *J* = 6.7, 2H), 2.39 (m, 9H), 2.15 (t, *J* = 11.0, 2H), 1.91 (d, *J* = 16.8, 2H), 1.49 (m, 2H), 1.14 (s, 9H); **^{13}C NMR** (126 MHz, MeOD) δ 172.20 (C), 158.53 (C), 155.44 (CH), 154.22 (C), 151.00 (C), 144.89 (C), 129.52 (C), 127.69 (C), 123.12 (CH), 120.22 (CH), 110.74 (CH), 97.79 (C), 62.24 (CH), 56.24 (CH_2), 55.08 (CH_3), 52.23 (2x CH_2), 49.79 (CH_2), 44.04 (CH_2), 40.11 (2x CH_3), 30.67 (C), 28.81 (3x CH_3), 27.31 (2x CH_2); **MS** (ES +ve) $[M+H]^+$: 509.6; **HRMS** (ES +ve), $C_{27}H_{41}N_8O_2$ $[M+H]^+$: calculated 509.33470, found 509.3363.

Synthesis of 1-[4-[4-amino-1-[2-[4-(dimethylamino)-1-piperidyl]ethyl]pyrazolo[3,4-d]pyrimidin-3-yl]-2-methoxy-phenyl]-3-tert-butyl-urea (64):

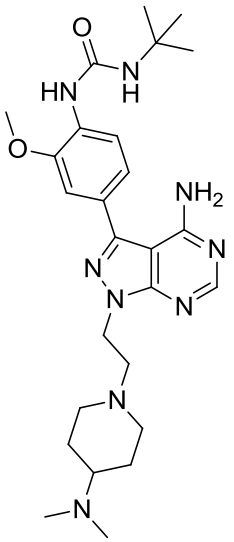

To a solution of 1-[2-[4-(dimethylamino)-1-piperidyl]ethyl]-3-iodo-pyrazolo[3,4-d]pyrimidin-4-amine (50 mg, 0.1205 mmol) in dioxane/water (4.5/0.5 ml) was added 1-tert-butyl-3-[2-methoxy-4-(4,4,5,5-tetramethyl-1,3,2-dioxaborolan-2-yl)phenyl]urea (1.5 eq., 62.9 mg, 0.181 mmol), potassium carbonate (1.5 eq., 25.0 mg, 0.181 mmol) and triphenylphosphine (20 mol %, 9.5 mg) followed by palladium acetate (5 mol %) and the mixture heated in the microwave at 120 ^{o}C for 30 mins. The mixture was concentrated *in vacuo* and purified by column chromatography, MeOH/DCM (10% then 0-30 drops of NEt_3 per 100 ml) to give a light brown solid, (30.4 mg, 0.0597 mmol, 49.5 %). **^{1}H NMR** (500 MHz, MeOD) δ 8.24 (s, 1H), 8.16 (d, *J* = 8.3, 1H), 7.25 (d, *J* = 1.8, 1H), 7.19 (dd, *J* = 8.3, 1.9, 1H), 4.53 (t, *J* = 6.7, 2H), 3.96 (s, 3H), 3.12 (d, *J* = 11.9, 2H), 2.92 (t, *J* = 6.7, 2H), 2.36 (m, 7H), 2.12 (t, *J* = 11.1, 2H), 1.87 (d, *J* = 12.5, 2H), 1.51 – 1.42 (m, 2H), 1.38 (s, 9H); **^{13}C NMR** (126 MHz, MeOD) δ 155.74 (C), 155.40 (CH), 154.09 (C), 148.52 (C), 145.33 (C), 130.34 (C), 125.66 (C), 120.49 (CH), 118.66 (CH), 110.02 (CH), 97.73 (C), 62.27 (CH), 56.23 (CH_2), 55.02 (CH_3), 52.22 (2x CH_2), 49.71 (C), 43.97 (CH_2), 40.07 (2x CH_3), 28.15 (3x CH_3), 27.20 (2x CH_2); **MS** (ES +ve) $[M+H]^+$: 510.8; **HRMS** (ES +ve), $C_{26}H_{40}N_9O_2$ $(M+H)^+$: calculated 510.32995, found 510.32830.

Synthesis of 3-(4-amino-3-methoxy-phenyl)-1-[2-[4-(dimethylamino)-1-piperidyl]ethyl]pyrazolo[3,4-d]pyrimidin-4-amine (65*):

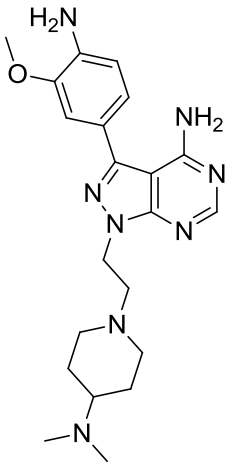

To a solution of 1-[2-[4-(dimethylamino)-1-piperidyl]ethyl]-3-iodo-pyrazolo[3,4-d]pyrimidin-4-amine (50 mg, 0.1205 mmol) in dioxane/water (4.5 ml/0.5 ml) was added phenyl N-[2-methoxy-4-(4,4,5,5-tetramethyl-1,3,2-dioxaborolan-2-yl)phenyl]carbamate (1.5 eq., 66.8 mg, 0.181 mmol), potassium carbonate (1.5 eq., 25.0 mg, 0.181 mmol) and triphenylphosphine (20 mol %, 9.5 mg) followed by palladium acetate (5 mol %) and the mixture heated in the microwave at 120 ^{o}C for 30 mins. The mixture was concentrated in vacuo and the product purified by column chromatography, MeOH/DCM (10% then 0-30 drops of NEt_3 per 100 ml) to give a brown solid, (19.4 mg, 0.0473 mmol, 39.2 %). **^{1}H NMR** (600 MHz, MeOD) δ 8.25 (s, 1H), 7.16 (d, J = 1.8, 1H), 7.09 (dd, J = 7.9, 1.8, 1H), 6.91 (d, J = 7.9, 1H), 4.54 (t, J = 6.7, 2H), 3.95 (s, 3H), 3.14 (d, J = 12.0, 2H), 2.93 (t, J = 6.7, 2H), 2.40 (m, 7H), 2.14 (t, J = 11.0, 2H), 1.90 (d, J = 12.3, 2H), 1.49 (d, J = 12.1, 2H); **^{13}C NMR** (126 MHz, MeOD) δ 158.62 (C), 155.35 (CH), 153.98 (C), 147.74 (C), 146.01 (C), 138.32 (C), 121.70 (CH), 121.07 (C), 114.69 (CH), 110.25 (CH), 109.97 (C), 62.19 (CH_2), 56.24 (CH_3), 54.74 (2x CH_2), 52.29 (CH), 43.91 (CH_2), 40.14 (2x CH_3), 27.35 (2x CH_2); **MS** (ES +ve) $(M+H)^+$: 411.6; **HRMS** (ES +ve), $C_{21}H_{31}N_8O_1$ $(M+H)^+$: calculated 411.26208, found 411.26270.

Synthesis of 3-[4-(benzylamino)-3-methoxy-phenyl]-1-[2-[4-(dimethylamino)-1-piperidyl]ethyl]pyrazolo[3,4-d]pyrimidin-4-amine (66*):

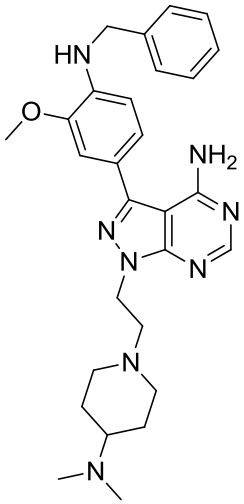

To a solution of 1-[2-[4-(dimethylamino)-1-piperidyl]ethyl]-3-iodo-pyrazolo[3,4-d]pyrimidin-4-amine (50 mg, 0.1205 mmol) in dioxane/water (4.5 ml/0.5 ml) was added N-benzyl-2-methoxy-4-(4,4,5,5-tetramethyl-1,3,2-dioxaborolan-2-yl)aniline (1.5 eq., 61.4 mg, 0.181 mmol), potassium carbonate (1.5 eq., 25.0 mg, 0.181 mmol) and triphenylphosphine (20 mol %, 9.5 mg) followed by palladium acetate (5 mol %) and the mixture heated in the microwave at 120 ^{o}C for 30 mins. The mixture was concentrated in vacuo without and purified by column chromatography, MeOH/DCM (10% then 5-20 drops of NEt_3 per 100 ml) to give a light brown coloured solid, (31.8 mg, 0.0584, 48.5 %). **^{1}H NMR** (400 MHz, MeOD) δ 8.24 (s, 1H), 7.40 (d, *J* = 7.5, 2H), 7.33 (t, *J* = 7.5, 2H), 7.24 (t, *J* = 7.3, 1H), 7.15 (d, *J* = 1.8, 1H), 7.08 (dd, *J* = 8.1, 1.8, 1H), 6.67 (d, *J* = 8.1, 1H), 4.52 (t, *J* = 6.7, 2H), 4.47 (s, 2H), 3.98 (s, 3H), 3.13 (d, *J* = 11.9, 2H), 2.92 (t, *J* = 6.7, 2H), 2.37 (s, 7H), 2.13 (t, *J* = 11.0, 2H), 1.88 (d, *J* = 12.3, 2H), 1.47 (d, *J* = 8.5, 2H); **^{13}C NMR** (126 MHz, MeOD) δ 166.23 (C), 158.62 (C), 155.34 (CH), 153.97 (C), 147.34 (C), 139.75 (C), 139.27 (C), 128.13 (2x CH), 126.78 (2x CH), 126.58 (CH), 121.15 (CH), 119.94 (C), 109.78 (CH), 109.27 (CH), 97.66 (C), 62.17 (CH), 56.20 (CH_2), 54.81 (CH_3), 52.22 (2x CH_2), 46.71 (CH_2), 43.89 (CH_2), 40.08 (2x CH_3), 27.28 (2x CH_2); **MS** (ES +ve) $[M+H]^+$: 501.4; **HRMS** (ES +ve), $C_{28}H_{37}N_8O_1$ $[M+H]^+$: calculated 501.30848, found 501.3087.

Synthesis of N-[4-[4-amino-1-[2-[4-(dimethylamino)-1-piperidyl]ethyl]pyrazolo[3,4-d]pyrimidin-3-yl]-2-methoxy-phenyl]-2-phenyl-acetamide (67):

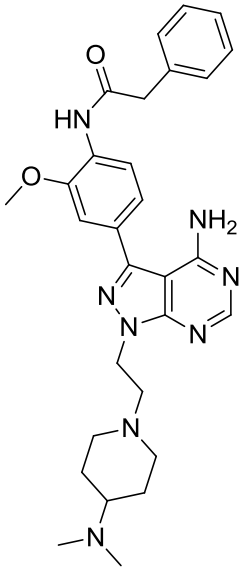

To a solution of 1-[2-[4-(dimethylamino)-1-piperidyl]ethyl]-3-iodo-pyrazolo[3,4-d]pyrimidin-4-amine (50 mg, 0.1205 mmol) in dioxane/water (4.5 ml/0.5 ml) was added N-[2-methoxy-4-(4,4,5,5-tetramethyl-1,3-dioxolan-2-yl)phenyl]-2-phenyl-acetamide (1.5 eq., 66.5 mg, 0.181 mmol), potassium carbonate (1.5 eq., 25.0 mg, 0.181 mmol) and triphenylphosphine (20 mol %, 9.5 mg) followed by palladium acetate (5 mol %) and the mixture heated in the microwave at 120 ^{o}C for 30 mins. The product was concentrated *in vacuo* and purified by column chromatography, MeOH/DCM (10% then 0-30 drops of triethylamine per 100 ml) to give a light brown solid, (37.9 mg, 0.0717 mmol, 59.5 %). **^{1}H NMR** (600 MHz, MeOD) δ 8.27 (s, 1H), 8.20 (d, *J* = 8.2, 1H), 7.40 (dt, *J* = 15.2, 7.5, 4H), 7.32 (dd, *J* = 11.0, 4.4, 2H), 7.26 (dd, *J* = 8.2, 1.8, 1H), 4.56 (t, *J* = 6.7, 2H), 3.95 (s, 3H), 3.83 (s, 2H), 3.13 (d, *J* = 11.8, 2H), 2.93 (t, *J* = 6.7, 2H), 2.34 (d, *J* = 13.6, 7H), 2.13 (t, *J* = 11.0, 2H), 1.88 (d, *J* = 12.7, 2H), 1.47 (dt, *J* = 12.2, 8.6, 2H); **^{13}C NMR** (126 MHz, MeOD) δ 171.20 (C), 158.51 (C), 155.42 (CH), 154.17 (C), 150.35 (C), 144.81 (C), 135.19 (C), 129.30 (C), 128.98 (2x CH), 128.38 (2x CH), 127.83 (C), 126.78 (CH), 122.00 (CH), 120.30 (CH), 110.62 (CH), 97.77 (C), 62.25 (CH), 56.21 (CH_2), 55.12 (CH_3), 52.24 (2x CH_2), 44.05 (CH_2), 43.30 (CH_2), 40.09 (2x CH_3), 27.29 (2x CH_2); **MS** (ES +ve) $[M+H]^+$: 529.6; **HRMS** (ES +ve), $C_{29}H_{37}N_8O_2$ $[M+H]^+$: calculated 529.30340, found 529.3051.

Synthesis of N-[4-[4-amino-1-[2-[4-(dimethylamino)-1-piperidyl]ethyl]pyrazolo[3,4-d]pyrimidin-3-yl]-2-methoxy-phenyl]-3-phenyl-propanamide (68):

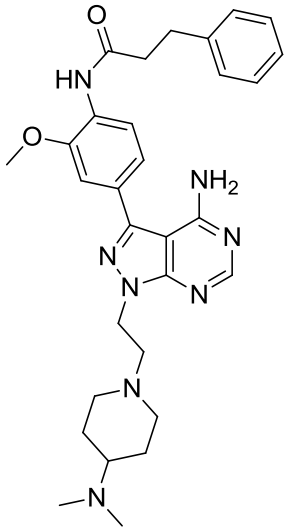

To a solution of 1-[2-[4-(dimethylamino)-1-piperidyl]ethyl]-3-iodo-pyrazolo[3,4-d]pyrimidin-4-amine (50 mg, 0.1205 mmol) in dioxane/water (4.5 ml/0.5 ml) was added N-[2-methoxy-4-(4,4,5,5-tetramethyl-1,3,2-dioxaborolan-2-yl)phenyl]-3-phenyl-propanamide (1.5 eq., 69.0 mg, 0.181 mmol), potassium carbonate (1.5 eq., 25.0 mg, 0.181 mmol) and triphenylphosphine (20 mol %, 9.5 mg) followed by palladium acetate (5 mol %) and the mixture heated in the microwave at 120 ^{o}C for 30 mins. The product was concentrated *in vacuo* and purified by column chromatography, MeOH/DCM (10% then 0-30 drops of triethylamine per 100 ml) to give a light brown solid, (36.0 mg, 0.0664 mmol, 55.1 %). **^{1}H NMR** (600 MHz, MeOD) δ 8.27 (s, 1H), 8.13 (d, *J* = 8.1, 1H), 7.27 (d, *J* = 1.7, 5H), 7.26 (dd, *J* = 8.2, 1.8, 1H), 7.21 (dd, *J* = 8.6, 4.4, 1H), 4.57 (t, *J* = 6.7, 2H), 3.95 (s, 3H), 3.15 (d, *J* = 11.8, 2H), 3.05 (m, 3H), 2.95 (t, *J* = 6.7, 2H), 2.81 (t, *J* = 7.7, 2H), 2.41 (s, 6H), 2.14 (t, *J* = 11.0, 2H), 1.91 (d, *J* = 17.2, 3H), 1.49 (d, *J* = 8.7, 2H); **^{13}C NMR** (126 MHz, MeOD) δ 172.65 (C), 158.53 (CH), 155.44 (C), 154.18 (C), 150.64 (C), 144.88 (C), 140.73 (C), 129.32 (C), 128.15 (CH), 127.76 (C), 125.85 (CH), 122.70 (CH), 120.20 (CH), 110.65 (CH), 97.77 (CH), 62.38 (C), 56.18 (CH_2), 55.06 (CH_3), 52.14 (2x CH_2), 46.33 (CH_2), 44.04 (CH_2), 39.99 (2x CH_3), 38.18 (CH_2), 31.38 (CH_2), 27.17 (2x CH_2); **MS** (ES +ve) $[M+H]^+$: 543.6; **HRMS** (ES +ve), $C_{30}H_{39}N_8O_2$ $[M+H]^+$: calculated 543.31905, found 543.3204.

10.6.3 Synthesis of Compounds 69-72

Synthesis of 2-methoxy-N-(2-pyridylmethyl)-4-(4,4,5,5-tetramethyl-1,3,2-dioxaborolan-2-yl)aniline (69):

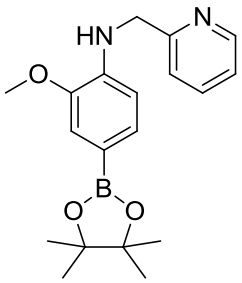

To a solution of 4-Amino-3-methoxybenzeneboronic acid, pinacol ester (150 mg, 0.602 mmol) in DCM (5 ml) was added triethylamine (3 eq., 1.806 mmol, 182.7 mg, 251.9 µl) followed by 2-(bromomethyl)pyridine hydrobromide (2.4 eq., 1.44 mmol, 362.2 mg) and the mixture allowed to stir for 72 hours. Water and DCM were added and the organic layer separated, dried over $MgSO_4$ and concentrated *in vacuo*. The product was purified by column chromatography, EtOAc/Hexane (20 %), to give a dark brown solid, (86.2 mg, 0.253 mmol, 42.1 %). **^{1}H NMR** (500 MHz, CDCl3) δ 8.59 (d, *J* = 4.2, 1H), 7.68 (d, *J* = 7.6, 1H), 7.37 (d, *J* = 7.9, 1H), 7.31 (dd, *J* = 7.8, 1.2, 1H), 7.23 (d, *J* = 6.8, 1H), 7.18 (d, *J* = 1.1, 1H), 6.79 (d, *J* = 8.0, 1H), 6.50 (d, *J* = 7.8, 1H), 4.60 (s, 2H), 3.92 (s, 3H), 1.31 (s, 12H); **^{13}C NMR** (126 MHz, CDCl3) δ 158.33 (C), 148.11 (CH), 147.04 (C), 146.18 (C), 140.29 (C), 137.81 (CH), 129.23 (CH), 122.39 (CH), 121.24 (CH), 114.68 (CH), 109.22 (CH), 83.30 (C), 55.56 (CH_3), 48.14 (CH_2), 24.73 (4x CH_3); **MS** (ES +ve) $(M+H)^+$: 341.2

Synthesis of 2-methoxy-N-(3-pyridylmethyl)-4-(4,4,5,5-tetramethyl-1,3,2-dioxaborolan-2-yl)aniline (70):

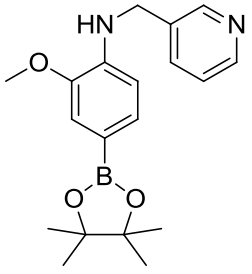

To a solution of 4-Amino-3-methoxybenzeneboronic acid, pinacol ester (150 mg, 0.602 mmol) in THF (5 ml) was added triethylamine (6 eq., 3.612 mmol, 365.4.7 mg, 503.8 µl)

followed by 3-(bromomethyl)pyridine hydrobromide (2.4 eq., 1.444 mmol, 362.2 mg) and the mixture heated to 180°C in the microwave for 4 hours. Water and DCM were added and the organic layer separated, dried over $MgSO_4$ and concentrated *in vacuo*. The product was purified by column chromatography, EtOAc/Hexane (20-50 %) to give a dark brown solid, (80.9 mg, 0.238 mmol, 39.5 %). **^{1}H NMR** (500 MHz, CDCl3) δ 8.63 (d, *J* = 1.6, 1H), 8.53 (dd, *J* = 4.9, 1.5, 1H), 7.75 (d, *J* = 8.2, 1H), 7.36 – 7.29 (m, 2H), 7.19 (d, *J* = 1.1, 1H), 6.51 (d, *J* = 7.8, 1H), 4.93 (s, 1H), 4.43 (d, *J* = 11.7, 2H), 3.90 (s, 3H), 1.33 (s, 12H); **^{13}C NMR** (126 MHz, CDCl3) δ 148.03 (CH), 147.60 (CH), 146.06 (C), 140.12 (C), 136.07 (CH), 135.46 (C), 129.22 (CH), 123.90 (CH), 114.76 (CH), 109.13 (CH), 83.36 (C), 55.59 (CH_3), 44.96 (CH_2), 29.71 (), 24.84 (4x CH_3); **MS** (ES +ve) $(M+H)^+$: 341.6, 363.6 (+Na).

Synthesis of 1-[2-[4-(dimethylamino)-1-piperidyl]ethyl]-3-[3-methoxy-4-(2-pyridylmethylamino)phenyl]pyrazolo[3,4-d]pyrimidin-4-amine (71):

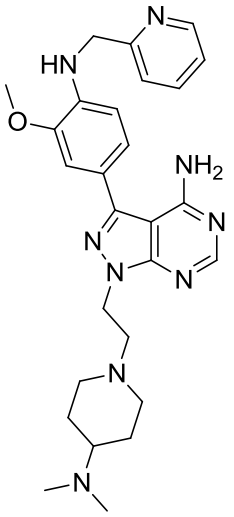

To a solution of 1-[2-[4-(dimethylamino)-1-piperidyl]ethyl]-3-iodo-pyrazolo[3,4-d]pyrimidin-4-amine (50 mg, 0.1205 mmol) in dioxane/water (4.5/0.5 ml) was 2-methoxy-N-(2-pyridylmethyl)-4-(4,4,5,5-tetramethyl-1,3,2-dioxaborolan-2-yl)aniline (1 eq., 41 mg, 0.1205 mmol), potassium carbonate (1.5 eq., 25.0 mg, 0.181 mmol) and triphenylphosphine (20 mol %, 9.5 mg) followed by palladium acetate (5 mol %) and the mixture heated in the microwave at 120 °C for 30 mins. The mixture was concentrated *in vacuo* and purified by column chromatography, MeOH/DCM (10 % then 10-30 drops of NEt_3 per 100 ml) to give a sand coloured solid, (37 mg, 0.0738 mmol, 61.3 %). **^{1}H NMR** (500 MHz, MeOD) δ 8.50 (d, *J* = 4.2, 1H), 8.21 (s, 1H), 7.77 (dd, *J* = 7.7, 6.0, 1H), 7.46 (d, *J* = 7.9, 1H), 7.29 (d, *J* = 5.3, 1H), 7.14 (d, *J* = 1.8, 1H), 7.05 (dd, *J* = 8.1, 1.9, 1H), 6.58 (d, *J* = 8.1, 1H), 4.55 (s, 2H), 4.49

(t, *J* = 6.6, 2H), 3.96 (s, 3H), 3.12 (d, *J* = 12.5, 2H), 2.90 (t, *J* = 6.6, 2H), 2.64 – 2.58 (m, 1H), 2.50 (s, 6H), 2.12 (t, *J* = 11.0, 2H), 1.90 (s, 2H), 1.49 (d, *J* = 8.4, 2H); **^{13}C NMR** (126 MHz, MeOD) δ 159.35 (C), 158.62 (C), 155.36 (CH), 154.03 (C), 148.39 (CH), 147.49 (C), 146.03 (C), 138.91 (C), 137.40 (CH), 122.27 (CH), 121.57 (CH), 121.15 (CH), 120.38 (C), 109.62 (CH), 109.42 (CH), 97.64 (C), 62.72 (CH), 56.04 (CH_2), 54.85 (CH_3), 51.85 (2x CH_2), 47.48 (CH_2), 43.92 (CH_2), 39.73 (2x CH_3), 26.86 (2x CH_2); **MS** (ES +ve) $[M+H]^+$: 502.2; **HRMS** (ES +ve), $C_{27}H_{36}N_9O_1$ $[M+H]^+$: calculated 502.30373, found 502.30320.

Synthesis of 1-[2-[4-(dimethylamino)-1-piperidyl]ethyl]-3-[3-methoxy-4-(3-pyridylmethylamino)phenyl]pyrazolo[3,4-d]pyrimidin-4-amine (72):

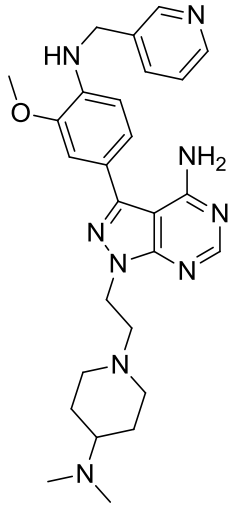

To a solution of 1-[2-[4-(dimethylamino)-1-piperidyl]ethyl]-3-iodo-pyrazolo[3,4-d]pyrimidin-4-amine (50 mg, 0.1205 mmol) in dioxane/water (4.5/0.5 ml) was 2-methoxy-N-(3-pyridylmethyl)-4-(4,4,5,5-tetramethyl-1,3,2-dioxaborolan-2-yl)aniline (1.5 eq., 61.6 mg, 0.181 mmol), potassium carbonate (1.5 eq., 25.0 mg, 0.181 mmol) and triphenylphosphine (20 mol %, 9.5 mg) followed by palladium acetate (5 mol %) and the mixture heated in the microwave at 120 ^{o}C for 30 mins. The mixture was concentrated *in vacuo* and purified by column chromatography, MeOH/DCM (10 % then 0-25 drops of NEt_3 per 100 ml), to give a light brown solid, (41.6 mg, 0.083 mmol, 68.9 %). **^{1}H NMR** (500 MHz, MeOD) δ 8.57 (s, 1H), 8.42 (d, *J* = 3.4, 1H), 8.23 (s, 1H), 7.87 (d, *J* = 7.9, 1H), 7.41 (dd, *J* = 7.9, 4.9, 1H), 7.16 (d, *J* = 1.8, 1H), 7.08 (dd, *J* = 8.1, 1.9, 1H), 6.65 (d, *J* = 8.1, 1H), 4.55 (s, 2H), 4.51 (t, *J* = 6.6, 2H), 3.97 (s, 3H), 3.13 (d, *J* = 7.3, 2H), 2.92 (t, *J* = 6.6, 2H), 2.59 (s, 1H), 2.50 (s, 6H), 2.14 (t, *J* = 11.0, 2H), 1.91 (d, *J* = 9.2, 2H), 1.50 (d, *J* = 8.5, 2H); **^{13}C NMR** (126 MHz, MeOD) δ 158.61 (C), 155.36 (CH), 154.02 (C), 147.77 (CH), 147.48

(C), 147.18 (CH), 146.00 (C), 138.73 (C), 136.44 (C), 135.79 (CH), 123.80 (CH), 121.13 (CH), 120.43 (C), 109.71 (CH), 109.45 (CH), 97.64 (C), 62.71 (CH), 55.96 (CH_2), 54.84 (CH_3), 51.85 (2x CH_2), 43.95 (CH_2), 43.92 (CH_2), 39.71 (2x CH_3), 26.84 (2x CH_2); **MS** (ES +ve) $[M+H]^+$: 502.4; **HRMS** (ES +ve), $C_{27}H_{36}N_9O_1$ $[M+H]^+$: calculated 502.30373, found 502.30140.

10.6.4 Synthesis of Compounds 73-95

Synthesis of tert-butyl N-(4-bromo-2-hydroxy-phenyl)carbamate (73):

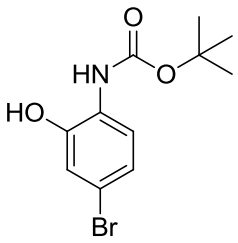

2-amino-5-bromophenol (250 mg, 1.34 mmol) was suspended in DCM (5 ml). Di-tertbutyldicarbonate (1 eq., 1.34 mmol, 292.2 mg) was added followed by a small spatula of DMAP and the reaction allowed to stir for 18 hours. Water was added and the organic layer separated, dried over $MgSO_4$ and concentrated *in vacuo*. The product was purified by column chromatography, EtOAc/Hexane (0-20 %) to give a cream solid, (177.3 mg, 0.618 mmol, 46.1 %). **^{1}H NMR** (500 MHz, MeOD) δ 7.63 (d, J = 8.4, 1H), 6.97 (d, J = 2.2, 1H), 6.93 (dd, J = 8.6, 2.2, 1H), 1.54 (s, 9H); **^{13}C NMR** (126 MHz, MeOD) δ 153.72 (C), 147.85 (C), 126.01 (C), 121.88 (CH), 120.93 (CH), 117.43 (CH), 84.51 (C), 80.08 (C), 27.19 (3x CH_3); **MS** (ES +ve) $(M+H)^+$: 286.0/288.0

Synthesis of tert-butyl N-[2-hydroxy-4-(4,4,5,5-tetramethyl-1,3,2-dioxaborolan-2-yl)phenyl]carbamate (74):

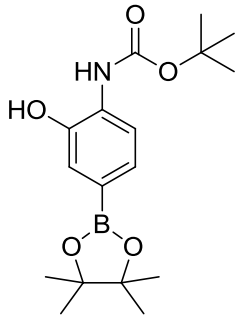

To a solution of tert-butyl N-(4-bromo-2-hydroxy-phenyl)carbamate (50 mg, 0.174 mmol) in dioxane/water (4.5/0.5 ml) was added bis(pinacolato)diboron (1.5 eq., 66.4 mg, 0.261 mmol), potassium carbonate (1.5 eq., 36.1 mg, 0.261 mmol) and triphenylphosphine (20 mol %, 13.7 mg) followed by palladium acetate (5 mol %) and the mixture heated in the microwave at 120 ^{o}C for 30 mins. EtOAc and water were added to the mixture and the organic layer separated, dried over $MgSO_4$ and concentrated *in vacuo*. The product was purified by column chromatography, EtOAc/Hexane (0-20%) to give a white solid (26.4 mg, 0.0788 mmol, 22.6 %). The reaction was repeated to give a second batch of product. **^{1}H NMR** (500 MHz, CDCl3) δ 7.35 (s, 1H), 7.33 – 7.28 (m, 2H), 6.78 (s, 1H), 1.52 (s, 9H), 1.34 (d, J = 10.2, 12H); **^{13}C NMR** (126 MHz, CDCl3) δ 154.27 (C), 145.75 (C), 128.66 (C), 127.70 (CH), 124.11 (CH), 119.94 (CH), 119.84 (C), 83.76 (C), 81.86 (C), 28.27 (3x CH_3), 24.86 (4x CH_3).

Synthesis of tert-butyl N-[4-[4-amino-1-[2-[4-(dimethylamino)-1-piperidyl]ethyl]pyrazolo[3,4-d]pyrimidin-3-yl]-2-hydroxy-phenyl]carbamate (75):

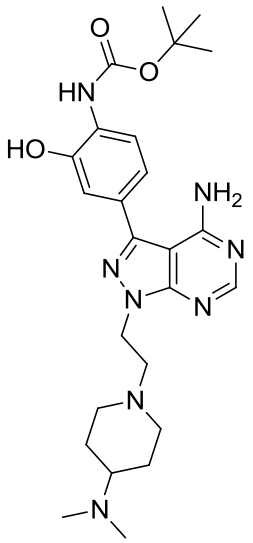

To a solution of 1-[2-[4-(dimethylamino)-1-piperidyl]ethyl]-3-iodo-pyrazolo[3,4-d]pyrimidin-4-amine (42.7 mg, 0.103 mmol) in dioxane/water (4.5/0.5 ml) was added tert-butyl N-[2-hydroxy-4-(4,4,5,5-tetramethyl-1,3,2-dioxaborolan-2-yl)phenyl]carbamate (1 eq., 34.4 mg, 0.103 mmol, limiting reagent), potassium carbonate (1.5 eq., 21.3 mg, 0.154 mmol) and triphenylphosphine (20 mol %, 8.1 mg) followed by palladium acetate (5 mol %) and the mixture heated in the microwave at 120 ^{o}C for 30 mins. MS showed the reaction was complete. The product was purified by column chromatography, MeOH/DCM (10 % then 10-40 drops of NEt_3 per 100 ml) to give a light brown/grey solid, (27.1 mg, 0.0546 mmol, 53.0 %). **^{1}H NMR** (500 MHz, MeOD) δ 8.26 (s, 1H), 7.95 (d, J = 8.1, 1H), 7.17 (d, J = 1.9, 1H), 7.14 (dd, J = 8.2, 1.9, 1H), 4.60 – 4.52 (m, 2H), 3.14 (m, 2H), 3.01 – 2.90 (m, 2H), 2.36 (m, 7H), 2.14 (t, J = 12.0, 2H), 1.88 (m, 2H), 1.57 (s, 9H), 1.47 (m, 2H); **^{13}C NMR** (126 MHz, MeOD) δ 158.53 (C), 155.40 (CH), 147.42 (C), 145.04 (C), 144.84 (C), 144.67 (C), 141.18 (C), 127.83 (C), 126.66 (C), 120.09 (CH), 119.29 (CH), 114.47 (CH), 110.24 (C), 97.09 (C), 62.20 (CH), 56.22 (CH_2), 52.27 (2x CH_2), 44.00 (CH_2), 40.14 (2x CH_3), 27.37 (2x CH_2), 27.22 (3x CH_3); **MS** (ES +ve) $(M+H)^+$: 497.4; **HRMS** (ES +ve), $C_{25}H_{37}N_8O_3$ $(M+H)^+$: calculated 497.29831, found 497.29770.

Synthesis of tert-butyl N-[4-[4-amino-1-[2-[4-(dimethylamino)-1-piperidyl]ethyl]pyrazolo[3,4-d]pyrimidin-3-yl]phenyl]carbamate (76):

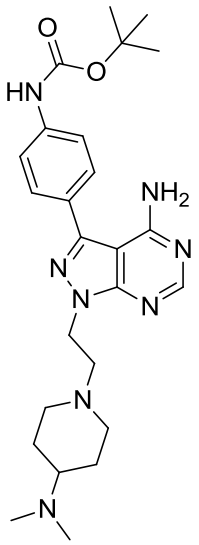

To a solution of 1-[2-[4-(dimethylamino)-1-piperidyl]ethyl]-3-iodo-pyrazolo[3,4-d]pyrimidin-4-amine (50 mg, 0.1205 mmol) in dioxane/water (4.5/0.5 ml) was added 3-(boc-amino)benzeneboronic acid (1.5 eq., 42.9 mg, 0.181 mmol), potassium carbonate (1.5 eq., 25.0 mg, 0.181 mmol) and triphenylphosphine (20 mol %, 9.5 mg) followed by palladium acetate (5 mol %) and the mixture heated in the microwave at 120 ^{o}C for 30 mins. The mixture was concentrated *in vacuo* and purified by column chromatography, MeOH/DCM (10% then 0-30 drops NEt_3 per 100 ml) to give a light brown coloured solid, (26.0 mg, 0.0541 mmol, 44.9 %). **^{1}H NMR** (500 MHz, MeOD) δ 8.24 (s, 1H), 7.65 – 7.57 (m, 4H), 4.53 (t, *J* = 6.6, 2H), 3.12 (d, *J* = 12.0, 2H), 2.92 (t, *J* = 6.6, 2H), 2.41 (m, 7H), 2.12 (t, *J* = 11.0, 2H), 1.88 (d, *J* = 14.4, 2H), 1.54 (s, 9H), 1.47 (m, 2H); **^{13}C NMR** (126 MHz, MeOD) δ 158.54 (C), 155.40 (CH), 154.15 (C), 153.74 (C), 144.96 (C), 140.47 (C), 128.68 (2x CH), 126.62 (C), 118.79 (2x CH), 97.74 (C), 79.76 (C), 62.43 (CH), 56.15 (CH_2), 52.09 (2x CH_2), 43.99 (CH_2), 39.95 (2x CH_3), 27.27 (3x CH_3), 27.13 (2x CH_2); **MS** (ES +ve) $[M+H]^+$: 481.6; **HRMS** (ES +ve), $C_{25}H_{37}N_8O_2$ $[M+H]^+$: calculated 481.30340, found 481.3046.

Synthesis of tert-butyl N-[3-[4-amino-1-[2-[4-(dimethylamino)-1-piperidyl]ethyl]pyrazolo[3,4-d]pyrimidin-3-yl]phenyl]carbamate (77):

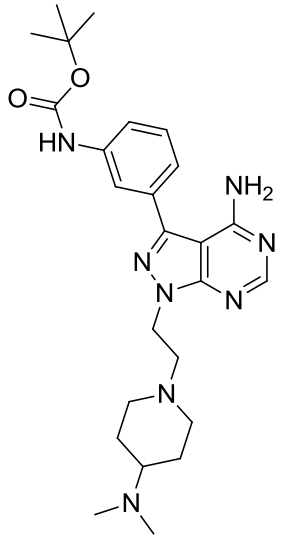

To a solution of 1-[2-[4-(dimethylamino)-1-piperidyl]ethyl]-3-iodo-pyrazolo[3,4-d]pyrimidin-4-amine (50 mg, 0.1205 mmol) in dioxane/water (4.5/0.5 ml) was added 3-(boc-amino)benzeneboronic acid (1.5 eq., 42.9 mg, 0.181 mmol), potassium carbonate (1.5 eq., 25.0 mg, 0.181 mmol) and triphenylphosphine (20 mol %, 9.5 mg) followed by palladium acetate (5 mol %) and the mixture heated in the microwave at 120 ^{o}C for 30 mins. The mixture was concentrated *in vacuo* and purified by column chromatography, MeOH/DCM (10% then 0-30 drops NEt_3 per 100 ml) to give a cream solid, (28.0 mg, 0.0583 mmol, 48.4 %). **^{1}H NMR** (500 MHz, MeOD) δ 8.27 (s, 1H), 7.88 (s, 1H), 7.50 – 7.44 (m, 2H), 7.37 (d, *J* = 7.0, 1H), 4.57 (t, *J* = 6.7, 2H), 3.16 – 3.10 (m, 2H), 2.95 (t, *J* = 6.7, 2H), 2.35 (m, 7H), 2.14 (t, *J* = 11.0, 2H), 1.88 (d, *J* = 12.7, 2H), 1.56 (s, 9H), 1.47 (m, 2H); **^{13}C NMR** (126 MHz, MeOD) δ 158.42 (C), 155.37 (CH), 154.22 (C), 154.00 (C), 144.97 (C), 140.14 (C), 133.30 (C), 129.46 (CH), 122.27 (CH), 119.16 (CH), 118.54 (CH), 97.74 (C), 79.72 (C), 62.16 (CH), 56.21 (CH_2), 52.29 (2x CH_2), 44.06 (CH_2), 40.16 (2x CH_3), 27.38 (2x CH_2), 27.28 (3x CH_3); **MS** (ES +ve) $[M+H]^+$: 481.4; **HRMS** (ES +ve), $C_{25}H_{37}N_8O_2$ $[M+H]^+$: calculated 480.30340, found 481.30540.

Synthesis of tert-butyl N-[5-[4-amino-1-[2-[4-(dimethylamino)-1-piperidyl]ethyl]pyrazolo[3,4-d]pyrimidin-3-yl]-2-pyridyl]carbamate (78):

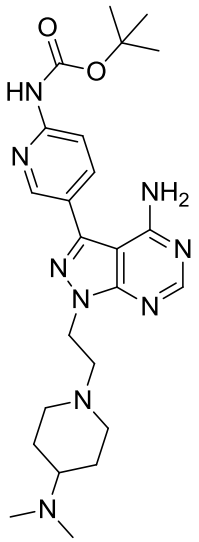

To a solution of 1-[2-[4-(dimethylamino)-1-piperidyl]ethyl]-3-iodo-pyrazolo[3,4-d]pyrimidin-4-amine (50 mg, 0.1205 mmol) in dioxane/water (4.5/0.5 ml) was added (6-((tert-Butoxycarbonyl)amino)pyridin-3-yl)boronic acid (1.5 eq., 43.1 mg, 0.181 mmol), potassium carbonate (1.5 eq., 25.0 mg, 0.181 mmol) and triphenylphosphine (20 mol %, 9.5 mg) followed by palladium acetate (5 mol %) and the mixture heated in the microwave at 120 ^{o}C for 30 mins. The mixture was concentrated *in vacuo* and purified by column chromatography, MeOH/DCM (10 % then 10-30 drops of NEt_3 per 100 ml) to give a white solid, (23.8 mg, 0.0495 mmol, 41.0 %). **^{1}H NMR** (500 MHz, MeOD) δ 8.55 – 8.51 (m, 1H), 8.26 (s, 1H), 8.06 – 8.01 (m, 2H), 4.55 (t, *J* = 6.5, 2H), 3.14 (d, *J* = 12.0, 2H), 2.94 (t, *J* = 6.5, 2H), 2.68 (m, 1H), 2.55 (s, 6H), 2.14 (t, *J* = 11.0, 2H), 1.92 (d, *J* = 12.7, 2H), 1.55 (s, 9H), 1.53 – 1.46 (m, 2H); **^{13}C NMR** (126 MHz, MeOD) δ 158.58 (C), 155.47 (CH), 154.40 (C), 153.05 (C), 152.96 (C), 147.13 (CH), 141.83 (C), 137.78 (CH), 123.46 (C), 112.28 (CH), 97.92 (C), 80.49 (C), 62.79 (CH), 56.00 (CH_2), 51.78 (2x CH_2), 44.12 (CH_2), 39.64 (2x CH_3), 27.16 (3x CH_3), 26.76 (2x CH_2); **MS** (ES +ve) $[M+H]^+$: 481.8; **HRMS** (ES +ve), $C_{24}H_{36}N_9O_2$ $[M+H]^+$: calculated 482.29865, found 482.30040.

Synthesis of tert-butyl 5-[4-amino-1-[2-[4-(dimethylamino)-1-piperidyl]ethyl]pyrazolo[3,4-d]pyrimidin-3-yl]indole-1-carboxylate (79):

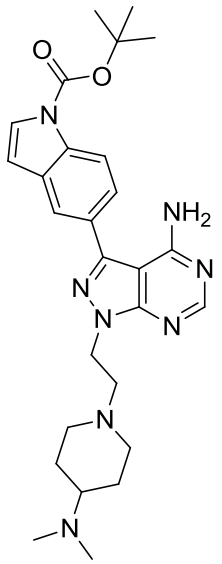

To a solution of 1-[2-[4-(dimethylamino)-1-piperidyl]ethyl]-3-iodo-pyrazolo[3,4-d]pyrimidin-4-amine (50 mg, 0.1205 mmol) in dioxane/water (4.5/0.5 ml) was added 1-Boc-indole-5-boronic acid pinacol ester (1.5 eq., 62.1 mg, 0.181 mmol), potassium carbonate (1.5 eq., 25.0 mg, 0.181 mmol) and triphenylphosphine (20 mol %, 9.5 mg) followed by palladium acetate (5 mol %) and the mixture heated in the microwave at 120 ^{o}C for 30 mins. The mixture was concentrated *in vacuo* and purified by column chromatography, MeOH/DCM (10 % then 10-30 drops of NEt_3 per 100 ml) to give a light cream solid, (31.2 mg, 0.0619 mmol, 51.3 %). **^{1}H NMR** (500 MHz, MeOD) δ 8.35 (d, *J* = 8.5, 1H), 8.29 (s, 1H), 7.92 (d, *J* = 1.3, 1H), 7.76 (d, *J* = 3.7, 1H), 7.65 (dd, *J* = 8.5, 1.7, 1H), 6.77 (d, *J* = 3.5, 1H), 4.58 (t, *J* = 6.6, 2H), 3.16 (d, *J* = 11.9, 2H), 2.97 (t, *J* = 6.6, 2H), 2.43 (s, 7H), 2.16 (t, *J* = 11.0, 2H), 1.91 (d, *J* = 12.7, 2H), 1.73 (s, 9H), 1.50 (td, *J* = 12.1, 8.5, 2H); **^{13}C NMR** (126 MHz, MeOD) δ 158.56 (C), 155.44 (CH), 154.16 (C), 149.49 (C), 145.58 (C), 135.55 (C), 131.29 (C), 127.17 (C), 126.91 (CH), 124.19 (CH), 120.88 (CH), 115.42 (CH), 107.14 (CH), 97.90 (C), 84.04 (C), 62.38 (CH), 56.19 (CH_2), 52.15 (2x CH_2), 44.02 (CH_2), 40.00 (2x CH_3), 27.19 (2x CH_2), 26.95 (3x CH_3); **MS** (ES +ve) $[M+H]^+$: 505.0.0; **HRMS** (ES +ve), $C_{27}H_{37}N_8O_2$ $[M+H]^+$: calculated 505.30340, found 505.30430.

Synthesis of [3-(tert-butoxycarbonylamino)-4-methoxy-phenyl]boronic acid (80):

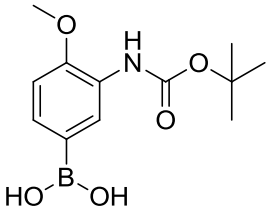

(3-Amino-4-methoxyphenyl)boronic acid (150 mg, 0.898 mmol) was suspended in DCM (5 ml). Di-tertbutyldicarbonate (1.5 eq., 1.347 mmol, 294.0 mg) was added followed by a small spatula of DMAP and the reaction allowed to stir for 18 hours. Water was added to the mixture and the organic layer separated, dried over $MgSO_4$ and concentrated *in vacuo*. The product was purified by column chromatography, MeOH/DCM (0-4 %) to give a dark brown solid (189.9 mg, 0.711 mmol, 79.2 %). **^{1}H NMR** (500 MHz, MeOD) δ 8.12 (s, 1H), 7.34 (dd, J = 8.2, 1.5, 1H), 6.98 (d, J = 8.2, 1H), 3.88 (s, J = 4.9, 3H), 1.53 (s, 9H); **^{13}C NMR** (126 MHz, MeOD) δ 153.77 (C), 150.52 (C), 129.82 (CH), 129.49 (CH), 126.76 (C), 125.18 (C), 109.48 (CH), 79.78 (C), 54.74 (CH_3), 27.26 (3x CH_3); **MS** (ES +ve) $[M+H]^+$: 268.5.

Synthesis of tert-butyl N-[5-[4-amino-1-[2-[4-(dimethylamino)-1-piperidyl]ethyl]pyrazolo[3,4-d]pyrimidin-3-yl]-2-methoxy-phenyl]carbamate (81):

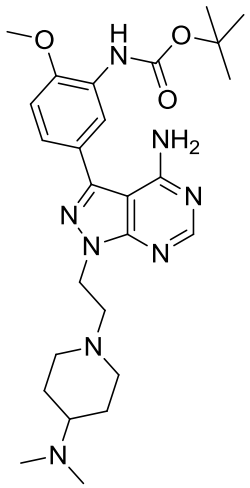

To a solution of 1-[2-[4-(dimethylamino)-1-piperidyl]ethyl]-3-iodo-pyrazolo[3,4-d]pyrimidin-4-amine (50 mg, 0.1205 mmol) in dioxane/water (4.5/0.5 ml) was added [3-(tert-butoxycarbonylamino)-4-methoxy-phenyl]boronic acid (1.5 eq., 48.4 mg, 0.181 mmol), potassium carbonate (1.5 eq., 25.0 mg, 0.181 mmol) and triphenylphosphine (20 mol %, 9.5 mg) followed by palladium acetate (5 mol %) and the mixture heated in the microwave at

120 ^{o}C for 30 mins. The mixture was concentrated *in vacuo* and purified by column chromatography, MeOH/DCM (0-10 % then 0-20 drops of NEt_3 per 100 ml) to give a light brown solid, (32.9 mg, 0.0645 mmol, 53.5 %). **^{1}H NMR** (500 MHz, MeOD) δ 8.26 (d, J = 5.2, 1H), 8.19 (d, J = 2.1, 1H), 7.41 (dd, J = 8.4, 2.2, 1H), 7.19 (d, J = 8.5, 1H), 4.56 (t, J = 6.6, 2H), 3.99 (d, J = 5.1, 3H), 3.15 (d, J = 12.1, 2H), 2.96 (t, J = 6.6, 2H), 2.54 (m, 1H), 2.48 (s, 6H), 2.16 (t, J = 10.9, 2H), 1.92 (d, J = 10.5, 2H), 1.56 (d, J = 5.1, 9H), 1.55 – 1.46 (m, 2H); **^{13}C NMR** (126 MHz, MeOD) δ 158.48 (C), 155.35 (CH), 154.20 (C), 153.82 (C), 149.93 (C), 145.03 (C), 128.25 (C), 124.95 (C), 123.27 (CH), 119.69 (CH), 111.00 (CH), 97.67 (C), 80.15 (C), 62.52 (CH), 56.07 (CH_2), 55.11 (CH_3), 51.99 (2x CH_2), 44.01 (CH_2), 39.86 (2x CH_3), 27.22 (3x CH_3), 27.03 (2x CH_2); **MS** (ES +ve) $[M+H]^+$: 511.4; **HRMS** (ES +ve), $C_{26}H_{39}N_8O_3$ $[M+H]^+$: calculated 511.31396, found 511.31660.

Synthesis of tert-butyl 2-[2-methoxy-4-(4,4,5,5-tetramethyl-1,3,2-dioxaborolan-2-yl)phenyl]acetate (82):

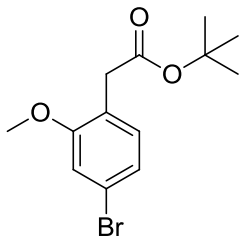

2-(4-Bromo-2-methoxyphenyl)acetic acid (2 g, 8.198 mmol) was dissolved in 20 ml of dry THF. Thionyl chloride (1.2 eq., 9.837 mmol, 1.17 g, 0.714 ml) was added followed by a drop of DMF and the reaction heated to reflux (80^{o}C) for 2 hours. The reaction was cooled to r.t. then t-butylalcohol (5 eq., 40.99 mmol, 3.04 g, 3.92 ml) and triethylamine (2.5 eq., 20.49 mmol, 2.86 ml) added and the mixture left to stir for 20 hours. Water and EtOAc were added to the mixture and the organic layer separated, dried over $MgSO_4$ and concentrated *in vacuo*. The product was purified by column chromatography, EtOAC/Hexane (0-4%) to give a light orange liquid, (694.8 mg, 2.316 mmol, 28.2 %). **^{1}H NMR** (500 MHz, MeOD) δ 7.10 (s, 1H), 7.07 – 7.02 (m, 2H), 3.81 s, 3H), 3.47 (s, 2H), 1.42 (s, 9H); **^{13}C NMR** (126 MHz, MeOD) δ 171.39 (C), 158.43 (C), 131.77 (CH), 122.99 (C), 122.98 (CH), 121.02 (C), 113.67 (CH), 80.51 (C), 54.84 (CH_3), 36.42 (CH_2), 26.85 (3x CH_3); **MS** (ES +ve) $(M+H)^+$: 323.2/324.8 (+Na).

Synthesis of tert-butyl 2-[2-methoxy-4-(4,4,5,5-tetramethyl-1,3,2-dioxaborolan-2-yl)phenyl]acetate (83):

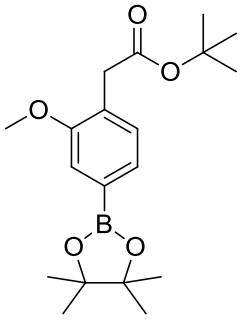

To a solution of tert-butyl 2-[2-methoxy-4-(4,4,5,5-tetramethyl-1,3,2-dioxaborolan-2-yl)phenyl]acetate (600 mg, 2.0 mmol) in dioxane/water (18/2 ml) was added bis(pinacolato)diboron (1.5 eq., 762.6 mg, 3.0 mmol), potassium carbonate (1.5 eq., 414.6 mg, 3.0 mmol) and triphenylphosphine (20 mol %, 104.9 mg) followed by palladium acetate (5 mol %, 22.5 mg) and the mixture heated in the microwave at 120 ^{o}C for an hour. MS showed a little SM so the mixture was heated for another hour. MS and TLC showed the reaction was complete. EtOAc and water were added to the mixture and the organic layer separated, dried over $MgSO_4$ and concentrated *in vacuo*. The product was purified by column chromatography, EtOAc/Hexane (0-10%) to give a colourless oil, (322.4 mg, 0.926 mmol, 46.3 %). **^{1}H NMR** (500 MHz, CDCl3) δ 7.37 (d, *J* = 8.0, 1H), 7.26 (d, *J* = 3.0, 1H), 7.18 (d, *J* = 7.3, 1H), 3.86 (s, 3H), 3.54 (s, 2H), 1.42 (s, 9H), 1.34 (s, 12H); **^{13}C NMR** (126 MHz, CDCl3) δ 170.96 (C), 157.02 (C), 130.25 (CH), 127.29 (C), 127.28 (CH), 115.89 (CH), 109.97 (C), 83.75 (C), 80.34 (C), 55.46 (CH_3), 37.58 (CH_2), 28.03 (3x CH_3), 24.85 (4x CH_3); **MS** (ES +ve) $[M+H]^+$: 349.7.

Synthesis of tert-butyl 2-[4-[4-amino-1-[2-[4-(dimethylamino)-1-piperidyl]ethyl]pyrazolo[3,4-d]pyrimidin-3-yl]-2-methoxy-phenyl]acetate (84):

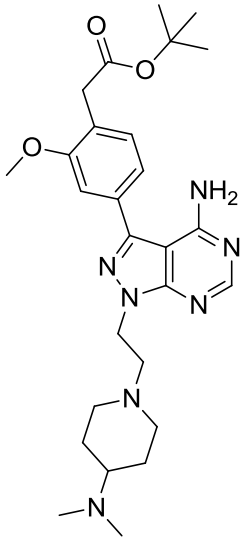

To a solution of 1-[2-[4-(dimethylamino)-1-piperidyl]ethyl]-3-iodo-pyrazolo[3,4-d]pyrimidin-4-amine (34.7 mg, 0.0836 mmol) in dioxane/water (4.5/0.5 ml) was added tert-butyl 2-[2-methoxy-4-(4,4,5,5-tetramethyl-1,3,2-dioxaborolan-2-yl)phenyl]acetate (1 eq., 29.1 mg, 0.0836 mmol), potassium carbonate (1.5 eq., 17.3 mg, 0.125 mmol) and triphenylphosphine (20 mol %, 4.4 mg) followed by palladium acetate (5 mol %) and the mixture heated in the microwave at 120 ^{o}C for 30 mins. The mixture was concentrated *in vacuo* and purified by column chromatography, MeOH/DCM (0-10 % then 0-30 drops of NEt_3 per 100 ml) to give a cream solid, (19 mg, 0.0373 mmol, 44.6 %). **^{1}H NMR** (500 MHz, MeOD) δ 8.26 (s, 1H), 7.35 (d, J = 7.6, 1H), 7.26 (d, J = 1.4, 1H), 7.22 (dd, J = 7.5, 1.6, 1H), 4.56 (t, J = 6.7, 2H), 3.91 (s, 3H), 3.64 (s, 2H), 3.13 (d, J = 11.9, 2H), 2.94 (t, J = 6.7, 2H), 2.37 (m, 7H), 2.13 (t, J = 11.0, 2H), 1.91 – 1.85 (m, 2H), 1.48 (m, 11H); **^{13}C NMR** (126 MHz, MeOD) δ 172.07 (C), 158.55 (C), 158.18 (C), 155.46 (CH), 154.14 (C), 145.09 (C), 133.02 (C), 131.48 (CH), 124.76 (C), 120.21 (CH), 110.45 (CH), 97.82 (C), 80.76 (C), 62.26 (CH), 56.22 (CH_2), 54.70 (CH_3), 52.24 (2x CH_2), 44.04 (CH_2), 40.09 (2x CH_3), 36.61 (CH_2), 27.28 (2x CH_2), 26.90 (3x CH_3); **MS** (ES +ve) $[M+H]^+$: 510.2; **HRMS** (ES +ve), $C_{27}H_{40}N_7O_3$ $[M+H]^+$: calculated 510.31872, found 510.31850.

Synthesis of tert-butyl 2-[4-(4,4,5,5-tetramethyl-1,3,2-dioxaborolan-2-yl)phenyl]acetate (85):

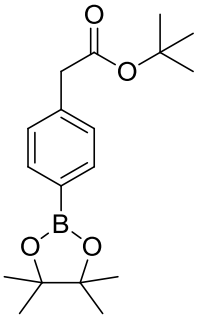

4-(Carboxymethyl)phenylboronic acid pinacol ester (150 mg, 0.572 mmol) was dissolved in 5 ml of dry toluene. Thionyl chloride (1.2 eq., 0.686 mmol, 81.6 mg, 49.8 ul) was added followed by a drop of DMF and the reaction heated to reflux (120^{o}C) for 2 hours. The reaction was cooled to r.t. then t-butylalcohol (5 eq., 2.86 mmol, 211.8 mg, 0.273 ml) and triethylamine (2.5 eq., 1.43 mmol, 199.3 ul) added and the mixture allowed to stir for 18 hours. Water and DCM were added to the mixture and the organic layer separated, dried over $MgSO_4$ and concentrated *in vacuo*. The crude product was purified by column chromatography, (100 % DCM), to give a light brown oil, (60 mg, 0.189 mmol, 33.0 %). **MS** (ES +ve) $(M+H)^+$: 340.8 (+Na)

Synthesis of tert-butyl 2-[4-[4-amino-1-[2-[4-(dimethylamino)-1-piperidyl]ethyl]pyrazolo[3,4-d]pyrimidin-3-yl]phenyl]acetate (86):

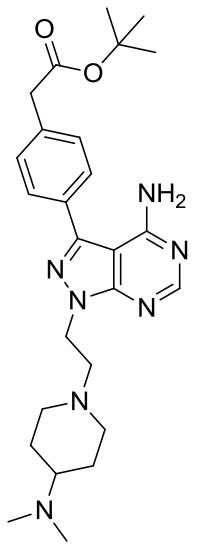

To a solution of 1-[2-[4-(dimethylamino)-1-piperidyl]ethyl]-3-iodo-pyrazolo[3,4-d]pyrimidin-4-amine (50 mg, 0.1205 mmol) in dioxane/water (4.5/0.5 ml) was added tert-butyl 2-[4-(4,4,5,5-tetramethyl-1,3,2-dioxaborolan-2-yl)phenyl]acetate (1.5 eq., 57.6 mg, 0.181 mmol), potassium carbonate (1.5 eq., 25.0 mg, 0.181 mmol) and triphenylphosphine (20 mol %, 9.5 mg) followed by palladium acetate (5 mol %) and the mixture heated in the microwave at 120 ^{o}C for 30 mins. The mixture was concentrated *in vacuo* and purified by column chromatography, MeOH/DCM (10 % then 0-30 drops of NEt_3 per 100 ml) to give a light brown thick oil, (40.5 mg, 0.0845 mmol, 70.1 %). **^{1}H NMR** (500 MHz, MeOD) δ 8.26 (s, 1H), 7.68 – 7.63 (m, 2H), 7.47 (d, *J* = 8.2, 2H), 4.55 (t, *J* = 6.6, 2H), 3.68 (s, 2H), 3.12 (d, *J* = 11.9, 2H), 2.93 (t, *J* = 6.6, 2H), 2.43 (m, 7H), 2.13 (t, *J* = 11.0, 2H), 1.87 (m, 2H), 1.47 (m, 11H); **^{13}C NMR** (126 MHz, MeOD) δ 171.52 (C), 158.52 (C), 155.44 (CH), 154.21 (C), 144.85 (C), 136.00 (C), 131.41 (C), 129.95 (2x CH), 128.45 (2x CH), 97.81 (C), 81.01 (C), 62.40 (CH), 56.15 (CH_2), 52.10 (2x CH_2), 44.04 (CH_2), 41.58 (CH_2), 39.95 (2x CH_3), 27.13 (2x CH_2), 26.88 (3x CH_3); **MS** (ES +ve) $[M+H]^+$: 480.0; **HRMS** (ES +ve), $C_{26}H_{38}N_7O_2$ $[M+H]^+$: calculated 480.30815, found 480.31210.

Synthesis of 2-[4-[4-amino-1-[2-[4-(dimethylamino)-1-piperidyl]ethyl]pyrazolo[3,4-d]pyrimidin-3-yl]phenyl]acetic acid (87):

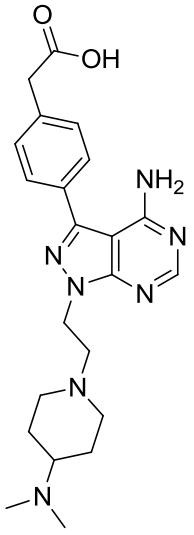

To a solution of 1-[2-[4-(dimethylamino)-1-piperidyl]ethyl]-3-iodo-pyrazolo[3,4-d]pyrimidin-4-amine (50 mg, 0.1205 mmol) in dioxane/water (4.5/0.5 ml) was added 4-(Carboxymethyl)phenylboronic acid pinacol ester (1.5 eq., 47.4 mg, 0.181 mmol), potassium carbonate (1.5 eq., 25.0 mg, 0.181 mmol) and triphenylphosphine (20 mol %, 9.5 mg)

followed by palladium acetate (5 mol %) and the mixture heated in the microwave at 120 ^{o}C for 30 mins. The mixture was concentrated *in vacuo* and purified by column chromatography, MeOH/DCM (10 % then 0-50 drops of NEt_3 per 100 ml) to give a cream solid, (25.0 mg, 0.0591 mmol, 49.0 %). **^{1}H NMR** (500 MHz, MeOD) δ 8.26 (s, 1H), 7.59 (d, *J* = 8.2, 2H), 7.49 (d, *J* = 8.2, 2H), 4.55 (t, *J* = 6.3, 2H), 3.62 (s, 2H), 3.20 – 3.15 (m, 2H), 2.98 (t, *J* = 6.3, 3H), 2.74 (s, 6H), 2.18 (t, *J* = 11.0, 2H), 2.03 – 1.96 (m, 2H), 1.56 (dd, *J* = 12.1, 3.9, 2H); **^{13}C NMR** (126 MHz, MeOD) δ 177.81 (C), 158.57 (C), 155.42 (CH), 154.16 (C), 145.31 (C), 139.11 (C), 130.29 (C), 129.88 (2x CH), 128.10 (2x CH), 97.82 (C), 63.29 (CH_2), 55.78 (CH_2), 51.37 (2x CH_2), 44.08 (CH_2), 39.26 (2x CH_3), 29.53 (CH), 26.34 (2x CH_2); **MS** (ES +ve) $[M+H]^+$: 424.4; **HRMS** (ES +ve), $C_{22}H_{30}N_7O_2$ $[M+H]^+$: calculated 424.24555, found 424.2475.

Synthesis of 2-(4-bromo-2-methoxy-phenyl)-1-pyrrolidin-1-yl-ethanone (88):

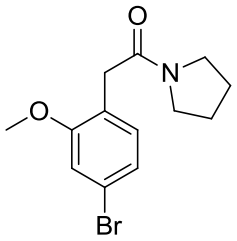

2-(4-Bromo-2-methoxyphenyl)acetic acid (300 mg, 1.229 mmol) was dissolved in 5 ml of dry toluene. Thionyl chloride (1.2 eq., 1.476 mmol, 175.6 mg, 107.0 ul) was added followed by a drop of DMF and the reaction heated to reflux (120^{o}C) for 1.5 hours. The reaction was cooled to r.t. then pyrrolidine (2.5 eq., 3.073 mmol, 218.6 mg, 0.257 ml) and triethylamine (2.5 eq., 3.073 mmol, 0.428 ml) added and the reaction left to stir for 18 hours. Water and DCM were added to the mixture and the organic layer, separated, dried over $MgSO_4$ and concentrated *in vacuo*. The product was purified by column chromatography, EtOAc/hexane (20-60 %), to give a cream coloured solid, (238.7 mg, 0.804 mmol, 65.4 %). **^{1}H NMR** (500 MHz, CDCl3) δ 7.10 (d, *J* = 8.0, 1H), 7.05 (dd, *J* = 8.0, 1.8, 1H), 6.98 (d, *J* = 1.8, 1H), 3.81 (s, 3H), 3.56 (s, 2H), 3.46 (m, 4H), 1.87 (m, 4H); **^{13}C NMR** (126 MHz, CDCl3) δ 169.26 (C), 157.78 (C), 131.58 (CH), 123.69 (CH), 123.05 (C), 121.10 (C), 114.00 (CH), 55.76 (CH_3), 46.72 (CH_2), 45.91 (CH_2), 35.37 (CH_2), 26.16 (CH_2), 24.39 (CH_2); **MS** (ES +ve) $(M+H)^+$: 298.2/300.2, 320.2/322.2 (+Na)

Synthesis of 2-[2-methoxy-4-(4,4,5,5-tetramethyl-1,3,2-dioxaborolan-2-yl)phenyl]-1-pyrrolidin-1-yl-ethanone (89):

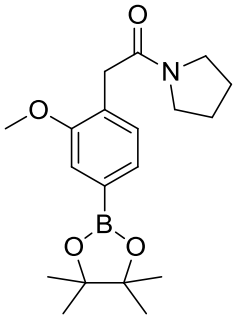

To a solution of 2-(4-bromo-2-methoxy-phenyl)-1-pyrrolidin-1-yl-ethanone (150 mg, 0.505 mmol) in dioxane/water (4.5/0.5 ml) was added bis(pinacolato)diboron (1.5 eq., 192.5 mg, 0.758 mmol), potassium carbonate (1.5 eq., 104.8 mg, 0.758 mmol) and triphenylphosphine (20 mol %, 26.5 mg) followed by palladium acetate (5 mol %) and the mixture heated in the microwave at 120 ^{o}C for an hour. Water and DCM were added to the mixture and the organic layer, separated, dried over $MgSO_4$ and concentrated *in vacuo*. The product was purified by column chromatography, EtOAc/hexane (20-80 %) to give a pale yellow oil, (85.6 mg, 0.248 mmol, 49.1 %). **^{1}H NMR** (500 MHz, CDCl3) δ 7.40 (dd, J = 7.4, 0.9, 1H), 7.31 – 7.27 (m, 2H), 3.88 (s, 3H), 3.69 (d, J = 5.0, 2H), 3.53 – 3.39 (m, 4H), 1.92 – 1.84 (m, 4H), 1.36 (s, 12H); **^{13}C NMR** (126 MHz, CDCl3) δ 169.83 (C), 156.58 (C), 132.95 (C), 129.61 (CH), 127.54 (CH), 127.19 (C), 115.86 (CH), 83.77 (C), 55.52 (CH_3), 46.71 (CH_2), 45.87 (CH_2), 35.99 (CH_2), 26.13 (CH_2), 24.72 (4x CH_3), 24.43 (CH_2); **MS** (ES +ve) $(M+H)^+$: 346.4

Synthesis of 2-[4-[4-amino-1-[2-[4-(dimethylamino)-1-piperidyl]ethyl]pyrazolo[3,4-d]pyrimidin-3-yl]-2-methoxy-phenyl]-1-pyrrolidin-1-yl-ethanone (90):

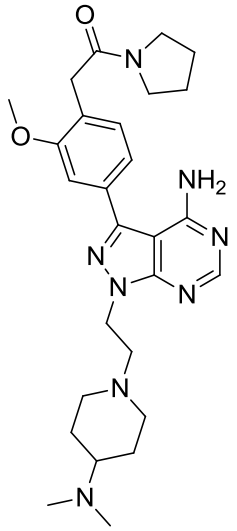

To a solution of 1-[2-[4-(dimethylamino)-1-piperidyl]ethyl]-3-iodo-pyrazolo[3,4-d]pyrimidin-4-amine (50 mg, 0.1205 mmol) in dioxane/water (4.5/0.5 ml) was added 2-[2-methoxy-4-(4,4,5,5-tetramethyl-1,3,2-dioxaborolan-2-yl)phenyl]-1-pyrrolidin-1-yl-ethanone (1.5 eq., 62.5 mg, 0.181 mmol), potassium carbonate (1.5 eq., 25.0 mg, 0.181 mmol) and triphenylphosphine (20 mol %, 9.5 mg) followed by palladium acetate (5 mol %) and the mixture heated in the microwave at 120 ^{o}C for 30 mins. The mixture was concentrated *in vacuo* and purified by column chromatography, MeOH/DCM (10 % then 0-30 drops of NEt_3 per 100 ml) to give a white solid, (34.6 mg, 0.0683 mmol, 56.7 %). **^{1}H NMR** (500 MHz, MeOD) δ 8.25 (s, 1H), 7.33 (d, J = 7.6, 1H), 7.23 (s, 1H), 7.21 (dd, J = 7.5, 1.6, 1H), 4.54 (t, J = 6.7, 2H), 3.89 (s, 3H), 3.74 (s, 2H), 3.64 (t, J = 6.8, 2H), 3.46 (t, J = 6.9, 2H), 3.11 (d, J = 11.9, 2H), 2.92 (t, J = 6.7, 2H), 2.34 (m, 7H), 2.12 (t, J = 10.9, 2H), 2.02 (dd, J = 13.3, 6.7, 2H), 1.96 – 1.90 (m, 2H), 1.86 (d, J = 12.7, 2H), 1.46 (m, 2H); **^{13}C NMR** (126 MHz, MeOD) δ 170.77 (C), 158.57 (C), 158.03 (C), 155.45 (CH), 154.13 (C), 145.18 (C), 132.80 (C), 131.39 (CH), 125.01 (C), 120.32 (CH), 110.50 (CH), 97.84 (C), 62.22 (CH), 56.23 (CH_2), 54.76 (CH_3), 52.27 (2x CH_2), 46.79 (CH_2), 45.71 (CH_2), 44.05 (CH_2), 40.11 (2x CH_3), 35.42 (CH_2), 27.32 (2x CH_2), 25.63 (CH_2), 24.02 (CH_2); **MS** (ES +ve) $[M+H]^+$: 507.6; **HRMS** (ES +ve), $C_{27}H_{39}N_8O_2$ $[M+H]^+$: calculated 507.31905, found 507.31830.

Synthesis of 2-(4-bromo-2-methoxy-phenyl)-N-prop-2-ynyl-acetamide (91):

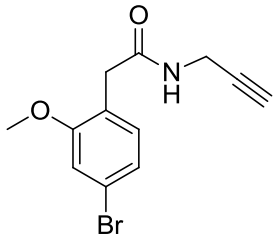

2-(4-Bromo-2-methoxyphenyl)acetic acid (500 mg, 2.049 mmol) was dissolved in 5 ml of dry toluene. Thionyl chloride (1.2 eq., 2.46 mmol, 292.7 mg, 178.3 ul) was added followed by a drop of DMF and the reaction heated to reflux (120^{o}C) for 3 hours. The reaction was cooled to r.t. then propargylamine (2.5 eq., 5.12 mmol, 282.2 mg, 0.328 ml) and triethylamine (2.5 eq., 5.12 mmol, 0.714 ml) added and the reaction left to stir for 20 hours. DCM and water were added to the mixture and the organic layer separated, dried over $MgSO_4$ and concentrated *in vacuo*. The product was purified by column chromatography, MeOH/DCM (0-3 %) to give a cream coloured solid, (458.2 mg, 1.631 mmol, 79.6 %). **^{1}H NMR** (500 MHz, CDCl3) δ 7.13 – 7.07 (m, 2H), 7.04 (s, 1H), 5.78 (s, 1H), 3.99 (dd, *J* = 5.2, 2.6, 2H), 3.86 (s, 3H), 3.51 (s, 2H), 2.21 – 2.16 (m, 1H); **^{13}C NMR** (126 MHz, CDCl3) δ 170.11 (C), 157.79 (C), 132.32 (CH), 124.16 (CH), 122.35 (C), 122.07 (C), 114.50 (CH), 79.53 (C), 71.45 (CH), 55.85 (CH_3), 38.02 (CH_2), 29.23 (CH_2); **MS** (ES +ve) $(M+H)^+$: 281.6/283.6, 303.8/306.0 (+Na)

Synthesis of 2-[(4-bromo-2-methoxy-phenyl)methyl]-5-methyl-oxazole (92):

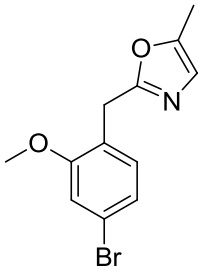

2-(4-bromo-2-methoxy-phenyl)-N-prop-2-ynyl-acetamide (200 mg, 0.713 mmol) was dissolved in 2 ml of 1,2-dichloroethane in a microwave vial. $FeCl_3$ (0.5 eq., 57.6 mg, 0.356 mmol) was added and the mixture heated to 150^{o}C for 90 mins. Water and DCM were added to the mixture and the organic layer separated, dried over $MgSO_4$ and concentrated *in vacuo*. The product was purified by column chromatography, MeOH/DCM (1 %), to give a light

yellow/orange oil, (108.7 mg, 0.389 mmol, 54.3 %). **^{1}H NMR** (500 MHz, CDCl3) δ 7.09 – 7.03 (m, 2H), 7.01 (s, 1H), 6.65 (d, *J* = 1.1, 1H), 4.04 (s, 2H), 3.82 (s, 3H), 2.26 (d, *J* = 1.2, 3H); **^{13}C NMR** (126 MHz, CDCl3) δ 161.66 (C), 157.87 (C), 148.90 (C), 131.42 (CH), 123.66 (CH), 123.09 (C), 122.03 (CH), 121.65 (C), 114.31 (CH), 55.83 (CH_3), 28.30 (CH_2), 10.88 (CH_3); **MS** (ES +ve) $(M+H)^+$: 281.6/283.6, 303.8/306.0 (+Na).

Synthesis of 2-[[2-methoxy-4-(4,4,5,5-tetramethyl-1,3,2-dioxaborolan-2-yl)phenyl]methyl]-5-methyl-oxazole (93):

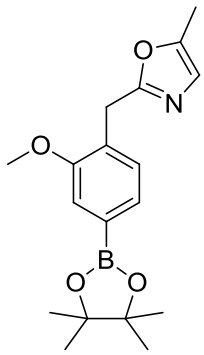

To a solution of 2-[(4-bromo-2-methoxy-phenyl)methyl]-5-methyl-oxazole (80 mg, 0.285 mmol) in dioxane/water (4.5/0.5 ml) was added bis(pinacolato)diboron (1.5 eq., 108.5 mg, 0.427 mmol), potassium carbonate (1.5 eq., 59.0 mg, 0.427 mmol) and triphenylphosphine (20 mol %, 15.0 mg) followed by palladium acetate (5 mol %) and the mixture heated in the microwave at 120 ^{o}C for 30 mins. The mixture was concentrated *in vacuo* and purified by column chromatography, EtOAc/hexane (30-40 %) to give a clear oil, (37.0 mg, 0.1124 mmol, 39.4 %). **^{1}H NMR** (500 MHz, MeOD) δ 7.35 – 7.30 (m, 1H), 7.20 – 7.12 (m, 1H), 6.69 – 6.65 (m, 1H), 5.97 (s, 1H), 4.51 (s, 2H), 4.08 (s, 3H), 2.28 (s, 3H), 1.37 (s, 12H); **MS** (ES +ve) $(M+H)^+$: 329.18.

Synthesis of 1-[2-[4-(dimethylamino)-1-piperidyl]ethyl]-3-[3-methoxy-4-[(5-methyloxazol-2-yl)methyl]phenyl]pyrazolo[3,4-d]pyrimidin-4-amine (94):

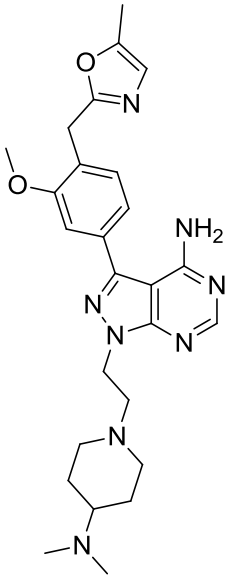

To a solution of 1-[2-[4-(dimethylamino)-1-piperidyl]ethyl]-3-iodo-pyrazolo[3,4-d]pyrimidin-4-amine (50 mg, 0.1205 mmol) in dioxane/water (4.5/0.5 ml) was added 2-[[2-methoxy-4-(4,4,5,5-tetramethyl-1,3,2-dioxaborolan-2-yl)phenyl]methyl]-5-methyl-oxazole (1 eq., 39.7 mg, 0.1205 mmol), potassium carbonate (1.5 eq., 25.0 mg, 0.181 mmol) and triphenylphosphine (20 mol %, 9.5 mg) followed by palladium acetate (5 mol %) and the mixture heated in the microwave at 120 ^{o}C for 30 mins. The mixture was concentrated *in vacuo* and purified by column chromatography, MeOH/DCM (10% then 0-30 drops of NEt_3 per 100 ml) to give a pale yellow solid, (36.8 mg, 0.0751 mmol, 62.3 %). **^{1}H NMR** (500 MHz, MeOD) δ 8.28 (s, 1H), 7.38 (d, J = 7.6, 1H), 7.29 (s, 1H), 7.26 (dd, J = 7.6, 1.6, 1H), 6.69 (d, J = 1.2, 1H), 4.57 (t, J = 6.6, 2H), 4.15 (s, 2H), 3.91 (s, 3H), 3.17 (d, J = 7.4, 2H), 2.96 (t, J = 6.6, 2H), 2.69 (m, 1H), 2.56 (s, 6H), 2.31 (s, 3H), 2.17 (t, J = 11.0, 2H), 1.94 (m, 2H), 1.54 (m, 2H); **^{13}C NMR** (126 MHz, MeOD) δ 162.54 (C), 158.55 (C), 157.95 (C), 155.47 (CH), 154.21 (C), 149.33 (C), 145.01 (C), 133.18 (C), 130.96 (CH), 124.85 (C), 121.56 (CH), 120.34 (CH), 110.70 (CH), 97.78 (C), 62.77 (CH), 56.03 (CH_2), 54.78 (CH_3), 51.82 (2x CH_2), 44.08 (CH_2), 39.66 (2x CH_3), 28.17 (CH_2), 26.79 (2x CH_2), 9.16 (CH_3); **MS** (ES +ve) $[M+H]^+$: 491.8; **HRMS** (ES +ve), $C_{26}H_{35}N_8O_2$ $[M+H]^+$: calculated 491.28775, found 491.28620.

Synthesis of 2-[4-[4-amino-1-[2-[4-(dimethylamino)-1-piperidyl]ethyl]pyrazolo[3,4-d]pyrimidin-3-yl]phenyl]acetonitrile (95):

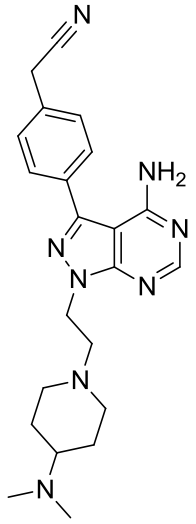

To a solution of 1-[2-[4-(dimethylamino)-1-piperidyl]ethyl]-3-iodo-pyrazolo[3,4-d]pyrimidin-4-amine (50 mg, 0.1205 mmol) in dioxane/water (4.5/0.5 ml) was added 4-(Cyanomethyl)benzeneboronic acid, (1 eq., 29.1 mg, 0.181 mmol), potassium carbonate (1.5 eq., 25.0 mg, 0.181 mmol) and triphenylphosphine (20 mol %, 9.5 mg) followed by palladium acetate (5 mol %) and the mixture heated in the microwave at 120 ^{o}C for 30 mins. The mixture was concentrated *in vacuo* and purified by column chromatography, MeOH/DCM (5-10 % then 20 drops of NEt_3 per 100 ml) to give a cream solid, (41.8 mg, 0.1034 mmol, 85.8 %). **^{1}H NMR** (500 MHz, MeOD) δ 8.27 (s, 1H), 7.79 – 7.70 (m, 2H), 7.59 (d, J = 8.3, 2H), 4.56 (t, J = 6.4, 2H), 4.03 (s, 2H), 3.18 (d, J = 5.8, 2H), 3.04 – 2.93 (m, 3H), 2.74 (s, 6H), 2.17 (dd, J = 15.1, 6.9, 2H), 1.99 (d, J = 12.8, 2H), 1.61 – 1.51 (m, 2H); **^{13}C NMR** (126 MHz, MeOD) δ 158.49 (C), 155.47 (CH), 154.36 (C), 144.35 (C), 132.22 (C), 128.84 (2x CH), 128.70 (2x CH), 117.95 (C), 110.00 (C), 97.74 (C), 63.27 (CH), 55.84 (CH_2), 51.39 (2x CH_2), 44.11 (CH_2), 39.27 (2x CH_3), 26.32 (2x CH_2), 21.98 (CH_2); **MS** (ES +ve) $[M+H]^+$: 405.0; **HRMS** (ES +ve), $C_{22}H_{29}N_8$ $(M+H)^+$: calculated 405.25097, found 405.24950.

10.6.5 Synthesis of Compounds 96-101

Synthesis of 3-iodo-1-[2-(4-methylpiperazin-1-yl)ethyl]pyrazolo[3,4-d]pyrimidin-4-amine (96):

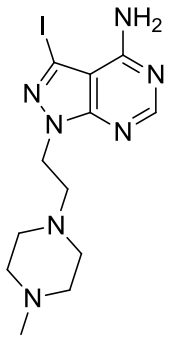

100 mg, 0.265 mmol of 1-(2,2-diethoxyethyl)-3-iodo-pyrazolo[3,4-d]pyrimidin-4-amine was added to a 5 ml microwave tube. 2.5 ml of water and 2.5 ml of TFA were then added and the mixture heated to 100 ^{o}C for 30 mins in the microwave. The solvents were removed *in vacuo* to give a dark brown oil. 0.265 mmol of 2-(4-amino-3-iodo-pyrazolo[3,4-d]pyrimidin-1-yl)acetaldehyde was suspended in 3 ml of DCM. 1-methylpiperizine (1.5 eq., 0.399 mmol, 39.8 mg, 44.1 ul) was added followed by a drop of acetic acid and the mixture allowed to stir for 10 mins. Sodium triacetoxyborohydride (1.5 eq., 0.399 mmol, 84.6 mg) was added and the mixture allowed to stir for 17 hours overnight. The mixture was concentrated *in vacuo* and purified by column chromatography, MeOH/DCM (5-10 % then 0-15 drops of NEt_3 per 100 ml) to give a light orange thick oil, (89.1 mg, 0.2302 mmol, 86.9 %). **^{1}H NMR** (500 MHz, MeOD) δ 8.22 (s, 1H), 4.51 (t, J = 6.0, 2H), 3.33 (d, J = 1.7, 4H), 3.20 – 3.04 (m, 4H), 2.98 (t, J = 6.0, 2H), 2.83 (s, 3H); **^{13}C NMR** (126 MHz, MeOD) δ 158.05 (C), 155.67 (CH), 153.80 (C), 103.55 (C), 87.02 (C), 55.51 (CH_2), 53.44 (CH_2), 49.45 (CH_2), 44.18 (CH_2), 43.07 (CH_2), 42.03 (CH_3); **MS** (ES +ve) $(M+H)^{+}$: 388.4.

Synthesis of 3-iodo-1-[2-(4-methoxy-1-piperidyl)ethyl]pyrazolo[3,4-d]pyrimidin-4-amine (97):

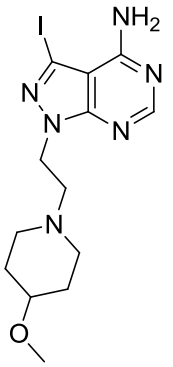

100 mg, 0.287 mmol of 1-(2,2-dimethoxyethyl)-3-iodo-pyrazolo[3,4-d]pyrimidin-4-amine was added to a 5 ml microwave tube. The mixture was then concentrated *in vacuo*. 0.287 mmol of 2-(4-amino-3-iodo-pyrazolo[3,4-d]pyrimidin-1-yl)acetaldehyde was suspended in 3 ml of DCM. 4-methoxypiperidine (1.5 eq., 0.430 mmol, 49.5 mg) was added followed by a drop of acetic acid and the mixture allowed to stir for 10 mins. Sodium triacetoxyborohydride (1.5 eq., 0.430 mmol, 91.1 mg) was then added and the mixture allowed to stir for 72 hours. The product was concentrated *in vacuo* and the product purified by column chromatography, MeOH/DCM (0-8 %) to give a pale yellow solid, (112 mg, 0.279 mmol, 97.1 %). **^{1}H NMR** (500 MHz, MeOD) δ 8.23 (s, 1H), 4.53 (t, J = 6.6, 2H), 3.29 (s, 1H), 2.98 (t, J = 6.5, 2H), 2.91 (s, 2H), 2.45 (s, 2H), 1.89 (s, 2H), 1.57 (s, 2H); **^{13}C NMR** (126 MHz, MeOD) δ 158.09 (C), 155.71 (CH), 153.68 (C), 103.71 (C), 87.16 (C), 75.13 (CH), 56.19 (CH_2), 54.43 (CH_3), 50.24 (2x CH_2), 43.96 (CH_2), 29.68 (2x CH_2); **MS** (ES +ve) $(M+H)^+$: 403.0.

Synthesis of 1-[2-[3-(dimethylamino)-1-piperidyl]ethyl]-3-iodo-pyrazolo[3,4-d]pyrimidin-4-amine (98):

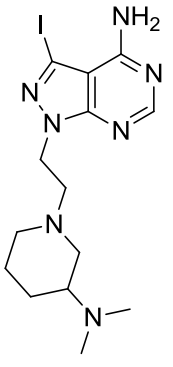

100 mg, 0.287 mmol of 1-(2,2-dimethoxyethyl)-3-iodo-pyrazolo[3,4-d]pyrimidin-4-amine was added to a 5 ml microwave tube. 2.5 ml of water and 2.5 ml of TFA were then added and the mixture heated to 100 ^{o}C for 30 mins in the microwave. The product was then concentrated *in vacuo*. 0.287 mmol of 2-(4-amino-3-iodo-pyrazolo[3,4-d]pyrimidin-1-yl)acetaldehyde was suspended in 3 ml of DCM. 3-dimethylaminopiperidine (1.5 eq., 0.430 mmol, 55.1 mg) was added followed by a drop of acetic acid and the mixture allowed to stir for 10 mins. Sodium triacetoxyborohydride (1.5 eq., 0.430 mmol, 91.1 mg) was added and the mixture allowed to stir for 18 hours. The mixture was concentrated *in vacuo* and purified by column chromatography, MeOH/DCM (5-10 %) to give a cream solid, (117.5 mg, 0.283 mmol, 98.6 %). **^{1}H NMR** (500 MHz, MeOD) δ 8.22 (s, 1H), 4.54 – 4.43 (m, 2H), 3.08 (m, 1H), 2.99 – 2.90 (m, 3H), 2.84 (s, 6H), 2.65 (m, 2H), 2.38 (m, 1H), 1.88 (m, 1H), 1.75 – 1.65 (m, 2H), 1.55 – 1.47 (m, 1H); **^{13}C NMR** (126 MHz, MeOD) δ 158.13 (C), 155.80 (CH), 153.62 (C), 103.65 (C), 87.01 (C), 62.48 (CH), 56.37 (CH_2), 52.78 (CH_2), 52.75 (CH_2), 44.50 (CH_2), 40.40 (2x CH_3), 24.67 (CH_2), 21.95 (CH_2); **MS** (ES +ve) $(M+H)^+$: 415.8

Synthesis of tert-butyl N-[4-[4-amino-1-[2-(4-methylpiperazin-1-yl)ethyl]pyrazolo[3,4-d]pyrimidin-3-yl]-2-methoxy-phenyl]carbamate (99):

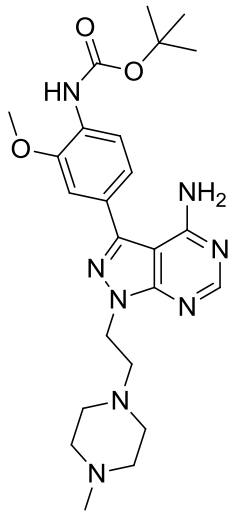

To a solution 3-iodo-1-[2-(4-methylpiperazin-1-yl)ethyl]pyrazolo[3,4-d]pyrimidin-4-amine (50 mg, 0.129 mmol) in dioxane/water (4.5 ml/0.5 ml) was added [4-(tert-butoxycarbonylamino)-3-methoxy-phenyl]boronic acid (1.5 eq., 51.8 mg, 0.194 mmol), potassium carbonate (1.5 eq., 26.8 mg, 0.194 mmol) and triphenylphosphine (20 mol %, 10.2 mg) followed by palladium acetate (5 mol %) and the mixture heated in the microwave at 120 ^{o}C for 30 mins. The mixture was concentrated *in vacuo* and purified by column

chromatography, MeOH/DCM (10 % then 0-20 drops of NEt_3 per 100 ml) to give a brown solid, (55.4 mg, 0.115 mmol, 89.0 %). **^{1}H NMR** (500 MHz, MeOD) δ 8.25 (s, 1H), 8.06 (d, J = 8.2, 1H), 7.29 (d, J = 1.8, 1H), 7.24 (dd, J = 8.2, 1.8, 1H), 4.55 (t, J = 6.5, 2H), 3.97 (s, 3H), 2.95 (t, J = 6.5, 2H), 2.57 (s, 8H), 2.35 (s, 3H), 1.55 (s, 9H); **^{13}C NMR** (126 MHz, MeOD) δ 158.54 (C), 155.42 (CH), 154.21 (C), 153.48 (C), 149.29 (C), 145.02 (C), 128.80 (C), 127.42 (C), 120.44 (CH), 119.61 (CH), 110.16 (CH), 97.74 (C), 80.21 (C), 56.21 (CH_2), 55.10 (CH_3), 54.16 (2x CH_2), 51.64 (2x CH_2), 44.06 (CH_3), 43.84 (CH_2), 27.21 (3x CH_3); **MS** (ES +ve) $(M+H)^+$: 483.6; **HRMS** (ES +ve), $C_{24}H_{35}N_8O_3$ $(M+H)^+$: calculated 483.28266, found 483.28200.

Synthesis of tert-butyl N-[4-[4-amino-1-[2-(4-methoxy-1-piperidyl)ethyl]pyrazolo[3,4-d]pyrimidin-3-yl]-2-methoxy-phenyl]carbamate (100):

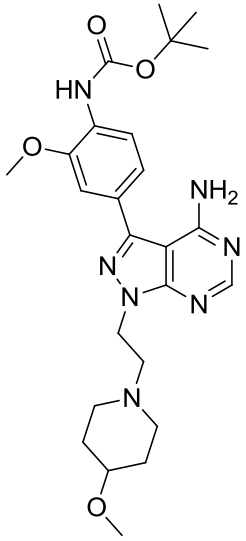

To a solution of 3-iodo-1-[2-(4-methoxy-1-piperidyl)ethyl]pyrazolo[3,4-d]pyrimidin-4-amine (50 mg, 0.124 mmol) in dioxane/water (4.5 ml/0.5 ml) was added [4-(tert-butoxycarbonylamino)-3-methoxy-phenyl]boronic acid (1.5 eq., 49.8 mg, 0.187 mmol), potassium carbonate (1.5 eq., 25.8 mg, 0.181 mmol) and triphenylphosphine (20 mol %, 6.5 mg) followed by palladium acetate (5 mol %) and the mixture heated in the microwave at 120 ^oC for 30 mins. The mixture was concentrated *in vacuo* and purified by column chromatography, MeOH/DCM (0-10 %) to give a cream coloured solid, (60.0 mg, 0.121 mmol, 97.3 %). **^{1}H NMR** (500 MHz, MeOD) δ 8.29 (s, 1H), 8.08 (d, J = 8.2, 1H), 7.31 (d, J = 1.8, 1H), 7.27 (dd, J = 8.2, 1.8, 1H), 4.63 (t, J = 6.6, 2H), 3.98 (s, 3H), 3.34 (s, 3H), 3.12 (m, 2H), 3.02 (m, 2H), 2.60 (m, 2H), 1.93 (m, 2H), 1.65 (m, 2H), 1.57 (s, 9H); **^{13}C NMR**

(126 MHz, MeOD) δ 158.53 (C), 155.46 (CH), 154.22 (C), 153.42 (C), 149.28 (C), 145.17 (C), 128.73 (C), 127.38 (C), 120.44 (CH), 119.50 (CH), 110.33 (CH), 97.94 (C), 80.15 (C), 75.12 (CH), 56.21 (CH_2), 55.10 (CH_3), 54.79 (CH_3), 50.02 (2x CH_2), 43.60 (CH_2), 29.69 (2x CH_2), 27.21 (3x CH_3); **MS** (ES +ve) $[M+H]^+$: 498.2; **HRMS** (ES +ve), $C_{25}H_{35}N_7O_4$ $[M+H]^+$: calculated 498.28233, found 498.2850.

Synthesis of tert-butyl N-[4-[4-amino-1-[2-[3-(dimethylamino)-1-piperidyl]ethyl]pyrazolo[3,4-d]pyrimidin-3-yl]-2-methoxy-phenyl]carbamate (101):

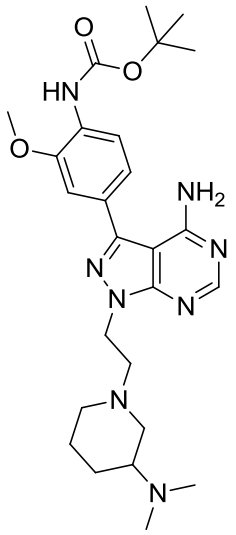

To a solution of 1-[2-[3-(dimethylamino)-1-piperidyl]ethyl]-3-iodo-pyrazolo[3,4-d]pyrimidin-4-amine (50 mg, 0.1205 mmol) in dioxane/water (4.5 ml/0.5 ml) was added [4-(tert-butoxycarbonylamino)-3-methoxy-phenyl]boronic acid (1.5 eq., 48.3 mg, 0.181 mmol), potassium carbonate (1.5 eq., 25.0 mg, 0.181 mmol) and triphenylphosphine (20 mol %, 9.5 mg) followed by palladium acetate (5 mol %) and the mixture heated in the microwave at 120 ^oC for 30 mins. The mixture was concentrated *in vacuo* and purified by column chromatography, MeOH/DCM (5-10 %) to give a dark red solid, (60.5 mg, 0.119 mmol, 98.4 %). **^{1}H NMR** (500 MHz, MeOD) δ 8.25 (s, 1H), 8.05 (d, *J* = 8.2, 1H), 7.26 (d, *J* = 1.8, 1H), 7.22 (dd, *J* = 8.2, 1.8, 1H), 4.58 – 4.48 (m, 2H), 3.94 (s, 3H), 3.13 (m, 1H), 2.97 (m, 3H), 2.82 (s, 6H), 2.66 (m, 2H), 2.42 (m, 1H), 1.86 (m, 1H), 1.71 (m, 2H), 1.52 (m, 10H); **^{13}C NMR** (126 MHz, MeOD) δ 158.61 (C), 155.59 (CH), 154.11 (C), 153.49 (C), 149.33 (C), 145.10 (C), 128.93 (C), 127.24 (C), 120.44 (CH), 119.66 (CH), 110.28 (CH), 97.76 (C), 80.24 (C), 62.58 (CH), 56.39 (CH_2), 55.12 (CH_3), 52.86 (CH_2), 52.73 (CH_2), 44.28 (CH_2),

40.32 (2x CH_3), 27.20 (3x CH_3), 24.59 (CH_2), 21.84 (CH_2); **MS** (ES +ve) $[M+H]^+$: 511.0; **HRMS** (ES +ve), $C_{26}H_{39}N_8O_3$ $(M+H)^+$: calculated 511.31396, found 511.31140.

10.6.6 Synthesis of Compounds 102-104

Synthesis of 1-(2,2-dimethoxyethyl)-3-iodo-pyrazole (102):

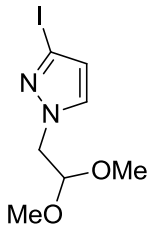

To a solution of 3-iodo-1H-pyrazole (500 mg, 2.578 mmol) in DMF (10 ml) was added sodium hydride (1.5 eq., 3.867 mmol, 60% dispersion in mineral oil, 154.7 mg) and the suspension allowed to stir for 30 mins until the gas evolution had subsided. Bromoacetaldehyde dimethyl acetal (1.5 eq. 3.867 mmol, 649.6 mg, 0.454 ml) was then added dropwise and the mixture heated at 150 ^oC in the microwave for an hour. The mixture was concentrated *in vacuo* in order to remove as much DMF as possible. EtOAc and water were then added to the mixture and the organic layer separated. The aqueous layer was washed twice with EtOAc and organics combined, dried over $MgSO_4$ and concentrated *in vacuo*. The product was purified by column chromatography, MeOH/DCM (0-1 %) to give a light orange solid, (519.2 mg, 1.841 mmol, 71.4 %). **^{1}H NMR** (500 MHz, CDCl3) δ 7.28 (d, *J* = 2.3, 1H), 6.40 (d, *J* = 2.3, 1H), 4.62 (t, *J* = 5.4, 1H), 4.20 (d, *J* = 5.4, 2H), 3.37 (d, *J* = 2.4, 6H); **^{13}C NMR** (126 MHz, CDCl3) δ 132.61 (CH), 114.84 (CH), 103.29 (CH_2), 94.49 (C), 55.20 (2x CH_3), 54.55 (CH); **MS** (ES +ve) $(M+H)^+$: 304.6 (+Na).

Synthesis of 1-[2-(3-iodopyrazol-1-yl)ethyl]-N,N-dimethyl-piperidin-4-amine (103):

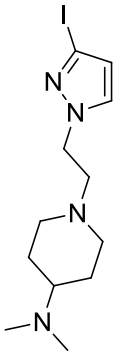

1-(2,2-dimethoxyethyl)-3-iodo-pyrazole (250 mg, 0.887 mmol) was added to a microwave vial followed by water (0.25 ml) and TFA (0.25 ml) and the mixture heated to 100 ^{o}C in the microwave for an hour. The product was concentrated *in vacuo* and used without further purification. 0.887 mmol of 2-(3-iodopyrazol-1-yl)acetaldehyde was suspended in 5 ml of DCM. N,N-dimethylpiperidine-4-amine (1.5 eq., 1.33 mmol, 170.5 mg) was added followed by a drop of acetic acid and the mixture allowed to stir for 10 mins. Sodium triacetoxyborohydride (1.5 eq., 1.33 mmol, 281.9 mg) was added and the mixture allowed to stir for 72 hours. The mixture was concentrated *in vacuo* and purified by column chromatography, MeOH/DCM (5-10 % then 10-20 drops of NEt_3 per 100 ml) to give a thick light orange oil, (306.3 mg, 0.880 mmol, 99.2 %). **^{1}H NMR** (500 MHz, MeOD) δ 7.54 (d, J = 2.3, 1H), 6.43 (d, J = 2.3, 1H), 4.27 (t, J = 6.4, 2H), 3.10 – 3.05 (m, 1H), 3.05 – 2.99 (m, 2H), 2.85 – 2.76 (m, 8H), 2.17 (td, J = 12.0, 2.3, 2H), 2.01 (d, J = 13.2, 2H), 1.67 (tt, J = 12.1, 6.1, 2H); **^{13}C NMR** (126 MHz, MeOD) δ 132.70 (CH), 114.34 (CH), 93.40 (C), 63.39 (CH), 56.57 (CH_2), 51.40 (2x CH_2), 49.59 (CH_2), 39.17 (2xCH_2), 26.24 (CH_2); **MS** (ES +ve) $(M+H)^+$: 348.8.

Synthesis of tert-butyl N-[4-[1-[2-[4-(dimethylamino)-1-piperidyl]ethyl]pyrazol-3-yl]-2-methoxy-phenyl]carbamate (104):

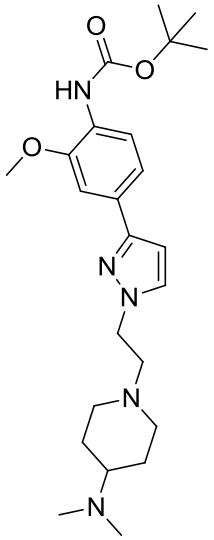

To a solution of 1-[2-(3-iodopyrazol-1-yl)ethyl]-N,N-dimethyl-piperidin-4-amine (50 mg, 0.1436 mmol) in dioxane/water (4.5 ml/0.5 ml) was added [4-(tert-butoxycarbonylamino)-3-methoxy-phenyl]boronic acid (1.5 eq., 57.6 mg, 0.215 mmol), potassium carbonate (1.5 eq., 29.7 mg, 0.215 mmol) and triphenylphosphine (20 mol %, 7.5 mg) followed by palladium acetate (5 mol %) and the mixture heated in the microwave at 120 ^{o}C for an hour. The reaction was concentrated *in vacuo* and purified by column chromatography, MeOH/DCM (5-10 %) to give a dark orange solid, (42.7 mg, 0.0963 mmol, 67.1 %). **^{1}H NMR** (500 MHz, MeOD) δ 7.88 (s, 1H), 7.69 (d, *J* = 2.3, 1H), 7.42 (d, *J* = 1.7, 1H), 7.33 (dd, *J* = 8.3, 1.8, 1H), 6.62 (d, *J* = 2.3, 1H), 4.33 (t, *J* = 6.4, 2H), 3.96 (s, 3H), 3.22 – 3.15 (m, 1H), 3.11 (s, 2H), 2.94 (s, 2H), 2.85 (d, *J* = 14.6, 6H), 2.26 (s, 2H), 2.05 (s, 2H), 1.73 (d, *J* = 8.3, 2H), 1.55 (d, *J* = 4.2, 9H); **^{13}C NMR** (126 MHz, MeOD) δ 153.56 (C), 151.55 (C), 149.10 (C), 131.77 (CH), 128.50 (C), 127.36 (C), 123.00 (C), 119.24 (CH), 117.75 (CH), 107.31 (CH), 102.25 (CH), 63.48 (CH), 56.69 (CH_2), 54.95 (CH_3), 51.21 (2x CH_2), 49.11 (CH_2), 39.19 (2x CH_3), 27.23 (3x CH_3), 26.22 (2x CH_2); **MS** (ES +ve) $(M+H)^+$: 444.2; **HRMS** (ES +ve), $C_{24}H_{38}N_5O_3$ $(M+H)^+$: calculated 444.29692, found 444.29650.

10. Experimental

10.7 Biology Methods

10.7.1 Cell Culture General

MCF7, MDA-MB-231 and SYF cells were grown in Dulbecco's Modified Eagle medium (DMEM) and PC3 cells were grown in Roswell Park Memorial Institute medium (RPMI), supplemented with serum (10% fetal bovine serum) and L-glutamine (2 mM) and incubated in a Heracell 240i tissue culture incubator at 37 °C and 5 % CO2.

10.7.2 Cell Viability Assay

Cells were plated in 96-well plates at 2000 cells/well in 100 µl of DMEM medium containing 10% FBS and 2 mM L-glutamine and incubated for 48 h in an incubator at 37 ^{o}C and 5% CO_2. After 48 hours, the media was aspirated from each well and replaced with 95 µl of fresh medium. Compounds, including DMSO, were prepared at 20X in DMEM medium in a separate 96-well intermediate plate. 5 µl from the intermediate plate was then added to each well containing cells. Untreated cells were incubated with DMSO (0.1% v/v). After 5 days, PrestoBlue™ cell viability reagent (10 µl) was added to each well and the plates incubated for 60 - 90 min. Fluorescence emission was detected using a fluorescence plate reader (excitation 540 nm, emission 590 nm). All conditions were normalised to the untreated cells (100%) and curves were fitted using a four parameter logistic fit with minimum value constrained to zero using GraphPad Prism software, to calculate EC_{50} values.

10.7.3 Apoptosis Assay - Using the IncuCyte

Cells were plated in 96-well Nunc™ black optical-bottom plates (Thermo Scientific) at 3000 cells/well in 100 µl of DMEM medium containing 10% FBS and 2 mM L-glutamine and incubated for 48h in an incubator at 37 ^{o}C and 5% CO_2. The media was replaced with 95 µl of fresh media containing NucView™ 488 from Biotium, at 1 µM concentration and drugs or DMSO added along a concentration gradient, as described in the cell viability assay, and the plates placed in the IncuCyte for incubation. Cell growth was monitored over 5 days

using phase and green fluorescence (excitation 460 nm, emission 524 nm) microscopy. Cell confluence and apoptotic (green) count was performed by the IncuCyte software.

10.7.4 Cell Cycle Assay

Cells were plated at 5000 cell/well in 100 µl of DMEM or RPMI medium containing 10% FBS and 2 mM L-glutamine in 96-well Nunc™ black optical-bottom plates and incubated at 37 ^{o}C with 5% CO_2. After 48 hours, the media was aspirated off and replaced with 95 µl of fresh media. Compounds, including DMSO, were prepared at 20X in DMEM or RMPI medium in a separate plate and 5 µl then added to each well containing cells. Untreated cells were incubated with DMSO (0.1% v/v). The cells were incubated for 24 hours at 37 ^{o}C then 100 µl of 8% PFA in PBS was added to each well and left to incubate at room temperature for 20 mins. The media/PFA was removed and wells washed with 100 µl of PBS (x3). 100 µl of blocking buffer (PBS containing 1.1% BSA and 0.2% Trixton X100) was added to each well and left for 30 minutes. 30 µl of a primary antibody solution containing anti-Cyclin B1 mixed mouse monoclonal antibody (1:300) and anti-pHH3 rabbit polyclonal antibody (1:800) was added to each well and plates incubated for an hour at room temperature. The solution was then removed and wells washed with 100 µl of blocking buffer (x3). 100 µl of blocking buffer was added to each well and plates incubated for 30 minutes at room temperature. 30 µl of a secondary antibody solution containing 4 µg/ml of DAPI, AlexaFluor® 488 Donkey anti-mouse antibody (1:500) and AlexaFluor® 594 Goat anti-rabbit antibody (1:500) was added to each well and left to incubate for 45 mins at room temperature in the dark. The solution was then removed and plates washed with 100 µl of PBS (x3) and stored in 100 µl PBS in the dark until imaged. Images were acquired using the scan^R fluorescence microscope from Olympus or ImageXpress System from Molecular Devices and analysed using scan^R or ImageXpress software. Cells were sorted according to their cell cycle state by DNA content and intensity.

10.7.5 Western Blotting Protocol

Cells were plated at 1x10^{6} cells/well in 2 ml of DMEM medium containing 10% FBS and 2 mM L-glutamine in 6-well plates and incubated at 37 ^{o}C with 5% CO_2. After 24 hours, the media was aspirated and replaced with 2 ml of DMEM medium containing 0.1 % FBS and 2 mM L-glutamine and the cells incubated for a further 24 hours. 2 µl of compounds dissolved in DMSO at appropriate concentration was then added to each well and plates incubated for

30 mins. 222 µl of FBS was then added to each well (giving a final concentration of 10%) and cells incubated for one hour. Cell lysates were then prepared using 100 µl of MD Anderson lysate buffer per well. The total cell protein concentration in each lysate was determined using Precision Red Advanced Protein Reagent #2 from Cytoskeleton. 25 µl of SDS-PAGE sample loading buffer, 10 µl of 1M DDT, lysate and water up to 100 µl to give solutions of 2-3 mg/ml were boiled at 100 ^{o}C for 3 mins. Samples were subjected to SDS-PAGE on BioRad 4-15% precast gels over 60 mins at 140 V and transferred to PVDF membranes over 150 mins at 210 mA. Membranes were blocked for an hour at room temperature using Roche's blocking buffer then primary antibodies added in 0.5 % blocking buffer at 4^{o}C overnight. Membranes were washed with TBS/T (x3, 5 mins) then secondary antibody linked to horseradish peroxidase (HRP) added for an hour at room temperature. Following further washing with TBS/T (x3, 5 mins) and TBS (x2, 5 mins) HRP was detected by peroxidase enhanced chemiluminescence (POD ECL from Roche) and bands visualised using X-ray film or the ChemiDoc™ MP Imaging System from BioRad.

10.7.6 Cell Migration Assay

Cells were plated at 50000 cells/well in 100 µl of DMEM medium containing 10% FBS and 2 mM L-glutamine in a 96-well ImageLock plate from Essen BioScience and left overnight to adhere in an incubator at 37 ^{o}C and 5% CO_2. Scratch wounds were created in each well using the WoundMaker™ supplied by Essen BioScience and each well washed with media (100 µl, x2) to remove floating cells. 95 µl of fresh media was added in each well. Compounds, including DMSO, were prepared at 20X in DMEM medium in a separate plate and 5 µl then added to each well containing cells. Untreated cells were incubated with DMSO (0.1% v/v). Images were recorded every 30 mins using the IncuCyte-ZOOM™ for 24 hours. Analysis was performed using the IncuCyte software.

10.7.7 Zebra Fish Toxicology Assay (Work performed by Dr Liz Patton and Reece Dowling, The University of Edinburgh)

Wild-type zebrafish embryos were collected from AB-TPL breeding pairs and reared at 28 °C in E3 embryo media. The embryos, 2 days post fertilisation (dpf), were treated with compound **52** or Dasatinib at 100µM, and DMSO (0.1 % v/v) as negative control, for 2 hours prior to tail amputation. The tails were then clipped from the

embryos. The embryos were incubated with drug for a further 2 hours before being washed off and replaced with fresh E3 media. For PP20 treatment, the fish were incubated for 1 hour pre-amputation and 1 hour post-amputation then replaced with fresh E3 media. The embryos were left to develop in E3 media at 28 ^{o}C for 2 days, after which, they were imaged by light microscopy.

10.7.8 hERG Channel Inhibition (Work performed by CYPROTEX DISCOVERY LIMITED)

The experiments are performed on an IonWorks™ HT Instrument (Molecular Devices Corporation), which automatically performs electrophysiology measurements in 48 single cells simultaneously. In a specialised 384-well plate (PatchPlate™), all cell suspensions, buffers and test compound solutions are at room temperature during the experiment. The cells used are Chinese hamster ovary (CHO) cells stably transfected with hERG (cell-line obtained from Cytomyx, UK). A single-cell suspension is prepared in extracellular solution (Dulbecco's phosphate buffered saline with calcium and magnesium pH 7-7.2) and aliquots added automatically to each well of a PatchPlate™. The cells are then positioned over a small hole at the bottom of each well by applying a vacuum beneath the plate to form an electrical seal. The vacuum is applied through a single compartment common to all wells which is filled with intracellular solution (buffered to pH 7.2 with HEPES). The resistance of each seal is measured via a common ground-electrode in the intracellular compartment and individual electrodes placed into each of the upper wells. Electrical access to the cells is then achieved by circulating a perforating agent, amphotericin, underneath the PatchPlate™ and then measuring the pre-compound hERG current. An electrode is positioned in the extracellular compartment and a holding potential of -80 mV applied for 15 sec. The hERG channels are then activated by applying a depolarising step to +40 mV for 5 sec and then clamped at -50 mV for 4 sec to elicit the hERG tail current, before returning to -80 mV for 0.3 s. The compound is then added automatically to the upper wells of the PatchPlate™ from a 96-well *microtitre* plate containing a range of concentrations of each compound. Solutions are prepared by diluting 10 mM DMSO solutions of the test compound into extracellular buffer such that the final concentrations tested are 0.008, 0.04, 0.2, 1, 5 and 25 µM *(*final DMSO concentration 0.25%). The test compound is left in contact with the cells for 300 sec before recording currents using the some voltage-step protocol as in the pre-compound scan. Quinidine, an established hERG inhibitor, is included as a positive control and buffer containing 0.25% DMSO is included as a negative control. The results for all compounds on the plate are rejected and the experiment repeated if the IC_{50} value for quinidine or the

negative control is outside quality-control limits. Each concentration is tested in 4 replicate wells on the PatchPlate™. However, only cells with a seal resistance greater than 50 MOhm and a pre-compound current of at least 0.1 nA are used to evaluate hERG blockade. Post-compound currents are then expressed as a percentage of pre-compound currents and plotted against concentration for each compound. Where concentration-dependent inhibition is observed, the data are fitted to the following equation and an IC_{50} value calculated:

$$Y = (V_{max}-V_{min})/(1+X/X_{50})^3 + Y_{min}$$

10.7.9 Cytochrome P450 Enzyme Inhibition (Work performed by Dr Scott Webster, The University of Edinburgh)

The P450-Glo screening system (Promega) was used to determine any effects of compounds on the activity of the CYP450 enzymes responsible for drug metabolism. The substrates used in this system are converted to a luciferin product by the CYP enzymes; luminescence is measured and represents the activity of the relevant enzyme. The hit compounds were assayed at a concentration of 10 µM. Assay buffer, substrate, positive inhibitor control and incubation times varied for each CYP enzyme assayed, these variables and concentrations for each are summarised in Table 2.3. Each compound was added at 40 µM to a separate well of a white walled 96 well plate in a volume of 12.5 µL. Compounds were prepared in luciferin-free water (with a final DMSO concentration of 1%) and assayed in duplicate. High controls contained luciferin-free water with DMSO (final concentration 1%) and low controls contained luciferin-free water only. Positive control inhibitors were assayed at a final concentration of 10 µM. Reaction mixture containing 12.5 µL of the relevant assay buffer, substrate and CYP membranes were added to the hit compounds, positive inhibitor and high control wells. To the low control wells, 12.5 µL of reaction mixture was added which contained CYP-free control membranes. The plates were sealed and placed on a plate shaker briefly to mix the contents of each well. Plates were then pre-incubated at the assay reaction temperature of 37 °C for ten minutes. The reaction was initiated by the addition of 25 µL of NADPH regeneration system. Plates were incubated at 37 °C for the duration of the activity assay (incubation time for each enzyme are shown in Table 2.3). Following incubation, luciferin detection reagent was added at a volume of 50 µL per well and the luminescence signal was left to stabilize for twenty minutes at room temperature. The luminescence signal in each well was read using a TECAN M1000 Infinite plate reader with an integration time of 1 second. The signal detected in the low control wells was averaged and subtracted from the average signal from all other wells. The signal was represented in

relative light units (RLU). Measurements obtained in the high control (vehicle only) wells were used to calculate the % inhibition of CYP activity for each compound tested.

10.7.10 Plasma Protein Binding (Work performed by Dr Scott Webster, The University of Edinburgh)

The degree of plasma protein binding was determined for each compound using rapid equilibrium dialysis (RED) device inserts in their corresponding base plates according to the protocol reported by Waters *et al* (2008). Each compound was diluted separately to a concentration of 10 µM in 200 µL of human plasma and transferred to the sample chamber of the RED device (indicated by red ring). 350 µL of PBS was added to the buffer chamber before the plate was sealed and incubated for 24 hours at 37˚C with rotation at 100 rpm. Following equilibrium dialysis, a 50 µL sample was obtained from both chambers of the RED device for each compound tested. 50 µL of PBS was added to the plasma samples (from the sample chamber) and 50 µL of plasma was added to the PBS samples (from the buffer chamber). To precipitate protein in the samples, 300 µL of ice-cold 90:10 acetonitrile:water with 0.1% formic acid (F.A.) was added to each sample. Samples were vortexed briefly then incubated on ice for 30 minutes. Samples were subject to centrifugation at 13,000 rpm for 10 minutes before the supernatant fraction was transferred to a 96 well deep well block. The supernatant was dried down under nitrogen and re-constituted in 70 µL of solvent (90:10 acetonitrile:water with 0.1% F.A.) before being transferred to a U-bottom 96 well plate for MS analysis. Zero time point samples for each compound (no 24 hour dialysis) were prepared and used as controls. Plates were frozen at -20˚C prior to MS analysis. LC-MS/MS was used to quantify the peak area of each compound in each compartment of the RED devices using MS tune settings established and validated for each compound. The peak areas detected in the 0 and 24 hour time point samples were utilised to calculate the % of compound which is bound to plasma protein.

10.7.11 Human Liver Microsome Stability (Work performed by Dr Scott Webster, The University of Edinburgh)

The microsomal stability of each compound was determined using human (or rat) liver microsomes. Microsomes were thawed and diluted to a concentration of 2 mg/mL in 50 mM $NaPO_4$ buffer pH 7.4. Each compound was diluted in 4 mM NADPH (made in the phosphate buffer above) to a concentration of 10 µM. Two identical incubation plates were prepared to act as a 0 minute and a 30 minute time point assay. 30 µL of each compound

dilution was added in duplicate to the wells of a U-bottom 96 well plate and warmed at 37˚C for approximately 5 minutes. Verapamil, lidocaine and propranolol were utilised as reference compounds in this experiment. Microsomes were also pre-warmed at 37˚C before the addition of 30 µL to each well of the plate resulting in a final concentration of 1 mg/mL. The reaction was terminated at the appropriate time point (0 or 30 minutes) by addition of 60 µL of ice-cold 0.3M trichloroacetic acid (TCA) per well. The plates were centrifuged for 10 minutes at 1000 rpm and the supernatant fraction transferred to a fresh U-bottom 96 well plate. Plates were sealed and frozen at -20˚C prior to MS analysis. LC-MS/MS was used to quantify the peak area response of each compound before and after incubation with human liver microsomes using MS tune settings established and validated for each compound. These peak intensity measurements were used to calculate the % remaining after incubation with human microsomes for each hit compound.

10.7.12 Human, Mouse and Rat Plasma Stability (Work performed by CYPROTEX DISCOVERY LIMITED)

Plasma is adjusted to pH 7.4 using either hydrochloric acid or sodium hydroxide depending on the initial pH of the plasma. Incubations are performed at a test or control compound concentration of 1 µM in plasma, pH 7.4, at 37^{o}C. The final DMSO concentration in the incubation is 2.5%. Reactions are terminated following 0, 15, 30, 60 and 120min by methanol containing internal standard. The sampling plate is centrifuged (2500rpm, 45min, 4^{o}C) and the supernatants from each time point pooled in cassettes of up to 4 compounds. Samples are analysed for parent compound by LC-MS/MS using Cyprotex generic analytical conditions. The percentage of parent compound remaining at each time point relative to the 0 min sample is then calculated from LC-MS/MS peak area ratios (compound peak area/internal standard peak area).

10.7.13 Hepatocyte Stability (Work performed by CYPROTEX DISCOVERY LIMITED)

Cryopreserved pooled hepatocytes are purchased from a reputable commercial supplier and stored in liquid nitrogen prior to use. Williams E media supplemented with 2 mM L-glutamine and 25 mM HEPES and test compound (final substrate concentration 3 µM; final DMSO concentration 0.25 %) are pre-incubated at 37°C prior to the addition of a suspension of cryopreserved hepatocytes (final cell density 0.5 x $l0^{6}$ viable cells/ml in Williams E media

supplemented with 2 mM L-glutamine and 25 mM HEPES) to initiate the reaction. The final incubation volume Is 500 µl. A control incubation is included for each compound tested where lysed cells are added instead of viable cells. Two control compounds are included with each species. The reactions are stopped by transferring 50 µl of incubate to 100 µl methanol containing internal standard at the appropriate time points. The control (lysed cells) is incubated for 60 min only. The termination plates are centrifuged at 2500 rpm at 4 °C for 30 min to precipitate the protein. Following protein precipitation, the sample supernatants are combined in cassettes of up to 4 compounds and analysed using Cyprotex generic LC-MS/MS conditions. From a plot of in peak area ratio (compound peak area/internal standard peak area) against time, the gradient of the line is determined. Subsequently, half-life ($t_{1/2}$) and intrinsic clearance (CL_{int}) are calculated using the equations below:

$$\text{Elimination rate constant (k)} = (-\text{gradient})$$

$$\text{Half-life } (t_{1/2}) \text{ (min)} = 0693/k$$

$$\text{Intrinsic clearance } (CL_{int}) \text{ (µl/min/million cells)} = (V \times 0.393)/t_{1/2}$$

Where V = incubation volume (µl)/number of cells.

*10.7.14 **Pharmacokinetic Analysis** (Work performed by CYPROTEX DISCOVERY LIMITED)*

Three female CD1 mice, 25-30g, were dosed per administration route per time point, per compound. The test compound was administered either orally or intravenously (typical dose level of 10 mg compound per kg body weight). Animals were given free access to food throughout the study. At the following time points, the animals were anaesthetised, blood collected in heparinised tubes and animals sacrificed:

Oral dosing: 0.08, 0.25, 0.5, 1, 2, 4 and 8 hour post dose.

IV dosing: 0.08, 0.25, 0.5, 1, 2, 4 and 8 hour post dose.

*10.7.15 **Kinase Screening Assay** (Work performed by Reaction Biology Corp.)*

Compound IC_{50} values were determined from 10-point, 1:3 dilution curves starting at either 100 µM or 10 µM with 10µM ATP, by Reaction Biology Corp. For the whole kinome screen

compounds were screened against 340 wild type kinases at a single dose of 10 or 1 μM, in duplicate, with 10 μM of ATP. The data was averaged and plotted as percentage enzyme activity relative to DMSO, as negative control, using DiscoverRX TREEspot™ software.

References

1. Bleicher, K.H., Böhm, H. J., Müller, K., and Alanine, A. I., *Hit and lead generation: beyond high-throughput screening. .* Nature Reviews Drug Discovery, 2003. **2**: p. 369-378.
2. Holdgate, G., Geschwindner, S., Breeze, A., Davies, G., Colclough, N., Temesi, D. and Ward, L., *Biophysical Methods in Drug Discovery from Small Molecule to Pharmaceutical. .* Methods in Molecular Biology, 2013. **1008**: p. 327-355.
3. Hughes, J.P., Rees, S., Kalindjian, S. B. and Philpott, K. L., *Principles of early drug discovery* British Journal of Pharmacology, 2011. **162**: p. 1239-1249.
4. McInnes, C., *Virtual screening strategies in drug discovery.* Current Opinion in Chemical Biology, 2007. **11**: p. 494-502.
5. Smith, A., *Screening for drug discovery.* Nature, 2002. **418**: p. 451-463.
6. Kamb, A., Wee, S. and Lengauer, C., *Why is cancer drug discovery so difficult?* Nature Reviews Drug Discovery, 2007. **6**: p. 115-120.
7. Chin, L., and Gray, J. W. , *Translating insights from the cancer genome into clinical practice. .* Nature, 2008. **452**: p. 553-563.
8. Stommel, J.M., Kimmelman, A. C., Ying, H., Nabioullin, R., Ponugoti, A. H., Wiedemeyer, R., Stegh, A. H., Bradner, J. E., Ligon, K. L., Brennan, C., Chin, L. and DePinho, R. A., *Coactivation of receptor tyrosine kinases affects the response of tumor cells to targeted therapies. .* Science, 2007. **318**: p. 287-290.
9. Mullard, A., *New drugs cost US$2.6 billion to develop.* Nature Reviews Drug Discovery, 2014. **13**: p. 877.
10. Swinney, D.C., and Anthony, J., *How were new medicines discovered?* Nature Reviews Drug Discovery, 2011. **10**: p. 507-519.
11. Carragher, N., Unciti-Broceta, A., and Cameron, D., *Advancing cancer drug discovery towards more agile development of targeted combination therapies. .* Future Medicinal Chemistry, 2012. **4**: p. 87-105.
12. Knight, Z.A., Lin, H. and Shokat, K. M. , *Targeting the cancer kinome through polypharmacology. .* Nature Reviews Cancer, 2010. **10**: p. 130-137.
13. Mangana, J., Levesque, M. P., Karpova, M. B. and Dummer, R., *Sorafenib in melanoma.* Expert Opinion Investigational Drugs, 2012. **21**: p. 557-568.
14. Zhang, J., Yang, P. L. and Gray, N. S., *Targeting cancer with small molecule kinase inhibitors.* Nature Reviews, 2009. **9**: p. 28-39.
15. Basilico, C., et. Al., *Tivantinib (ARQ 197) displays cytotoxic activity that is independant of its ability to bind MET.* Clinical Cancer Research, 2013. **19**: p. 2381-2392.
16. Katayama, R.e.A., *Cytotoxic activity of tivantinib (ARQ 197) is not due solely to c-MET inhibition.* Cancer Research, 2013. **73**: p. 3087-3096.
17. Lee, J.A., Uhlik, M. T., Moxham, C. M., Tomandl, D. and Sall, D. J., *Modern phenotypic drug discovery is a viable, neoclassic pharma strategy.* Journal of Medicinal Chemistry, 2012. **55**: p. 4527-4538.
18. Weiss, J.T., Dawson, J. C., Macleod, K. G., Rybski, W., Fraser, C., Torres-Sánchez, C., Patton, E. E., Bradley, M., Carragher, N. O. and Unciti-Broceta, A. , *Extracellular palladium-catalyzed dealkylation of 5-fluoro-1-propargyl-uracil as a bioorthogonally-activated prodrug approach. .* Nature Communications, 2014. **5**: p. 3277-3286.

19. Carragher N. O., B.V.G., and Frame M.C. , *Combining imaging and pathway profiling: an alternative approach to cancer drug discovery.* Drug Discovery Today, 2012. **17**: p. 203-214.
20. Swinney, D.C., *Phenotypic versus target-based drug discovery for first-in-class medicines.* Clinical Pharmacology & Therapeutics, 2013. **93**: p. 299-301.
21. DeVita, V.T., and Chu, E., *A history of cancer chemotherapy.* Cancer Research, 2008. **68**: p. 8643-8653.
22. Terstappen, G.C., Schlüpen, C., Raggiaschi, R. and Gaviraghi, G., *Target deconvolution stategies in drug discovery.* Nature Reviews Drug Discovery, 2007. **6**: p. 891-903.
23. Moffat, J.G., Rudolph, J. and Bailey, D., *Phenotypic screening in cancer drug discovery - past, present and future.* Nature Reviews Drug Discovery, 2014. **13**: p. 588-602.
24. Justoni, R., and Fusco, R., Gazzetta Chimica Italiana, 1938. **68**: p. 66.
25. Robins, R.K., *Potential Purine Antagonists. I. Synthesis of Some 4,6-Substituted Pyrazolo [3,4-d] pyrimidines.* Journal of the American Chemical Society, 1955. **78**: p. 784-790.
26. Davies, L.P., Brown, D. J., Chow, S. C., and Johnston, G. A. R., *Pyrazolo [3,4-d] pyrimidines, a new class of adenosine antagonists.* Neuroscience Letters, 1983. **41**: p. 189-193.
27. Davies, L.P., Chow, S. C., Skerritt, J. H., Brown, D. J., and Johnston, G. A. R., *Pyrazolo[3, 4-d]pyrimidines as adenosine antagonists.* Life Science, 1984. **34**: p. 2117-2128.
28. Cottam, H.B., Petrie, C. R., McKernan, P. A., Goebel, R. J., Dalley, N. K., Davidson, R. B., Robins, R. K., and Revankar, G. R., *Synthesis and Biological Activity of Certain 3,4-Disubstituted Pyrazolo[3,4-d]pyrimidine Nucleosides.* Journal of Medicinal Chemistry, 1984. **27**: p. 1119-1137.
29. Cohen, P., *Protein Kinases - The Major Drug Targets of the Twenty-First Century?* Nature Reviews, 2002. **1**: p. 6.
30. Cottam H. B., W.D.B., Shih H. C., Raychaudhuri A., Pasquale G. D., and Carson D. A., *New Adenosine Kinase Inhibitors with Oral Antiinflammatory Activity: Synthesis and Biological Evaluation.* Journal of Medicinal Chemistry, 1993. **36**: p. 3424-3430.
31. Fincham, V., Frame, M., Haefner, B., Unlu, M., Wyke, A. and Wyke, J., *Functions of the v-SRC protein tyrosine kinase.* Cell Biology International, 1994. **18**: p. 337-344.
32. Aleshin, A., and Finn, R. S., *SRC: A Century of Science Brought to the Clinic.* Neoplasia, 2010. **12**: p. 599-607.
33. Hanke, J.H., Gardner, J. P., Dow, R. L., Changelian, P. S., Brissette, W. H., Weringer, E. J., Pollok, B. A. and Connelly, P. A., *Discovery of a Novel, Potent, and Src Family-selective Tyrosine Kinase Inhibitor: Study of LCK and FYNT-Dependent T Cell Activation.* Journal of Biological Chemistry, 1996. **271**(2): p. 6.
34. Bishop, A.C., Kung, C., Shah, K., Witucki, L., Shokat, K. M., and Liu, Y., *Generation of Monospecific Nanomolar Tyrosine Kinase Inhibitors via a Chemical Genetic Approach.* Journal of the American Chemical Society, 1999. **121**: p. 627-631.
35. Hsieh, A.C., et. Al., *The translational landscape of mTOR signalling steers cancer initiation and metastasis.* Nature, 2012. **485**: p. 55-61.
36. Laplante, M.a.S., D. M., *mTOR Signaling in Growth Control and Disease.* Cell, 2012. **149**: p. 274-293.
37. Laplante, M.a.S., D. M., *mTOR signaling at a glance.* Journal of Cell Science, 2009. **122**: p. 3589-3594.

38. Guertin, D.A.a.S., D. M., *Defining the Role of mTOR in Cancer.* Cancer Cell, 2007. **12**: p. 9-22.
39. Sarbassov, D.D., Ali, S. M., Kim, D. H., Guertin, D. A., Latek, R. R., Erdjument-Bromage, H., Tempst, P. and Sabatini, D. M., *Rictor, a novel binding partner of mTOR, defines a rapamycin-insensitive and raptor independent pathway that regulates the cytoskeleton.* Current Biology, 2004. **14**: p. 1296-1302.
40. Jacinto, E., Loewith, R., Schmidt, A., Lin, S., Ruegg, M.A., Hall, A., and Hall, M.N., *Mammalian TOR complex 2 controls the actin cytoskeleton and is rapamycin insensitive.* Nature Cell Biology, 2004. **6**: p. 1122-1128.
41. Richter, J.D.a.S., N., *Regulation of cap-dependent translation by eIF4E inhibitory proteins.* Nature, 2005. **433**: p. 477-480.
42. Ma, X.M.a.B., J., *Molecular mechanisms of mTOR-mediated translational control.* Nature Reviews Molecular Cell Biology, 2009. **10**: p. 307-318.
43. Codogno, P., and Meijer, A. J., *Autophagy and signaling: their role in cell survival and cell death.* Cell Death & Differentiation, 2005. **12**: p. 1509-1518.
44. Ganley, I.G., Lam du, H., Wang, J., Ding, X., Chen, S. and Jiang, X., *ULK1.ATG13.FIP200 complex mediates mTOR signaling and is essential for autophagy.* Journal of Biological Chemistry, 2009. **284**: p. 12297-12305.
45. Hosokawa, N., Hara, T., Kaizuka, T., Kishi, C., Takamura, A., Miura, Y., Iemura, S., Natsume, T., Takehana, K., Yamada, N. et. Al., *Nutrient dependent mTORC1 association with the ULK1-Atg13-FIP200 complex required for autophagy.* Molecular Biology of the Cell, 2009. **20**: p. 1981-1991.
46. Jung, C.H., Jun, C. B., Ro, S. H., Kim, Y. M., Otto, N. M., Cao, J., Kundu, M. and Kim, D. H., *ULK-Atg13-FIP200 complexes mediate mTOR signaling to the autophagy machinery.* Molecular Biology of the Cel, 2009. **20**: p. 1992-2003.
47. Porstmann, T., Santos, C. R., Griffiths, B., Cully, M., Wu, M., Leevers, S., Griffiths, J. R., Chung, Y. L. and Schulze, A., *SREBP activity is regulated by mTORC1 and contributes to Akt-dependent cell growth.* Cell Metabolism, 2008. **8**: p. 224-236.
48. Kim, J.E., and Chen, J., *Regulation of peroxisome proliferator-activated receptor-gamma activity by mammalian target of rapamycin and amino acids in adipogenesis.* Diabetes, 2004. **53**: p. 2748-2756.
49. Hardie, D.G., *AMP-activated/SNF1 protein kinases: conserved guardians of cellular energy.* Nature Reviews Molecular Cell Biology, 2007. **8**: p. 774-785.
50. Wouters, B.G., and Koritzinsky, M., *Hypoxia signalling through mTOR and the unfolded protein response in cancer.* Nature Reviews Cancer, 2008. **8**: p. 851-864.
51. Kim, E., Goraksha-Hicks, P., Li, L., Neufeld, T. P. and Guan, K. L., *Regulation of TORC1 by Rag GTPases in nutrient response.* Nature Cell Biology, 2008. **10**: p. 935-945.
52. Sancak, Y., Peterson, T. R., Shaul, Y. D., Lindquist, R. A., Thoreen, C. C., Bar-Peled, L. and Sabatini, D. M., *The Rag GTPases bind raptor and mediate amino acid signaling to mTORC1.* Science, 2008. **320**(1496-1501).
53. Feng, Z., Zhang, H., Levine, A. J. and Jin, S., *The coordinate regulation of the p53 and mTOR pathways in cells.* Proceedings of the National Academy of Sciences USA, 2005. **102**: p. 8204-8209.
54. Lee, D.F., Kuo, H. P., Chen, C. T., Hsu, J. M., Chou, C. K., Wei, Y., Sun, H. L., Li, L. Y., Ping, B., Huang, W. C. et. Al., *IKK beta suppression of TSC1 links inflammation and tumor angiogenesis via the mTOR pathway.* Cell, 2007. **130**: p. 440-455.
55. Sarbassov, D.D., Ali, S.M., Sengupta, S., Sheen, J.H., Hsu, P.P., Bagley, A.F., Markhard, A.L., and Sabatini, D.M., *Prolonged rapamycin treatment inhibits mTORC2 assembly and Akt/PKB.* Molecular Cell, 2006. **22**: p. 159-168.

56. Sarbassov, D.D., Guertin, D.A., Ali, S.M., and Sabatini, D.M., *Phosphorylation and regulation of Akt/PKB by the rictor-mTOR complex.* Science, 2005. **307**: p. 1098-1101.
57. Fayard, E., Tintignac, L. A., Baudry, A. and Hemmings, B. A., *Protein kinase B/Akt at a glance.* Journal of Cell Science, 2005. **118**: p. 5675-5678.
58. Yuan, T., and Cantley, L. C., *PI3K pathway alterations in cancer: variations on a theme.* Oncogene, 2008. **27**: p. 5497-5510.
59. Zoncu, R., Efeyan, A., and Sabantini, D. M., *mTOR: from growth signal integration to cancer, diabetes and ageing.* Nature Reviews, 2011. **12**: p. 12-35.
60. Dowling, R.J., Topisirovic, I., Alain, T., Bidinosti, M., Fonseca, B.D., Petroulakis, E., Wang, X., Larsson, O., Selvaraj, A., Liu, Y., et. Al., *mTORC1-mediated cell proliferation, but not cell growth, controlled by the 4E-BPs.* Science, 2010. **328**: p. 1172-1176.
61. Menendez, J.a.L., R., *Fatty acid synthase and the lipogenic phenotype in cancer pathogenesis.* Nature Reviews Cancer, 2007. **7**: p. 763-777.
62. Thomas, G.V.e.A., *Hypoxia-inducible factor determines sensitivity to inhibitors of mTOR in kidney cancer.* Nature Medicine, 2006. **12**: p. 122-127.
63. Guertin, D.A., Stevens, D.M., Saitoh, M., Kinkel, S., Crosby, K., Sheen, J.H., Mullholland, D.J., Magnuson, M.A., Wu, H., and Sabatini, D.M., *mTOR complex 2 is required for the development of prostate cancer induced by Pten loss in mice.* Cancer Cell, 2009. **15**: p. 148-159.
64. Masri, J., Bernath, A., Martin, J., Jo, O.D., Vartanian, R., Funk, A., and Gera, J., *mTORC2 activity is elevated in gliomas and promotes growth and cell motility via overexpression of rictor.* Cancer Research, 2007. **67**: p. 11712-11720.
65. Ballou, L.M., and Lin. R. Z., *Rapamycin and mTOR kinase inhibitors.* Journal of Chemical Biology, 2008. **1**: p. 27-36.
66. Neshat, M.S., Mellinghoff, I.K., Tran, C., Stiles, B., Thomas, G., Petersen, R., Frost, P., Gibbons, J.J., Wu, H., and Sawyers, C.L., *Enhanced sensitivity of PTEN-deficient tumors to inhibition of FRAP/mTOR.* Proceedings of the National Academy of Sciences USA, 2001. **98**: p. 10314-10319.
67. Wan, X., Harkavy, B., Shen, N., Grohar, P. and Helman L. J., *Rapamycin induces feedback activation of Akt signaling through an IGF-1R-dependent mechanism.* Oncogene, 2007. **26**: p. 1932-1940.
68. Wang, B.T., Ducker, G.S., Barczak, A.J., Barbeau, R., Erle, D.J., and Shokat, K.M., *The mammalian target of rapamycin regulates cholesterol biosynthetic gene expression and exhibits a rapamycin-resistant transcriptional profile.* Proceedings of the National Academy of Sciences USA, 2011. **108**: p. 15201-15206.
69. Guertin, D.A., Stevens, D.M., Thoreen, C.C., Burds, A.A., Kalaany, N.Y., Moffat, J., Brown, M., Fitzgerald, K.J., and Sabatini, D.M., *Ablation in mice of the mTORC components raptor, rictor, or mLST8 reveals that mTORC2 is required for signaling to Akt-FOXO and PKCalpha, but not S6K1.* Developmental Cell, 2006. **11**: p. 859-871.
70. Zhang, Y., Duan, Y. and Zheng, S., *Targeting the mTOR kinase domain: the second generation of mTOR inhibitors.* Drug Discovery Today, 2011. **16**: p. 325-331.
71. Martin, G.S., *The hunting of the Src.* Nature Reviews Molecular Cell Biology, 2001. **2**: p. 467-475.
72. Yeatman, T.J., *A RENAISSANCE FOR SRC.* Nature Reviews Cancer, 2004. **4**: p. 470-480.
73. Parsons, S.J., and Parsons, J. T., *Src family kinases, key regulators of signal transduction.* Oncogene, 2004. **23**: p. 7906-7909.

74. Masaki, T., Okada, M., Tokuda, M., Shiratori, Y., Hatase, O., Shirai, M., Nishioka, M. and Omata, M., *Reduced C-terminal Src kinase (CSK) activities in hepatocellular carcinoma.* Hepatology, 1999. **29**: p. 379-384.
75. Schaller, M.D., Hildebrand, J. D., Shanon, J. D., Fox, J. W., Vines, R. R. and Parsons, J. T., *Autophosphorylation of the focal adhesion kinase, pp125FAK, directs SH2-dependent binding of pp60src.* Molecular and Cellular Biology, 1994. **14**: p. 1680-1688.
76. Westhoff, M.A., Serrels, B., Fincham, V. J., Frame, M. C. and Carragher, N. O., *SRC-mediated phosphorylation of focal adhesion kinase couples actin and adhesion dynamics to survival signaling.* Molecular and Cellular Biology, 2004. **24**: p. 8113-8133.
77. Hanahan, D., and Weinber, R. A., *Hallmarks of Cancer: The Next Generation.* Cell, 2011. **144**: p. 646-674.
78. Roche, S., Fumagalli, S. and Courtneige, S. A., *Requirement for Src family protein tyrosine kinases in G2 for fibroblast cell division.* Science, 1995. **269**: p. 1567-1569.
79. Frame, M.C., Fincham, V. J., Carragher, C. O. and Wyke, J. A., *v-SRC's hold over actin and cell adhesions.* Nature Reviews Molecular Cell Biology, 2002. **3**: p. 233-245.
80. Bjorge, J.D., Jakymiw, A., and Fujita, D. J., *Selected glimpses into the activation and function of Src kinase.* Oncogene, 2000. **19**: p. 5620-5635.
81. Nam, J.S., Ino, Y., Sakamoto, M. and Hirohashi, S., *Src family kinase inhibitor PP2 restores the E-cadherin/catenin cell adhesion system in human cancer cells and reduces cancer metastasis.* Clinical Cancer Research, 2002. **8**: p. 2430-2436.
82. Irby, R.B.a.Y., T. J., *Increased Src activity disrupts cadherin/catenin–mediated homotypic adhesion in human colon cancer and transformed rodent cells.* Cancer Research, 2002. **62**: p. 2669-2674.
83. Guarino, M., *Src signaling in cancer invasion.* Journal of Cell Physiology, 2010. **223**: p. 14-26.
84. McLean, G.W., Carragher, N. O., Avizienyte, E., Evans, J., Brunton, V. G. and Frame, M. C., *The role of focal-adhesion kinase in cancer—a new therapeutic opportunity.* Nature Reviews Cancer, 2005. **5**: p. 505-515.
85. Yu, C.L., Meyer, D. J., Campbell, G. S., Larner, A. C., Carter-Su, C., Schwartz, J. and Jove, R., *Enhanced DNA-binding activity of a Stat3-related protein in cells transformed by the Src oncoprotein.* Science, 1995. **269**: p. 81-83.
86. Niu, G.e.A., *Constitutive Stat3 activity up-regulates VEGF expression and tumor angiogenesis.* Oncogene, 2002. **21**: p. 2000-2008.
87. Kilarski, W.W., Jura, N. and Gerwins, P., *Inactivation of Src family kinases inhibits angiogenesis in vivo: implications for a mechanism involving organization of the actin cytoskeleton.* Experimental Cell Research 2003. **291**: p. 70-82.
88. Werdich, X.Q., and Penn, J. S., *Src, Fyn and Yes play differential roles in VEGF-mediated endothelial cell events.* Angiogenesis, 2005. **8**: p. 315-326.
89. Miyazaki, T., Tanaka, S., Sanjay, A. and Baron, R., *The role of c-Src kinase in the regulation of osteoclast function.* Modern Rheumatology, 2006. **16**: p. 68-74.
90. Boyce, B.F., Xing, L., Yao, Z., Yamashita, T., Shakespeare, W. C., Wang, Y., Metcalf, C. A., Sundaramoorthi, R., Dalgarno, D. C., Iuliucci, J. D., and Sawyer, T. K. , *SRC inhibitors in metastatic bone disease.* Clinical Cancer Research, 2006. **12**: p. 6291-6295.
91. Hanke, J.H., Gardner, J. P., Dow, R. L., Changelian, P. S., Brissette, W. H., Weringer, E. J., Pollok, B. A. and Connelly, P. A., *Discovery of a novel, potent, and Src family-selective tyrosine kinase inhibitor. Study of Lck- and FynT-dependent T cell activation.* Journal of Biological Chemistry, 1996. **271**: p. 695-701.

92. Apsel, B., Blair, J. A., Gonzalez, B., Nazif, T. M., Feldman, M. E., Aizenstein, B., Hoffman, R., Williams, R. L., Shokat, K. M., and Knight, Z. A., *Targeted polypharmacology: discovery of dual inhibitors of tyrosine and phosphoinositide kinases.* Nature Chemical Biology, 2008. **4**: p. 691-699.
93. Puls, L.N., Eadens, M. and Messersmith, W., *Current Status of Src Inhibitors in Solid Tumor Malignancies.* The Oncologist, 2011. **16**: p. 566-578.
94. Duxbury, M.S., Ito, H., Zinner, M. J., Ashley, S. W., and Whang, E. E., *siRNA directed against c-Src enhances pancreatic adenocarcinoma cell gemcitabine chemosensitivity.* Journal of the American Collage of Surgeons, 2004. **198**: p. 953-959.
95. George, J.A., Chen, T., and Taylor, C. C., *SRC tyrosine kinase and multidrug resistance protein-1 inhibitions act independently but cooperatively to restore paclitaxel sensitivity to paclitaxel-resistant ovarian cancer cells.* Cancer Research, 2005. **65**: p. 10381-10388.
96. Kopetz, S., et. Al., *Synergistic activity of the SRC family kinase inhibitor dasatinib and oxaliplatin in colon carcinoma cells is mediated by oxidative stress.* Cancer Research, 2009. **69**: p. 3842-3849.
97. Hiscox, S., Jordan, N. J., Smith, C., James, M., Morgan, L., Taylor, K. M., Green, T. P., and Nicholson, R. I., *Dual targeting of Src and ER prevents acquired anti-hormone resistance in breast cancer cells.* Breast Cancer Research and Treatment, 2009. **115**: p. 57-67.
98. Wheeler, D.L., Iida, M., Kruser, T. J., Nechrebecki, M. M., Dunn, E. F., Armstrong, E. A., Huang, S., and Harari, P. M., *Epidermal growth factor receptor cooperates with Src family kinases in acquired resistance to cetuximab.* Cancer Biology & Therapy, 2009. **8**: p. 696-703.
99. Paul, S.M., Mytelka, D. S., Dunwiddie, C. T., Persinger, C. C., Munos, B. H., Lindborg, S. R. and Schacht, A. L., *How to improve R&D productivity: the pharmaceutical industry's grand challenge.* Nature Reviews Drug Discovery, 2010. **9**: p. 203-214.
100. Yildirim, M.A., Goh, K., Cusick, M. E., Barabási, A. and Vidal, M., *Drug-target network.* Nature Biotechnology, 2007. **25**: p. 1119-1126.
101. Fabian, M.A., et. Al., *A small molecule–kinase interaction map for clinical kinase inhibitors.* Nature Biotechnology, 2005. **23**: p. 329-336.
102. Bishop, A.C., Buzko, O., and Shokat, K. M., *Magic bullets for protein kinases.* Trends in Cell Biology, 2001. **11**(4): p. 167-172.
103. Tatton, L., Morley, G. M., Chopra, R. and Khwaja, A., *The Src-selective Kinase Inhibitor PP1 Also Inhibits Kit and Bcr-Abl Tyrosine Kinases.* Journal of Biological Chemistry, 2003. **278**: p. 4847-4853.
104. Jester, B.W., Gaj, A., Shomin, C. D., Cox, K. J., and Ghosh, I., *Testing the Promiscuity of Commercial Kinase Inhibitors Against the AGC Kinase Group Using a Split-luciferase Screen.* Journal of Medicinal Chemistry, 2012. **55**: p. 1526-1537.
105. Dinér, P., Alao, J. P., Söderlund, J., Sunnerhagen, P., and Grøtli, M., *Preparation of 3-Substituted-1-Isopropyl-1H-pyrazolo[3,4-d]pyrimidin-4-amines as RET Kinase Inhibitors.* Journal of Medicinal Chemistry, 2012. **55**: p. 4872-4876.
106. Bain, J., McLauchlan, H., Elliott, M., and Cohen, P., *The specificities of protein kinase inhibitors: an update.* Biochemical Journal, 2003. **371**: p. 199-204.
107. Hay, N., and Sonenber, N., *Upstream and downstream of mTOR.* Genes and Development, 2004. **18**: p. 1926-1945.
108. Pike, K.G., Malagu, K., Hummersone, M. G., Menear, K. A., Duggan, H. M. E.,Gomez, S., Martin, N. M. B., Ruston, L., Pass, S. L. and Pass, M., *Optimization of potent and*

selective dual mTORC1 and mTORC2 inhibitors: The discovery of AZD8055 and AZD2014. Bioorganic & Medicinal Chemistry Letters, 2013. **23**: p. 1212-1216.
109. Yang, H., Rudge, D. G., Koos, J. D., Vaidialingam, B., Yang, H. J. and Pavletich, N. P., *mTOR kinase structure, mechanism and regulation.* Nature, 2013. **497**: p. 217-224.
110. Hsu, F., Zhang, S., and Chen, B. P.C., *Role of DNA-dependent protein kinase catalytic subunit in cancer development and treatment.* Translational Cancer Research, 2012. **1**: p. 22-34.
111. Miao, L., Zhu, S., Wang, Y., Li., Ding, J., Dai, J., Cai, H., Zhang, D. and Song, Y., *Discoidin domain receptor 1 is associated with poor prognosis of non-small cell lung cancer and promotes cell invasion via epithelial-to-mesenchymal transition.* Medical Oncology, 2013. **30**: p. 626-635.
112. Soliman, G.A., Acosta-Jaquez, A., Dunlop, E. A., Ekim, B., Maj, N. E., Tee, A. R. and Fingar, D. C., *mTOR Ser-2481 Autophosphorylation Monitors mTORC-specific Catalytic Activity and Clarifies Rapamycin Mechanism of Action.* The Journal of Biological Chemistry, 2009. **285**: p. 7866-7879.
113. Chiang, G.G., and Abraham, R. T., *Phosphorylation of Mammalian Target of Rapamycin (mTOR) at Ser-2448 Is Mediated by p70S6 Kinase.* The Journal of Biological Chemistry, 2005. **280**: p. 25485-25490.
114. Brandvold, K.R., Steffey, M. E., Fox, C. C., and Soellner, M. B., *Development of a Highly Selective c-Src Kinase Inhibitor.* ACS Chemical Biology, 2012. **7**: p. 1393-1398.
115. Allington, T.M., and Schiemann, W. P., *The Cain and Abl of Epithelial-Mesenchymal Transition and Transforming Growth Factor-β in Mammary Epithelial Cells.* Cells Tissues Organs, 2011. **193**: p. 98-113.
116. Manning, G., Whyte, D. B., Martinez, R., Hunter, T. and Sudarsanam, S., *The Protein Kinase Complement of the Human Genome.* Science, 2002. **298**: p. 1912-1934.
117. Ostrander, J.H., Daniel, A. R. and Lange, C. A., *Brk/PTK6 Signaling in Normal and Cancer Cell Models.* Current Opinion in Pharmacology, 2010. **10**: p. 662-669.
118. Anderson, T.M.R., et. Al., *Breast Tumor Kinase (Brk/PTK6) Is a Mediator of Hypoxia-Associated Breast Cancer Progression.* Cancer Research, 2013. **73**: p. 5810-5820.
119. Chen, H., Shen, C., Tsai, Y., Lin, F., Huang, Y. and Chen R., *Brk Activates Rac1 and Promotes Cell Migration and Invasion by Phosphorylating Paxillin.* Molecular and Cellular Biology, 2004. **24**: p. 10558-10572.
120. Kramer, N., Walzl, A., Unger, C., Rosner, M., Krupitza, G., Hengstschläger, M. and Dolznig, H., *In vitro cell migration and invasion assays.* Mutation Research, 2013. **752**: p. 10-24.
121. Chen, R., Kim, O., Yang, J., Sato, K., Eisenmann, K. M., McCarthy, J., Chen, H. and Qiu, Y., *Regulation of Akt/PKB Activation by Tyrosine Phosphorylation.* Journal of Biological Chemistry, 2001. **276**: p. 31858-31862.
122. Zheng, Y., and Tyner, A. L., *Context-specific protein tyrosine kinase 6 (PTK6) signalling in prostate cancer.* European Journal of Clinical Investigation, 2013. **43**: p. 397-404.
123. Lieschke, G.J.a.C., P. D., *Animal models of human disease: zebrafish swim into view.* Nature Reviews, 2007. **8**: p. 353-367.
124. White, R., Rose, K. and Zon, L., *Zebrafish cancer: the state of the art and the path forward.* Nature Reviews, 2013. **13**: p. 624-636.
125. Yoo, S.K., Freisinger, C. M., LeBert, D. C. and Huttenlocher, A., *Early redox, Src family kinase, and calcium signaling integrate wound responses and tissue regeneration in zebrafish.* Journal of Cell Biology, 2012. **199**: p. 225-234.
126. Kerkelä, R., et. Al., *Cardiotoxicity of the cancer therapeutic agent imatinib mesylate.* Nature Medicine, 2006. **12**: p. 908-916.

127. Chen, M.H., Kerkelä, R. and Force, T., *Mechanisms of Cardiac Dysfunction Associated With Tyrosine Kinase Inhibitor Cancer Therapeutics.* Circulation, 2008. **118**: p. 84-95.
128. Yeh, E.T.H.a.B., C. L., *Cardiovascular Complications of Cancer Therapy.* Journal of the American College of Cardiology, 2009. **53**: p. 2231-2247.
129. Qui, Z., Cang, Y. and Goff, S. P., *c-Abl tyrosine kinase regulates cardiac growth and development.* Proceedings of the National Academy of Sciences USA, 2010. **107**(1136-1141).
130. Knowles, P.P., Murray-Rust, J., Klær, S., Scott, R. P., Hanrahan, S., Santoro, M., Ibañez, C. F. and McDonald N. Q., *Structure and Chemical Inhibition of the RET Tyrosine Kinase Domain.* The Journal of Biological Chemistry, 2006. **281**: p. 33577-33587.
131. Sundaramoorthi, R.e.A., *Bone-Targeted Src Kinase Inhibitors: Novel Pyrrolo and Pyrazolopyrimidine Analogues.* Bioorganic & Medicinal Chemistry Letters, 2003. **13**: p. 3063-3066.
132. Lipinski, C.A., Lombardo, F., Dominy, B. W. and Feeney, P. J., *Experimental and computational approaches to estimate solubility and permeability in drug discovery and development settings* Advanced Drug Delivery Reviews, 1997. **23**: p. 3-25.
133. Ertl, P., Rohde B. and Selzer P., *Fast Calculation of Molecular Polar Surface Area as a Sum of Fragment-Based Contributions and Its Application to the Prediction of Drug Transport Properties.* Journal of Medicinal Chemistry, 2000. **43**: p. 3714-3717.
134. Palm, K., Stenberg, P., Luthman, K. and Artursson, P., *Polar Molecular Surface Properties Predict the Intestinal Absorption of Drugs in Humans.* Pharmaceutical Research, 1997. **14**: p. 568-571.
135. Pollard, C.E., Gerges, N. A., Bridgland-Taylor, M. H., Easter, A., Hammond, T. G. and Valentin J-P, *An introduction to QT interval prolongationand non-clinical approaches to assessing and reducing risk.* British Journal of Pharmacology, 2010. **159**(12-21).
136. Sanguinetti, M.C.a.T.-F., M., *hERG potassium channels and cardiac arrhythmia.* Nature, 2006. **440**: p. 463-469.
137. Guth, B.D.a.R., G., *Dealing with hERG liabilities early: diverse approaches to an important goal in drug development.* British Journal of Pharmacology, 2010. **159**: p. 22-24.
138. Cavalli, A., Poluzzi, E., Ponti, F. D. and Recanatini, M., *Toward a Pharmacophore for Drugs Inducing the Long QT Syndrome: Insights from a CoMFA Study of HERG K+ Channel Blockers.* Journal of Medicinal Chemistry, 2002. **45**: p. 3844-3853.
139. Pearlstein, R., Vaz, R. and Rampe, D., *Understanding the Structure-Activity Relationship of the Human Ether-a-go-go-Related Gene Cardiac K+ Channel. A Model for Bad Behavior.* Journal of Medicinal Chemistry, 2003. **46**: p. 2017-2022.
140. Ekins, S., Crumb, W. J., Sarazan R. D., Wikel, J. H., and Wright, S. A., *Three-Dimensional Quantitative Structure-Activity Relationship for Inhibition of Human Ether-a-Go-Go-Related Gene Potassium Channel.* Journal of Pharmacology and Experimental Therapeutics, 2002. **301**: p. 427-434.
141. Rampe, D., and Brown A. M., *A history of the role of the hERG channel in cardiac risk assessment.* Journal of Pharmacological and Toxicological Methods, 2013. **68**: p. 13-22.
142. Gibbons, G.F., *The role of cytochrome P450 in the regulation of cholesterol biosynthesis.* Lipids, 2002. **12**: p. 1163-1170.
143. Li, A.P., *Preclinical in vitro screening assays for drug-like properties.* Drug Discovery Today: Technologies, 2005. **2**: p. 179-185.

144. Law, V.e.A., *DrugBank 4.0: shedding new light on drug metabolism.* Nucleic Acids Research, 2014. **42**: p. 1091-1097.
145. Liu, X., Wright, M. and Hop, C. E. C. A., *Rational Use of Plasma Protein and Tissue Binding Data in Drug Design.* Journal of Medicinal Chemistry, 2014. **57**: p. 8238-8248.
146. *Cancer Survival - Cancer Statistics Report.* Cancer Research UK, 2014.
147. *Cancer Incidence and Mortality in the UK - Cancer Statistics Report.* Cancer Research UK, 2014.
148. Boyle, P., *Triple-negative breast cancer: epidemiological considerations and recommendations.* Annals of Oncology, 2012. **23**: p. 7-12.
149. Luo, F.R., et. Al., *Dasatinib (BMS-354825) Pharmacokinetics and Pharmacodynamic Biomarkers in Animal Models Predict Optimal Clinical Exposure.* Clinical Cancer Research, 2006. **12**: p. 7180-7186.

Appendix 1

ABL1	CHK1	FLT4/VEGFR3	MEK3	PKA	STK38L/NDR2
ABL2/ARG	CHK2	FMS	MEKK1	PKAcb	STK39/STLK3
ACK1	CK1a1	FRK/PTK5	MEKK2	PKAcg	SYK
AKT1	CK1d	FYN	MEKK3	PKCa	TAK1
AKT2	CK1epsilon	GCK/MAP4K2	MELK	PKCb1	TAOK1
AKT3	CK1g1	GLK/MAP4K3	MINK/MINK1	PKCb2	TAOK2/TAO1
ALK	CK1g2	GRK1	MKK4	PKCd	TAOK3/JIK
ALK1/ACVRL1	CK1g3	GRK2	MKK6	PKCepsilon	TBK1
ALK2/ACVR1	CK2a	GRK3	MLCK/MYLK	PKCeta	TEC
ALK3/BMPR1A	CK2a2	GRK4	MLCK2/MYLK2	PKCg	TESK1
ALK4/ACVR1B	CLK1	GRK5	MLK1/MAP3K9	PKCiota	TGFBR2
ALK5/TGFBR1	CLK2	GRK6	MLK2/MAP3K10	PKCmu/PRKD1	TIE2/TEK
ARAF	CLK3	GRK7	MLK3/MAP3K11	PKCnu/PRKD3	TLK1
ARK5/NUAK1	CLK4	GSK3a	MNK1	PKCtheta	TLK2
ASK1/MAP3K5	COT1/MAP3K8	GSK3b	MNK2	PKCzeta	TNIK
Aurora A	CSK	Haspin	MRCKa/CDC42BPA	PKD2/PRKD2	TNK1
Aurora B	DAPK1	HCK	MRCKb/CDC42BPB	PKG1a	TRKA
Aurora C	DAPK2	HGK/MAP4K4	MSK1/RPS6KA5	PKG1b	TRKB
AXL	DCAMKL1	HIPK1	MSK2/RPS6KA4	PKG2/PRKG2	TRKC
BLK	DCAMKL2	HIPK2	MSSK1/STK23	PKN1/PRK1	TSSK2
BMPR2	DDR1	HIPK3	MST1/STK4	PKN2/PRK2	TSSK3/STK22C
BMX/ETK	DDR2	HIPK4	MST2/STK3	PKN3/PRK3	TTBK1
BRAF	DLK/MAP3K12	HPK1/MAP4K1	MST3/STK24	PLK1	TTBK2
BRK	DMPK	IGF1R	MST4	PLK2	TXK
BRSK1	DMPK2	IKKa/CHUK	MUSK	PLK3	TYK1/LTK
BRSK2	DRAK1/STK17A	IKKb/IKBKB	MYLK3	PLK4/SAK	TYK2
BTK	DYRK1/DYRK1A	IKKe/IKBKE	MYO3b	PRKX	TYRO3/SKY
c-Kit	DYRK1B	IR	NEK1	PYK2	ULK1
c-MER	DYRK2	IRAK1	NEK11	RAF1	ULK2
c-MET	DYRK3	IRAK4	NEK2	RET	ULK3
c-Src	DYRK4	IRR/INSRR	NEK3	RIPK2	VRK1
CAMK1a	EGFR	ITK	NEK4	RIPK3	VRK2
CAMK1b	EPHA1	JAK1	NEK5	RIPK5	WEE1
CAMK1d	EPHA2	JAK2	NEK6	ROCK1	WNK1
CAMK1g	EPHA3	JAK3	NEK7	ROCK2	WNK2
CAMK2a	EPHA4	JNK1	NEK9	RON/MST1R	WNK3
CAMK2b	EPHA5	JNK2	NLK	ROS/ROS1	YES/YES1
CAMK2d	EPHA6	JNK3	OSR1/OXSR1	RSK1	ZAK/MLTK
CAMK2g	EPHA7	KDR/VEGFR2	P38a/MAPK14	RSK2	ZAP70
CAMK4	EPHA8	KHS/MAP4K5	P38b/MAPK11	RSK3	ZIPK/DAPK3
CAMKK1	EPHB1	LATS1	P38d/MAPK13	RSK4	
CAMKK2	EPHB2	LATS2	P38g	SGK1	
CDC7/DBF4	EPHB3	LCK	p70S6K/RPS6KB1	SGK2	
CDK1/cyclin A	EPHB4	LCK2/ICK	p70S6Kb/RPS6KB2	SGK3/SGKL	
CDK1/cyclin B	ERBB2/HER2	LIMK1	PAK1	SIK1	
CDK1/cyclin E	ERBB4/HER4	LIMK2	PAK2	SIK2	
CDK16/cyclin Y (PCTAIRE)	ERK1	LKB1	PAK3	SIK3	
CDK2/cyclin A	ERK2/MAPK1	LOK/STK10	PAK4	SLK/STK2	
CDK2/Cyclin A1	ERK5/MAPK7	LRRK2	PAK5	SNARK/NUAK2	
CDK2/cyclin E	ERK7/MAPK15	LYN	PAK6	SRMS	
CDK3/cyclin E	FAK/PTK2	LYN B	PASK	SRPK1	
CDK4/cyclin D1	FER	MAPKAPK2	PBK/TOPK	SRPK2	
CDK4/cyclin D3	FES/FPS	MAPKAPK3	PDGFRa	SSTK/TSSK6	
CDK5/p25	FGFR1	MAPKAPK5/PRAK	PDGFRb	STK16	
CDK5/p35	FGFR2	MARK1	PDK1/PDPK1	STK22D/TSSK1	
CDK6/cyclin D1	FGFR3	MARK2/PAR-1Ba	PHKg1	STK25/YSK1	
CDK6/cyclin D3	FGFR4	MARK3	PHKg2	STK32B/YANK2	
CDK7/cyclin H	FGR	MARK4	PIM1	STK32C/YANK3	
CDK9/cyclin K	FLT1/VEGFR1	MEK1	PIM2	STK33	
CDK9/cyclin T1	FLT3	MEK2	PIM3	STK38/NDR1	

Appendix 1a: *List of 340 wild type kinases used in whole kinome screen for compounds* ***41*** *and* ***52****.*

EEF2K	**EIF2AK3**
mTOR/FRAP1	**EIF2AK2**
AMPK(A2/B2/G2)	**EIF2AK4**
PDK1/PDHK1	**AMPK(A1/B1/G1)**
PDK2/PDHK2	**AMPK(A1/B1/G2)**
PDK3/PDHK3	**AMPK(A1/B1/G3)**
PDK4/PDKH4	**AMPK(A1/B2/G1)**
DNA-PK	**AMPK(A2/B1/G1)**
TRPM7/CHAK1	**AMPK(A2/B2/G1)**
EIF2AK1	

Appendix 1b: *List of 19 atypical kinases used in whole kinome screen for compound* ***41.***

PI3Kalpha	**PI3KC3/hVPS34**
PI3Kbeta	**PI4KA**
PI3Kgamma	**PI4KB**
PI3Kdelta	**SPHK1**
PI3K (p110a/p65a)	**SPHK2**
PI3K (p110a/ (E542K)/p85a)	**PI4K2A**
PI3K (p110a (E545K)/p85a)	**PIP5K1A**
PI3K (p110a (H1047R)/p85a)	**PIP5K1C**
PI3KC2a/PIK3C2A	

Appendix 1c: *List of 17 lipid kinases used in whole kinome screen for compound* ***41.***

Appendix 2

Kinase Tested	% Inhibition
ABL1	48
AKT1 (PKB alpha)	0
ALK	18
AURKA (Aurora A)	13
ABL1 E255K	45
ABL1 G250E	27
ABL1 T315I	9
ABL1 Y253F	62
ABL2 (Arg)	39
ACVR1B (ALK4)	25
ADRBK1 (GRK2)	3
ADRBK2 (GRK3)	-4
AKT2 (PKB beta)	5
AKT3 (PKB gamma)	19
AMPK A1/B1/G1	2
AMPK A2/B1/G1	16
AURKB (Aurora B)	8
AURKC (Aurora C)	4
AXL	6
BLK	50
BMX	13
BRAF	9
BRAF V599E	8
BRSK1 (SAD1)	2
BTK	13
CAMK1 (CaMK1)	-14
CAMK1D (CaMKI delta)	8
CAMK2A (CaMKII alpha)	2
CAMK2B (CaMKII beta)	7
CAMK2D (CaMKII delta)	15
CAMK4 (CaMKIV)	0
CDC42 BPA (MRCKA)	2
CDC42 BPB (MRCKB)	2
CDK1/cyclin B	-2
CDK2/cyclin A	-7
CDK5/p25	4
CDK5/p35	1
CDK7/cyclin H/MNAT1	-37
CHEK1 (CHK1)	2
CHEK2 (CHK2)	15
CLK1	6
CLK2	5
CLK3	3
CSF1R (FMS)	76
CSK	23
CSNK1A1 (CK1 alpha 1)	13
CSNK1D (CK1 delta)	73
CSNK1E (CK1 epsilon)	87
CSNK1G1 (CK1 gamma 1)	2
CSNK1G2 (CK1 gamma 2)	4
CSNK1G3 (CK1 gamma 3)	12
CSNK2A1 (CK2 alpha 1)	1
CSNK2A2 (CK2 alpha 2)	4
DAPK1	13
DAPK3 (ZIPK)	-1
DCAMKL2 (DCK2)	2
DYRK1A	-1
DYRK1B	3
DYRK3	31
DYRK4	-4
EEF2K	6
EGFR (ErbB1)	10
EGFR (ErbB1) L858R	11
EGFR (ErbB1) L861Q	13
EGFR (ErbB1) T790M	5
EGFR (ErbB1) T790M L858R	9
EPHA1	37
EPHA2	21
EPHA3	4
EPHA4	11
EPHA5	16
EPHA8	29
EPHB1	16
EPHB2	15
EPHB3	10
EPHB4	9
ERBB2 (HER2)	3
ERBB4 (HER4)	5
FER	-4
FES (FPS)	5
FGFR1	27
FGFR2	36
FGFR3	17
FGFR3 K650E	37
FGFR4	32
FGR	76
FLT1 (VEGFR1)	5
FLT3	81
FLT3 D835Y	25
FLT4 (VEGFR3)	20
FRAP1 (mTOR)	101
FRK (PTK5)	36
FYN	55
GRK4	-3
GRK5	4
GRK6	-5
GRK7	-2
GSK3A (GSK3 alpha)	5
GSK3B (GSK3 beta)	-2
HCK	41
HIPK1 (Myak)	1
HIPK4	7
IGF1R	3
IKBKB (IKK beta)	1
IKBKE (IKK epsilon)	1
INSR	4
INSRR (IRR)	14
IRAK4	5
ITK	0
JAK1	4
JAK2	-2
JAK2 JH1 JH2	-11
JAK2 JH1 JH2 V617F	4
JAK3	3
KDR (VEGFR2)	30
KIT	13
KIT T670I	4
LCK	66
LRRK2	16
LRRK2 G2019S	7
LTK (TYK1)	9
LYN A	63
LYN B	65
MAPK1 (ERK2)	-1
MAP2K1 (MEK1)	18
MAP2K2 (MEK2)	28
MAP2K6 (MKK6)	-3
MAP3K8 (COT)	2
MAP3K9 (MLK1)	16
MAP4K2 (GCK)	6
MAP4K4 (HGK)	15
MAP4K5 (KHS1)	6
MAPK10 (JNK3)	-5
MAPK11 (p38 beta)	13
MAPK12 (p38 gamma)	7
MAPK13 (p38 delta)	1
MAPK3 (ERK1)	6
MAPK8 (JNK1)	12
MAPK9 (JNK2)	4
MAPKAPK2	4
MAPKAPK3	2
MAPKAPK5 (PRAK)	1
MARK1 (MARK)	9
MARK2	13
MARK3	6
MARK4	13
MATK (HYL)	3
MET (cMet)	7
MELK	32
MERTK (cMER)	16
MET M1250T	3
MINK1	4
MST1R (RON)	1
MST4	-5
MUSK	15
MYLK2 (skMLCK)	15
NEK1	7
NEK2	1
NEK4	2
NEK6	-2
NEK7	13
NEK9	-4
NTRK1 (TRKA)	33
NTRK2 (TRKB)	29
NTRK3 (TRKC)	66
PAK2 (PAK65)	9
PAK3	-17
PAK4	4
PAK6	5
PAK7 (KIAA1264)	-4
PASK	0
PDGFRA (PDGFR alpha)	50
PDGFRA D842V	50
PDGFRA T674I	8
PDGFRA V561D	81
PDGFRB (PDGFR beta)	24
PDK1	14
PHKG1	5
PHKG2	2
PIM1	-2
PIM2	0
PKN1 (PRK1)	0
PLK1	-1
PLK2	3
PLK3	-3
PRKACA (PKA)	39
PRKCA (PKC alpha)	22
PRKCB1 (PKC beta I)	8
PRKCB2 (PKC beta II)	3
PRKCD (PKC delta)	2
PRKCE (PKC epsilon)	9
PRKCG (PKC gamma)	23
PRKCH (PKC eta)	6
PRKCI (PKC iota)	4
PRKCN (PKD3)	17
PRKCQ (PKC theta)	4
PRKCZ (PKC zeta)	1
PRKD1 (PKC mu)	21
PRKD2 (PKD2)	11
PRKG1	4
PRKG2 (PKG2)	4
PRKX	0
PTK2 (FAK)	12
PTK2B (FAK2)	5
PTK6 (Brk)	53
RAF1 (cRAF) Y340D Y341D	34
RET	51
RET V804L	8
RET Y791F	71
ROCK1	0
ROCK2	1
ROS1	13
RPS6KA1 (RSK1)	1
RPS6KA2 (RSK3)	0
RPS6KA3 (RSK2)	4
RPS6KA4 (MSK2)	11
RPS6KA5 (MSK1)	4
RPS6KA6 (RSK4)	0
RPS6KB1 (p70S6K)	-23
SGK (SGK1)	4
SGK2	2
SGKL (SGK3)	2
SNF1LK2	20
SRC	12
SRC N1	23
SRMS (Srm)	30
SRPK1	-1
SRPK2	-3
STK22B (TSSK2)	1
STK22D (TSSK1)	1
STK23 (MSSK1)	5
STK24 (MST3)	-3
STK25 (YSK1)	1
STK3 (MST2)	1
STK4 (MST1)	3
SYK	-1
TAOK2 (TAO1)	6
TBK1	-4
TEK (Tie2)	-5
TYK2	2
TYRO3 (RSE)	18
YES1	43
ZAP70	2

Appendix 2: *List of 243 kinases used in whole kinome screen for INK-128.[35]*

Appendix 3

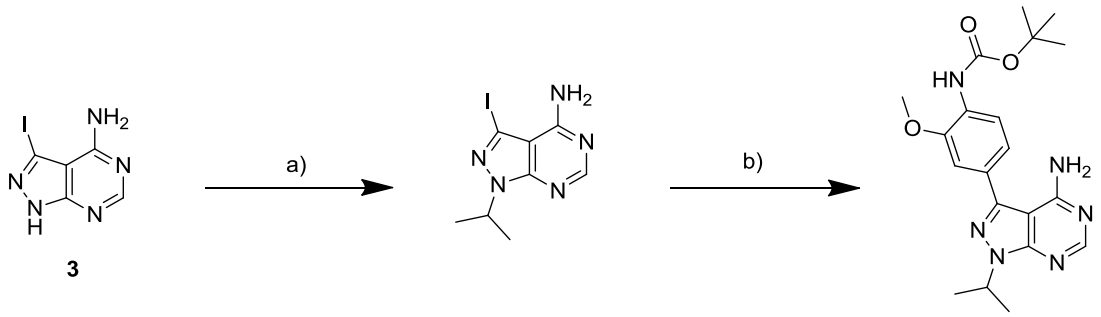

Synthesis of PP20: *a) 2-iodopropane, NaH, DMF, mw, 150 ^{o}C. b) [4-(tert-butoxycarbonylamino)-3-methoxy-phenyl]boronic acid, K_2CO_3, $Pd(OAc)_2$, PPh_3, 1,4-dioxane/water (10:1), 120 ^{o}C, mw.*